Light Harvesting and Orbital Tuning

Perylene Monoimides and Diimides for Photovoltaic Purposes

Dissertation
zur Erlangung des Grades
"Doktor der Naturwissenschaften"
im Promotionsfach Chemie

am Fachbereich
Chemie, Pharmazie und Geowissenschaften
der Johannes Gutenberg-Universität
in Mainz

Henrike Wonneberger

geboren in Hamburg

Mainz – 2012

Die vorliegende Arbeit wurde in der Zeit vom Juni 2008 bis November 2011 am Max-Planck-Institut für Polymerforschung Mainz unter Anleitung von [redacted] durchgeführt und wurde in LaTeX gesetzt.

Dekan: [redacted]

1. Berichterstatter: [redacted]

2. Berichterstatter: [redacted]

Tag der mündlichen Prüfung: 11. September 2012

Contents

List of Figures

List of Tables

Abbreviations

ATR	attenuated total reflectance
BG	band gap
BINAP	2,2-Bis(diphenylphosphino)-1,1'-binaphthyl
CB	conduction band
COSY	correlation spectroscopy
CT	charge transfer
CV	cyclic voltammetry
DFT	density functional theory
DCM	dichloromethane
DMF	dimethylformamide
DMSO	dimethyl sulfoxide
DSSC	dye-sensitised solar cell
DπA	donor π-spacer acceptor
EA	electron affinity
ESI	electrospray ionisation
EQE	external quantum efficiency
eV	electron volt
FD	field desorption
FF	fill factor
FRET	Förster resonance energy transfer

FT-IR	Fourier-transform infrared spectroscopy
FTO	fluorine-doped tin oxide
HOMO	highest occupied molecular orbital
HTM	hole transporting material
I	photocurrent in Am^{-2}
ICT	intramolecular charge transfer
IP	ionisation potential
IPCE	incident power conversion efficiency
I_{SC}	short-circuit current
IV curve	current-voltage curve
LUMO	lowest unoccupied molecular orbital
MALDI-TOF	matrix-assisted laser desorption/ionisation time-of-flight
MLCT	metal to ligand charge transfer
MPP	maximum power point
NBS	*N*-bromosuccinimide
n-DSSC	n-type DSSC
NHE	normal hydrogen electrode
NIR	near infrared
NOESY	nuclear Overhauser enhancement spectroscopy
NMI	naphthalene monoimide
NMP	*N*-Methyl-2-pyrrolidon
NMR	nuclear magnetic resonance
OFET	organic field effect transistor
OP	orbital partitioning
OPV	organic photovoltaics

P	incident light power in Wm^{-2}
PDI	perylene diimide
p-DSSC	p-type DSSC
PET	photoinduced electron transfer
PMI	perylene monoimide
PV	photovoltaics
sDSSC	solid-state dye-sensitised solar cell
SPC	synthetic procedures and characterisation
spiro-MeOTAD	2,2'7,7'-tetrakis-(*N,N*-di-*p*-methoxyphenyl-amine)-9,9'-spirobifluorene
THF	tetrahydrofuran
TMS	trimethylsilyl
UV-vis	ultraviolet-visible
V	voltage
VB	valence band
V_{OC}	open-circuit voltage
Wp	peak Watt
x	excitation wavelength
$	US dollar
δ	chemical shift
ϵ	extinction coefficient
η	power conversion efficiency
λ	wavelength

We are like tenant farmers chopping down
the fence around our house for fuel
when we should be using Nature's
inexhaustible sources of energy —
sun, wind and tide. ...

I'd put my money
on the sun and solar energy.
What a source of power!
I hope we don't have to wait
until oil and coal run out
before we tackle that.[4]

– Thomas Edison –

Chapter 1

Introduction

It is 80 years since Thomas Edison voiced his concerns about society's energy procurement and, at the same time, pointed out a possible solution to the arising shortage of fossile resources – renewable erergy and in particular the sun! Though maybe not the first one to realise and mention this issue, he hit the nail on the head, his words sounding like a prophecy which has materialised over the years. Today, discussions about peak oil, energy shortage, and climate change due to CO_2-emissions have become omnipresent. At the same time research efforts in the direction of renewable energies have been strongly intensified. Many private households have furnished their roofs with solar panels, wind generators have become a usual sight along coastlines as well as in the inland but traditional biomass[1], currently the most intensively used

[1]Biomass produced in a sustainable way – the so-called modern biomass – excludes traditional uses of biomass as fuelwood and includes electricity generation and heat production, as well as transportation fuels, from agricultural and forest residues and solid waste. On the other hand, "traditional biomass" is produced in an unsustainable way and it is used as a non-commercial source-usually with very low efficiencies for cooking in many countries.[5]

renewable energy worldwide, held only 10 % of the world's final energy consumption in 2009.[6] We certainly have not *tackled it*!

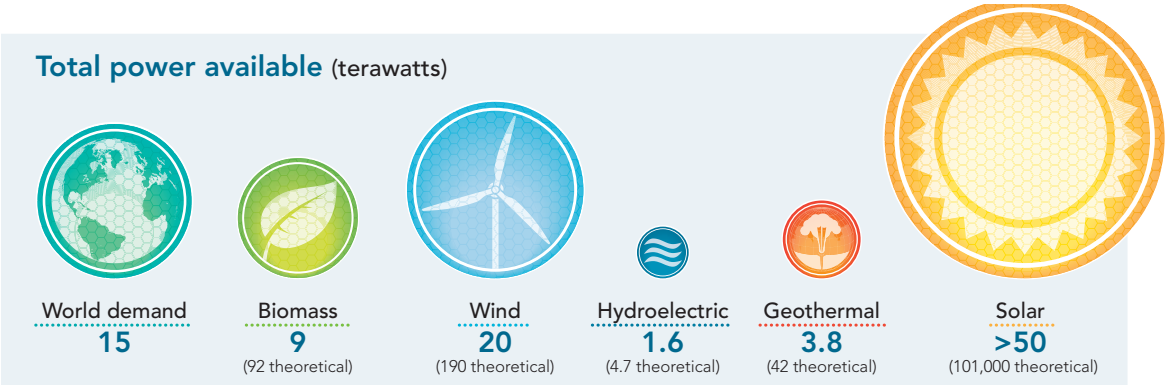

From: Adrian Cho, *Science*, **2010**, *329*, 786. Reprinted with permission from AAAS. SOURCE: WORLD ENERGY ASSESSMENT 2000/UNDP; WEA 2004/UNDP; REPORT OF THE INTL. GEOTHERMAL ASSOCIATION TO THE U.N. COMMISSION ON SUSTAINABLE DEVELOPMENT 2001; SCLATER ET AL., JOURNAL OF GEOPHYSICAL RESEARCH 86 (1981); NASA

Figure 1.1: Estimation of the available power of various renewable energies and the current world demand

10 % for traditional biomass and 3.4 % for hydropower are respectable shares, the other renewable energies (wind, solar, geothermal and biomass), however, reach only 2.8 %, an almost negligible number compared to 81 % global final energy consumption of fossil fuels.[6] The residual 2.8 % are allotted to nuclear power[6], a technology which is often praised as long-lasting, strongly efficient and CO_2-poor, but which bears other pitfalls, namely the devastating consequences of radiation for mankind, animals, and the environment in the case of severe and uncontrollable accidents, which have happened regularly in the past (e. g. Kyschtym 1957, Tschernobyl 1986) and unfortunately with Fokushima in 2011 also in the present. Moreover the question of final storage of the nuclear waste has not been answered yet.

When pondering the different possibilities of energy production, various characteristics need to be considered. In August 2010 Cho[7] gave a short overview on today's energy mix and the implications of the individual technologies. One main prerequisite of course is the availability of resources. Currently hydroelectric power is the main producer of energy besides the above mentioned traditional biomass with a current worldwide capacity of around 1 terawatt.[6] Even if the theoretical maximum for this source could be reached, it would still only account for a third of current world demand (figure 1.1). Biomass seems to offer a greater potential of 9 terawatts but would require stiff competition with food production and is often connected to deforestation. In contrast, the sun's potential is estimated to exceed 50 terawatts, thus more than three times the current global demand (figure 1.1).[7] *What a source of power!*

Coal, natural gas, and oil, the resources we rely on today, are limited. Depending

on the oil price and the costs of the competing technologies, some resources may or may not be made accessible, new deposits might be detected, and depending on the consumption and energy mix of the following years, it is hard to say excactly, how long coal, natural gas, and oil will last. Cho[7] mentions a timescale of 40-125 years for oil, 65-210 years for natural gas and 250-360 years for coal – timescales, which range from our lifetimes to the next 10-15 generations. A fact is, however, that we consume more than what is recreated, hence that gas, *oil and coal* will *run out* and especially as oil is a very important feedstock for other industries, e. g. the synthetic materials industry, we need to make use of it very carefully.

Other implications which need to be considered are water-consumption, land demand, and CO_2-emissions. Though not the top-saver in all three categories, solar energy shows a good balance, needing more land than fossile fuels, nuclear and hydroelectric power but considerably less than wind and biomass. Its CO_2-emissions balance sheet looks less appealing, here solar energy emits more than all other renewables and nuclear power but not even a tenth of natural gas, the CO_2-poorest fossile energy. Regarding water consumption, however, solar energy comes in first together with wind with zero-water-consumption.[7] So Thomas Edison was absolutely right: with its large availability and acceptable eco-balance with respect to land demand, CO_2-emissions, and water consumption, *the sun and solar energy* are highly promising to play a major role in our solution to the energy problem, and the related technologies, summarised as "photovoltaics", are worth being thouroughly investigated and developed.

1.1 Photovoltaics

Photovoltaics date back to the 1950s when the Bell laboratories presented the first silicon-based solar cell. At the time solar cells were too expensive to conquer the consumer market but found use in aeronoautics and other applications like oil rigs where alternative powering meant even higher costs.[8] By this first use of photovoltaics, one of the major advantages besides the above mentioned eco-friendliness becomes evident: solar energy is generally available wherever[2] it is consumed and can therefore be used in self-sufficient devices or small local grids. The implications of this advantage go far beyond environmental sustainability. If research efforts and scale-up will allow for prices to drop, photovoltaics will be a means to equip poor remote regions with electricity, and therefore stimulate socio-economic development. One early example for this is Mali, where photovoltaic pumps have provided people and farms with water since 1980.[8]

Since then, photovoltaics (PV) have developed dramatically. Various types of solar

[2]Of course, here the term "everywhere" is somewhat imprecise, if indoors and underground is considered, and must be understood as "everywhere within a short distance".

cells are now in the market, which can be roughly subdivided into silicon wafers and thin film technologies. Silicon wafers, the first generation solar cells, still holds the largest share in the market. In 2010 it accounted for approximatly two thirds, the other third falling on thin film PV, the fast developing second generation.[9] Inorganic solar cells reach efficiencies up to approximately 20% in modules.[10] Besides efficiency, long-term stability and low costs are main prerequisites for a PV technology to be successful. In inorganic PV the issue of stability seems to be solved, most producers giving a guarantee of 80% efficiency for 20 years. The target price for photovoltaics is 1$/peak Watt (1$/Wp) in order to be able to compete with other power generating technologies.[10] The American company First Solar LLC. was able to even underprice this with 0.81$/Wp production costs in 2010.[9] In 2010 the global capacity of photovoltaics was 40 GW, 17 GW of which had been installed in 2010, so the capacities almost doubled over the past 12 months.[6] A strong impetus has driven the PV market throughout the last years but still today's capacities are negligible considering what the sun has to offer (figure 1.1 on page 2).

1.2 Organic Photovoltaics

In the 1980s, with first single-layer cells[11] and later with the first heterojunction device presented by Tang[12], a new branch of photovoltaics, namely "organic photovoltaics" arose and has been developed throughout the past two decades.

Main advantages of organic photovoltaics are that i) organic materials are abundant, ii) all organic photovoltaics are thin-film technologies, implying low material requirement, iii) diffuse light can be converted almost as well as direct irradiation, and iv) the aspired processing techniques allow roll-to-roll printing. All three points hold the promise of organic photovoltaics to become a powerful cheap technology for the mass market.

Organic photovoltaics of today can be divided into three main cell types: flat-heterojunction cells, bulk-heterojunction cells, and dye-sensitised solar cells. In flat-heterojunction cells donor and acceptor materials are deposited as two seperate layers on top of each other between two electrodes. As mainly vacuum deposition is used, most flat-heterojunction cells are based on organic small molecules. Upon irradiation both donor and acceptor material absorb photons leading to exciton formation. These excitons diffuse to the interface where the charges are seperated and transported to the electrodes. Limitations are the small interface and confined exciton diffusion lengths. These limitations are addressed in bulk-heterojunction cells, where the donor and acceptor material is blended forming donor and acceptor domains within the active material. This way, the interface area is raised and the length is shortened which needs to be travelled by the excitons. Small molecules as well as polymers can be used

in bulk-heterojunction devices, mostly processed from solution, a cheaper technique than the vacuum depostion. Dye-sensitised solar cells, also called "Grätzel-cells" after Prof. Dr. Michael Grätzel, the pioneer in the field of dye-sensitised solar cells, are quite different in their working principle and cell setup. They will be the main field of application of the materials presented in this thesis and will therefore be presented in more depth in the following section.

With companies like G24Innovation (G24i), Konarka, and Solarmer, organic photovoltaics have entered the market, slowly evolving as commercialised products. Generally their efficiencies and stabilities still lag behind those of inorganic photovoltaics though with the just recently validated 8.3 %[13] efficiency single-junction polymer cell of Konarka, OPV is slowly becoming serious competition.

1.3 Dye-Sensitised Solar Cells

Dye-sensitised solar cells (DSSCs) mimic Nature's photosynthesis. The chlorophyll in the plant is the dye in the DSSC, absorbing light resulting in electron excitation. In DSSCs the electrons are subsequently injected into the conduction band of a semiconductor, the oxidised dye molecules recovered by either a liquid electrolyte system for liquid DSSCs or a solid-state hole transporting material (HTM) for soldid-state DSSCs (sDSSCs). Semiconductor and HTM are flanked by electrodes and connected via an external circuit (figure 1.2).

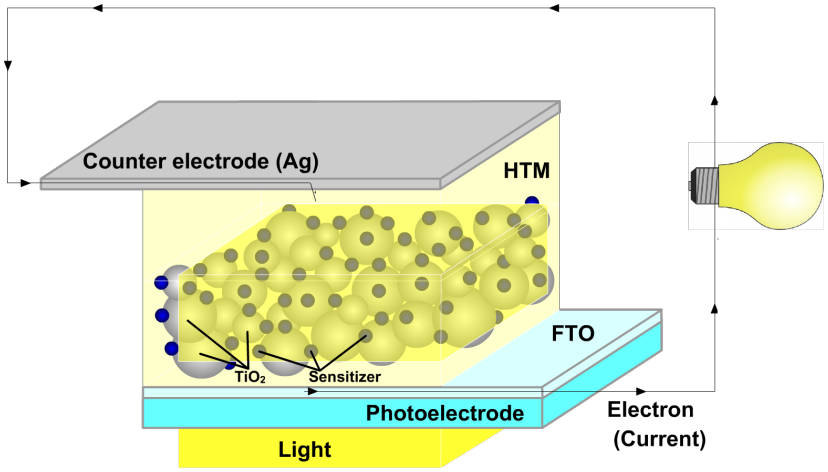

HTM: hole transporting material; FTO: fluorine-doped tin oxide

Figure 1.2: Device structure of a solid-state dye-sensitised solar cell

Dye-sensitised solar cells (DSSCs) are often distinguished from the other organic photovoltaics technologies as "hybrid systems" because inorganic semiconductors are used in all cell set-ups. The first efficient DSSCs were reported by O'Regan and Grätzel[14]. A ruthenium-complex served as the sensitiser anchored on titanium dioxide

nanocrystals producing large current density (higher than 12 $mAcm^{-2}$) and efficiencies exceeding 7 %[14] in cells with good stability. To date, ruthenium complexes are the most widely explored and efficient class of sensitisers, and titanium dioxide is the most widely used semiconductor.[15]

With efficiencies exceeding 12 % for liquid[16] and up to 7.2 % for organic-based[3] solid-state devices[18], DSSCs are one of the more efficient organic photovoltaic technologies and a serious competition or complement of inorganic photovoltaics. The advantages of DSSCs, some of which are also valid for organic photovoltaics in general[8], are outlined below.

Potentially low costs: DSSCs are thin-layer devices with low material usage. Moreover, metal-free sensitisers can be made by numerous synthetic pathways from feedstocks considered abundant. The most widely used semiconductor, titanium dioxide, though inorganic, is cheap and sufficiently available. Solution processing and the prospects of efficient roll-to-roll printing are another important factor allowing for low cost fabrication.

Flexible: Thin as they are, DSSCs can be deposited onto flexible substrates, e. g. plastic foil. This opens up a whole new field of applications, for example on textiles (like the DSSC bags of G24i which are already in the market) in roller blinds or to jacket any other bent object.

Light weight: As a thin-layer technology DSSCs have a very low net weight. The total weight of the device is strongly influenced by the substrate material. Especially DSSCs on plastic foil are extremely light, on the one hand improving the carbon footprint of the product, on the other hand enabling additional applications where weight is a key criterion, e. g. the above mentioned application on bags.

Semi-transparent and coloured: Semi-transparent and coloured is a combination of characteristics which has already been used for a long time in tinted windows in cars or buildings to ensure privacy, for aesthetic reasons of just to block the sun. DSSCs can be easily deposited on glass and offer the added value of power generation. As sensitisers are available in all designated colours, architects or product designers have all freedom of scope.[19]

Efficient conversion of diffuse light: Whereas conventional crystalline silicon based devices unfold their high efficiencies primarily upon direct beam radiation, DSSCs like other organic photovoltaics technologies work almost as well with diffuse light[20], making them particularly attractive for locations distal to the equator as well as indoor-applications.

Having listed all these promising advantages of DSSCs, it needs to be mentioned that also in inorganic photovoltaics, research efforts to meet these requirements have

[3] Very recently, results of a mainly inorganic sDSSC (ruthenium-based sensitiser and inorganic hole conductor) have caused a stir with an overall power conversion efficiency of 10.2 %.[17]

been made. Amorphous silicon cells, for example, are already less dependent on the irradiation angle. Moreover, Yoon et al.[21] presented in 2008 a first ultra-thin bendable silicon-based solar cell of high transparency. With an efficiency of 11.6%, its performance is, however, not superior to liquid DSSCs. The device based on the porphyrine-sensitiser **YD2** presented by Bessho et al.[22] for example showing an efficiency of 11%. The performance of this sensitiser was even improved to 12.3 % when cosensitised with **YD2-*o*-C8** in combination with a cobalt (II/III) electrolyte (figure 1.3).[16] Whereas in liquid DSSCs after a long prevailance of ruthenium-based sensitisers, the porphyrin dyes have taken the lead, in solid-state devices the highest efficiency of an organic-based system could be reached by a metal-free sensitiser, namely **Y123** (figure 1.3), a cyclopentadithiophene bridged donor-acceptor dye, reaching an outstanding efficiency of 7.2 %.[18] **Y123** is one of the few sensitisers reaching good efficiencies both in liquid as well as solid-state devices.[23] In general, inorganic and organic photovoltaics, particularly the highly efficient DSSC can either be regarded as rivals, or the two technologies can be seen as complementary to form a sound solar cell market.

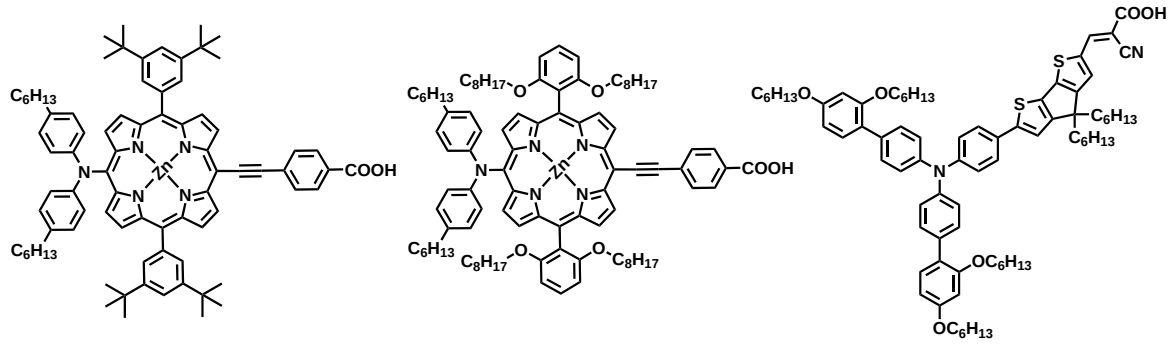

YD2 **YD2-*o*-C8** **Y123**

Figure 1.3: Top efficiency sensitisers: porphyrine-based **YD2** and **YD2-*o*-C8** and cyclopentadithiophene bridged donor-acceptor dye **Y123**

There are different types of DSSCs. In general n-type (n-DSSCs) and p-type DSSCs (p-DSSCs) need to be distinguished. N-type DSSCs work as photoanodes and are the more common and to date more efficient devices. P-type DSSCs working as photocathodes are not in the focus of this thesis and if not mentioned explicitely the term "DSSC" always relates to n-type DSSCs.

A second differentiation is according to the nature of the electrolyte system. Cells using liquid electrolyte systems, mostly the I^-/I_3^- redox system, to regenerate the oxidised dye, are the liquid DSSCs or what is generally understood when speaking of "Grätzel cells". To overcome the problems of leakage and degradation reactions, solid hole transporting materials (HTM) were introduced[24], spiro-MeOTAD currently the most widely used, these cells forming the class of solid-state DSSCs (sDSSCs) which are generally more stable than liquid DSSCs but inferior regarding their efficiency. Main reason for this is probably the lower conductivity of the spiro-MeOTAD compared to

the liquid electrolyte leading to higher interfacial recombination losses.[25,26]

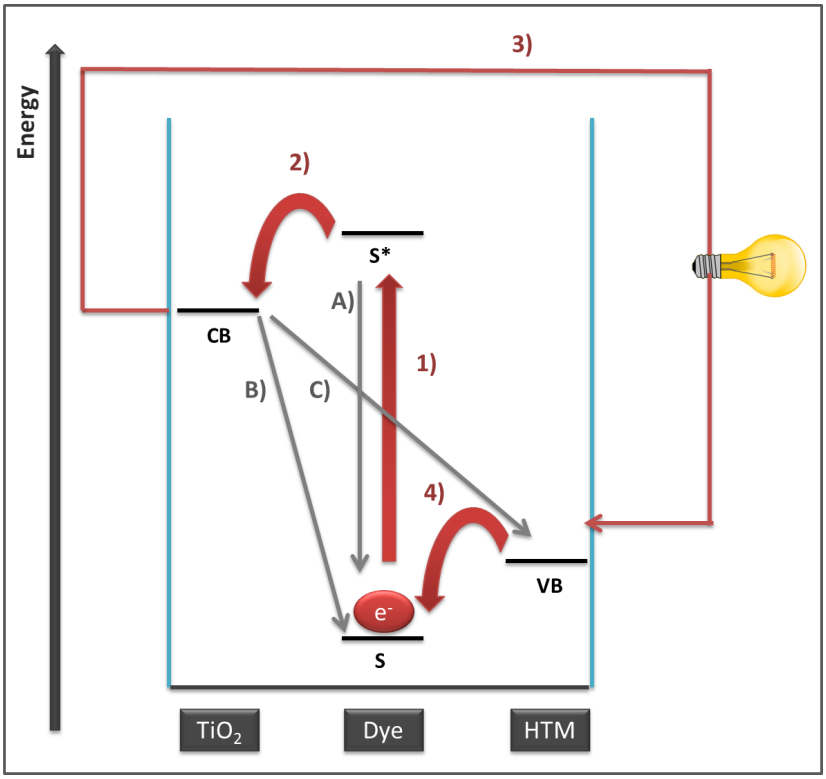

S: ground state; S*: excited state; CB: conduction band; VB: valence band; TiO_2: titanium dioxide; HTM: hole transporting material

1) excitation of dye; 2) electron injection into titanium dioxide (oxidation of dye); 3) regeneration of hole transporting material; 4) regeneration (reduction) of dye

A) dye-dye recombination; B) titanium dioxide-dye recombination; C) titanium dioxide-HTM recombination

Figure 1.4: Operation mechanism of an sDSSC

The components and the cell structure have been described and presented briefly above (figure 1.2 on page 5). The operating mechanism of the devices is demonstrated in figure 1.4. Upon irradiation of the dye, an electron is excited from the ground state (S) to the excited state (S*) of the dye (1). If enough driving force is provided, this electron is injected into the conduction band of titanium dioxide (2) leaving an oxidised dye molecule behind. Via the electrode the electron travels through an external circuit to the counter-electrode to recover the hole transporting material (3) which in return reduces the oxidised dye (4). An external load (here represented as a light bulb) can be interposed in the external circuit between the electrodes allowing to use (or store) the generated current.

This desired pathway (red) competes with several unwanted recombination reactions. One is the dye-dye recombination (A) which can occur between neighbouring dye molecules or the electron falls back into its ground state, if it is not injected into the titanium dioxide. The second unwanted recombination is the back-transfer of the injected electron to the dye molecule (B). The third recombination between titanium

dioxide and the hole transporting material occurs if the titanium dioxide layer is not separated well enough from the hole transporting material layer. Then the electron choses the direct path (C) from titanium dioxide to the hole transporting material not through the external circuit.

With help of clever molecular design by the chemists and skillful processing by the device physiscists, the desired mechanisms can be enhanced, the undesired ones suppressed. How to approach this from the chemistry side will be discussed in more depth in section 1.5 on page 17.

Device processing is of course just as complex but not the focus of this work. What is important for this work, however, is to know that besides the standard components (electrodes, semiconductor, sensitiser and hole transporting materials), additives can be used. These additives are used for two major reasons: i) small as they generally are, these molecules take up empty spaces between the dye-molecules preventing aggregation and the above undesired dye-dye recombination. Moreover they enforce the barrier between the semiconductor and the hole transporting material. Most of the time this use of additives leads also to lower dye concentration on the surface which is, however, generally overcompensated by the positive effects of the additives. ii) additives interact with the semiconductor lowering or elevating the conduction band that the dye injects into. This affects on the one hand the current as it favours or decelerates injection, on the other hand the voltage will be altered as a result of the change in the semiconductor conduction band-hole conductor valence band gap.

Another variable which was applied in the testing of the dyes in this thesis was the processing from different solvents like dichloromethane, tetrahydrofuran, and toluene. The choice of solvent always depends on the solubility of the dye. In general dichloromethane and toluene lead to better performance results than tetrahydrofuran. Toluene as a non-chlorinated solvent is favoured for health and environmental reasons. Different solvents also bring about varying drying speed of the cells due to their different vapour pressures. This may influence the uptake of the amount of dye and also the morphology of the molecules.

Working in the field of dye-sensitised solar cells, there are several performance indicators which need to be known and understood. Depending on the earth's tilt, the solar spectrum striking the earth differs from place to place and with the seasons. That is why scientists have agreed on standard conditions (AM 1.5 G[4]) regarding tilt, temperature, albedo, and turbidity with one standard spectrum (figure 1.5 on the next page) in order to make the test results of cells comparable. Roughly 40 % of the irradiation can be found in the UV-Vis region of the spectrum, around 60 % in the near infrared. Ideally a sensitiser would cover both visible and near infrared in absorption.

[4] Air Mass 1.5 G: further details provided by the NREL; http://rredc.nrel.gov/solar/spectra/am1.5/ (23.12.2011)

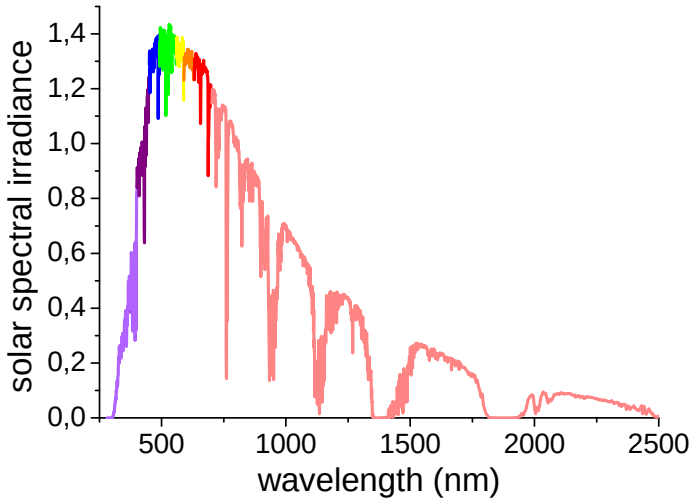

Figure 1.5: Solar spectrum under 1.5 AM standard conditions

Most sensitisers of today, however, absorb only in the UV-Vis region.

Moreover, besides the power conversion efficiency (η), the short-circuit current (I_{SC}), the open-circuit voltage (V_{OC}), and the fill factor (FF) are standard performance values that help comparing different cells. Other very important characteristics are the absorption spectrum of the sensitiser in solution, on titanium dioxide and the EQE (external quantum efficiency) spectrum of the cell. The EQE-spectrum strongly depends on the absorption and has a major influence on the current output. Definitions, demonstrations, and explanations are given below and in the figures 1.6 and 1.7 on the next page and the equations 1.1 on the facing page, 1.2 on page 12, and 1.3 on page 12.

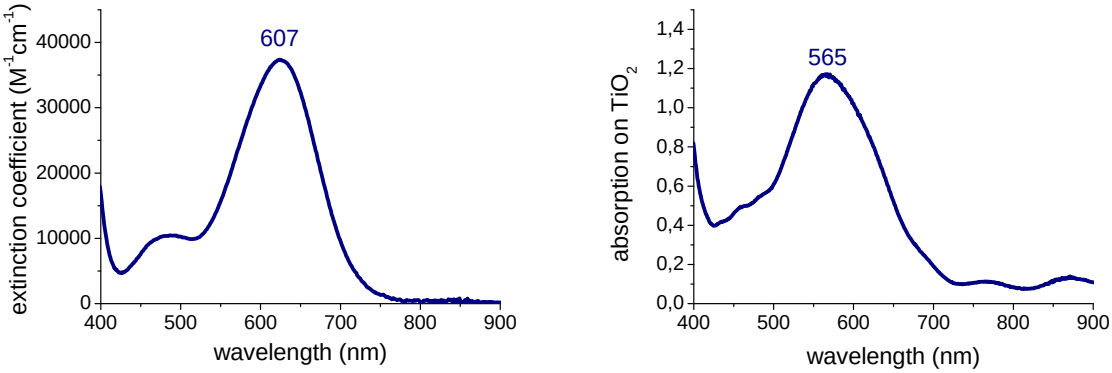

(a) solution absorption

(b) TiO_2 absorption

sensitiser **149** (chapter 5 on page 95)

Figure 1.6: Absorption in solution (a) and on titanium dioxide (b)

The solution absorption spectrum and the extinction coefficient provide a first indication how much irradiation and in what wavelength region the dye absorbs (figure 1.6 on the facing page). Once adsorbed on titanium dioxide (figure 1.6 on the preceding page), the absorption spectrum will look different from that in solution as can be seen in figure 1.6 on the facing page. Here the absorption maximum of the same dye, once adsorbed on titanium dioxide experiences a blue-shift of roughly 40 nm. The absorptivity on titanium dioxide is driven by three main factors: a) the already mentioned extinction coefficient, b) the amount of dye molecules adsorbed on the surface, and c) the morphology of the dye layer. The amount of dye molecules adsorbed on the titanium dioxide can vary upon different processing solvents, dye loading time and – what will also come into play later on in this thesis – the size of the dye molecules.[27]

$$EQE = \frac{n_{electrons}}{n_{photons}} = \frac{I/e}{P/h\,\nu} = \frac{I}{P}\,\frac{h\,c}{e\,\lambda} = \frac{I}{P}\,\frac{1240}{\lambda(nm)} \tag{1.1}$$

EQE: external quantum efficiency; I: photocurrent in Am^{-2}; P: incident light power in Wm^{-2}; *e*: elementary charge; *h*: Planck constant; *c*: speed of light; λ: wavelength

The EQE (external quantum efficiency)[5] represents the ratio of charge carriers generated to the incident photon flux. It is recorded as a function of the excitation wavelength (figure 1.7). A powerful EQE is a strong driver for high current.

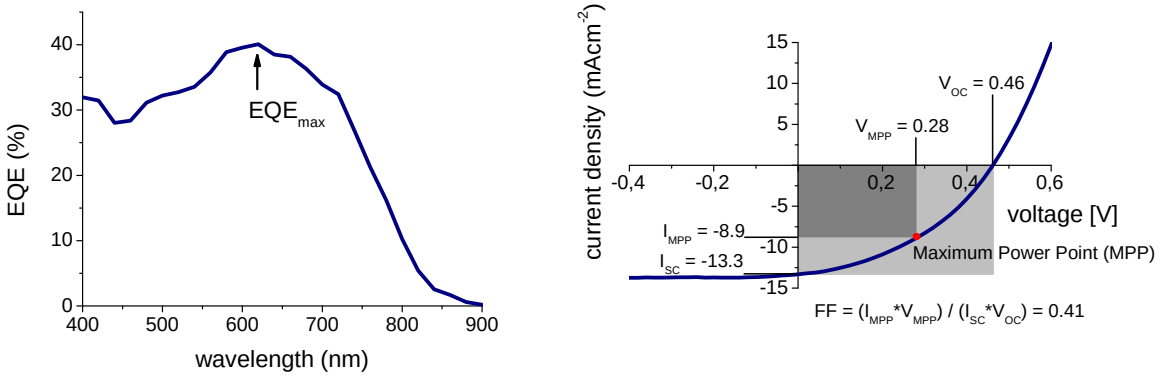

(a) EQE curve

(b) IV curve

sensitiser **149** (chapter 5 on page 95)

Figure 1.7: EQE (a) and IV curve (b) of an sDSSC

The open-circuit voltage (V_{OC}) is measured at zero output current and the short-circuit current (I_{SC}) accordingly at zero output voltage. Whereas the current is mainly driven by the absorption and extinction of the sensitiser as well as the efficieny of the electron injection and dye regeneration processes, the voltage is determined by the gap between the conduction band of the semiconductor and the valence band of the hole

[5]Sometimes also called IPCE (incident photon to current conversion efficiency)

transporting material (figure 1.4 on page 8). As mentioned above, it can be further tuned by the choice of appropriate additives.

$$\eta = \frac{P_{out}}{P_{in}} = FF\,\frac{I_{SC}\,V_{OC}}{P_{in}} \tag{1.2}$$

η: overall power conversion efficiency; FF: fill factor; I_{SC}: short-circuit current in Am^{-2}; V_{OC}: open-cicuit voltage

$$FF = \frac{I_{MPP}\,V_{MPP}}{I_{SC}\,V_{OC}} \tag{1.3}$$

MPP: maximum power point

The power conversion efficiency η (equation 1.2) is the ratio of power offered to the cell system by irradiation (P_{in}) and the power collected after conversion (P_{out}). This ratio can also be expressed by using besides the P_{in} the already presented V_{OC}, I_{SC}, and the fill factor (FF) which is defined in equation 1.3 as the ratio of the current-voltage product at the maximum power point (MPP) (dark grey rectangle) and the product of V_{OC} and I_{SC} (light grey rectangle), also graphically demonstrated in figure 1.7 on the preceding page. An ideal IV curve is more or less rectangular, thereby maximising the area of the MPP so both areas are congruent with each other.

1.4 Perylenes and Their Chemistry

One key material in DSSCs and object of this work is the dye. Many chromophore families like coumarines, porphyrines, merocyanines, squaraines or thiophenes have been investigated.[28,29,30,31,32,33] One very stable chromophore class are perylene and its imide derivatives. They have been amongst the first dyes used in organic photovoltaics and are still to date, of great importance to this field.

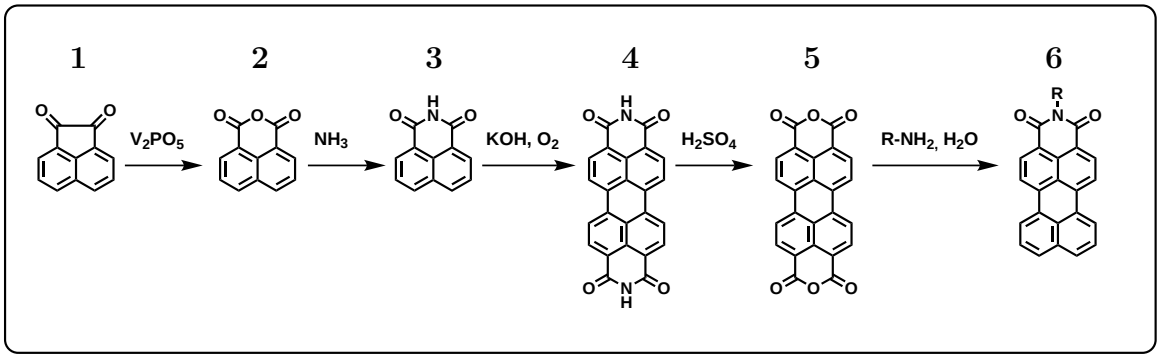

Figure 1.8: Industrial synthesis of perylene dianhydrides and one-pot imidisation-decarboxylation to perylene monoimide[1]

Perylene occurs like other polycyclic aromatic hydrocarbons in Nature, e. g. in marine, lake, and river sediments as well as peat accumulations, its origin still not

clearly identified.[34] Synthetically perylene derivatives have been developed for around 100 years now. Especially the perylene imides have gained more and more importance since Kardos[35] presented in 1913 a way to synthesise perylene diiimides. Perylene dianhydrides **5** are nowadays a commercialised product. They are synthesised by oxidising acenaphthylene **1** with vadium pentoxide, amination of the resulting naphthalene monoanhydride **2** with ammonia to achieve naphthalene monoimide **3** and subsequent oxidative coupling in alkali melt (figure 1.8 on the preceding page).[36] In 1995 Feiler et al.[1] showed a convenient one-pot reaction converting perylene dianhydrides into the asymmetric perlyene monoimide **6** with bulky primary amines in the presence of water (figure 1.8 on the facing page).

Perylene derivatives are a highly versatile chromophore class. First used mainly as vat dyes[37], they soon advanced to functional dyes for high-tech applications, such as biolabelling[38,39], sensing[40], single molecule spectroscopy[41,42,39], organic field effect transistors[43], and last but certainly not least in all kinds of organic photovoltaics[44,36].

The manifold applications of perylene derivatives are a result of the diverse chemical modification possibilities and their related characteristics. In the following the main synthesis options and related properties will be presented, dividing the perylene derivatives into two groups: i) the symmetric perylene diimides/-anhydrides and the asymmetric perylene monoimides/-anhydrides.

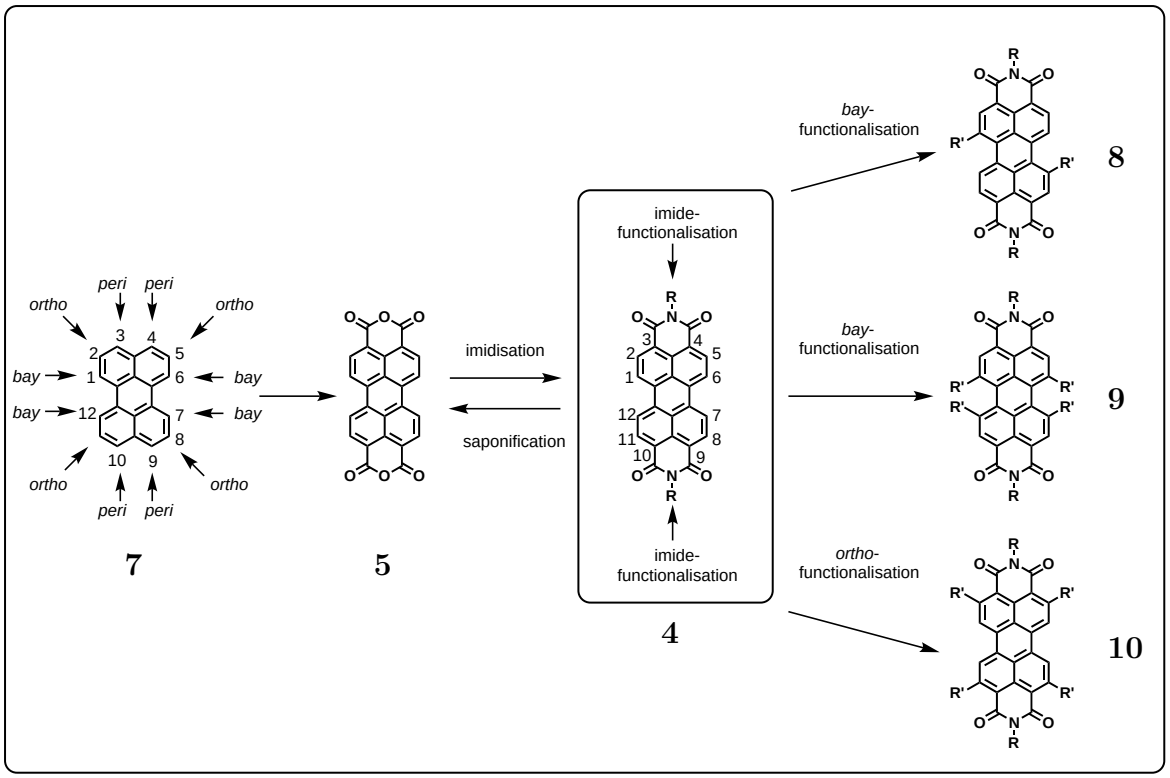

Figure 1.9: Synthesis: from perylene to perylene dianhydrides and diimides

Perylene diimides are known for their excellent chemical, thermal, and photosta-

bility.[45,46] Moreover, they are of intense colours with high extinction coefficients and can reach fluorescence quantum yields close to unity.[47]

The perylene core has twelve functionalisation positions which can be grouped as the *peri*-, *bay*-, and *ortho*-positions (figure 1.9 on the previous page). Functionalisation of the different positions can strongly influence their optical, electronic, and morphological properties as well as their solubility.[36]

The above mentioned synthesis of a perylene diimide or dianhydride constitutes the probably most typical *peri*-functionalisation of perylene. Along with it came the imide-substitution which can be easily achieved by imidisation of the perylene dianhydride **5** with the designated amine to achieve **4**. The imide-substitutent is electronically decoupled from the perylene core and therefore has no noteworthy influence on its electronic properties, i. e. HOMO and LUMO energy level.[36] It has, however, a strong effect on the solubility of the compounds, permitting the synthesis of insoluble pigments (imide substituent: H) or dyes highly soluble in many organic solvents (imide substitutent: aryl or (branched) alkyl chains) or even achieve water-solubility[48]. Morover the imide substituent can be used to tune the morphology of the compounds, bulkier imides for example preventing the otherwise intrinsically tight packing of the perylene cores.[49] The different morphologies play an important role in many applications, e. g. in organic field transistors where defects in packing hinder the charge transport considerably. Moreover, Hädicke and Graser[50,51] ascertained and investigated a chrystallochromic effect for different imide substituents leading to colours from red to black perylene diimides in solid-state. In solution, however, the absorption spectra are almost identical.

Tuning of the solution colour can be achieved by *bay*-substitution. BASF discovered a convenient way in 1984 to halogenate either just the 1,7- (**8**) or the 1,6,7,12-positions (**9**) (*bay*-positions) of perylene diimide[52], opening up the way to achieve manifold functionalities by subsequent reactions such as nucleophilic substitution or palladium-catalysed coupling. With the *bay*-functionalisation various donor-acceptor perylene diimides with different optical and electronic properties were synthesised throughout the past decades and *bay*-functionalisation remains a popular means to obtain perylene diimides with individually tailored properties. One examplary series of three 1,7-terthiophene substituted perylene diimides will be discussed later on in this thesis. Moreover, *bay*-functionalisation can be used to introduce water-solubilising groups, particularly important for bio-applications, and enables the synthesis of many donor-acceptor polymers with perylene diimides in the backbone. In general, *bay*-substitution of perylene diimides is accompanied by twisting of the perylene core. This of course affects the packing – depending on the application this effect can be favourable or undesired.

The functionalisation of the *ortho*-positions has been discovered and developed very

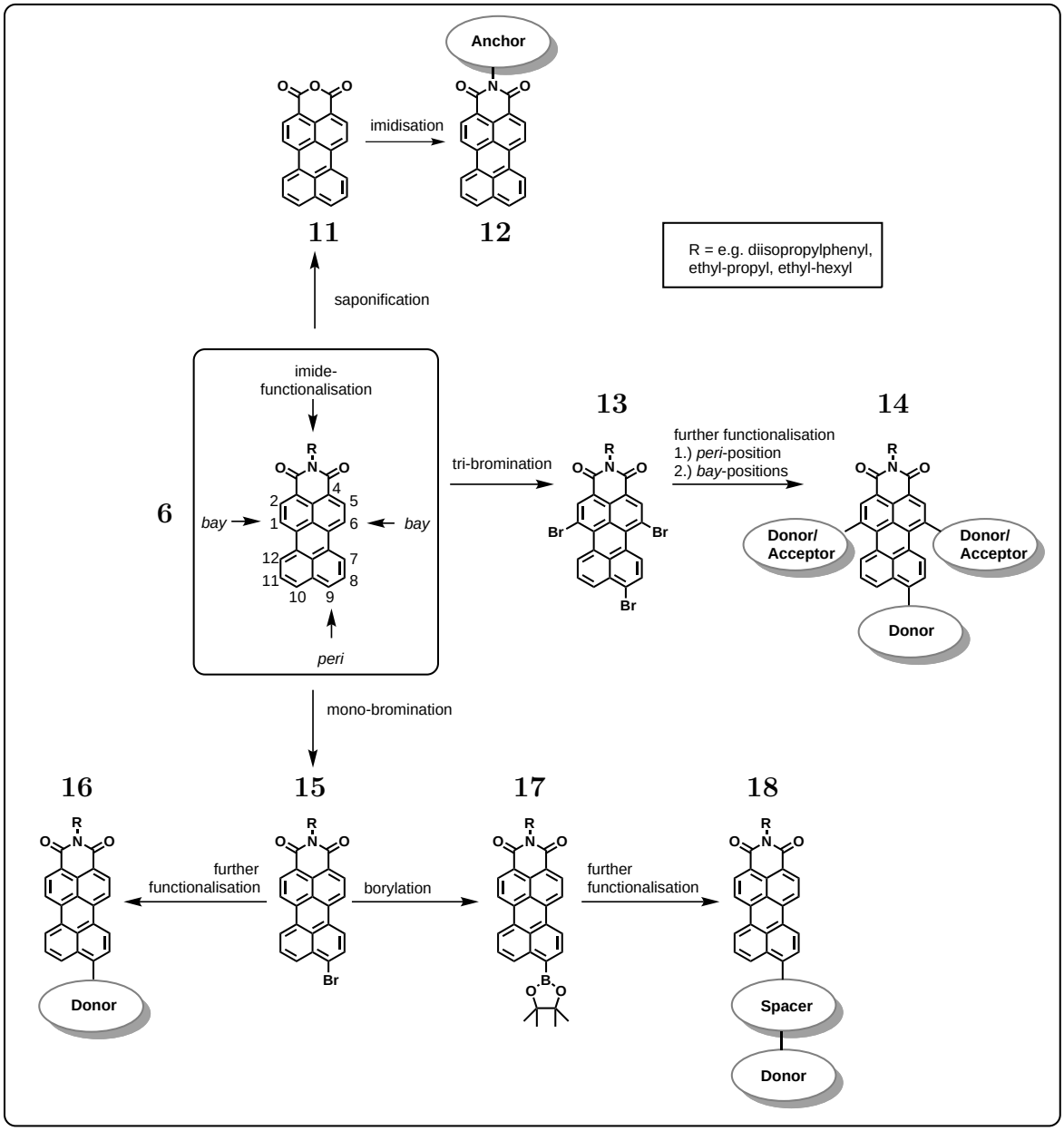

Figure 1.10: Synthesis: functionalisations of perylene monoimide

recently, first by alkylation in 2009[53] and arylation[54] and followed by presentation of borylated[55,56] and halogenated[57] perylene diimides, offering the most important building blocks for further functionalisations as known from the *bay*-positions.

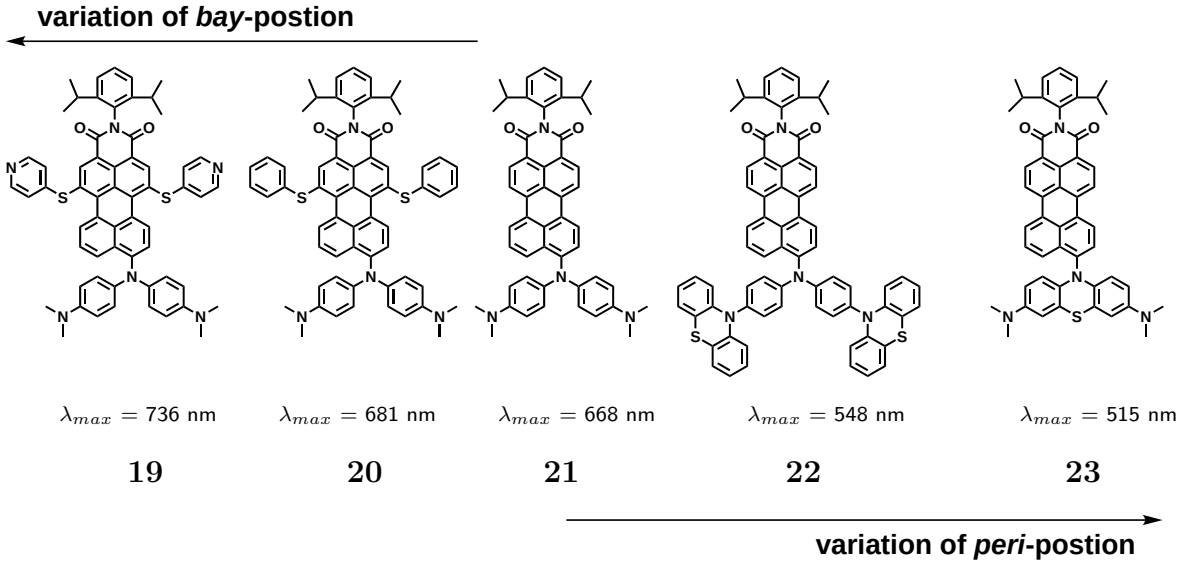

Figure 1.11: Rainbow perylenes – colour tuning via *peri*- and *bay*-substitution[2]

All perylene diimides are intrinsically symmetric. There is the possibility of introducing two different imide substituents, for example in dyad systems[58,59] or perform a monosaponification to achieve perylene monoimide monoanhydrides. Technically these molecules pass for asymmetric structures, electronically, however, the different imides and the anhydride – all strong acceptors – are very similar.

To really desymmetrise the molecule, the synthesis of perylene monoimides (**6**) is the most facile method. Unlike their related perylene diimides, they are asymmetric molecules along the long axis of the molecule with a dipole moment from the perylene core towards the imide acceptor. As mentioned above perylene monoimides can be synthesised via a one-pot reaction of perylene dianhydride under harsh conditions[46] (figure 1.8 on page 12). Moreover, they can be achieved by selective saponification and subsequent decarboxylation of the parent perylene diimides.[60,61,62] This dipole can be enhanced by donor functionalisation to give so called push-pull PMIs with broad spectral response, thus improving their light-harvesting ability, making them particularly favourable for the application in photovoltaics.[2] This has been demonstrated impressively by Li et al.[2] and their rainbow perylenes (figure 1.11), a series of *peri*- and *bay*-functionalised perylene monoimides exhibiting absorption spectra across the visible range of the spectrum.

Like perylene diimides, the monoimides possess excellent thermal, chemical and photochemical stability. Unlike the diimides, most PMIs especially PMIs with donor substituents show weaker or no fluorescence at all due to the push-pull effect.[36] For

their application in photovoltaics, however, this is not necessarily a disadvantage. Fluorescence does not play a major role in the processes of solar cells and is hence not a prerequisite of a good active material.

Perylene monoimides can be functionalised in various ways in both *peri* and *bay*-positions (figure 1.10 on page 15) allowing the tuning of HOMO and LUMO energy levels and subsequently of the absorption spectrum. The most easily accessible position of a perylene monoimide is the 9-position (*peri*-position). It can be addressed by a simple mono-bromination reaction (**15**) (Br_2, I_2, acetic acid, r.t., 4.5h) and subsequently be further functionalised (**16**, **17**, **18**), e. g. by nuclear substitution reactions or by palladium-mediated cross-coupling like C-C Suzuki or Sonogashira coupling as well as C-N coupling under Buchwald-Hartwig conditions.[46] Later in this thesis, in addition to the common 9-substitution examples of 8-, 8,11-, 8,10- and 9,10-functionalisation will be presented.

The 1,6-positions (*bay*-position), are easily accessible in connection with the 9-position. After bromination of the *peri*-position, the two *bay*-positions can be brominated under appropriate conditions **13** (Br_2, $CHCl_3$, reflux, 6 h).[46] In further functionalisations, these two *bay*-positions are more reactive than the *peri*-position. This allows for different functionalities to be introduced first in the *bay*-positions and then in the 9-position **14**.[2]

Last, but not least, the imide structure of the perylene monoimide can be varied. The perylene monoimide can be converted into a perylene monoanhydride by saponification (KOH, 2-methyl-2-butanol, reflux, 6h) and can be re-imidised with various amines.[63] This is particularly important for the application of perylene derivatives in dye-sensitsed solar cells, enabling the introduction of anchoring groups adjacent to the imide acceptor (**12**). These anchoring groups, e. g. carboxylates or phosphonates, are needed in DSSCs in order to bind the sensitiser to the metal oxide surface. The anhydride itself can also be used as an anchoring group. In its open form it allows anchoring via the two carboxyl groups and is one of the most widely used anchoring groups for perylene sensitisers in liquid dye-sensitised solar cells.

1.5 Design Principles of Sensitisers[6]

Perylene monoimides are amongst the most efficient sensitisers for dye-sensitised solar cells showing additional benefits like stability, comparatively low costs, and environmental safety.[20]

Metal complexes like the well-known ruthenium-complex **N3** (cis-di(thiocyanato)-

[6]This as well as the following section (modified) are part of the recently published review: Chen Li and Henrike Wonneberger: Perylene Imides for Organic Photovoltaics: Yesterday, Today, and Tomorrow, *Advanced Materials* **2012**, *24*, 613–636[36]

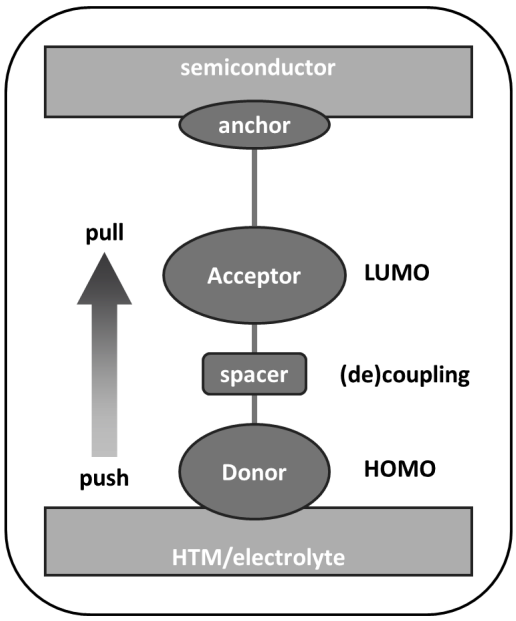

LUMO: lowest unoccupied molecular orbital; HOMO: highest occupied molecular orbital; HTM: hole transporting material

Figure 1.12: Design Principles for DSSC-Sensitiser

bis(2,2'-bipyridyl-4,4'-dicarboxylate)ruthenium(II)) have shown that charge separation within the sensitisers is an important characteristic for efficient charge transfer within the system. Spatial separation of the positive charge left on the dye and the injected electrons after the metal-to-ligand charge transfer (MLCT) decreases the rate of recombination between injected electrons and oxidised dye molecules considerably.[64,65] In metal-free sensitisers this orbital partitioning can only be achieved by push-pull design (figure 1.12), which means combining a strong donor with a strong acceptor and thus creating a powerful intramolecular dipole (figure 1.13 on the facing page). This will lead to a LUMO mainly located on the perylene core and imide/anhydride, thus close to the metal oxide, and a HOMO predominantly located on the donor part close to the electrolyte/hole transporting material. Such an approach will help 1) the intramolecular charge transfer, 2) the electron injection from the LUMO of the excited dye to the conduction band of the metal semiconductor[7], and 3) the regeneration of the dye by the electrolyte in liquid[8] or hole transporting material[9] in solid-state DSSCs (sDSSCs). Moreover, the push-pull system is beneficial for the light harvesting as it leads to broadening of the absorption spectrum of the dye and a bathochromic shift. In most push-pull-PMIs the donor is an alkyl or aryl amine in the *peri*-position.

To have both processes a) electron injection from the LUMO of the dye to the

[7]mostly titanium dioxide
[8]mostly I^-/I_3^-
[9]mostly spiro-MeOTAD (2,2',7,7'-tetrakis-(*N,N*-di-*p*-methoxyphenylamine)-9,9'-spirobifluorene)

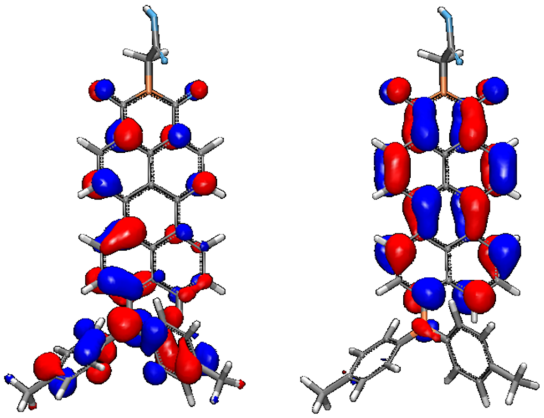

(DFT; performed by BASF SE)

Figure 1.13: Orbital partitioning on a donor-acceptor perylene monoimide sensitiser – HOMO (left); LUMO (right)

conduction band of the semiconductor and b) dye regeneration from the valence band of the hole transporting material/oxidation potential of the electrolyte work efficiently requires a certain minimum driving force which is said to be at least 0.2 eV.[66] Working in a set and well-proven cell system, these driving forces can be influenced especially well by the right sensitiser design, as HOMO and LUMO of the dye are strongly influenced by its molecular components and their interplay. A stronger donor directly connected to the acceptor will push up both HOMO and LUMO whereas strong orbital partitioning will result in a certain degree of independence. The LUMO of the dye is now being mainly directed by the LUMO energy level of the acceptor, the HOMO mainly influenced by the HOMO energy level of the donor moiety. Another option to adjust the energy levels in the injection process is by the introduction of additives influencing the energy level of the valence band of the metal oxide. This modification, however, is within the domain of cell processing and is an additional second step towards optimisation succeeding intelligent sensitiser design.

Moreover, the two electron transfer sites require good interactions of the dye with both the semiconductor and the hole transporting material/electrolyte. Binding on the semiconductor is achieved by anchoring groups like carboxylates, phosphonates or anhydride which opens upon anchoring to give two carboxyl groups.[67,66] The interaction with the hole transporting material (HTM) is dependent on many factors not yet fully understood, e. g. the orientation of the dye on the surface und subsequently the orientation of the donor towards the hole transporting material. Donor groups are often sterically demanding and frequently come decorated with alkyl chains. The alkyl chains supposedly interact with the HTM or electrolyte and, along with the bulky donor group itself, act as a barrier between the HTM/electrolyte and the semiconductor. The alkyl chains also help preventing aggregation of the dye molecules. Together

these features minimise unwanted recombination reactions between semiconductor and HTM/electrolyte or between neighbouring dye molecules. This is especially important in the case of perylene sensitisers as the flat, rigid and relatively large perylene cores show a strong tendency to aggregate.[68]

Another important tool for molecular design is a spacer between donor and acceptor or the deliberate avoidance of one. Spacer molecules are used for fine tuning of absorption and orbital energies. If the spacer takes part in conjugation between the donor and acceptor it can enhance absorption. In contrast if the spacer hinders conjugation either by twist or an interruption of the aromatic conjugation system it should lead to a stronger orbital separation. As mentioned above efficient partitioning will result in a HOMO mainly located on the donor and a LUMO located mainly on the acceptor of the molecule. In the case of complete separation the LUMO level energy will be determined mainly the the acceptor, thus the perylene monoimide. The HOMO level energy will be strongly influenced by the donor moiety. The decoupling will lessen the push of the donor and subsequently narrow the absorption back towards the absorption of the perylene or – if the donor is a chromophore itself – towards the absorption of this bichromophoric or dyad system in which energy transfer (via FRET - Förster resonance energy transfer) from the donor to the acceptor is still possible. Moreover a spacer and strong orbital partitioning may constrain the back-transfer of charges from the acceptor to the donor, making the charges better available for the injection into the semiconductor conduction band.

1.6 Perylene Sensitisers

There are two ways to group perylene sensitisers for dye-sensitised solar cells. One is by the cell type: a) p-type dye-sensitised solar cells and b) n-type dye-sensitised solar cells, with the subgroups b1) liquid and b2) solid-state cells. The other one is the classification into i) perylene diimide derivatives and ii) perylene monoimide derivatives.

Perylene diimide derivatives were the first perylene sensitisers in liquid dye-sensitised solar cells presented by Ferrere et al.[69] in 1997. Various sensitisers, perylene diimdes[70], perylene monoimide monoanhydrides[71] or bichromophoric systems[72,73] followed (all in liquid cells). The top sensitiser, a 1,6-pyrrolidine-substituted perylene diimide[74], however, reached an efficiency of only 2.6 %, thus not even half of what Grätzel's first efficient sensitiser yielded in 1991.[14] One intrinsic problem of the perylene diimides and their derivatives is the lack of a noteworthy molecular dipole which is yet so important for efficient charge transport within the molecule, for injection and recombination (quod vide section 1.5 on page 17) This is why perylene diimides and their derivatives – though a very potent class of chromophores for many organic electronics

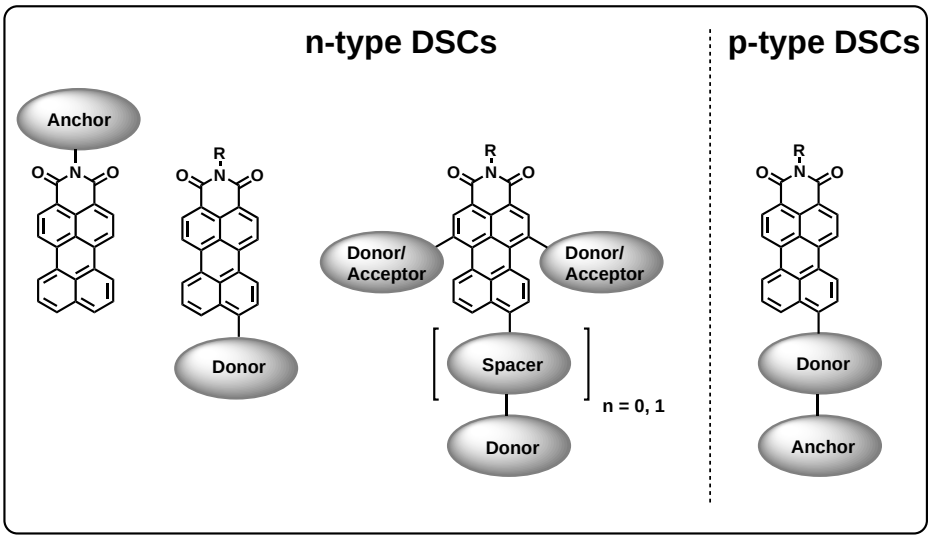

Figure 1.14: Major design concepts of PMIs for n-type and p-type DSSCs

applications – play no important role in dye-sensitised solar cell sensitisers.[36]

The asymmetric perylene monoimides, however, all possess this dipole, mostly enhanced by additional donor groups in the *peri*-position opposite to the imide acceptor (quod vide section 1.5 on page 17). Up to now most perylene sensitisers were designed for and used in liquid cells. The main design concepts for perylene monoimide sensitisers already briefly explained in the preceding section on design principles are presented in figure 1.14.

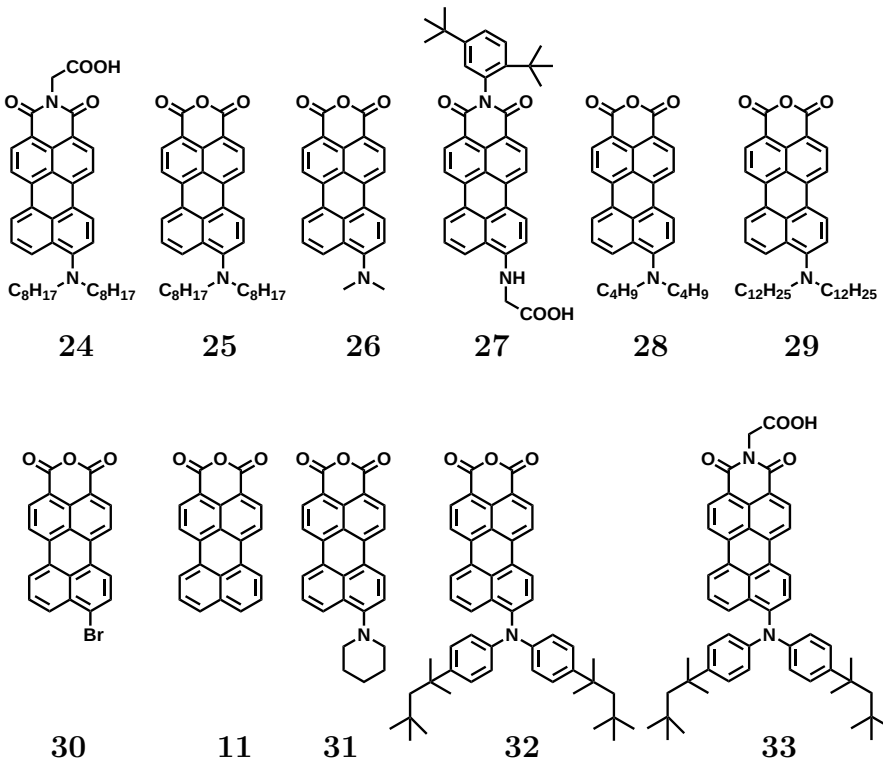

Figure 1.15: *Peri*-donor-functionalised perylene monoimides

Peri-Donor-Functionalisation and Steric Effects of Substituents on the Donor Amine The first perylene monoimide sensitisers were presented by Gregg et al.[75,76] in 2001, five years after their first perylene diimide sensitisers and ten years after Grätzel's first efficient ruthenium sensitiser[14]. This was a breakthrough in dye-sensitised solar cells. The authors kept to a very simple concept of just functionalising the *peri*-position with various amine donors bearing alkyl chains of different chain lengths. Moreover, with the carboxylate group in **24** and the anhydrides in **25** and **26** an anchor variation was investigated, introducing the two important anchoring groups for perylene sensitisers (figure 1.15 on the preceding page). Sensitiser **24-26** are classic push-pull dyes with strong coupling of the amine donor with the perylene imide. Their efficiencies in liquid cells (titanium dioxide, I^-/I_3^-) of up to 1.92 % (I_{SC} = 8.9 mA/cm^2, V_{OC} = 540 mV) for **26** were a promising start for perylene sensitisers and soon this concept was picked up and compounds **28-31** presented.[77,78] The main purpose of all these sensitisers was to investigate the steric and morphological effects of the alkyl substituents on the donor group as well as trying them in zinc oxide cells[10]. It was only quite recently, that sensitiser **31** was able to outperform the earlier sensitisers[75,76] with an efficiency of 3.1 % (I_{SC} = 7.7 mA/cm^2, V_{OC} = 570 mV) in a liquid titanium dioxide-based cell. However, as it was only compared to **11** in a joint testing, it is unclear whether the improved efficiency is really a result of the piperidine donor or of improved cell processing.

In terms of performance sensitiser **27** and **33** stand out of the crowd. **27** also belongs to the group of the earliest perylene monoimide sensitisers.[75,76] Interestingly, here the anchor is not attached to the perylene imide but rather on the opposite side to the donor group. This is a typical design of sensitisers for p-type cells (figure 1.14 on the previous page), which will be discussed later. Nevertheless, **27** was used in a liquid titanium dioxide-based cell and shows, with 1.3 % (I_{SC} = 9.8 mA/cm^2, V_{OC} = 410 mV), a respectable efficiency. Sensitiser **33** with a carboxylic anchor and an alkyl-substituted aryl-amine is the first and only designated perylene monoimide sensitiser[11] for solid-state dye-sensitised solar cells (titanium dioxide, spiro-MeOTAD) until this doctoral thesis[12]. **33** was tested in both cell types, yielding with 3.2 % (I_{SC} = 8.7 mA/cm^2, V_{OC} = 640 mV) a much higher efficiency in solid-state than in liquid dye-sensitised solar cells (η = 1.2 %, I_{SC} = 4.2 mA/cm^2, V_{OC} = 440 mV).[79] Especially remarkable is the high photocurrent achieved in the solid-state cells, the main reason for the improved performance of the dye by change of cell type. The authors suggest injection and regeneration mechanisms differ in the two cell types. This comparison makes it evident that sensitiser design for liquid and solid-state DSSCs must have

[10] Zink oxide cells: ZnO instead of TiO_2 is used as the semiconductor.

[11] Designated because of the for solid-state devices suitable carboxylic acid anchor.

[12] The second solid-state sensitiser presented in literature[63] was synthesised in the course of this doctoral thesis and is described in chapter 3 on page 57.

individual approaches.[36]

Peri-Donor- and Additional Bay-Functionalisation *Peri*-functionalisation on the one hand is a means to fine tune colour and energy levels of HOMO and LUMO. On the other hand the *bay*-substituents, by suppressing aggregation, also exert a strong influence on the morphological behaviour upon film formation. This was systematically proven by comparing the *peri*-substituted sensitiser **32** with the *bay*-phenoxy-substituted **35** and **36** bearing bulky dendritic substituents on the phenoxy-groups in the *bay* (figure 1.16 on the next page).[80] The efficiencies of the sensitisers drop with increasing size of the *bay*-substituents from 2.9 % over 2.7 % to 2.5 %, proving that the benefit of maximised dye loading overcompensates the losses from dye-dye recombination due to aggregation.[36]

By introducing sulfur bridges, the to date most efficient perylene sensitiser for liquid dye-sensitised solar cells, **34**, could be synthesised (η = 6.8 %, I_{SC} = 12.6 mA/cm^2, V_{OC} = 730 mV).[81] With this efficiency, perylene monoimide sensitisers have managed to achieve the original efficiencies of ruthenium-complexes and, considering their many advantages (metal-free, low cost, abundance etc.), may now be considered a viable alternative to the metal-based dyes. Though not particularly designed for sDSSCs, this sensitiser was also tested in a solid-state device. Here it could, however, only reach an efficiency of 1.8 %, once again showing that sensitiser design needs to be adapted to the cell type. Reason for the lower efficiency of **34** in the sDSSC device can be found mainly in the lower current (I_{SC} = 2.87 mA/cm^2). One major reason for the lower current achieved is the reduced titanium dioxide film thickness in the solid state device of only 1.8 μm compared to 4 μm in the liquid DSSC.[81] Currently the film thickness of sDSSCs is limited to around 2 μm. Main reason for this is the poor pore penetration of most solid hole conducting materials including the state-of-the-art material spiro-MeOTAD.[82] Therefore in solid sDSSC high extinction and broad absorption of the sensitiser on the titanium dioxide is even more important in order to achieve currents as high as in liquid cells.

Peri-Donor-, Bay-Functionalisation and Spacer-Insertion Sensitisers **38**, **39** (figure 1.16 on the following page) now follow the third major concept for n-type dye-sensitised solar cells (figure 1.14 on page 21).[66] Additionally, with the rigid and fully conjugated acetylene bridge in **38** and the flexible phenylene spacer in **39** two different spacer concepts were employed. These two spacer dyes were compared to the already established *peri*-substituted sensitiser **32** and the additionally *bay*-substituted **37**. Hence, the authors managed to use all three major sensitiser concepts for n-type cells within one study. One of the main differences of the sensitisers was the change in intramolecular charge transfer (ICT) which is rising from **39** → **38** → **37**/**32**. This

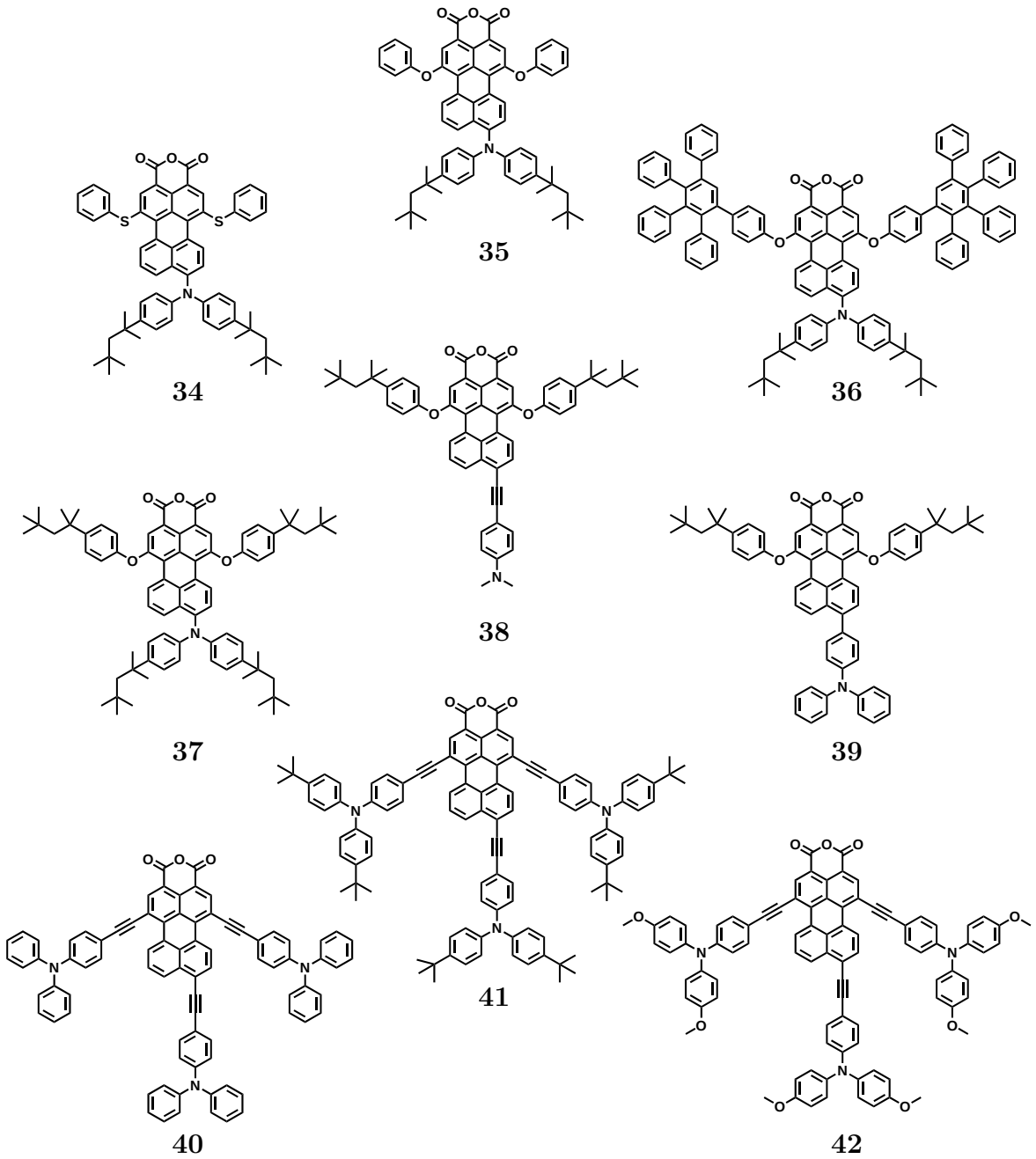

Figure 1.16: Tri-substituted perylene monoimide sensitisers with and without spacers

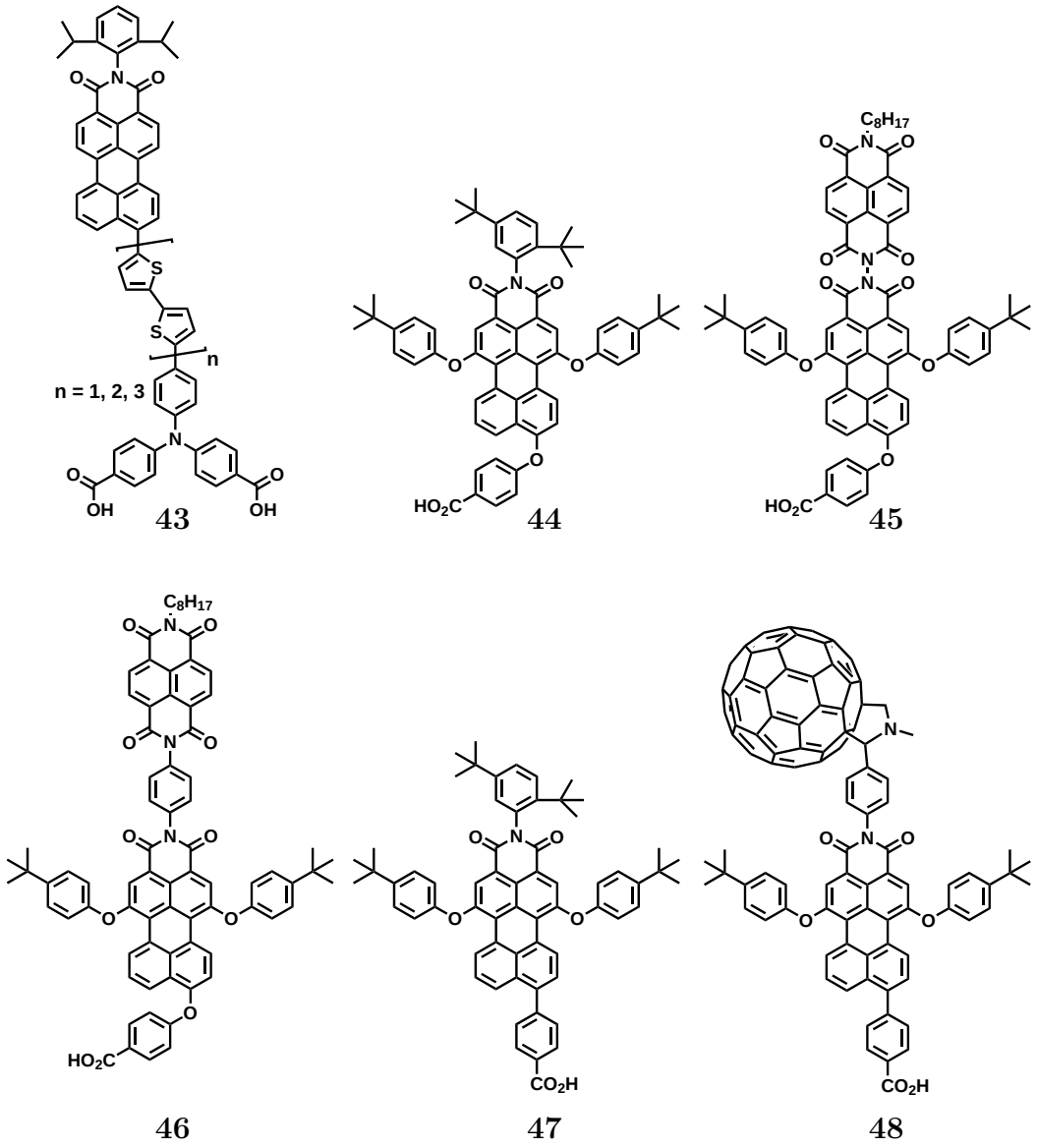

Figure 1.17: Perylene monoimide sensitisers for p-type DSSCs

is not surprising, given that the spacer and its degree of coupling has strong influence on the molecular dipole. The strongest donor-acceptor coupling is of course achieved in the cases of the directly attached amine-donors to the perylene core. For its rigidity the acetylene spacer allows unhindered conjugation and only increases the distance between donor and acceptor, whereas the flexible phenylene spacer weakens the donor ability by twisting out of the plane. Applied in a DSSC (titanium dioxide, I^-/I_3^-) the increase in ICT character seems to improve the efficiency in injection and subsequently the photocurrent achieving rising power conversion efficiencies from 2.2 %, 2.4 %, and 3.2 % for perylene **39**, **38**, and **37**, respectively. It is interesting to see, that perylene **32** with the simple concept (no spacer, no *bay*-functionalisation but only direct *peri*-functionalisation) still outclasses the other sensitisers in this series by reaching a power conversion efficiency of 3.9 %.[36] Another sensitiser series (**40**-**42**) with spacers

combines the acetylene with the phenylene and uses this spacer combination in the *peri*- and both *bay*-positions.[83] In addition, the influence of the sustituents (H for **40**, *t*-butyl for **41**, methoxy for **42**) was investigated. The increasing donor strength was noticeable as now the phenylene spacer is seperated from the perylene core by the acetylene bridge and not twisted out of the plane. Even though the efficiencies of the sensitisers with 2.1-2.9 % remain very limited compared to the current state of the art, the design approach involves all main setscrews, namely *peri*- and *bay*-functionalisation, spacer-insertion, variation of donor strength and steric demand.[36]

Reversed Sensitzers for pDSSCs One reversed sensitiser (**27**) has already been mentioned before though it was not used in a p-DSSC. Similar sensitisers (figure 1.17) have been made purposely for p-DSSCs (compound **44**, **47**).[84,85] Established concepts for n-type sensitisers like *bay*-functionalisation have been used but also new features like dyadic systems (**45**, **46**, **48**). In general this thesis does not aim for p-type applications, but for its concept, sensitiser **43** needs to be mentioned in more detail. It consists of a perylene monoimide with a flexible oligothiophene spacer and triphenylamine donor moiety.[86] Not only did this sensitiser reach – for p-DSSCs – excellent values of 0.41 % efficiency in a single junction device and an outstanding voltage of 1.079 V in a tandem cell, but later on in chapter 3 on page 57 a sensitiser with the same three components (perylene monoimide, oligothiophene, triphenylamine) will be presented for the use in n-DSSCs, setting a new literature-record for solid state perylene monoimide sensitisers at the time.[63]

1.7 Motivation

Perylene derivatives have developed alongside organic photovotaics. They are highly versatile in their synthetic pathways, optical and electronic properties and our group benefits from a long tradition and expertise in perylene chemistry. In dye-sensitised solar cells, perylenes have proven to be one of the most successful sensitiser classes. Especially the preceding work of Li[87] has led to major development and insights into structure-property relationships. His sensitisers have exhibited excellent performances, especially in liquid cells. To further develop the solid-state perylene-based sensitiser class on basis of the design principles developed by him was the starting point of this thesis. Till today compound **33** (ID176) with its broad absorption still is a highly potent sensitiser, its major "fault" being the low-lying LUMO energy.

As it is, tuning of the LUMO level energy often brings along also a change in the HOMO level energy and can cause a change in bandgap and therefore also absorption. This thesis aspires towards exploring the whole range of energy level tuning: from complete decoupling of donor and acceptor resulting in narrow and hypsochromic ab-

sorption over considerate orbital partitioning to strong coupling leading to broad and bathochromic absorption. New design principles for perylene sDSSC sensitisers shall be established and improved compounds developed, meeting the requirements of good sensitisers discussed earlier in this chapter. Besides contributing to the development of sDSSCs, this work moreover aims at launching new perylene chemistry which can thereafter be useful for various applications.

In the first part, the focus will lie on perylene monoimides and their use as sensitisers in sDSSC. In two cases, the naphthalene analogue will also be considered in order to allow comparison regarding the variation of conjugation of the chromophore core into the vertical direction. This is particularly interesting as naphthalene monoimide derivatives have rarely been used as sensitisers for sDSSC and have never led to meaningful device efficiencies.

In chapter 2 rigid aromatic spacer moieties will be introduced between the donor and acceptor to seperate the two moieties. Due to this decoupling of HOMO and LUMO, a hypsochromic shift in absorption is expected, corresponding to an enlarged bandgap and a hopefully higher lying LUMO level energy. The degree of coupling will be adjusted by the variation of spacer length and pathway. In comparison with **33** (ID176), now the strength of broad absorption may be replaced by the advantage of higher driving force, at the same time probably leading to reduced light harvesting. These competing features and the overall impact in a solar cell device will also be discussed. Moreover, donor groups will be changed to see the effect they have despite their decoupling. By introduction of a second chromophore like thiophenes and pyrenes on the donor, the concept of additional light harvesting and energy transfer will be investigated. Using similar donor and spacer building blocks, synthesis of the different variations is straight forward, involving palladium-catalysed reactions like Suzuki coupling and Buchwald amination to build up the PMI-spacer-donor systems. In chapter 2 the most extreme cases of orbital partitioning within the perylene monoimide sensitisers of this thesis will be demonstrated.

Using a similar building block approach but making use of a flexible spacer unit is pursued in chapter 3. This aims at partially retaining the orbital partitioning in order to keep the LUMO level energy high but at the same time trying to achieve broader absorption by better conjugation through the flexible spacer. As a spacer moiety, a branched terthiophene was chosen. Thiophenes have been widely used in organic electronics in general but they are also part of many sDSSC sensitisers.[88,89,20] They are known for excellent absorption and charge transport properties. Using thiophene together with perylene is an attempt to combine the outstanding properties of both chromophore classes. This has been tried before for various organic electronic applications including bulk heterojunction solar cells as well as p-type DSSCs but never for n-type sDSSCs.[90] In order to have a flexible spacer, at least two thiophene moieties are

required. By using a branched terthiophene, an extra thiophene moiety can be added without increasing the distance between the donor and acceptor, at the same time enlarging the conjugated system, especially by enabling the introduction of a second donor moiety.

Double donor systems are subsequently subject of chapter 4. The introduction of two donor moieties directly on the perylene core without spacer are now cases of strong coupling, aiming at achieving an even stronger push than in **33** (ID176) and therefore a more bathochromic shift. This is especially interesting as many sensisitisers can be found absorbing up to 600-700 nm, but only few beyond. In order to maintain the strong molecular dipole, the additional donor groups are not introduced to the easily accesible *bay*-positions, but to the *peri*- and the *edge*-positions (8,10-positions) further removed from the acceptor part of molecule. Selective functionalisation of the less reactive *edge*-positions of perylene monoimides by first borylation and then subsequent conversion into either a bromo or chloro functionality is presented here for the first time and brings along new and unexpected chemistry like the proposed aryne-mechanism during palladium-catalysed reactions like Buchwald amination.

After the spacer introduction and double donor functionalisation a third new design concept is looked into, namely core extension. This topic is touched already in chapter 4 combined with the concept of double donor functionalisation in the *peri*-pentannulated perylene monoimide. A second core extension by an indole moiety is presented in chapter 5. This is again achieved by new perylene chemistry, making use of the long-known *Cadogan chemistry*[91], often used to synthesise carbazole. The extension of the core in the vertical direction is another way to achieve a more bathochromic shift and moreover increase extinction. The whole chapter 5 will be dedicated to this very interesting and versatile core extension forming a new chromophore class. Not only will the perylene monoimide core be extended, but moreover, a donor group will be introduced to achieve another push-pull system. In this case, again, the naphthalene analogue will be used for comparison, the dye itself being an interesting candidate for sDSSCs. Besides the thorough investigation of these simple representatives of this chromophore class, some first continuative experiments are discussed to hold out the prospect of new fields like quinoline extension and double indole extension.

The last chapter 6 will be dedicated to the combination of different terthiophenes and perylene diimides. Here, the focus is not on sDSSC application but the series is a more general investigation of a combination of those two very interesting compound classes along the lines of *Light Harvesting and Orbital Tuning* and showing also the transferability of perylene monoimide concepts to perylene diimides. One terthiophene moiety used here is already known from chapter 3. Now the symmetrical perylene diimides are used and the terthiophenes are introduced in the *bay*-positions. Varying the architecture of the terthiophene moiety and connection to the perylene diimide

allows interesting HOMO level and colour tuning.

Chapter 2

Decoupling via Introduction of Rigid π-Spacers in Donor-Acceptor Systems

2.1 Introduction

Orbital partitioning has proven to be a key principle in sensitiser design, the separated charges on the molecule facilitating intramolecular charge transfer, electron injection into the semiconductor conduction band, and the regeneration of the dye by the hole transporting material. In this chapter a series of eleven donor-π-spacer-acceptor-PMIs (DπA-PMIs) is presented including **33** (ID176), taking the concept of orbital partitioning further to complete decoupling and showing different attempts at optimisation by variation of spacer structure and pathway, spacer length, and donor identity.

Especially the donor length is a powerful means to vary the degree of orbital communication, deciding what impact the donor group still has in a push-pull system. Starting from **33** (ID176) without a donor, three spacer moieties of different length are inserted between the donor group and the perylene imide acceptor. The spacer length should strongly influence the absorption properties, as the spacers will twist out of the plane of the perylene core and therefore weaken the conjugation. With regard to the application in dye-sensitised solar cells, increasing the orbital partitioning to full decoupling seems irrational as it implies narrowing of the absorption, and light harvesting of the sensitiser is what is needed in the first place to achieve an efficient DSSC. At the same time, the electron transfer mechanisms of the cell need strong driving forces for the cell to work properly. The aim of going from one extreme to the other in small steps within this series is to explore the whole band width of tuning and find an optimum of decoupling.

As charge transfer from the donor to the acceptor needs to pass the spacer moiety, apart from length also the nature of the spacer might play a role. One characteristic is of course the above mentioned length, another is the electronic nature which will be varied by a heteroatom change and connection pathway.

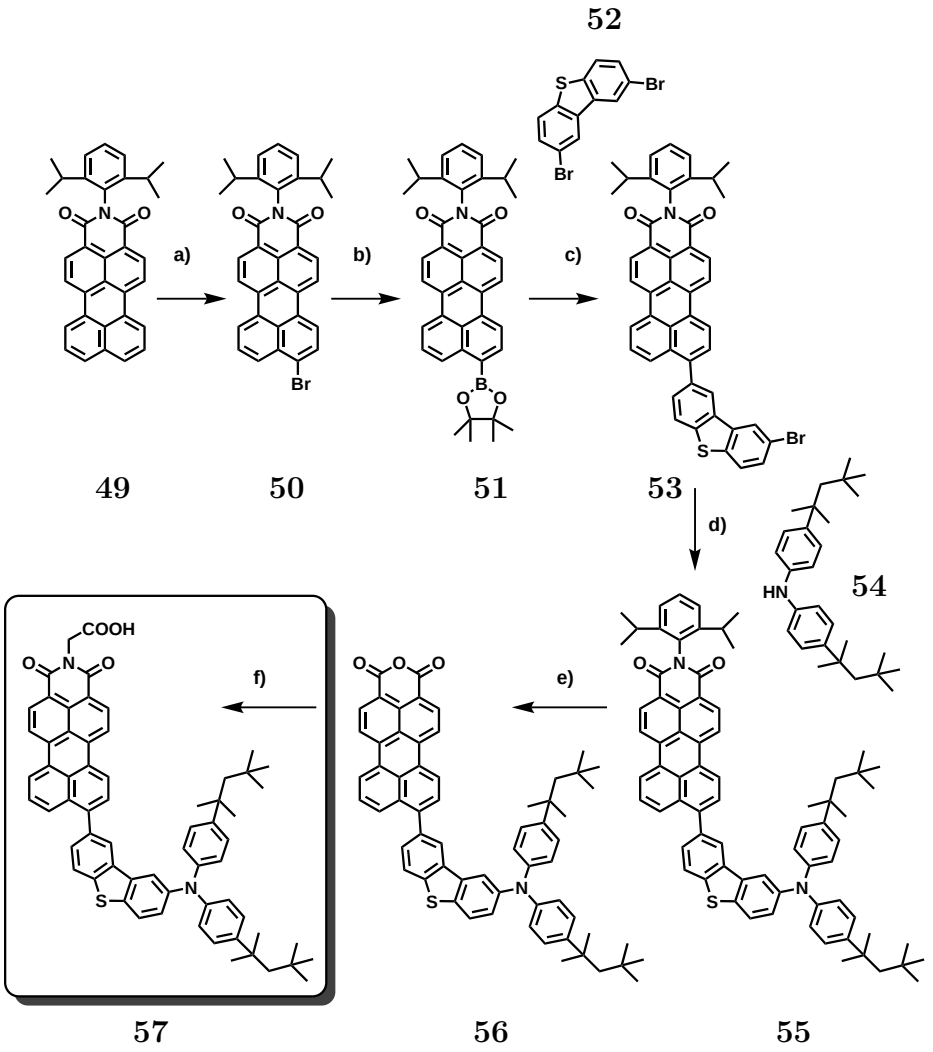

a) Br_2, I_2, rt, 4h, yield: 95 %; b) bispinacolatodiboron, potassium acetate, $Pd(dppf)Cl_2$, dioxane, 80°C, 15h, yield: 85 %; c) K_2CO_3, $Pd(PPh_3)_4$, toluene, water, ethanol, 80 °C, overnight; d) NaOtBu, $Pd_2(dba)_3$, tri-t-butylphosphine, 80°C, overnight, yield (step c+d): 25 %; e) 2-methyl-2-butanol, KOH, reflux, over night, yield: 80 %; f) glycine, imidazole, 140°C, over night, yield: 90 %

Figure 2.1: Synthesis of compound **57**

Last but not least, the influence of the donor group will be explored. In a decoupled donor-acceptor system, the nature of the donor group may at first glance seem secondary. The introduction of additional chromophores, however, will show that the donor groups can still have considerable influence on the absorption.

The central molecule of this series is a perylene monoimide with a 2,8-connected dibenzothiophene as the π-spacer moiety and a bis(4-tertoctylphenyl)amine donor, therefore a direct analogue of **33** (ID176), in which donor and acceptor are separated by one of the largest spacers in the series aiming at full decoupling. Its synthesis, ^{1}H-NMR and ^{1}H,^{1}H-cosy spectra for proof of structure as well as the absorption characteristics of this central compound and its precursors will be described in more depth in the beginning. The other target molecules in this series are comparable systems. Differences regarding their synthesis will be discussed. Otherwise the focus will be to

compare and contrast their optical, electrochemical and sDSSC device properties.

The synthesis scheme of compound **57** is shown in figure 2.1 on the preceding page as the model synthesis for the building block approach used for the majority of dyes in this chapter. A great advantage of this approch is, that many intermediates (e.g. **50**, **51**, **53**) can be utilised for different compounds and other commercial spacers can be used instead of **52**.

The first step is a monobromination of *N*-(2,6-di*iso*propylphenyl)-perylene monoimide (**49**) in the 9-position (**50**) and subsequent, palladium-catalysed conversion of **50** into a boronic ester (**51**). These first steps are known from literature and afford good yields of up to 95 % for the bromination[92] and 75 % for the borylation.[93,94] Compound **50** was kindly supplied by BASF for comparison. With a slightly modified protocol compared to literature, using dioxane instead of toluene in the borylation step, an even higher yield of 85 % could be reached. In the third step the 2,8-dibromodibenzothiophene **52** was introduced via palladium-catalysed Suzuki coupling, yielding 60 % of the coupled product **53**, however, containing also fair amounts of the debrominated species. Separation requires great effort and would entail loss of product. As the debrominated species does not interfere with the next palladium-catalysed carbon-nitrogen-coupling (Buchwald reaction) to attach the amine donor **54** to the spacer moiety, the mixture was used for this fourth step, understandibly leading to a comparatively low yield for a Buchwald amination of only 40 % of compound **55**. The anhydride **56** was subsequently achieved by saponification. In the last step the anchoring group was attached via imidisation with glycine to yield compound **57**. These last two steps proceed with good yields of 80 % and 90 %, respectively, the main losses in product occuring during chromatographic purification due to strong interactions of the carboxylic acid with the silica gel. 85 mg of the sensitiser **57** were obtained.

The ^{1}H-NMR spectrum and the ^{1}H,^{1}H-cosy spectrum of compound **55** measured in tetrahydrofuran are presented in figure 2.2 on the following page to prove the obtained structure of the DπA-PMI by the synthesis described above. Two very characteristic peaks are f and e, both giving doublets with small ^{4}J-coupling constants to h and i, respectively, marked by the green boxes in the 2D-spectrum. Because of its proximity to the nitrogen of the amine group, proton e is expected to be more shielded and thus shifted to the high field of the spectrum. Proton h and i are split into doublets of doublets because of their partners g and k and the already above mentioned long-range coupling with f and e. This splitting pattern is recognisable for the case of h and suspected likewise for i. Again the stronger shielding is reflected in their relative shifts. Protons g and k can be located through their coupling with h and i by the purple boxes, splitting into doublets with geminal coupling constants. A second characteristic pattern should be produced by the ABC system n, l, and m. The couplings are marked by the blue boxes in the 2D spectrum. In this case it is hard to say which proton is n

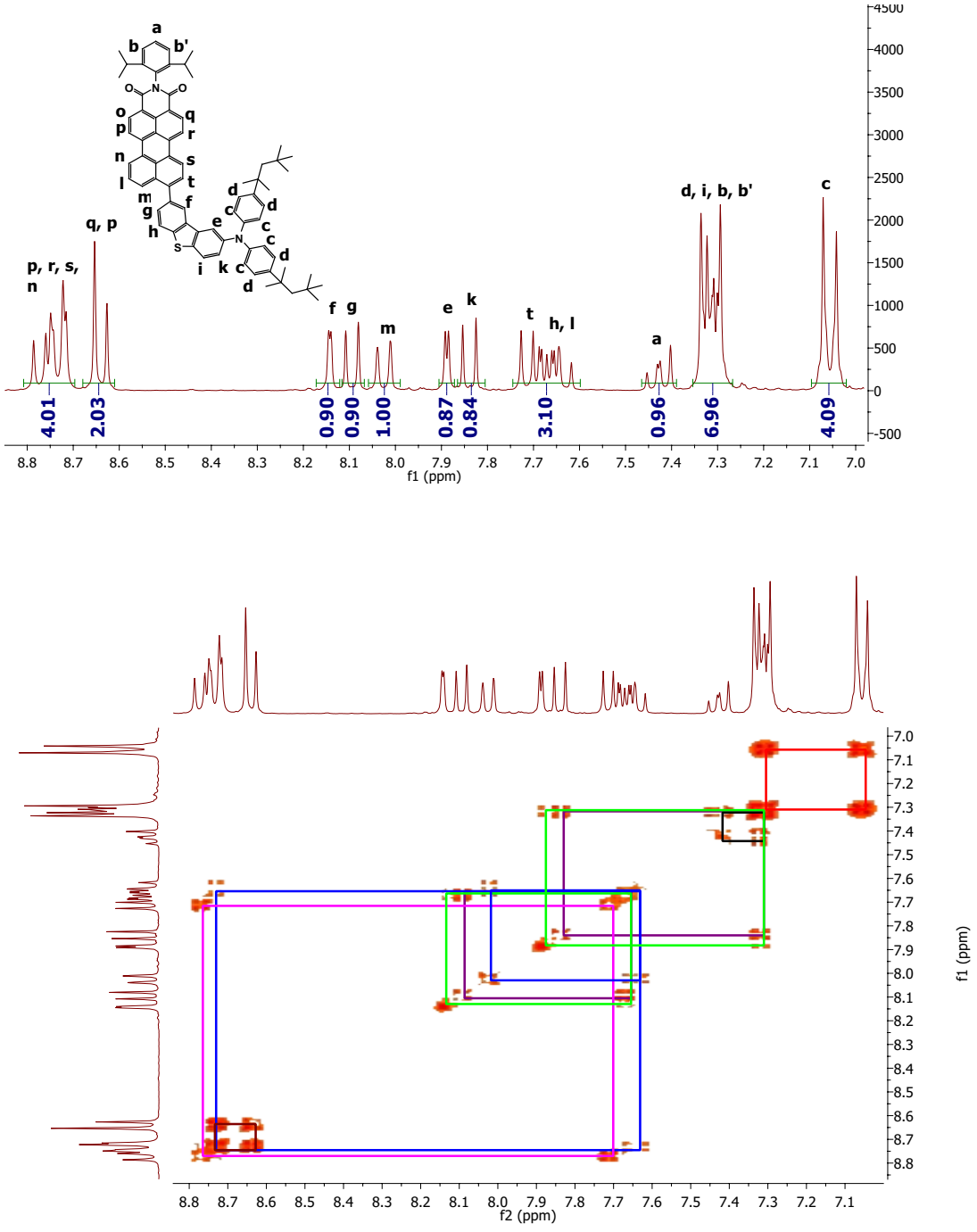

(300 MHz, THF, 298 K)

Figure 2.2: ^{1}H-NMR and ^{1}H,^{1}H-cosy spectra of **55**

and which one m, but as proton s is coupling with proton t in a ^{4}J-coupling marked by the pink box, n can be expected to be shifted to the low field because of its similar chemical sourroundings compared to s. Proton t, however, closer to the donor due to the banana shape of the molecular structure, is shifted significantly upfield. Within the multiplet and the doublet in the low field o, r, q, and p can be found. This leaves the protons of the *N*-(2,6-di*iso*propylphenyl)- and the donor-moiety, all well shielded in the high field. Proton a splits into a doublet of a triplet probably due to rotational hindrance of the diisopropyl-moieties and therefore inequality of b and b' (black box). Protons c and d (red box) split like expected for an AB system into doublets, c due to its vicintiy to the nitrogen is probably high field-shifted compared to d.

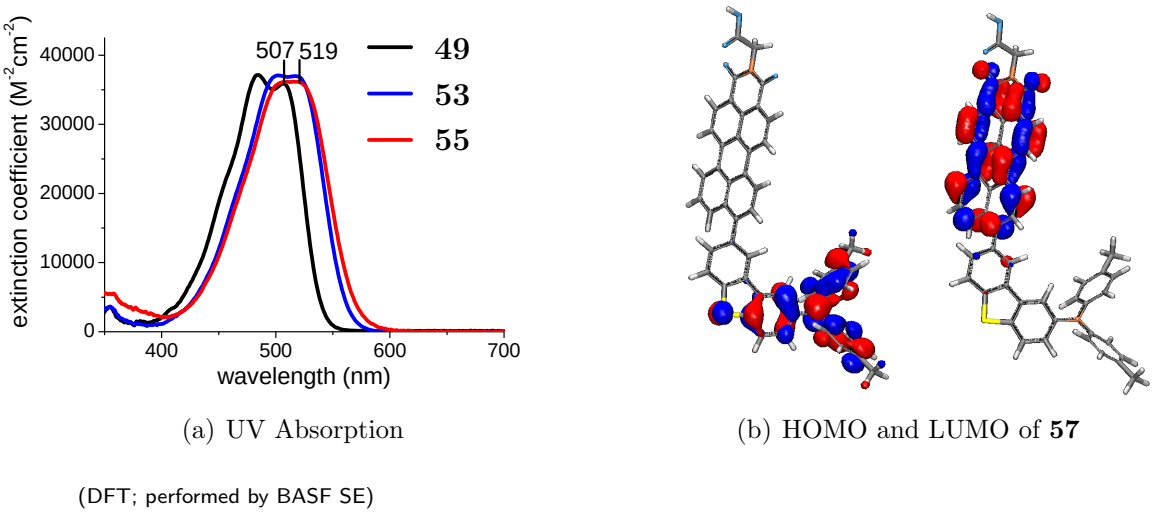

(a) UV Absorption

(b) HOMO and LUMO of **57**

(DFT; performed by BASF SE)

Figure 2.3: Change in absorption (in dichloromethane) during synthesis (a) and HOMO and LUMO of **57** (b)

The absorption spectra of the three key synthesis steps – starting material, introduction of the spacer, and functionalisation with the donor – are shown in 2.3. The unsubsituted *N*-(2,6-di*iso*propylphenyl)-perylene monoimide **49** absorbs in one slightly split band with an extinction of around 35.000 $M^{-1}cm^{-1}$ and a λ_{max} at 507 nm. This band can be attributed to the π-π*-transition of the perylene monoimide. The small split of the band is a hint of vibronic fine structure, in the perylene monoimide, however, not nearly as strong as in the parent perylene diimide.[95,96] Upon spacer introduction (**53**), the extinction is more or less unchanged[1]. Theoretically the additional spacer leads to a greater conjugation length and higher extinction could be expected. As both moieties, the perylene monoimide and the spacers are rotated into different planes, the conjugation is somewhat hindered. The spacer gives a small bathochromic shift of a little more than 10 nm and leads to a less defined, slightly broader shape of the band.

[1]A mixture of PMI-spacer-Br and PMI-spacer was used for the measurement. The extinction coefficient was determined assuming there was only PMI-spacer. In reality for the pure PMI-spacer the extinction coefficient will be slightly higher but within the same range.

The bathochromic shift of the π-π*-transition band can be explained by additional conjugation with the dibenzothiophene spacer. It is, however, just a small shift because of the considerable twisting of about 53°[2] and hence there is only weak communication between the dibenzothiophene and the perylene. The broadening of this band is typical for more flexible systems. The most interesting step is the introduction of the donor group. In other dyes like **33** (ID176) this amine group has induced a strong bathochromic shift.[79] In the case of **55** the absorption spectrum is almost identical to the one of the PMI-spacer.

This can be explained by the localisation of the coefficients of the orbitals. As mentioned in the introduction of the thesis orbital partitioning is one very important design principle in sensitiser dyes. The ionisation potential, the electron affinity, the localisation of the HOMO and LUMO coefficients, and electronic transitions and their oscillator strengths were calculated using density functional theory.[3] The results show that not only do we have a case of orbital partitioning but that the HOMO is located exclusively on the donor and spacer of the molecule and the LUMO on the acceptor (perylene monoimide core) with nearly no overlap of the orbitals (figure 2.3 on the preceding page), thus very limited communication. The S1-transition from the HOMO to the LUMO of the dye, thus a potential CT-transition is calculated at 684 nm, however, with an oscillator strenth (f1) of nearly 0. This is in good agreement with the measured absorption spectrum showing only the π-π*-transition at 512 nm. This S2-transition is calculated at 519 nm with a considerable oscillator strength of f2 = 0.8. As intended, complete decoupling could be achieved in compound **57**. Like in the cases of the two precursors the absorption band of the spectrum is still a result of the π-π*-transition of the perylene monoimide moiety.

This complete decoupling of HOMO and LUMO is the strongest possible form of orbital partitioning, well-known from multichromophore systems which are often connected by aliphatic or strongly twisted aromatic spacers where energy transfer occurs by FRET (Förster resonance energy transfer).[97,98] Mor et al.[99] made use of FRET in sDSSCs by adsorbing an IR-absorbing acceptor dye onto the titanium dioxide and blending a visible light absorbing donor dye into the hole conductor and thereby inproving the light harvesting and current of the cell. In perylene sensitisers for DSSCs this concept has been used in various p-type sensitisers as mentioned in the introduction.[85,84] Complete decoupling of the donor and acceptor is new in n-type perylene sensitiser design. Here, the rather large dibenzothiophene spacer was chosen deliberately in order to investigate the effect of decoupling on the optical, electronic and photovoltaic properties of a sensitiser.

The absorption spectrum of compound **57** in dichloromethane is shown in figure 2.4

[2] In the final molecule **57**, according to the DFT-calculations (2.1).

[3] Further details provided in the experimental part.

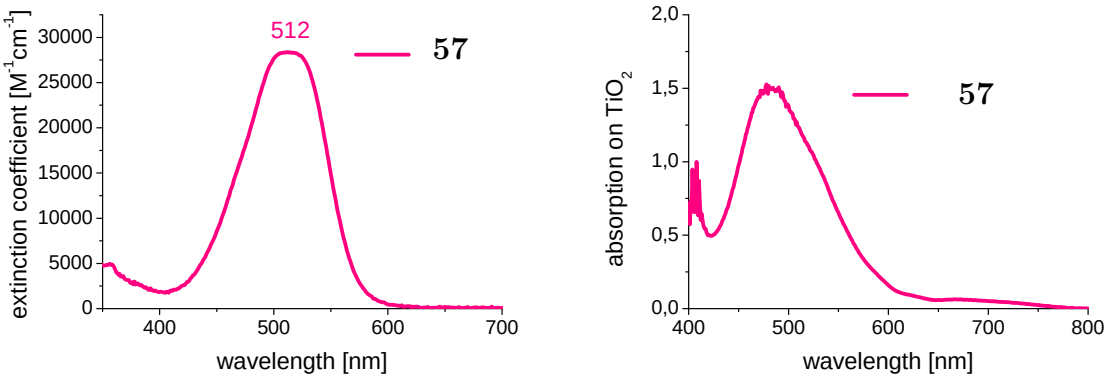

(a) Solution absorption (b) TiO_2 absorption

Figure 2.4: Absorption spectra of **57** in dichloromethane (a) and on titanium dioxide (b)

on the next page. As described above, a rather narrow π-π*-transition band with a maximum at 512 nm, similar to the absorption spectrum of perylene monoimide, can be observed with an extinction coefficient of around 28.000 $M^{-1}cm^{-1}$. The drop in extinction from the *N*-(2,6-di*iso*propylphenyl)-substituted compound **55** to the carboxymethyl-substituted compound **57** is a well-known characteristic and can be observed for all sensitisers presented in this thesis. Similar absorption with the maximum slighly hypsochromically shifted can be observed on titanium dioxide (figure 2.4).

The strong orbital partioning is not only reflected in the absorption spectrum but also in the energy level of the HOMO and LUMO. One weak point in sensitiser design of the already presented dye **33** (ID176) (later on also part of the spacer length comparison), was the rather low LUMO (0.68 eV vs. NHE) lying only little above the conduction band of the titanium dioxide (0.5 eV vs NHE), possibly resulting in too little driving force for efficient electron injection. Because of the decoupling, the LUMO level is essentially the one of perylene monoimide and the HOMO level is mainly influenced by the donor moiety. Cyclic voltammetry measurements have confirmed this, the LUMO level being at -3.5 eV in vacuum (0.9 eV vs. NHE), thus providing approximately 0.4 eV driving force for injection, the HOMO being located at -5.1 eV in vacuum, thus well below the ionisation potential of the hole transporting material spiro-MeOTAD (-4.77 eV in vacuum[100]). All measurement results (UV-Vis absorption, HOMO and LUMO) of the sensitisers are summarised in table 2.4 on page 55.

Solid-state dye-sensitised solar cells were processed on an FTO covered glass substrate with titanium dioxide as the semiconductor. The electrode was then dyed in a toluene solution of organic additive and dye and subsequently spin-coated with spiro-MeOTAD as the hole transporting material (HTM) followed by evaporation of the

silver counter electrode on top. Cell making and measurements[4] were undertaken at and by BASF, the performance data kindly provided and summarised in table 2.5 on page 55 (photovoltaic performance).

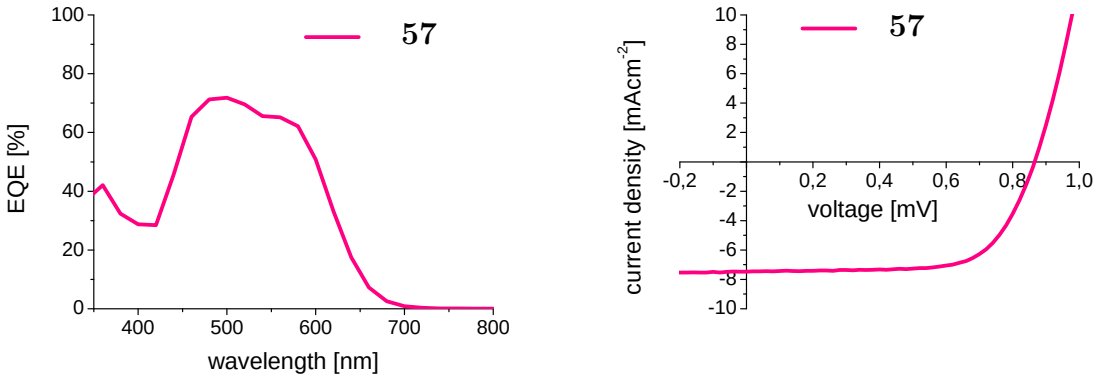

(a) EQE (b) IV

Figure 2.5: EQE (a) and IV-curve (b) of **57**; top performance

The EQE of the cell is considerably broader compared to the absorption in solution or on titanium dioxide gaining in the long wavelength region of the spectrum (figure 2.5). This effect can be observed in many perylene monoimide-based sensitisers and be ascribed to aggregation of the molecules. The EQE, though only reaching out to 700 nm shows high intensities of up to 70 %, leading to a good cell performance with a short circuit current of 7.47 $mAcm^{-2}$, an open circuit voltage of 860 mV, a fill factor of 69 %, and an overall power conversion efficiency of 4.5 % under 1 sun, outclassing to date all solid-state perylene sensitisers presented in literature.[36]

These outstanding results for a so narrow absorbing sensitiser seems at first glance quite incomprehensible. The good performance of this completely decoupled dye with rather narrow absorption and the results previously reported in literature of successful charge tranfer dyes like **33** (ID176) prove that both mechanisms – strong coupling or decoupling – can be beneficial for the sensitiser performance. In order to better understand the mechanisms within the molecule and design principles finding the right balance between decoupling and broad absorption, differents attempts of optimisation of compound **57**, namely variation of spacer structure and pathway, variation of spacer length, and variation of donor were carried out and are presented in the following.

2.2 Variation of Spacer Structure and Pathway

In a first variation series, different analogous spacers were introduced to better understand the role of this moiety. (figure 2.6 on the facing page) The dibenzothiophene

[4]Further details provided in the experimental part.

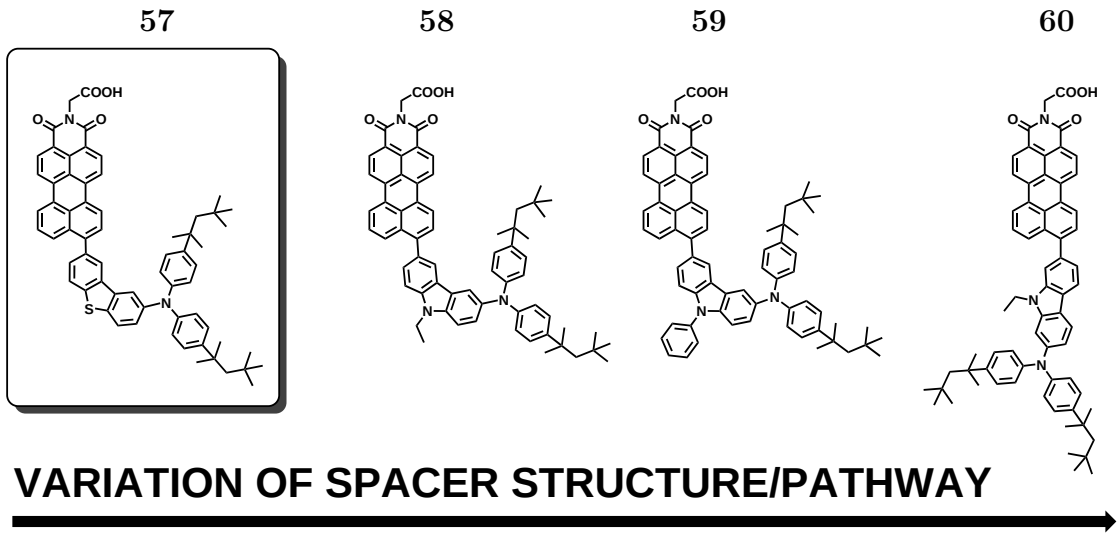

Figure 2.6: Variation of spacer structure and pathway

was exchanged for an ethyl-substituted (compound **58**) and a phenyl-substituted (compound **59**) carbazole but keeping the connection of the spacer in the *para*-positions of the heteroatom. In compound **60**, an isomer of compound **58**, the couplings were performed at the *meta*-positions of the carbazole nitrogen. Here, the coupling positions in the 2,7-positions of the carbazole force the molecule into a more linear shape. The carbazole was chosen for its structural similarity to the dibenzothiophene and because of a hoped-for additional push from the electron-rich nitrogen. The ethyl to phenyl variation from compound **58** to compound **59** was undertaken in order to find out if the carbazole subsituent has an effect on the sensitiser performance.

Compounds **58**, **59**, and **60** were made according to the synthesis of **57** described in figure 2.1 on page 32 using the respective dibromo-carbazoles. Again, the Suzuki coupling of the perylene monoimide boronic ester **51** with the different carbazole spacer moieties was the bottleneck of the syntheses. Like in the case of **53**, the mixture of the debrominated and brominated species was used for the subsequent Buchwald aminations leading to rather low yields of 32 %, 22 %, and 30 % for the *N*-(2,6-di*iso*-propylphenyl)-perylene monoimide precursors of **58**, **59**, and **60**, respectively, however, providing enough material for the final compounds and their testing in sDSSCs. Subsequent saponification and imidisation reactions produced overall yields between 65 % and 76 % for the two steps. 95 mg of **58**, 48 mg of **59**, and 105 mg of **60** were obtained.

Pictures of the HOMO and LUMO localisation on the molecules are shown in table 2.1 on the following page. Like in compound **57** complete decoupling can be found, the LUMO coefficients localised on the perylene monoimide acceptor, the HOMO coefficients on the donor and spacers. The strongest coupling amonst the four molecules is reached by compound **60** with the 2,7-carbazole-spacer. Even though the conjugation

Dye	Structure	HOMO	LUMO	
57	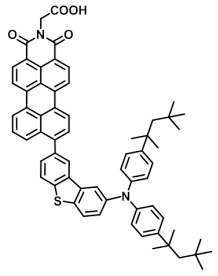	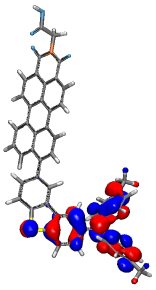	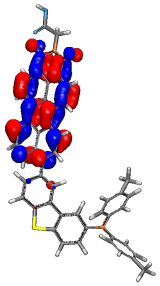	IP: 5.27 EA: 3.20 S1: 684 nm S2: 519 nm f1: 0.02 f2: 0.80
58	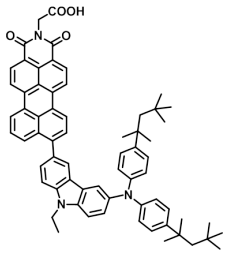	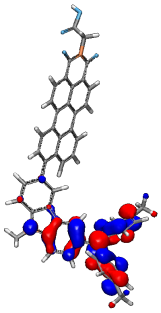	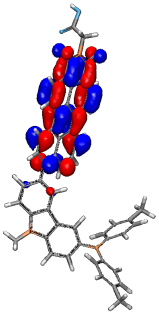	IP: 5.06 EA: 3.14 S1: 721 nm S2: 529 nm f1: 0.06 f2: 0.77
59	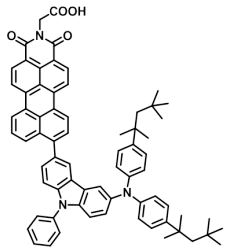	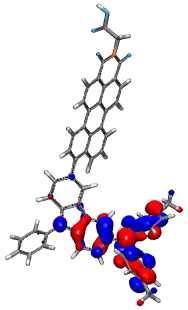	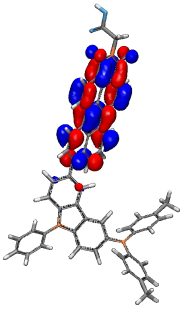	IP: 5.08 EA: 3.14 S1: 721 nm S2: 529 nm f1: 0.05 f2: 0.80
60	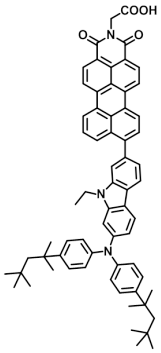	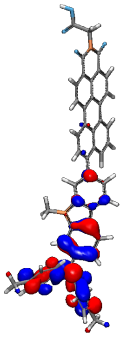	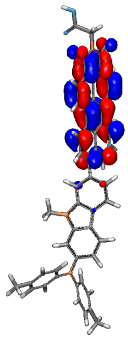	IP: 5.15 EA: 3.16 S1: 678 nm S2: 515 nm f1: 0.26 f2: 0.76

(DFT; performed by BASF SE)

Table 2.1: Calculated orbital surfaces, ionisation potential (IP), electron affinity (EA), transitions (S) and oscillator strengths (f) of compound **57**, **58**, **59**, and **60**

towards the carbazole nitrogen is weaker than in the 3,6-connected cases, the nitrogen of the amine donor is in the extended *peri*-position or rather *para*-connected.

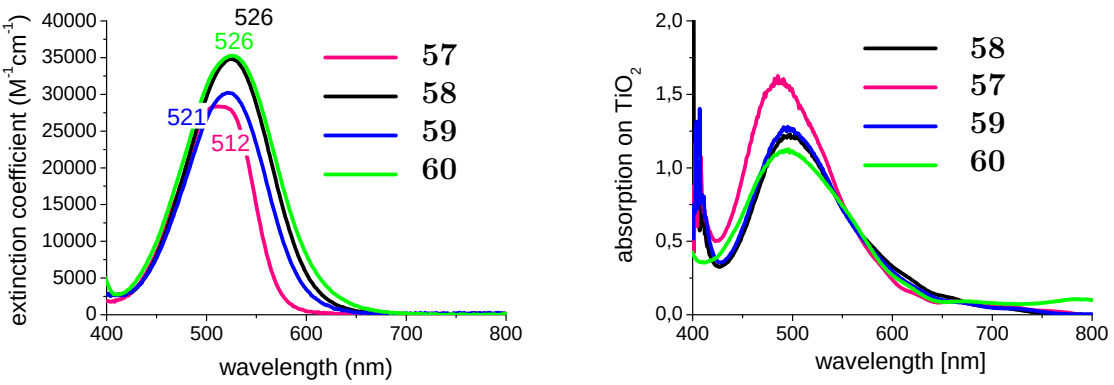

(a) Solution absorption

(b) TiO_2 absorption

Figure 2.7: Absorption spectra of the dyes **57**, **58**, **59**, and **60** in dichloromethane (a) and on titanium dioxide (b)

From the absorption spectra of compound **57** and its precursors we know that the spacer has only little influence on the absorption but also, that it is exactly that influence of the spacer which will in the end determine the absorption of the perylene monoimide-spacer-donor compound. And in fact, all three carbazole variations show as intended an additional bathochromic effect without loosing absorption on the short wavelength side (figure 2.7). This small broadening hints at a slightly increased charge transfer of the spacer towards the donor, in good coherence with the more electron-rich, hence more "'pushing"' nitrogen. But still, the band observed is no charge-transfer band but derives from the π-π^*-transition. The stronger bathochromic shifts with λ_{max} at 526 nm are achieved by the ethyl-substituted carbazole compounds (**58** and **60**), the phenyl-substituted compound **59** reaching a λ_{max} at 521 nm. Furthermore compound **58** and **60** show improved extinction (around 35.000 $M^{-1}cm^{-1}$) compared to compound **59** (ϵ = ca. 30.0000 $M^{-1}cm^{-1}$). The different pathways of compound **58** and **60** show no evident difference in absorption, only a small, almost negligible broadening of the band for compound **60** can be observed. As only the π-π^*-transition is visible in the absorption spectra, it is understandable that the differences in coupling for compound **60** compared to compound **57**, **58**, and **59** cannot be observed.

Turning to the absorption on titanium dioxide (figure 2.7), the picture looks quite changed. Compound **57**, in solution showing the weakest absorption, is now exceeding all carbazole spacer perylene monoimides, showing much higher extinction than compound **58**, **59**, and **60** and at the same time reaching out to similar wavelengths as the formerly more bathochromic carbazole derivatives. As the thickness of the titanium dioxide layer of all cells is identical (1.8 μm) and all dyes are processed from the same solvent in the same concentration (0.5 mM), this suggests that with **57** a higher degree

of dye-loading could be achieved.[5] The substitution of the carbazole nitrogen adds to the steric demand of the molecules which may be a reason for less dye-molecules to be adsorbed on the surface.

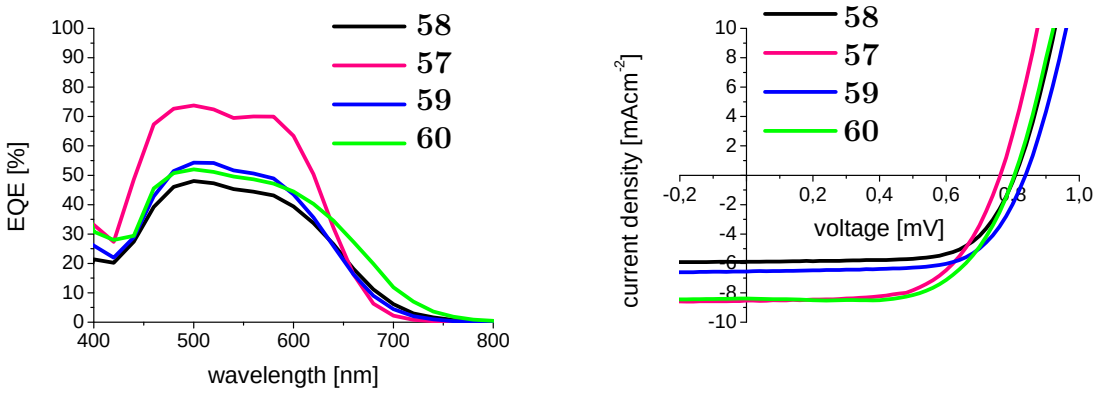

(a) EQE (b) IV

Figure 2.8: EQE (a) and IV-curve (b) of the dyes **57**, **58**, **59**, and **60**

Tested under the same conditions within one series, the solar cell performance of the different compounds was (table 2.5 on page 55) measured as follows: compound **60** (4.5 %) > compound **57** (4.0 %) > compound **59** (3.7 %) > compound **58** (3.2 %). Again, compound **57** shows an exceedingly good EQE with a maximum value at 74 %. The EQEs of the carbazole derivates are much lower with top values of only up to 54 % (figure 2.8), the broadest EQE achieved by compound **60**. In the IV-curve it is noticeable that all carbazole compounds reach higher open circuit voltages than compound **57** up to 840 mV (compound **59**). Only compound **60**, however, with -8.42 $mAcm^{-2}$, reaches a comparable short circuit current as compound **57** (-8.52 $mAcm^{-2}$). Together with its good open circuit voltage of 820 mV (compared to only 760 mV for compound **57**) compound **60** achieves a higher fill factor (65 % for compound **60**, 62 % for compound **57**) and a considerably higher overall power conversion than compound **57**.[6]

Seeing that compound **59** with the phenyl carbazole outperforms compound **58** with the ethyl carbazole leads to the speculation whether a phenyl on the 2,7-connected carbazole spacer in compound **60** might be able to improve the efficiency even further. However, the difference in power conversion efficiency is more or less within the error margin of +/-0.2 %[7]. Simple steric reasons and better shielding of the dye through a phenyl substituent on the carbazole might play a role and be beneficial. Comparing the

[5]Here the degree of dye-loading is estimated by comparing the ratio of extinction on titanium dioxide and extinction in solution. In this rough estimate the possible formation of multilayers is neglected.

[6]All performance values can be found in table 2.5 on page 55.

[7]For more details on the error margin see table 2.5

results oxidation and ionisation potential derived from the cyclic voltammetry measurements, the four dyes are very similar, leading to the assumption that also HOMO and LUMO energy levels are similar as well. One surprising value is definitely the oxidation potential of compound **58**, which compared to compound **59** is shifted around 0.1 eV into the negative direction. This is unexpected, the calculations predicting both dyes to be the same. It could be a larger bandgap of compound **59**, which resulting in the higher open-circuit voltage, drives up the efficiency. In solution, however, the absorption of both compounds is almost identical, implying also a similar bandgap. Overall, the small change of different substitution at the nitrogen of the carbazole spacer does not lead to a clear trend.

Comparing bandgaps of **57** and **60**, **57** with the presumabably higher bandgap is outperformed in current and efficiency by compound **60**. However, comparing these two molecules, one parameter is of course not enough to explain their difference in sensitiser performance. Other reasons like the shape of the molecule the connection pathway and the broader more bathochromic absorption of compound **60** might have led to that very good result. As mentioned above, the difference in performance of the two compounds is very small. The only clear outcome of this device series is the superiority in performance of the 2,7-connected compared to the 3,6-connected carbazole. Knowing, that in a different testing series as mentioned before **57** can also reach higher efficiencies ($\eta = 4.5\,\%$), a sensible optimisation attempt could be using a 3,7-connected dibenzothiophene spacer.

2.3 Variation of Spacer Length

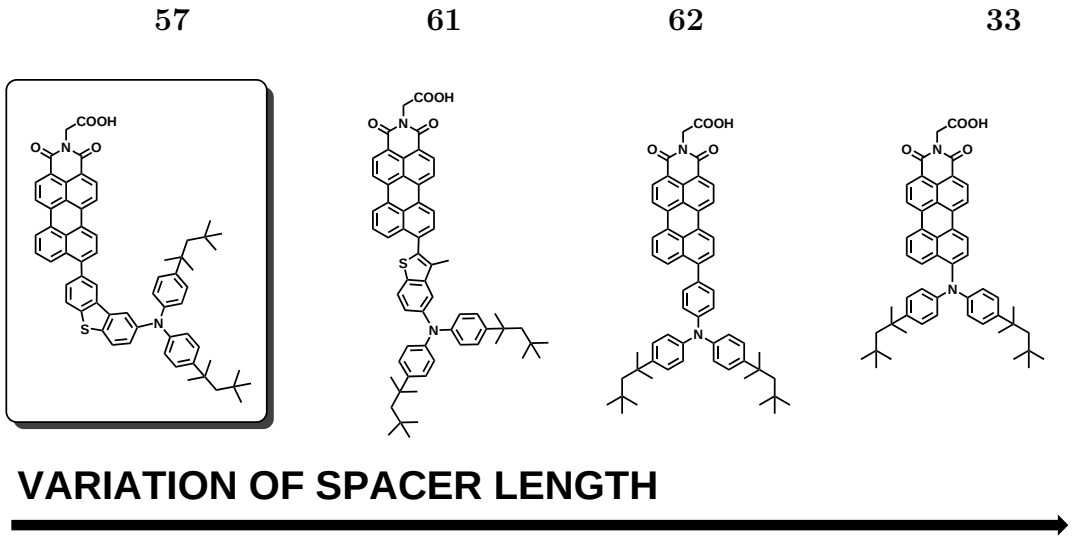

Figure 2.9: Variation of spacer length

In the preceding series of different spacers we have seen that in all cases HOMO and LUMO are decoupled as an extreme case of orbital partitioning. In the following section, compound **57** with its dibenzothiophene spacer will be compared to compound **61** with a methyl-substituted benzothiophene, compound **62**[8] with a phenylene spacer and compound **33**[9] without a spacer in order to allow more and more communication and possibly find the ideal spacer length within this series.

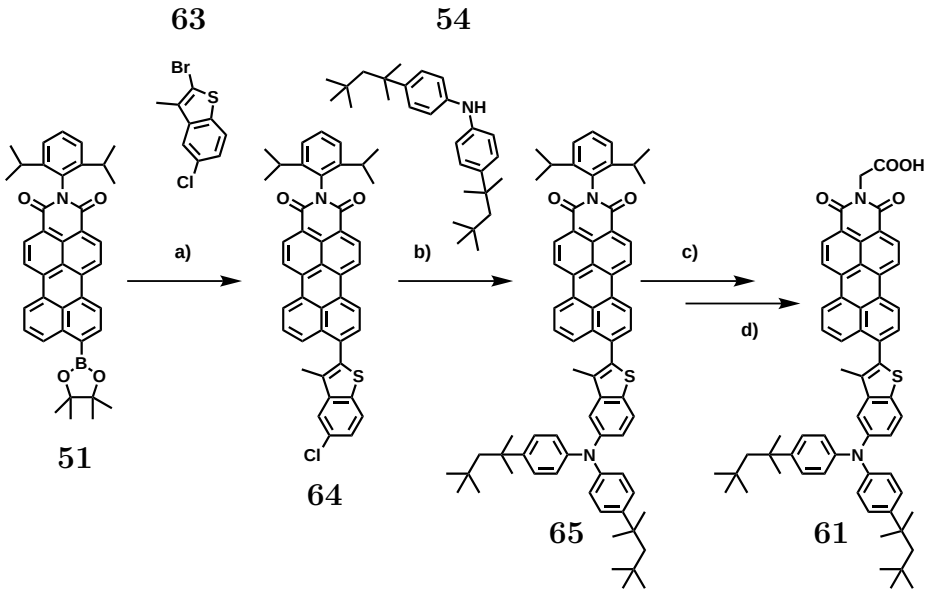

a) K_2CO_3, $Pd(PPh_3)_4$, toluene, water, ethanol, 80 °C, overnight, yield: 58 %; b) NaOtBu, $Pd_2(dba)_3$, tri-t-butylphosphine, 80°C, overnight, yield: 52 %; c) 2-methyl-2-butanol, KOH, reflux, over night, yield (crude): 88 %; d) glycine, imidazole, 140°C, over night, yield: 69 %.

Figure 2.10: Synthesis of compound **61**

For the synthesis of compound **61** (figure 2.10), 2-bromo-5-chloro-3-methylbenzo-*[b]*thiophene (**63**) was reacted with the perylene monoimide boronic ester, the coupling occurring selectively on the bromo site and without dechlorination, yielding 58 %. The main side product was the deborylated perylene monoimide. Like in the synthesis of **57**, the donor moiety was introduced using Buchwald conditions, however, using different conditions ($Pd_2(dba)_3$, BINAP, caesium carbonate, toluene, 100°C), which have in our group proven to be more suitable in the case that the halogen on the aromatic system is chlorine, yielding 52 %. Saponification and imidisation were performed under the same conditions as for **57** and all other compounds in this chapter (figure 2.1 on page 32) giving an overall yield of **61** of 60 % for the two steps. 103 mg of the final product **61** were obtained. The main loss in product occurred in the purification of the final compound due to strong interaction of the carboxylic acid with the silica gel combined with lower solubility compared to the other DπA-PMIs. Compound **33** was synthesised

[8] Synthesised by BASF SE

[9] Also known as ID176; first synthesised by Chen Li [87]

by Chen Li[87], and compound **62** by BASF SE, also kindly providing their data for this compound.

The pictures of the HOMO-LUMO localisation presented in table 2.2 on the following page show, that with shortening the spacer length more and more coupling of HOMO and LUMO occurs, the first considerable overlap in compound **62** with a phenylene spacer, where the HOMO reaches out into the perylene core up to the imide acceptor and the LUMO down into the phenylene spacer.

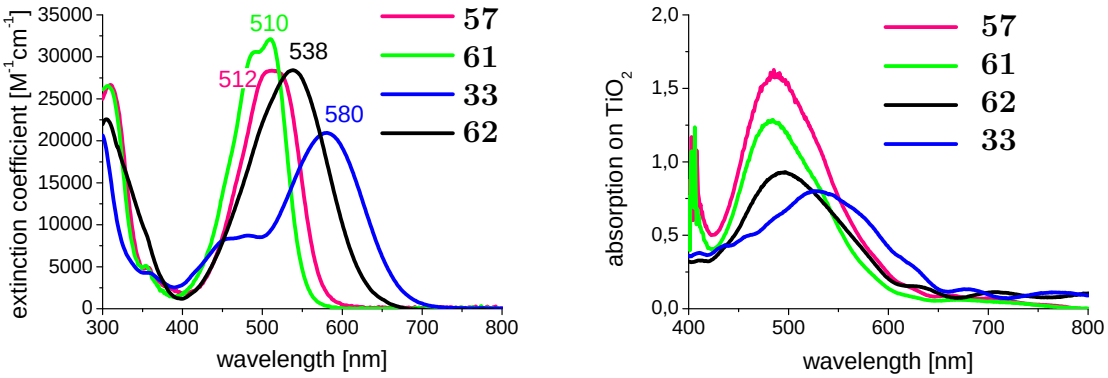

(a) Solution absorption

(b) TiO_2 absorption

33 processed in dichloromethane. All other dyes processed in toluene.

Figure 2.11: Absorption spectra of the dyes **57**, **61**, **62**, and **33** in dichloromethane (a) and on titanium dioxide (b)

When charge transfer comes into play, DFT calculations often reach their limitations.[101,102] Here, the quantum mechanical predictions seem to overestimate the coupling of HOMO and LUMO especially for compound **61** and **62**. The calculated orbital coefficients show a much better coupling of the orbitals for compound **61** compared to compound **57** and with an oscillator strength (f1) of 0.21 a weak CT-band is suggested at around 711 nm. The absorption of **61**, however, with its hypsochromic shift and more distinct fine structure shows great resemblance with the perylene monoimide absorption (figure 2.3 on page 35), showing only the π-π*-transition and no CT-band. Due to low solubility in dichloromethane, this compound's extinction had to be determined in tetrahydrofuran, but the fine structure and the hypsochromic shift are not solvatochromic effects as the *N*-(2,6-di*iso*propylphenyl)-precursor could be measured in dichloromethane and showed the same characteristics. Changing the imide substituent from a di*iso*propylphenyl to a carboxymethyl has generally only a negligible effect on the absorption. Maybe in this case the calculations underestimate the influence of the methyl group on the thiophene. The torsion angle of the optimised structure of **61** is with 54° predicted higher than for all other compounds, confirming the assumption, that despite the shorter spacer **61** is the most strongly decoupled system within this

Dye	Structure	HOMO	LUMO	
57	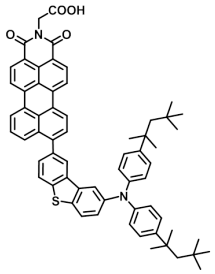	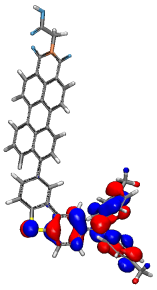	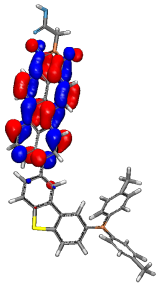	IP: 5.27 EA: 3.20 S1: 684 nm S2: 519 nm f1: 0.02 f2: 0.80
61	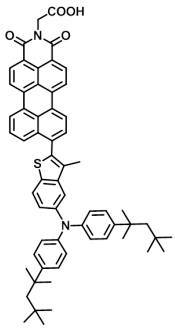	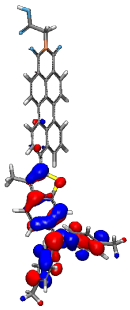	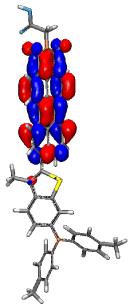	IP: 5.22 EA: 3.22 S1: 711 nm S2: 512 nm f1: 0.21 f2: 0.78
62	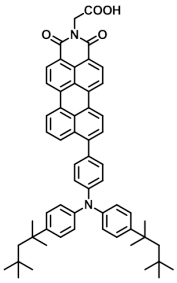	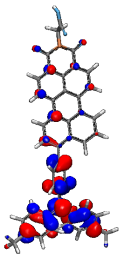	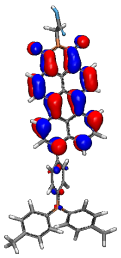	IP: 5.30 EA: 3.17 S1: 639 nm S2: 497 nm f1: 0.45 f2: 0.53
33	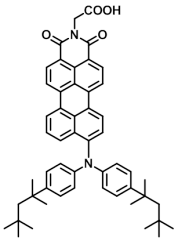	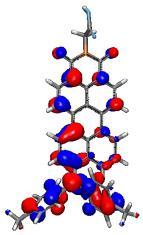	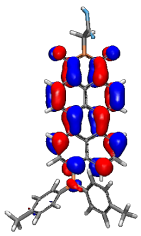	IP: 5.52 EA: 3.21 S1: 602 nm S2: 465 nm f1: 0.52 f2: 0.25

(DFT; performed by BASF SE)

Table 2.2: Calculated orbital surfaces, ionisation potential (IP), electron affinity (EA), transitions (S) and oscillator strengths (f) of compound **57**, **61**, **62**, and **33**

series. For the phenylene spacer, the torsion angle is estimated to be only 47°[10] and therefore considerably lower than for the dibenzothiophene and carbazole spacers, their predicted torsion angles varying between 51-53°.

Both compound **62** and **33** show a bathochromic shifted band owing to the stronger orbital overlap of HOMO and LUMO. The calculation data, however, suggests a more bathochromic S1 transition for **62** than for **33**, whereas the solution absorption spectra (figure 2.11 on page 45) of the two compounds show the opposite. In compound **62** the absorption band with its maximum at 538 nm can most probably still be assigned to the π-π*-transition. Two indicators for that lie in the experimentally determined absorption, namely the high extinction (similar to compound **57**), unusual for CT-bands as well as the shape of the band, the rising of it being congruent with the π-π*-transition bands of compound **57** and **61**. Like compound **60** the perylene monoimide core feels a much stronger push of the *para*-conjugated donor in the extended *peri*-position, even if the charge transfer is somewhat reduced by the phenylene spacer rotated out of the plane. Compound **33** with stronger orbital overlap shows a typical CT-band exhibiting a much stronger red-shift in absorption to λ_{max} at 580 nm at decidedly lower extinction. Adjacent to the CT-band towards the shorter wavelengths, a weaker π-π*-transition band of the perylene monoimide can still be observed.

The red-shift in absorption for compound **33** is also apparent on titanium dioxide (figure 2.12 on the next page). Compound **57** yields a much higher absorptivity than compound **61**, both compound **62** and **33** show much lower extinction than compound **57** and **60**, **62** slightly exceeding **33** but **33** showing a broader band. In general, CT results in a broader but lower absorption in donor-acceptor perylene monoimides. As compound **33** is the only compound showing a broadening of the band, this supports the assumption that the absorption band of **62** with its maximum at 538 nm is not a CT but a π-π*-transition band.

According to the calculation, the electron affinity (EA) is about the same for all four compounds (**57**, **61**, **62**, and **33**). The results of the cyclic voltammetry measurements, however, give different reduction potentials, pointing at the lowest lying LUMO for the CT-dye **33**, followed by the – according to absorption – strongest decoupled sensitiser **61**. Compound **62** shows a reduction potential comparable to compound **57**.

Unfortunately **33** was not tested together with the other dyes. Even though devices for **33** were made the same way using the same additives, only results from dichloromethane-processed cells were available. This might also have had an influence on the extinction of **33** on titanium dioxide.

The EQE curves show again considerable broadening for all dyes and is in good agreement with the solution absorption regarding the bathochromic shifts; compound **33** > compound **62** > compound **57** > compound **61**, again suggesting that compound

[10] In the final molecule **69**, according to the DFT-calculations (2.3).

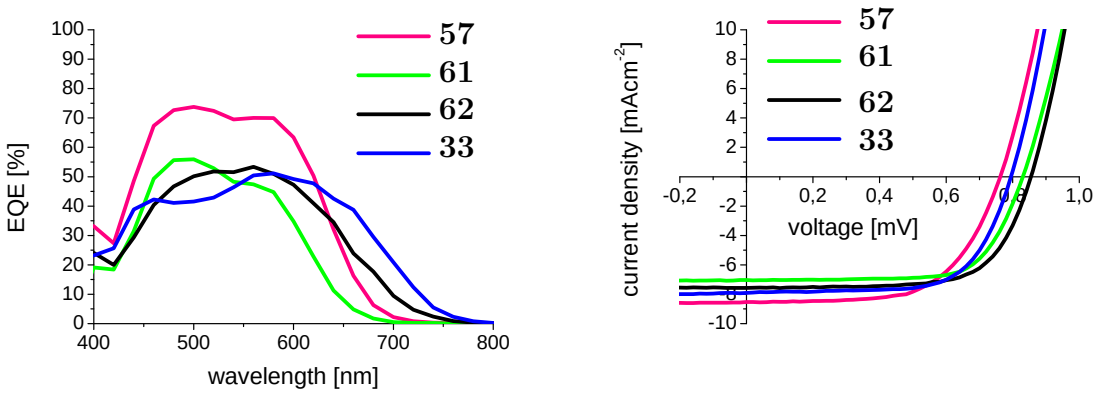

(a) EQE (b) IV

33 processed in dichloromethane. All other dyes processed in toluene.

Figure 2.12: EQE (a) and IV-curve (b) of the dyes **57**, **61**, **62**, and **33**

61 though bearing a shorter spacer is more strongly decoupled than compound **57**. In EQE intensity compound **61**, **62**, and **33** are very similar, their top EQE values ranging between 51 and 56 %, compound **57** far exceeding all three with its top EQE of up to 74 %.

Their order of overall power conversion measured is as follows: compound **62** (4.4 %) > compound **33** (4.1 %) > compound **57** (4.0 %) > compound **61** (3.9 %). Again these efficiencies are all very close. From the device performance, no clear conclusion can be drawn, especially as **33** was measured in a different solvent and testing series. Though spacer length does have a strong influence on the degree of orbital communication reflected in the absorption, the compounds without spacer, with the phenylene spacer and with the dibenzothiophene spacer reach effiencies greater than 4 %. Their optical properties vary strongly, the EQE spectra showing clearly how broad absorption (**33**) can be compensated by extinction (**57**).

2.4 Variation of Donor

In the introduction of this chapter the absorption measurements of the different synthesis steps already showed, that introduction of a donor on a dibenzothiophene spacer perylene monoimide does not result in broadening or bathochromic shift of the main absorption band. But different donor groups may have other benefits, i.e. better interaction with the hole transporting material through steric or electronic features[103], a stronger push maybe overcoming the strong decoupling or additional absorption in the shorter wavelenth region.

In the following, four different donor groups will be presented; the first three on the dibenzothiophene-perylene monoimide, thus a variation of compound **57**, the last

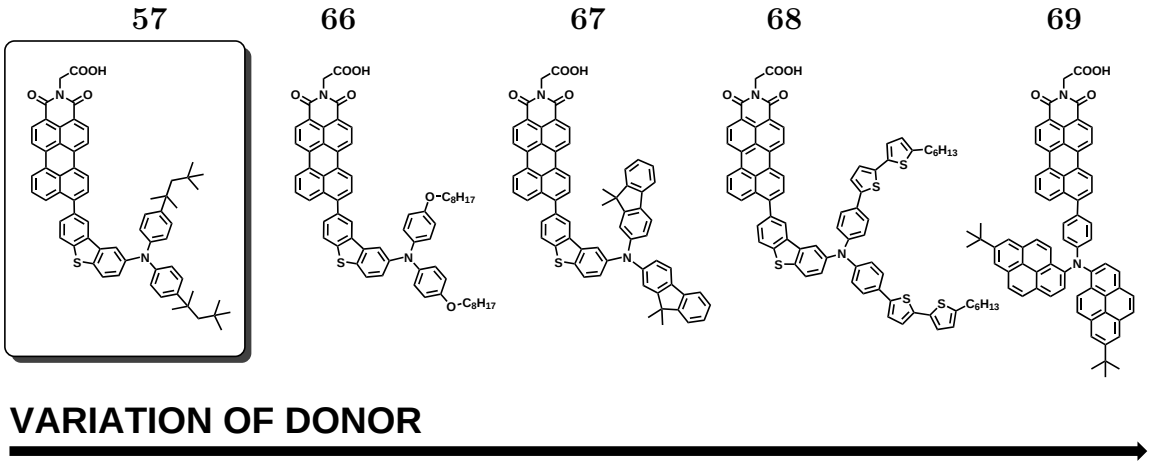

Figure 2.13: Variation of donor

donor group, a bis(pyrenyl)amine on the phenylene-perylene monoimide (figure 2.13) as an analogue of **62**.

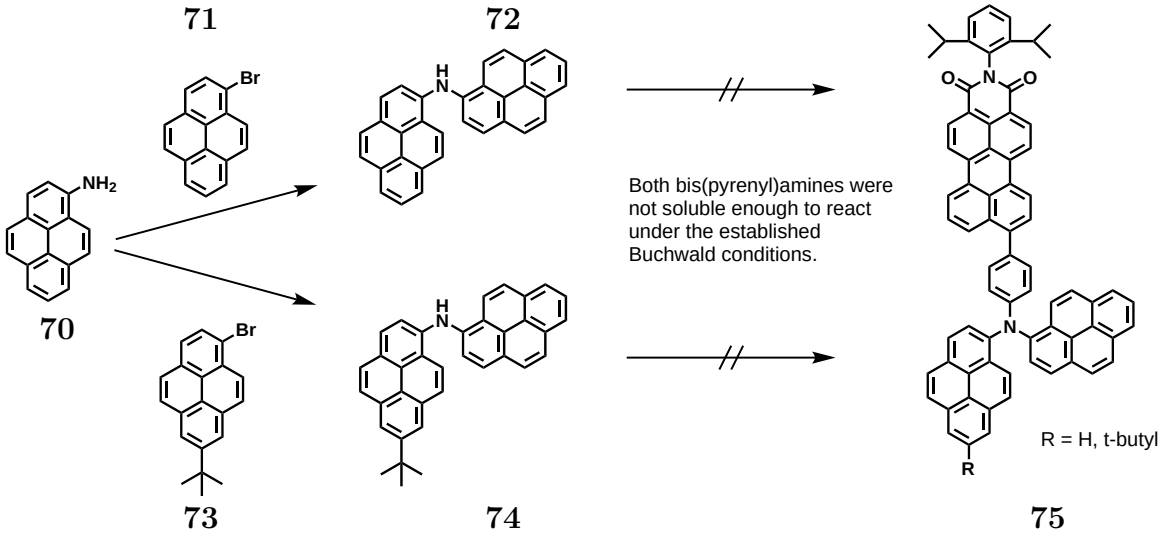

Figure 2.14: Synthesis of pyrene donor

Compounds **66**, **67**, and **68** were made according to the scheme presented for compound **57** (figure 2.1 on page 32) using the respective donor. Unlike the *tert*-octylated diphenyl amine donor, they were not commercial. The fluorenyl amine donor (compound **67**) was kindly provided by BASF, the alkoxylated diphenylamine (compound **66**) as well as the diphenyl amine donor with additional thiophenes (compound **68**) had been synthesised by Li and were still available in the group.[87] Again, using the building block **53** contaminated with debrominated species, the yields for the Buchwald amination reactions varied between 36 and 59 % while the yields for the subsequent saponification and imidisation reactions ranged between 73 and 82 % over both steps. 75 mg of **66**, 107 mg of **67**, and 80 mg of **68** were obtained.

A first attempt to synthesise compound **69** in a similar way failed because the bis(pyrenyl)amine donors (**72**, **74**) achieved by Buchwald coupling of amino-pyrene (**70**) with bromo-pyrene (**71**) and *t*-butylated bromo-pyrene (**73**) were too insoluble to couple with the 9-(4-chlorophenyl)-perylene monoimide under the established conditions (toluene, 100°C) described in figure 2.14 on the preceding page.

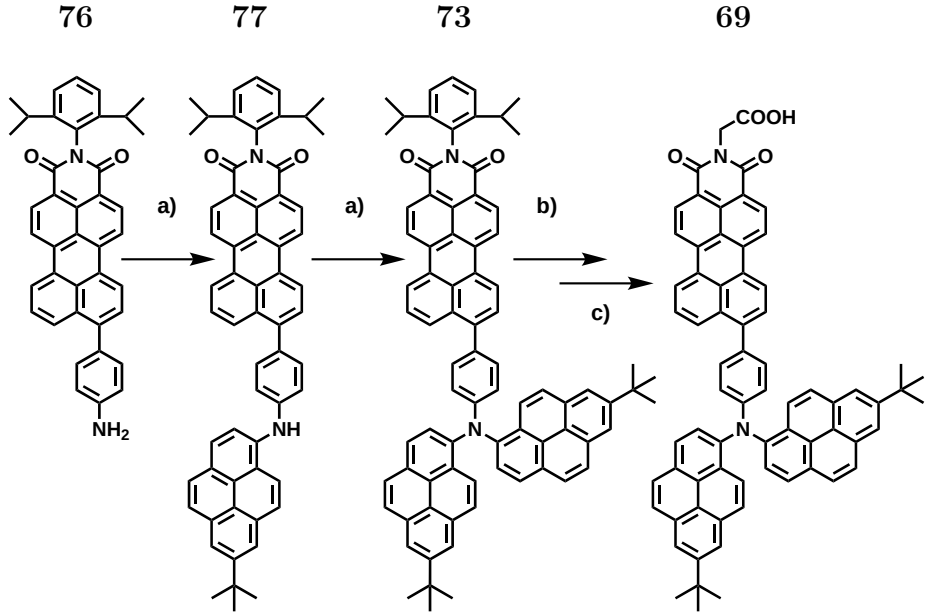

a) 1-bromo-7-(*t*-butyl)pyrene, NaOtBu, $Pd_2(dba)_3$, tri-*t*-butylphosphine, 80°C, overnight, yield: 32 %; e) 2-methyl-2-butanol, KOH, reflux, over night, yield (crude): 98 %; f) glycine, imidazole, 140°C, over night, yield: 90 %

Figure 2.15: Synthesis of compound **69**

Compound **69** was therefore built up according to the scheme presented in figure 2.15. Two *t*-butyl-pyrenyls (**73**) prepared by [redacted] were reacted with **76** reported in literature[104] via a two-step Buchwald reaction yielding overall 32 %. Main side product in this reaction was single substitution and the beginning of saponification. In order to attach an anchoring group, compound **73** was separated by column chromatography on silica gel with dichloromethane from the mono-functionalised analogue, saponified under basic conditions with potassium hydroxide in 2-methyl-2-butanol, and imidised with glycine in imidazole to yield 96 mg of the final product **69** with an overall yield of 88 % for the two last steps.

In compound **66**, the branched alkyl chains on the donor of compound **57** were exchanged for linear alkoxy chains, hoping for a stronger push. Moreover, long alkyl chains are used in many successful ruthenium-based sensitisers.[20] DFT-calculations (table 2.3 on the facing page) predict a considerable bathochromic shift of the S1-transition from 684 nm in compound **57** to 763 nm in compound **66** but as in both compounds f1 is only 0.02, this has no noticeable impact on the absorption spectrum

Dye	Structure	HOMO	LUMO	
57	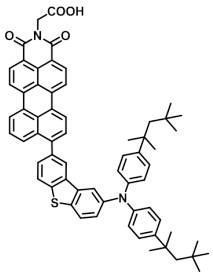	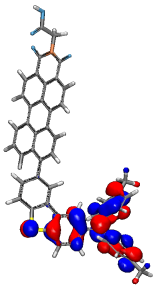	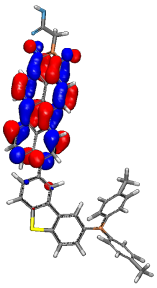	IP: 5.27 EA: 3.20 S1: 684 nm S2: 519 nm f1: 0.02 f2: 0.80
66	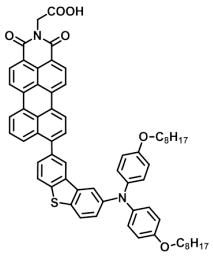	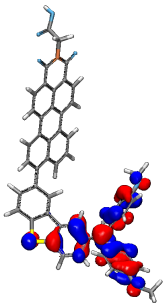	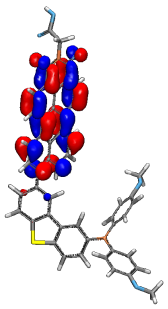	IP: 5.07 EA: 3.18 S1: 763 nm S2: 519 nm f1: 0.02 f2: 0.77
67	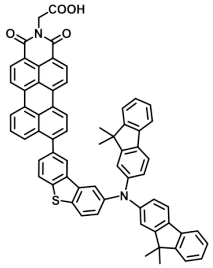	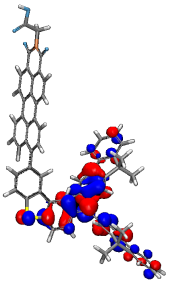	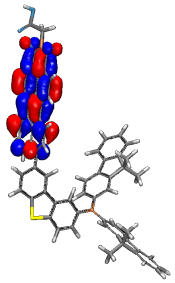	IP: 5.14 EA: 3.25 S1: 717 nm S2: 500 nm f1: 0.00 f2: 0.72
68	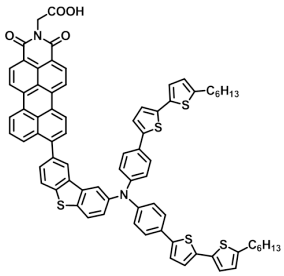	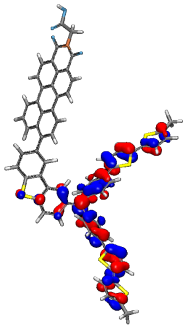	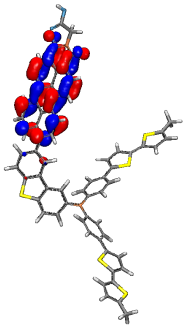	IP: 4.95 EA: 3.20 S1: 770 nm S2: 598 nm S3: 525 nm f1: 0.01 f2: 0.00 f3: 0.68
69	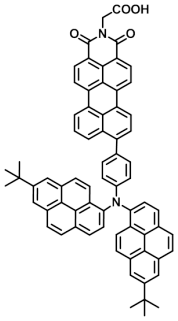	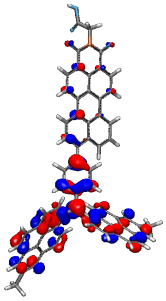	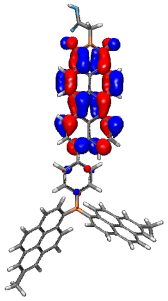	IP: 5.21 EA: 3.16 S1: 654 nm S2: 513 nm f1: 0.38 f2: 0.71

(DFT; performed by BASF SE)

Table 2.3: Calculated orbital surfaces, ionisation potential (IP), electron affinity (EA), transitions (S) and oscillator strengths (f) of compound **57**, **66**, **67**, **68**, and **69**

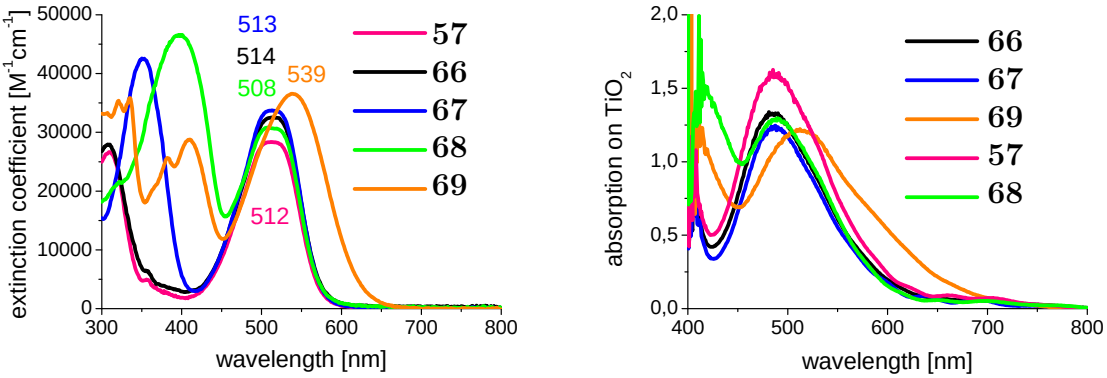

(a) Solution absorption (b) TiO_2 absorption

Figure 2.16: Absorption Spectra of the dyes **57**, **66**, **67**, **68**, and **69** in dichloromethane (a) and on titanium dioxide (b)

(compare figure 2.16). Only a rise in the extinction coefficient can be observed. The HOMO coefficients are similarly located as in compound **57** but the oxidation potential in the cyclic voltammetry measurements is shifted a little into the negative direction compared to the other dyes, suggesting a higher HOMO level energy and hence leading to a slightly reduced bandgap. The bulky bis(fluorenyl)donor in compound **67** shows similar calculation results and absorption spectrum. The fluorenes give additional absorption in the range up to 400 nm with a maximum at around 350 nm, however, the band falling mainly into the absorption range of the titanium dioxide which will mostly attenuate the effect.

Compound **68** follows a more complex concept of additional light harvesting. The dithiophene groups attached to the each phenyl of the amine spacer absorb in the typical dithiophene range of up to 450 nm and Förster resonance energy transfer (FRET) to the perylene monoimide takes place as confirmed by fluorescence measurements showing the perylene monoimide emission upon the excitation of the dithiophene band at 400 nm (figure 2.17 on the facing page), reaching 73 % of emission intensity compared to the emission upon excitation at λ_{max} 520 nm. This contribution from short-wave excitation is confirmed in the emission trend (excitation spectrum) demonstrated in 2.17 on the next page of **55** together with the one of the *N*-(2,6-di*iso*propylphenyl)-precursor of compound of **68**, both graphs normalised to their excitation maxima. The excitation spectrum of **55** is missing this strong short-wavelength contribution. Both excitation spectra are in good coherence with their respective absorption spectra. Compound **69** with its bis(pyrenyl)amine donor manages to provide absorption in the same range like the dithiophenes but with its higher orbital coupling through the smaller phenylene spacer also achieves a broader perylene monoimide absorption and therefore shows the broadest coverage within the visible spectrum. Like for compound **62**, the DFT-calculations predict a CT-band at 654 nm with an oscillator strength of

0.38. Again this can not be detected in the recorded spectrum which shows just a broader π-π*-transition band reaching out to 650 nm.

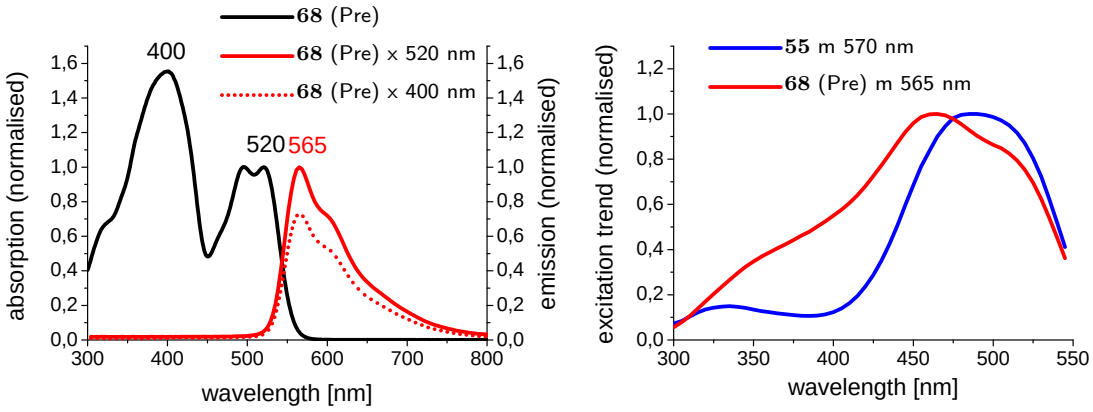

(a) Absorption and emission

(b) Excitation spectra

68(Pre): *N*-(2,6-di*iso*propylphenyl)-precursor of **68**; x: excitation wavelength; m: emission wavelength

Figure 2.17: Absorption (black) and emission (red) of the *N*-(2,6-di*iso*propylphenyl)-precursor of **68** in toluene (a) and excitation spectra of *N*-(2,6-di*iso*propylphenyl)-precursor of **68** and **55** in toluene (b)

The absorptivity of these compounds with variable donors on titanium dioxide is presented in figure 2.16 on the facing page. Again compound **57** – though in solution owning the poorest extinction – exceeds all other dyes in absorptivity. The short-wavelength absorption of the dithiophenes and pyrenes is also reflected on titanium dioxide, especially the dithiophenes leading to high absorptivity in the range of up to 350 nm. Compound **69** shows a much higher extinction on titanium dioxide up to 1.2 compared to compound **62** of the preceding section reaching only 0.6. What is remarkable about the shape of the absorption band on titanium dioxide of compound **69** is the tailing of the curve starting at 550 nm and reaching out to 700 nm. This may be a sign of aggregation or CT-character. A similar though much weaker tailing can also be observed for example in compound **57** and even in the presumably still stronger decoupled compound **61**, arguing in favour of donor impact even though not instantly observed in solution absorption.

Compound **57**, **66**, and **67** show very similar EQE curves (figure 2.18 on the next page) regarding their shape rising at aroung 420 nm and stretching out to 700 nm. Compound **57** and **67**, however, reach much higher intensities and compound **57** an additional broadening towards longer wavelengths. The effect of additional light harvesting of the dithiophenes in compound **68** is clearly visible, the dye achieving additional EQE in the area of 400-450 nm. Like in the solution absorption and on titanium dioxide the pyrenes of compound **69** contribute a little less in that area though still exceeding the intensities of compound **57**, **66**, and **67**. But towards longer wavelengths

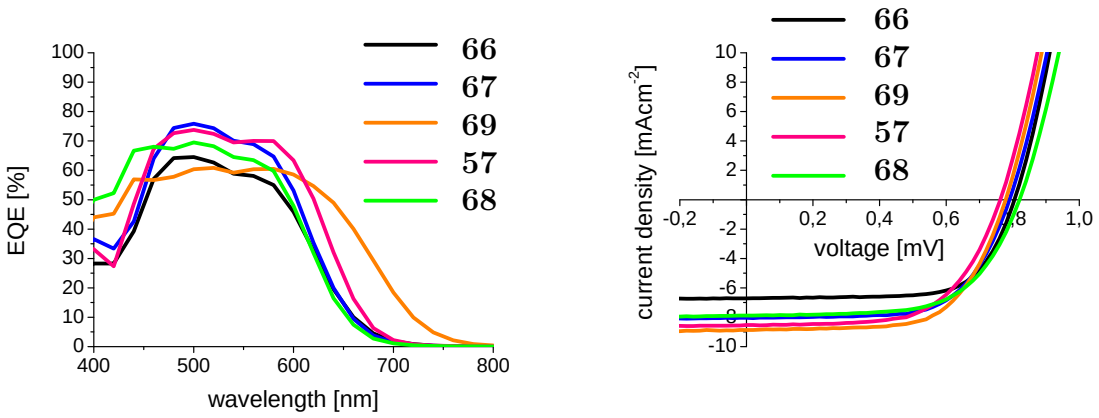

(a) EQE (b) IV

Figure 2.18: EQE (a) and IV-curve (b) of the dyes **57**, **66**, **67**, **68**, and **69**

the dye shows a much broader EQE, reaching out to 800 nm. This broadening goes along with flattening of the curve, the top intensities around 60 %, comparable with compound **66**.

The additional light harvesting of the dithiophenes could unfortunately not help the performance of the cell, compound **68** reaching an I_{SC} of only -7.88 $mAcm^{-2}$. Compound **69** exhibits not only the best short circuit current (I_{SC} = -10.33 $mAcm^{-2}$) but also by far the highest power conversion efficiency of 4.9 %. The high current density shows that the broadening of absorption and EQE could outweigh the loss in extinction and EQE intensity. Regarding current, all compounds are within the same range. The power conversion efficiencies measured within this series were as follows: compound **69** (4.9 %) > compound **57** (4.1 %) > compound **67** (4.0 %) and **68** (4.0 %) > compound **66** (3.8 %). Within the error of +/-0.2 %, compound **57**, **67**, **68**, and **66** show more or less the same efficiencies. The additional light harvesting of **68** in the short-wavelength region could be detected in the solution absorption and EQE but did not have a strong effect on the efficiency. Compound **69**, however, achieved a far better result, reaching also a slightly higher performance than **62** with the same spacer moiety, suggesting that the pyrenyl donor is not only helping the light harvesting but is also well compatible with the whole cell system. Besides influencing the optical properties the donor needs to have the ability to interact well with the hole transporting material, here with spiro-MeOTAD.[103]

2.5 Conclusion

With strong orbital partitioning and decoupling a series of sensitisers could be obtained, reaching power conversion efficiencies of up to 4.9 %, therefore being amongst the current top-sensitisers in solid-state dye-sensitised solar cells world-wide. Even though

Dye	λ_{max} [nm] / ϵ [$M^{-1}cm^{-1}$]	LUMO* [eV]	HOMO* [eV]	bandgap [eV]
57	512 / 28,382	-3.5	-5.1	1.6
58	526 / 34,806	-3.5	-4.9	1.4
59	521 / 30,219	-3.5	-5.0	1.5
60	526 / 35,621	-3.5	-5.0	1.5
61**	510 / 32,115	-3.6	-5.1	1.5
62	538 / 28,422	-3.5	-5.1	1.6
33	580 / 20,942	-3.7	-5.2	1.5
66	514 / 32,537	-3.5	-4.9	1.4
67	513 / 33,743	-3.5	-5.0	1.5
	350 / 42,575			
68	508 / 30,833	-3.5	-5.0	1.5
	397 / 46,574			
69	539 / 36,565	-3.5	-5.0	1.5
	410 / 28,794			

*determined by cyclic voltammetry; **absorption measured in tetrahydrofuran due to poor solubility in dichloromethane. All other absorption spectra measured in dichloromethane.

Table 2.4: Optical and electrochemical properties of the dyes

Dye	EQE_{max} [%]	V_{OC} [mV]	I_{SC} [$mAcm^{-2}$]	FF [%]	η [%]
57	74	760	-8.52	62	4.0
58	48	800	-5.88	69	3.2
59	54	840	-6.55	67	3.7
60	52	820	-8.42	65	4.5
61	56	840	-7.03	70	3.9
62	53	860	-7.57	68	4.4
33*	51	800	-7.91	66	4.1
66	76	800	-6.72	70	3.8
67	65	800	-8.04	64	4.1
68	70	820	-7.88	63	4.1
69	62	800	-10.33	59	4.9

*All dyes except for compound **33** are processed from toluene using the additive; cell performance was measured under 1 sun.

The cell making was undertaken by BASF SE. The cells were assembled manually, however, in some steps using apparatuses which allow the treatment of several substrates at the same time, minimising the error due to manual inaccuracies within one testing series. The titanium dioxide-substrates for example were made in large batches by screen printing in order to achieve the same layer thickness for the substrates and the back electrode can be vapour deposited on 10-16 substrates at the same time. In order to reduce measuring errors, two substrates of the same additive-solvent combination with four cells each were tested. The effiencies presented here are an average of the cell results. Cells, which did not reach 70 % efficiency of the top cell amongst the eight cells, were expected to have a major defect and were not included in the avarage. Still, cell results can vary. With help of one standard dye, which has been included in all measurement series for several years now, the error of a cell measurement could be estimated over the past years and is roughly +/-0.2 in efficiency.

Table 2.5: Photovoltaic performance of the the various spacer dyes

Figure 2.19: Solutions of **57**-**62**, **33**, and **66**-**69** (from left to right) in dichloromethane

complete decoupling like in case of compound **57** can achieve very high efficiencies, it seems that a small orbital overlap like in the compounds **60**, **62**, and **69** is favourable to ensure a minimum of communication between donor and acceptor moiety. At the same time, this series shows that broad absorption can be compensated by strong extinction, thus **33** and **57** showing similar device performance. This finding points up once more, how complex sensitiser design is and that the various setscrews of tuning are strongly interconnected. Increased light harvesting of a second chromophore on the donor moiety, like the dithiophenes in the case of compound **68** and the pyrenes in compound **69** may help the efficiency. This becomes apparent in the direct comparison of **62** and **69**, the pyrene moieties on the donor filling the short wavelength absorption gap, improving the current and at the same time efficiency. The lack of performance improvements in the case of compound **68** could be justified by unfavourable sterics. As with the poorly performing compound **66**, compound **68** bears long linear alkyl chains. Although these chains seem to be useful in metal-complex sensitisers, no beneficial impact can be observed within this series, and they might be even detrimental. A thorough investigation of steric effects was, however, beyond the scope of this study.

Chapter 3

Flexible π-Spacer for Improved Light Harvesting and Introduction of a Second Donor

3.1 Introduction

One conclusion drawn from the preceding chapter was that complete decoupling via introduction of rigid π-spacers leads without doubt to very good sensitisers for dye-sensitised solar cells but that a little overlap of HOMO and LUMO like in the compounds **60**, **62**, and **69** seems even more desirable, leading to improved efficiencies. The two main reasons for the decoupling concept were i) the balance of charge transfer from the donor to the acceptor and reduction of the unwanted back-transfer as well as ii) keeping a high LUMO for better driving force for the electron injection into the titanium dioxide conduction band. In this chapter a perylene monoimide with a flexible π-spacer and two donor groups will be presented, the flexible π-spacer allowing better orbital communication and the second donor group increasing the electron-push towards the acceptor and at the same time raising the LUMO level energy. The main results of this chapter have already been presented in literature.[63]

Like in the precding chapter a π-spacer unit was inserted between perylene monoimide and donor group, only that now the spacer unit is a branched terthiophene[105,106]. It is thus a flexible spacer moiety. Moreover, it makes the introduction of two triphenyl amine donor groups[107] possible. For comparison a naphthalene analogue was synthesised. Synthesis and structure of both perylene monoimide (**83**) and naphthalene monoimide (**84**) are described in figure 3.1 on page 59. As Thomas et al.[105] and Fischer et al.[106] showed the combination of a triphenylamine donor and branched oligothiophene spacer in combination with and a 2-cyanoacrylate acceptor gives good efficiencies up to 6.15 %[105] and 6.8 %[106] in liquid DSSCs and up to 2.6 %[106] in a solid-state DSSC. Furthermore three moieties - triphenylamine, oligothiophene, and

perylene monoimide - have recently received attention in a p-DSSC (NiO) reaching a sevenfold increase in energy conversion efficiencies compared to preceding sensitisers.[86] The herein presented sensitisers were designed for for solid-state n-DSSCs with titanium dioxide as the semiconductor, for which the perylene sensitiser **83** shows a good efficiency of 3.8 % under AM 1.5 illumination (1 sun). At the time of publication this was an unprecedented performance for a perylene sensitiser. Previously, to the best of our knowledge, the best perylene sensitiser reported in literature in solid state DSSCs had been **33** (ID176) with an efficiency of 3.2 %[1].[79]

The choice of the branched terthiophene spacer was made deliberately for thiophenes show excellent charge transport properties and enhance absorptivity.[26,67] As our group has shown before, and will be presented in the last chapter, the variation of architecture of a terthiophene moiety can alter the absorption properties decidedly.[108] Using the branched terthiophene instead of a single thiophene or linear oligothiphene followed the intention of adding more than two thiophenes, keeping the distance between donor and acceptor for efficient intramolecular charge transfer reasonably short and at the same time enabling the introduction of a second donor moiety. As one thiophene is α-β connected, this second donor loses some of its strength due to weak conjugation, but still can generate electron transfer towards the perylene (or naphthalene) core and will not only affect the HOMO level but furthermore shift the first reduction potential in the negative direction. This elevation of the LUMO level energy enhances the electron injection from the dye to the conduction band of the titanium dioxide. Moreover this second spacer-donor branch increases the bulkiness of the molecule and presumably prevents aggregation and hence unwanted recombination between the dyes.[109] Bulkiness can furthermore function as a barrier between the titanium dioxide and the hole transporting layer.[110] Obviously this effect is always a trade-off between the mentioned positive effects and the undesired consequence of lower dye concentration on the titanium dioxide leading to less light harvesting.[27]

3.2 Synthesis, Optical and Electronic Characteristics, and Photovoltaic Performance

Both compounds were prepared by first coupling the terthiophene spacer under Suzuki conditions with the brominated perylene or naphthalene imide with a satisfying yield of 77 % for the perylene and an excellent yield of 92% for the naphthalene case. In a second step the trimethylsilyl-groups were changed into bromo with N-bromosuccinimide in tetrahydrofuran with comparative yields of 82% and 84% for both derivatives. The

[1]The best published efficiency for ID176 is 3.2 % even though within the testing series described in the preceding chapter a higher efficiency of namely 4.4 % could be reached.

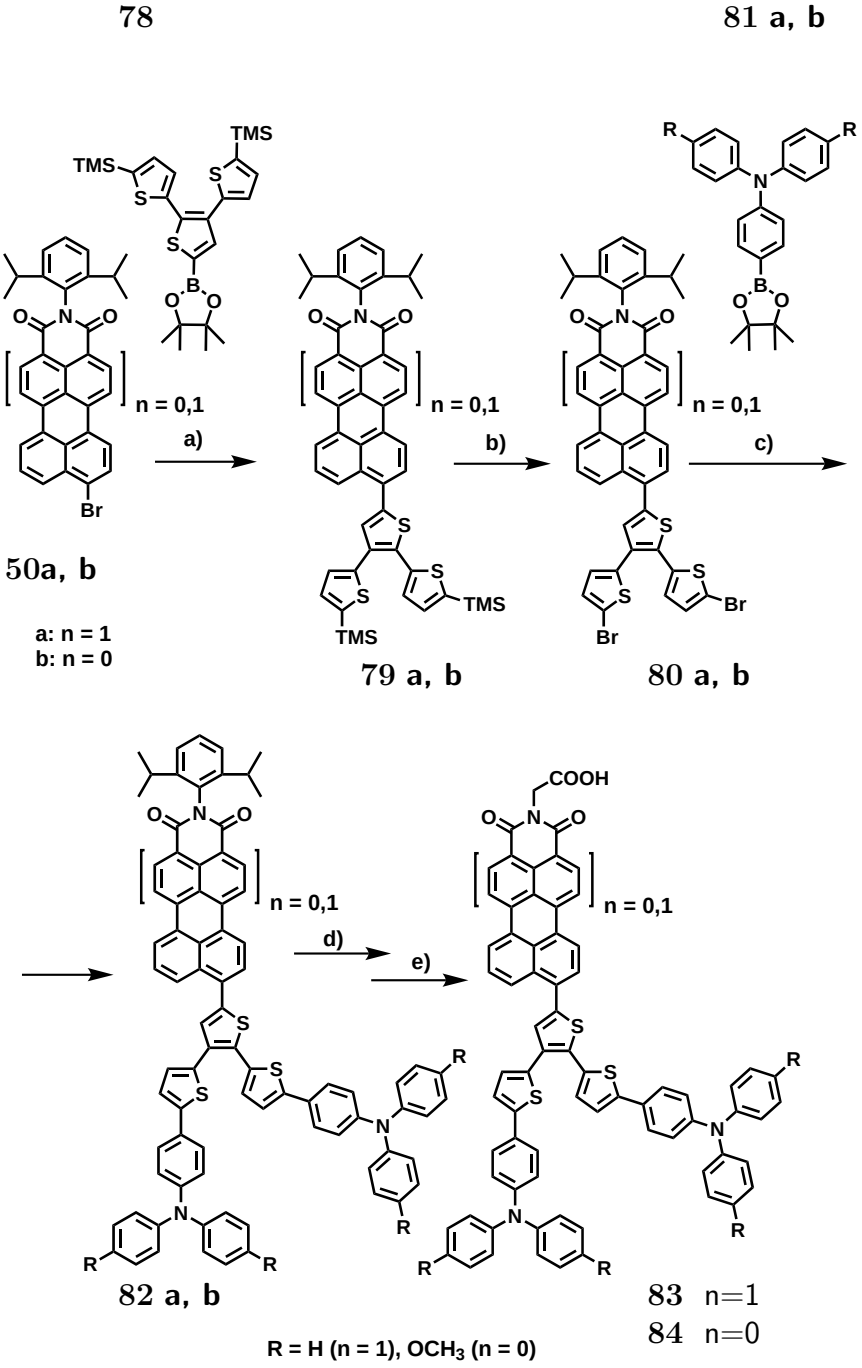

a) K_2CO_3, $Pd(PPh_3)_4$, toluene, water, ethanol, 80 °C, overnight (yields: 77% (**79a**), 92% (**79b**)); b) NBS, THF, 0 °C → rt, 24 h (yields: 82% (**80a**), 84% (**80b**)); c) K_2CO_3, $Pd(PPh_3)_4$, toluene, water, ethanol, 80 °C, overnight (a) / 1.5 days (b) (yields: 43% (**82a**), 19% (**82b**)); d) 2-methyl-2-butanol, KOH, reflux, overnight (yields: 90% (a), 92% (b)); e) glycine, imidazole, 140°C, overnight (yields: 89% (**83**), 91% (**84**)).

Figure 3.1: Synthesis of a donor-acceptor perylene monoimide with thiophene dendron spacer groups and its naphthalene analogue

triphenyl amine donor was introduced via a second Suzuki coupling with the respective donor moiety. This step clearly represents the chokepoint of the synthesis. In the case of the perylene derivative **82a** only 43% of the desired compound could be achieved, for **82b** the yield was as low as 19%. Both reactions proceeded very slowly compared to other Suzuki couplings described in this thesis. The perylene as well as the naphthalene case were left to react overnight. In the perylene case, FD-mass spectrum showed peaks at the masses of the desired product, single substitution with bromo and without. The FD-mass spectrum of the naphthalene reaction displayed peaks at the masses of the respective reaction products but in this case, even the peak of the starting material mass was still present. This is surprising as in many cases the naphthalene derivative reacts more readily. One reason for the sluggish reaction might have been the lower concentration of the reaction solution (0.013 mol/L for the perylene, 0.011 mol/L for the napththalene case). In the perylene case, the reaction was stopped after one night, the naphthalene reaction was left stirring at 80°C for one more day. After that the starting material peak could not be detected in FD-mass anymore but a few other peaks which could not be assigned. The thin layer chromatography as well showed several additional spots complicating the separation. Purification of this step for both derivatives was done by first column chromatography on silica gel and subsequent recycling gel permeation chromatography to eliminate the mono-coupled side products. Saponification and subsequent imidisation with glycine yielded the final product (figure 3.1 on the previous page) in the usual satisfactory yields of 89-92% for these steps (figure 3.1 on the preceding page). 103 mg of **83** and 77 mg of **84** were obtained.

The absorption spectra of the different synthesis steps are presented in figure 3.2 on the next page. The introduction of the terthiophene spacer results in a stronger bathochromic shift of 18 nm to $\lambda_{max} = 525$ nm than in the case of the dibenzothiophene in the preceding chapter and moreover a complete loss of the perylene monoimide fine structure. Both of these effects can be attributed to the flexibility of the thiophene dendron. The three thiophenes cannot all twist out of the perylene monoimide plane as the dibenzothiophene moiety could, leading to a higher degree of conjugation between the spacer moiety and the perylene monoimide core. Moreover the flexibility of the spacer allows stronger vibrational movement resulting in a smother absorption curve. Additionally the introduction of the terthiophene spacer enhances the absorptivitiy. So does the subsequent introduction of the donor groups which also brings up the absorption band at shorter wavelengths originating from the thiophenes and the triphenylamine moieties. The introduction of the donor groups leads to a small broadening of the curve but only negligible shift in absorption ($\lambda_{max} = 526$ nm).

As described above, both sensitisers consist of an acceptor unit with a carboxylic acid anchor in the imide structure, a branched terthiophene (α-α connection and α-β

connection of the thiophene units) and a triphenylamine donor. In order to achieve a stronger push-pull effect in the naphthalene sensitiser the outer benzene rings of the triphenylamine donor bear methoxy groups para to the nitrogen. It was attempted to reach an even higher push by attaching diphenylamine donor groups directyl to the thiophene dendron. The resulting products, however, were not stable. Most probably oxidation of the sulfurs took place.

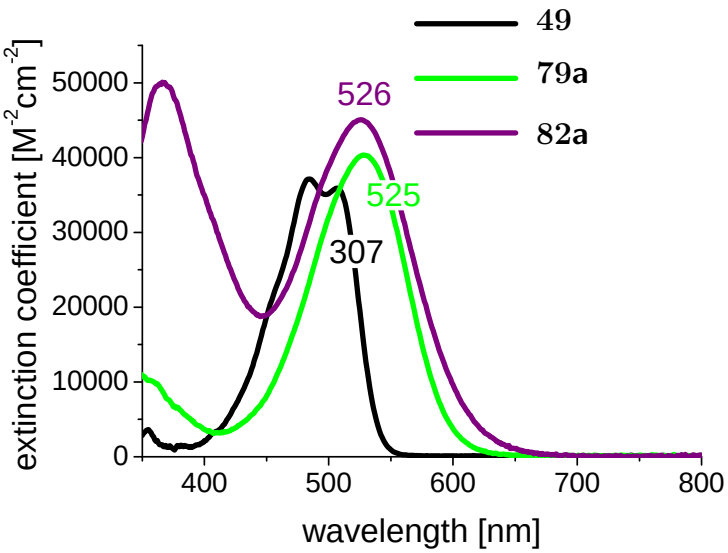

Figure 3.2: Change in absorption (in dichloromethane) during synthesis

It is in fact a strong push-pull effect which is desirable for broad absorption and which has been a basic concept in many donor-acceptor sensitisers. A strong vectorial excitation from the donor to the acceptor supports efficient charge separation. Insertion of a π-spacer leads to stronger orbital partitioning (OP), impeding the recombination of electrons in titanium dioxide with holes located on the dye molecules.[111] In fact, quantum mechanical calculations show that for compound **83** as well as **84** the LUMO is mainly located on the naphthalene and perylene core, respectively. The HOMO, on the other hand, can be found mainly on the donor moiety which is fully conjugated via the thiophenes. Both HOMO and LUMO also extend to the terthiophene spacer connecting the donor and acceptor. Considerable decoupling can be observed, however, still allowing communication between the donor and acceptor.

Concerning the absorption characteristics, in solid state **83** appears dark purple, **84** brownish-orange to the human eye. Their solution colours are violet and yellow, respectively (figure 3.5 on page 65). The absorption spectra of both dyes are displayed in figure 3.3 on page 63. **83** shows a very broad absorption over the whole visible region with two strong absorption bands, one band around $\lambda = 365$ nm and a strong band resulting from the π-π^* transition of the PMI derivative at $\lambda = 527$ nm with an extinction coefficient of roughly 35.000 $M^{-1}cm^{-1}$. **84** on the other hand shows

Structure	HOMO	LUMO	
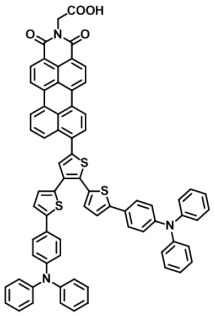 **83**	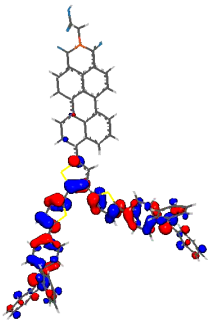	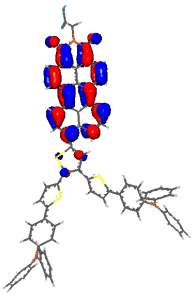	IP: 4.97 EA: 3.26 S1: 737 nm S2: 655 nm S3: 549 nm S4: 504 nm f1: 0.42 f2: 0.19 f3: 0.75 f4: 0.55
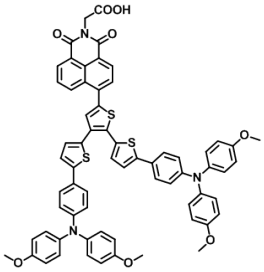 **84**	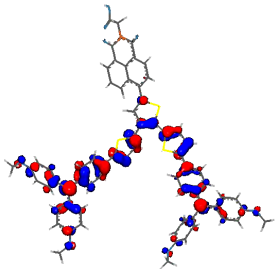	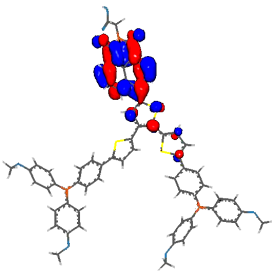	IP: 5.76 EA: 2.97 S1: 687 nm S2: 631 nm S3: 517 nm S4: 491 nm f1: 0.22 f2: 0.24 f3: 0.50 f4: 0.39

(DFT; performed by BASF SE)

Table 3.1: Calculated orbital surfaces, ionisation potential (IP), electron affinity (EA), transitions (S) and oscillator strengths (f) of compound **83** and **84**

mainly one strong band with an ϵ of around 48.000 $M^{-1}cm^{-1}$ in the visible region with an absorption maximum of λ_{max} = 378 nm. Moreover a weak charge transfer band around λ = 500 nm reaching out to 600 nm can be observed. The DFT-calculations expect much stronger charge transfer for both compounds, predicting the S1 transition at 737 nm with an f1 = 0.42 for **83** and at 687 nm with and f1 = 0.22. The absorption band with λ_{max} = 527 nm in compound **83** is most probably the S3 transition at 546 nm and f3 = 0.75 nm.

Both dyes were incorporated in sDSSCs following the same procedure (details provided in chapter 2 and the experimental part). The absorptivity on titanium dioxide as well as the EQEs show a clear superiority of the perylene sensitiser in the visible region relevant for the cell performance. Whereas **84** reaches a top EQE value of 42 % at 420 nm and dropping steadily with longer wavelength, **83** shows EQE values of

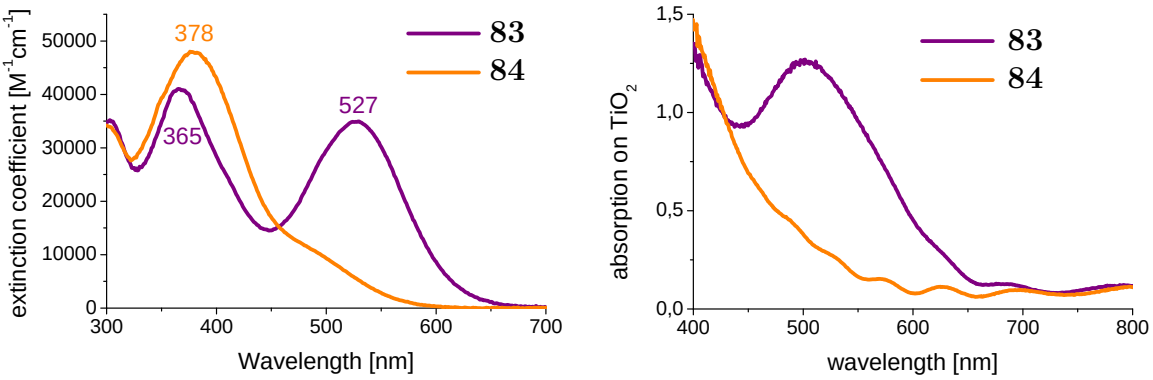

(a) Solution absorption (b) TiO_2 absorption

Figure 3.3: Absorption spectra of the two dyes in dichloromethane solution (a) and on titanium dioxide (b)

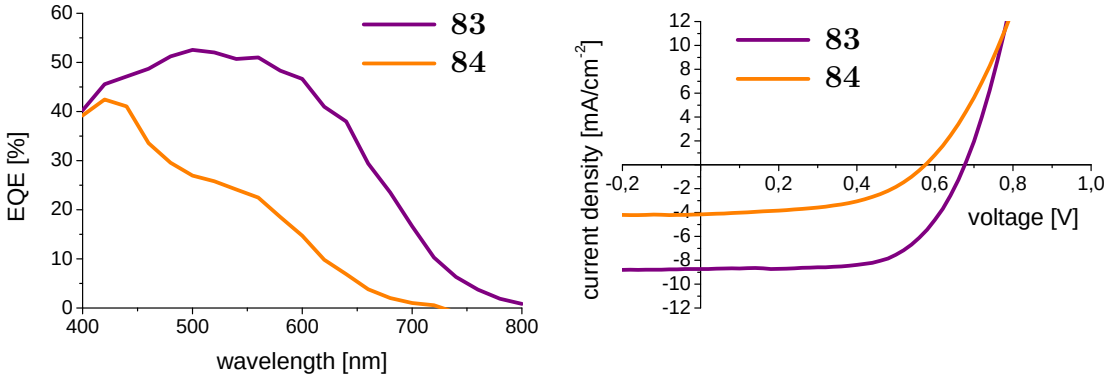

(a) EQE (b) IV

Figure 3.4: EQE (a) and I-V curves of the two dyes (b)

around 50 % (top EQE of 52% at 470 nm) from 460 to 580 nm and values of over 40 % from 400 to 630 nm. Moreover the EQE curve of **83** reaches out to 800 nm, roughly 100 nm more bathochromic than the one of **84**. Integration of the EQE spectra results in current densities of 8.6 $mAcm^{-2}$ for **83** and 3.7 $mAcm^{-2}$ for **84**, in good agreement with the I/V measurements.

As for the application in DSSC, not only the absorption of the dyes but also their energy levels play an important role in determining the efficiency. The energy levels of the HOMO and LUMO, i.e. the ionisation potential and the electron affinity, were calculated by Density Functional Theory (details provided in the experimental part) and afterwards determined by cyclic voltammetry. Theoretical predictions for **83** gave an energy level of -5.0 eV for the HOMO and -3.6 for the LUMO, cyclic voltammetry measurements in dry dichloromethane with 0.1 M tetrabutylammonium hexafluorophosphate as the supporting electrolyte resulted in -5.0 eV and -3.5 eV, respectively. For **84**, the calculated HOMO level energy was -4.7 eV and the LUMO level

Dye	λ_{max} [nm]/ ϵ [$M^{-1}cm^{-1}$]	LUMO*/ HOMO*/ bandgap [eV]	EQE_{max} [%]	V_{OC} [mV]	I_{SC} [$mAcm^{-2}$]	FF [%]	η [%]
83	365/41,033 527/34,881	-3.5/ -5.0/ 1.5	52	680	-8.7	63	3.8
84	378/47,967	-3.1/ -4.9/ 1.8	42	580	-4.2	51	1.2

*determined by cyclic voltammetry

Table 3.2: Photovoltaic performance of the perylene monoimide and naphthalene monoimidewith dendron spacer and triphenylamine donor

energy -3.0 eV. Again we can see good coherence with the values determined via cyclic voltammetry: -4.9 eV (HOMO), -3.1 eV (LUMO). This corresponds to 0.6 V (HOMO) and -0.9 V (LUMO) for **83** and 0.5 V (HOMO) and -1.3 V (LUMO) for **84** vs. NHE. Comparing the reduction potentials of **83** and **33** ID176 in solution, the LUMO of **83** is considerably higher than for **33** (ID176) (LUMO: -0.68 V vs. NHE). As the energy of the conduction band of titanium dioxide is approximately at -0.5 V vs. NHE the driving force of electron injection is roughly 0.4 eV for the perylene derivative **83** and 0.8 eV for the naphthalene derivative **84**. Thus the driving force lies well above the desired minimum driving force of 0.2 eV for efficient electron injection.[28] The ionisation potential of the hole transporting material spiro-MeOTAD -4.77 eV in vacuum[100] is above the HOMO values of both dyes, thus allowing efficient dye regeneration.

Considering the electrochemical properties, the naphthalene sensitiser **84** with its higher LUMO has the potential for much better electron injection, however, does not reach an efficiency as high as the perylene sensitiser **83**. One reason for this could be the lower driving force for the dye regeneration. Another cause can surely be found in the additional light harvesting of **83**. Even though the absorptivity for **84** in the region of 320-460 nm is higher **83** harvests and converts more sunlight through its additional absorption band in the visible region which - bearing in mind the solar spectrum - is of greater importance for photovoltaics than the UV region. This effect can already be suspected looking at the absorption spectra in dichloromethane or on titanium dioxide, is affirmed by the EQE spectrum and reflected in the I_{SC}. Furthermore also the V_{OC} of **83** and the fill factor (63 % for **83** compared to 51 % for **84**) are higher, resulting in a three times higher efficiency for **83**.

In order to be able to compare the two dyes within the same cell system, a rather low efficiency was presented above for **84**. Using, however, a different additive which

elevates the conduction band of the titanium dioxide, a device of the naphthalene derivative **84** reaching an overall efficiency of 3.3 % could be built. By raising the conduction band of the titanium dioxide, the gap between the conduction band and the valence band of the hole transporting material could be enlarged and a very good open-circuit voltage of 860 mV without losing current (I_{SC} = 5.9 mAcm^{-2}) combined with a fill factor of 64 % could be reached. As a prerequisite for this conduction band tuning a high lying LUMO is needed. According to the cyclic voltammetry and as confirmed in the device using the band-elevating additive that is the case for the naphthalene dye **84**. For compound **83**, however, using the same additive results despite an increased open-cirucit voltage of 780 mV and a similar fill factor (53 %) in a loss of current (I_{SC} of 5.1 mAcm^{-2}) and a reduced power conversion efficiency of only 2.3 %. This strong decrease in current implies that injection from the dye to the titanium dioxide was not efficient because of too little driving force. This is again in good coherence with the cyclic voltammetry results, suggesting a considerably lower LUMO level energy for the broad absorbing **83**. These are examples of successful device tuning, addressing and optimising individual performance indicators. Maximum power conversion efficiency is generally achieved with a moderate tuning in order to balance all factors.

Figure 3.5: Solutions of **84** and **83** (from left to right) in dichloromethane

3.3 Conclusion

In summary both dyes within their individual processing were able to reach good photovoltaic performance, 3.3 % being a respectable result for a naphthalene derivative [112] which are generally weaker absorbers than perylenes and 3.8 %, though not as high an efficiency as the ones presented in the preceding chapter, the record efficiency of perylene monoimide solid-state DSSC sensitisers at the time. Key factors in sensitiser design were i) the balance of the orbital energies, ii) colour tuning in order to achieve a broad spectrum with high absorptivity as well as a sound degree of orbital partitioning and iii) the steric demand of the molecule: the two bulky donor groups are expected to shield the hole conductor from the titanium dioxide surface to prevent shunt faults and to prevent aggregation of the dye molecules. With their spacer group and the

two donor moieties these two compounds build a link between the π-spacer perylene monoimides of the preceding and the different donor groups of the following chapter.

Chapter 4

Double Donor Systems

4.1 Introduction

To date, most DSSC sensitisers absorb mainly visible light while about 60 % of the irradiation striking the earth is in the NIR (figure 1.5 on page 10). Designing sensitisers with either more bathochromic absorption for the use in dye cocktails or with broad absorption as single sensitisers is a major challenge. One way to shift absorption to longer wavelengths is to extend the long axis of the molecule to a terrylene core or even further to higher rylene homologues.[113,114,115] Core extension in the *peri*-position of the perylene core and its periphery is a related concept of which examples will be demonstrated in the end of this chapter and the following chapter 5. A second way is increasing the donor concentration in the molecule. Introduction of a second donor group can increase the intramolecular dipole and enhance the charge transfer within the molecule. DFT-calculations[1] predict for example for the two molecules **33** and **85** a dipole of 7.91 Debye for the one *peri*-donor (compound **33**), and 12.43 Debye for the double-*peri*-donor (compound **85**, figure 4.1 on the next page), respectively. This gain in push-pull character should lead not mainly to a bathochromic shift but to a broadening of the absorption, a desirable characteristic of a DSSC sensitiser.

Another potential benefit is an expected increase of the LUMO energy of the dye by the introduction of a second donor on the perylene monoimide core. DFT-calculations of the double-donor analogue of **33**, a perylene monoimide with bis(4-(2,4,4-trimethylpentane-2-yl)phenyl)amine donor in both *peri*-positions, predict a electron affinity of 3.10 eV compared to 3.21 eV for **33**. A higher LUMO energy level would lead to increased driving force for electron injection from the dye into the titanium dioxide conduction band. This had been a crucial shortcoming of the very broadly absorbing and overall efficient 9-functionalised perylene monoimide sensitiser **33**.[79] So, by pursuing a double donor approach, favourable absorption and orbital tuning for sDSSC application could possibly be addressed at the same time.

[1] DFT-calculations performed by BASF SE.

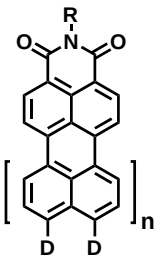

85

R = aryl, alkyl or H
n = 0, 1, 2
D = Donor, e.g. NH_2 or NR_2

Figure 4.1: Structure of desired double donor perylene monoimide

Not only for DSSC applications, the double donor compounds are of interest. For a long time the double-*peri*-functionalisation (compound **85**) has been a target of our group.[116] As a new functionalisation of the well-known perylene monoimide it would open up a path to new pigments and dyes for various NIR applications. In this chapter different attempts to achieve this double-*peri*-functionalised perylene monoimide will be presented. Though the desired product remains out of reach, smaller achievements, e. g. the tetrabromination of perylene monoimide were made. Other double donor systems, in order to prove the concepts described above, were also achieved, giving valuable insights into the chemistry of the yet to be functionalised *edge*-positions (8,11-position) of perylene monoimide.

4.2 Two Potential Routes to a 9,10-Functionalised Perylene Monoimide

One attempt to achieve the target structure was made by Müller[116] who tried coupling 1,8-dinitronaphthalene **87** with *N*-2,6-di*iso*propylphenyl-naphthtalene-1,8-dicarboximide **86** in a one-pot reaction (often used for terrylene synthesis) with 1,5-diazabicyclo[4.3.0]non-5-en (DBN) – however, without success (figure 4.2 on the facing page). Her second attempt was coupling the two components via a palladium-catalysed Suzuki-reaction and a base-induced fusion of the second bond, a method which is often used for building up higher rylene homolouges, e. g. terrylene and quaterrylene. Due to difficult accessability of 4-bromo-1,8-dinitro-naphthalene, 8-amino-4-bromo-1-nitro-naphthalene was used for the Suzuki coupling. Whereas the first step showed good conversion to give **89** together with a homo-coupled side product, the fusion of the second bond remained – even after protection of the free amino group (compound **91**) – unsuccessful.[116] One reason for these fusion failures could be the donor ability of the amino group weakening the acidity of the naphthalene unit which is then not as readily deprotonated in basic conditions. If the arylide anion is not formed, the fusion

cannot occur.

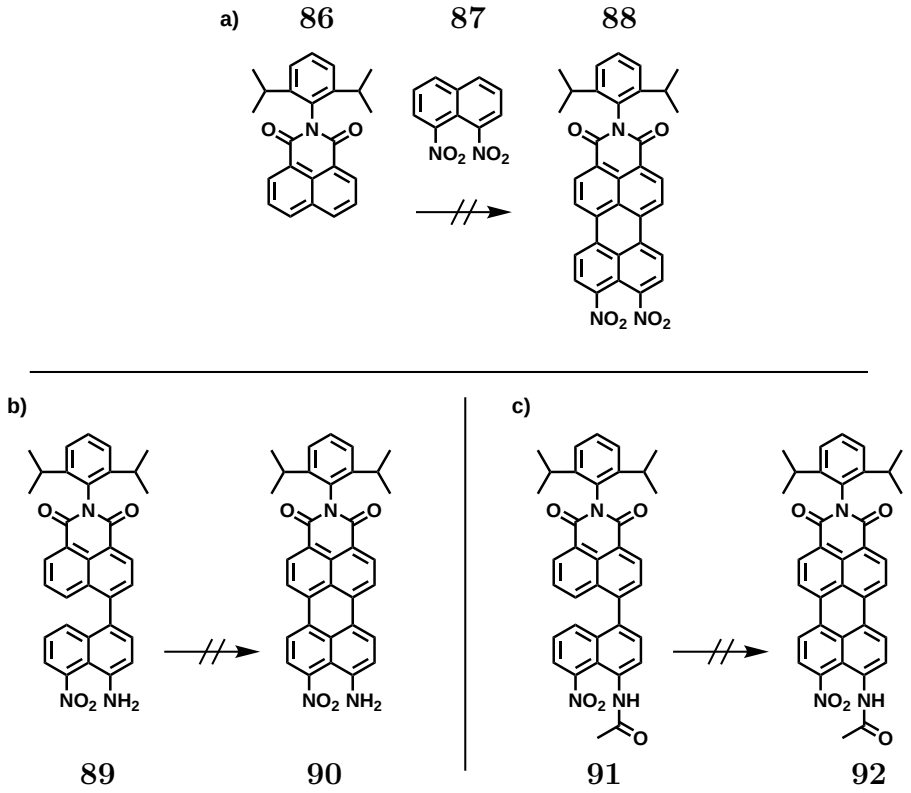

Figure 4.2: Failed fusion attempts to achieve a double-*peri*-functionalised terrylene monoimide

Even though these first attempts (figure 4.2) had failed, the route as such seemed a promising way to build up the desired double-amino-funtionalised structure **85** if the electronic properties of the naphthalene coupling partner could be adjusted. This was done by using a 1,4-bromo-5-nitro-naphthalene **95**, which was prepared by nitration of 1,4-dibromonaphthalene **94**. It was hoped that the neighbouring bromo would help the electron pull of the nitro-group and facilitate the ring fusion. Instead of a naphthalene dicarboximide, it was reacted with a perylene dicarboximide **93** aiming for the terrylene analogue **97** as the terrylene fusion conditions are well elaborated within the group (figure 4.3 on the following page).

As before, Suzuki coupling could be achieved, leading to the product **96** alongside with a homo-coupled side product. But in this case also the isomer of the product (coupling having occurred in the 4-position instead of the 1-position) was formed, lowering the yield to 30%. Unlike before the fusion of the second bond could be achieved, however, only with debromination, thus losing the desired second *peri*-functionality. After various attempts under different conditions [a) DBN, NaO*t*Bu, diglyme, 70°C,

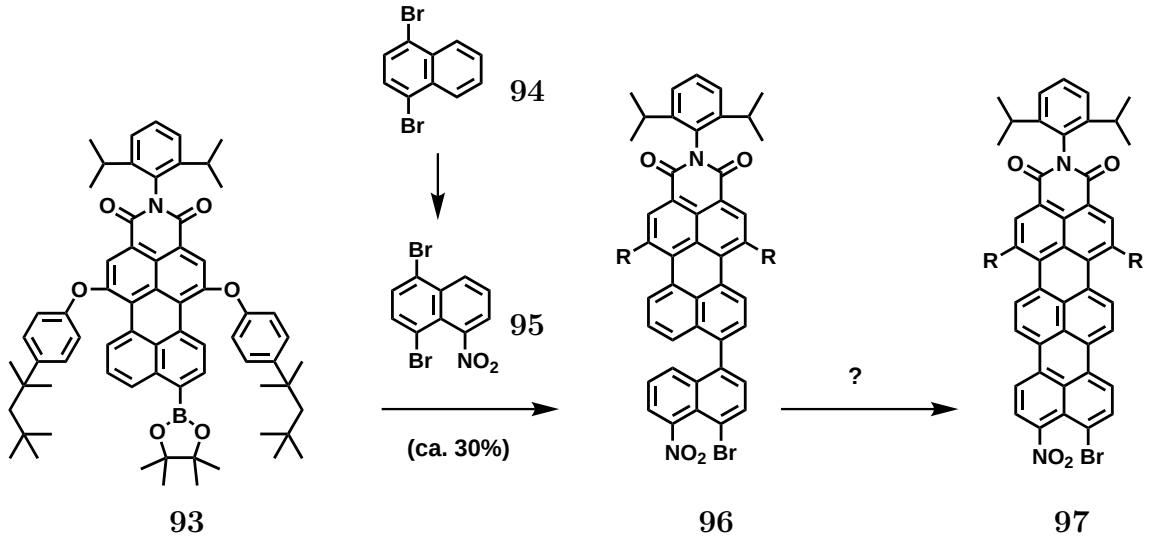

Figure 4.3: Synthesis of a double donor terrylene monoimide via coupling

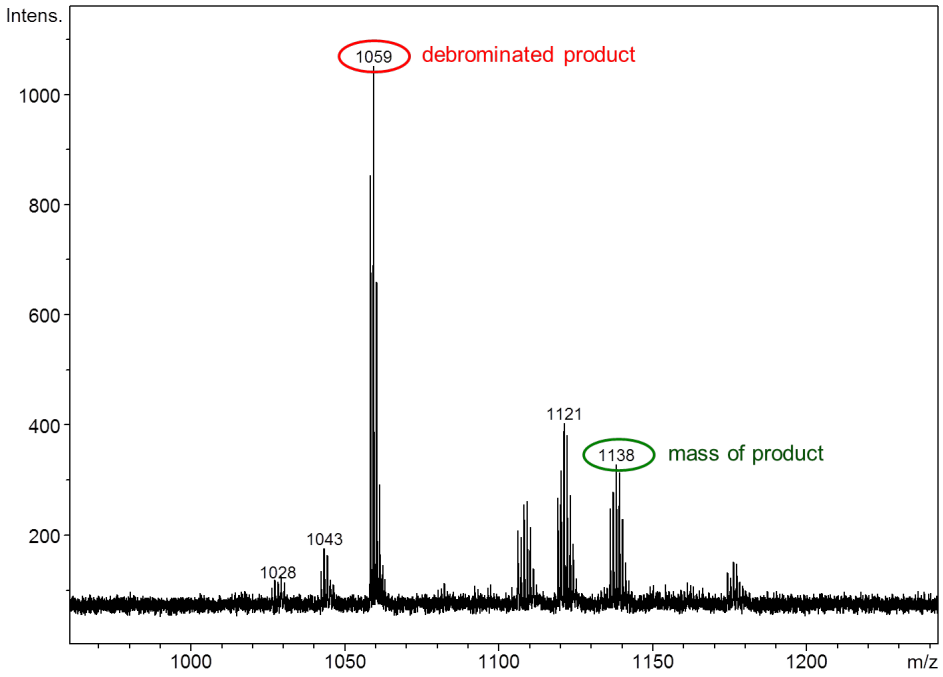

Figure 4.4: MALDI-TOF spectrum of the coupling reaction

2 h; b) $FeCl_3$, $MeNO_2$, DCM; c) ethanolamine, K_2CO_3, 120°C, 2h; d) ethanolamine, K_2CO_3, 160°C, 2h], the product mass (**97**) could be detected in the MALDI-TOF spectrum (figure 4.4 on the preceding page) using the following optimised conditions: DBN, NaOMe, diglyme, 70°C, 2h. The milder base apparently does not completely remove the bromo-functionality. Unfortunately it was not possible to isolate the product in this attempt due to the small quantities used for the test reaction. If the selectivity in the Suzuki reaction cannot be improved, a maximal overall yield of only 10% after ring fusion can be expected as the yields of the fusion are in the range of 35 %.[115] The route was put aside in order to try another route – building up the double-functionality by tetrabromination.

Bromination of the *N*-(2,6-di*iso*propylphenyl)-perylene-3,4-dicarboximide leads to a 9-monobrominated perylene monoimide or a 3,6,9-tribrominated derivative (figure 1.10 on page 15). If bromination is taken further, additional bromination occurs on the phenyl of the imide structure but not, as desired in the 10-position. Further bromination is expected to also occur in the 10-position, however, making subsequent functionalisation unneccessarily complex because of too many reactive sites.

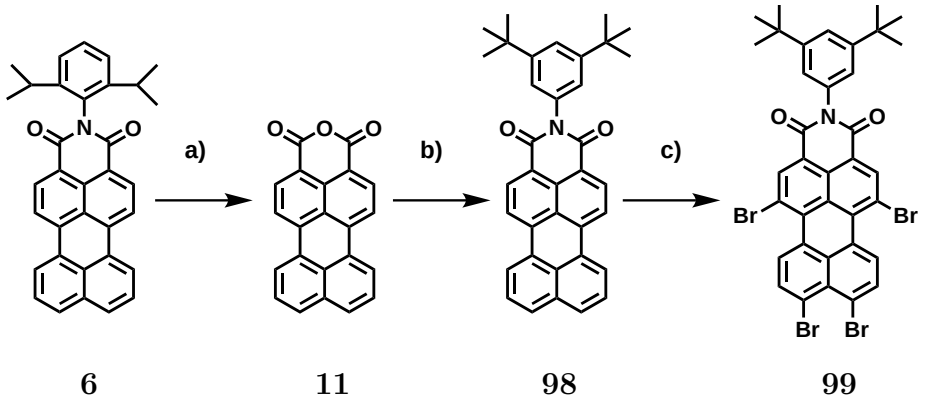

6 **11** **98** **99**

a) KOH, KF, isopropanol, 2-methyl-2-butanol, reflux, overnight; b) 3,5-di-*tert*-butylaniline, propionic acid, 140°C, overnight; yield: 23% c) Br_2, chloroform, rt, overnight, yield: approx. 60%

Figure 4.5: Tetrabromination of a perylene monoimide

In order to prevent this unwanted bromination, the 3,5-positions were blocked by using *N*-(3,5-Di*iso*butylphenyl)-perylene-3,4-dicarboximide **98** for the bromination reaction (figure 4.5). The perylene monoimide **98** was achieved by saponifying the standard *N*-(2,6-di*iso*propylphenyl)-perylene monoimide **6** and reacting the resulting perylene monoanhydride **11** with 3,5-di-*tert*-butylaniline. PMI **6** was saponified with KOH and KF in a mixture of isopropanol and 2-methyl-2-butanol under reflux overnight. The solvent was removed under reduced pressure and the reaction mixture stirred in acetic acid and subsequently precipitated by adding water. The precipitate was dissolved in hot potassium hydroxide solution and reprecipitated by adding hydrochloric acid. In thin layer chromatography analysis a similarly intense spot of the starting

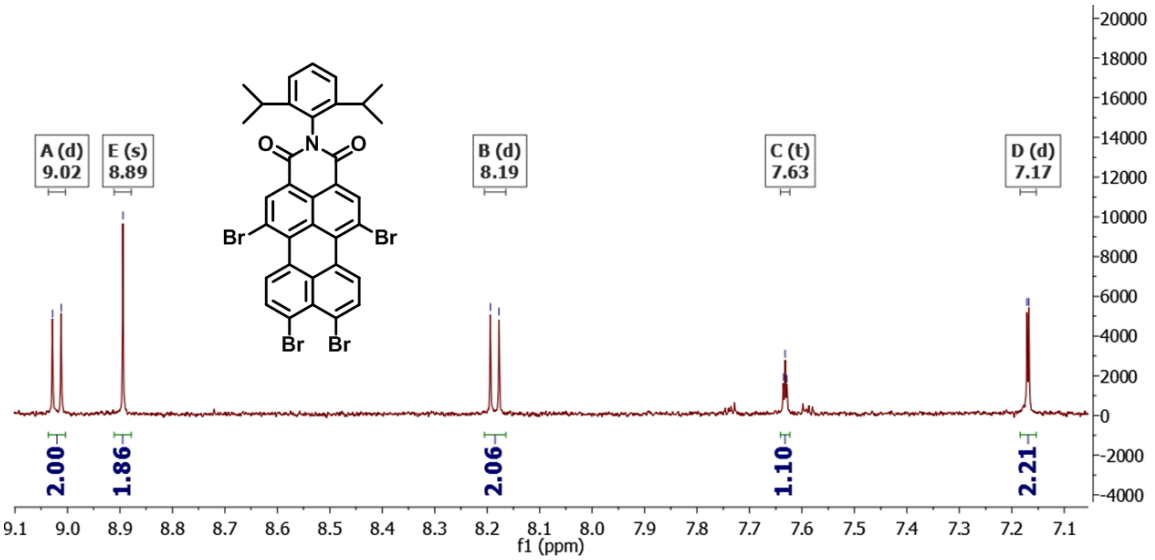

Figure 4.6: ^{1}H-NMR spectrum of the tetrabrominated perylene monoimide

material as the one of the desired product **11** indicated, that the conversion had been rather low (approximately 50%, jugdging by the intensity of the spots). Later on, the reaction and work-up protocol for saponification reactions could be optimised giving yields of 80-95%. These improved conditions (reflux with KOH in 2-methyl-2-butanol overnight) and work-up (precipitation of reaction mixture in acetic acid/ice water mixture, dissolving the precipitate in dichloromethane and after acidification with acetic acid stirring overnight at room temperature) was used for all other saponification reactions presented in this thesis. Chemically, to achieve the desired saponified product, not only the conversion to the dicarboxylic salt is important, but also the ring closure to form the anhydride. This ring closing requires some time and is much more effective in the acidified dichloromethane solution than in the precipitation before. Moreover, pure 2-methyl-2-butanol with its higher boiling point than isopropanol allows an increased reflux temperature facilitating the reaction and improving the solubility of the starting material. Nevertheless, for the synthesis of **98**, the only partially saponified product was used for the imidisation with 3,5-di-*tert*-butylaniline in propionic acid at 140°C overnight. Due to the low quality of the anhydride, only 23% of the desired imide **98** could be achieved. The imide **98** was purified via column chromatography on silica gel with dichloromethane. For bromination 80 mg of **98** were dissolved in chloroform and a large excess of bromine was added. For tri-bromation the reaction is generally stopped after 6 hours to avoid overbromination. Here the reaction was left to stir at 60°C overnight. In thin layer chromatography analysis three different spots with very similar retention factors in various eluents could be identified. With help of mass spectrometry of different mixed fractions seperated by preparational thin layer chro-

matography, these spots could be assigned to tri-, tetra-, and five times bromination. Full separation in order to determine the individual yields of the different bromination products was not possible due to their very similar properties. Judging from the colour intensities of their spots on thin layer chromatography the main product was tetrabromination with approximately 60%, the other side-products yielding ca. 20% each. For proof of concept, however, evidence was needed that the tetrabromation actually did occur in the second *peri*-position. It was possible to separate around 2 mg for that with analytic high pressure liquid chromatography allowing to record the ^{1}H-NMR spectrum presented in figure 4.5 on page 71, clearly showing the symmetry of the tetrabrominated product and proving that for the fourth bromination the 10-position was favoured.

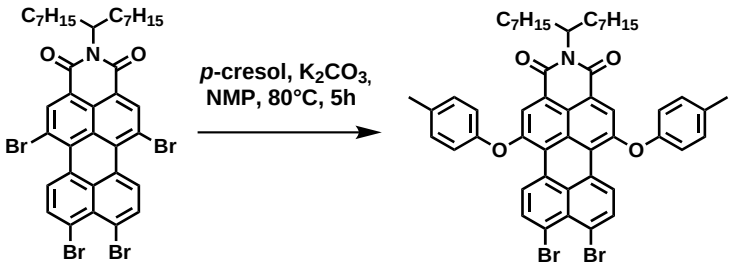

100 **101**

Figure 4.7: Phenoxylation of tetrabrominated perylene monoimide

Hoping for a more convenient purification, the tetrabromination was repeated using 500 mg of the C_7-swallow tail perylene monoimide which due to the long alkyl chains possesses an enhanced solubility, as well as being less prone to over bromination compared to a phenyl in the imide structure. Again, thin layer chromatography as well as FD-mass spectrometry showed tri-, tetra- and five times bromination, this time, however, showing mainly tri- and tetra-bromination (each approximately 40%, the larger scale probably being the reason for slower conversion. Controlling the reaction time therefore seems a feasible means to reduce five times bromination.

In a third reaction 800 mg of the C_7-swallow tail perylene monoimide were brominated, this time, however, at room temperature, hoping to fully avoid the five times bromination and facilitate purification. Unfortunately this was unsuccessfull, the five times bromination occuring just as readily at room temperature. Despite the solubilising C_7-chains, purification via column chromatography on silica gel proved to be difficult. Again, full separation could not be achieved but a fraction of 280 mg containing mainly the tetrabrominated species according to thin layer chromatography and FD-mass spectral data could be isolated. This was used for the phenoxylation reaction described in figure 4.7, aiming for selective substitution in the *bay*-positions **101** which – from the 1,6,9-tribromo-perylene monoimide – are known to be the more reactive sites. However, in this case, it seems that the *peri*-positions reacted just as willingly,

as several products could be identified with more than one of them showing a mass consistent with a di-substituted product. Taking into account that the 10-position was the last to be brominated, this is not surprising, the isomers probably being the 1,9-phenoxylated, the 1,10-phenoxylated, and possibly also the 1,6-phenoxylated product. Separation of the different products proved very difficult, and the synthesis route was given up.

By carrying out the tetrabromination two key ideas had been explored. One was to prove that this symmetric double bromination in the *peri*-position can actually occur. This was successfully proven. The other was to then take the synthesis further and try and introduce two donor moieties in the 9,10-position. Due to its complex intermediates this approach no longer seemed an efficient route to a double-*peri*-functionalised perylene monoimide **85**.

4.3 8,11- and 8,10-Functionalised Perylene Monoimide

Whilst at fist glance seeming straightforward, both routes towards the double-*peri*-functionalised perylene monoimide **85** – building up via coupling and functionalisation via tetrabromination – were not successful. Considering the original motivation for this work and hoped-for characteristics of this double donor, it was now logical to think about new structures which might offer the same or similar benefits, but which are synthetically better accessible.

One target structure was an 8,11-functionalised perylene monoimide (**106**), the 8,11-positions from here on also called "*edge*-positions". To date, these positions had never been functionalised as they had never been accessible by standard methods of substitution like halogenation. After Nakazono et al.[53] published a ruthenium-catalysed direct alkylation of PDI in the 2,5,8,11-positions, Battagliarin opened up a new area of functionalisation in our group by first ruthenium-catalysed borylation and halogenation of the 2,5,8,11-positions of perylene diimide[56,57] along with the iridium-catalysed borylation of the *edge*-positions of perylene monoimide and their subsequent conversion into chloro or bromo moieties.[2]

Looking back at the desired electronic characteristics, an 8,11-functionalised perylene monoimide would fulfill the requirements of higher donor concentration in one molecule and could possibly generate a higher LUMO-level, which is beneficial for efficient electron injection into a metal oxide electrode. Weak conjugation of the donors through the *meta*-like *edge*-positions will, however, not induce the strong desired bathochromic shift of the absorption. Last but not least the functionalisation

[2]Further details will be presented in his forthcoming thesis.

of the *edge*-positions will result in a sterically more demanding structure. This can be advantageous in a dye-sensitised solar cell as the bulky groups separate the dye molecules from each other, preventing aggregation of the perylene cores and thus unwanted intermolecular electron transfer.[49] It could at the same time be a disadvantage, lowering the overall dye concentration on the titanium dioxide surface, leading to less light harvesting[27], one major expected advantage of the slim and well-coupled double-*peri*-functionalised molecule.

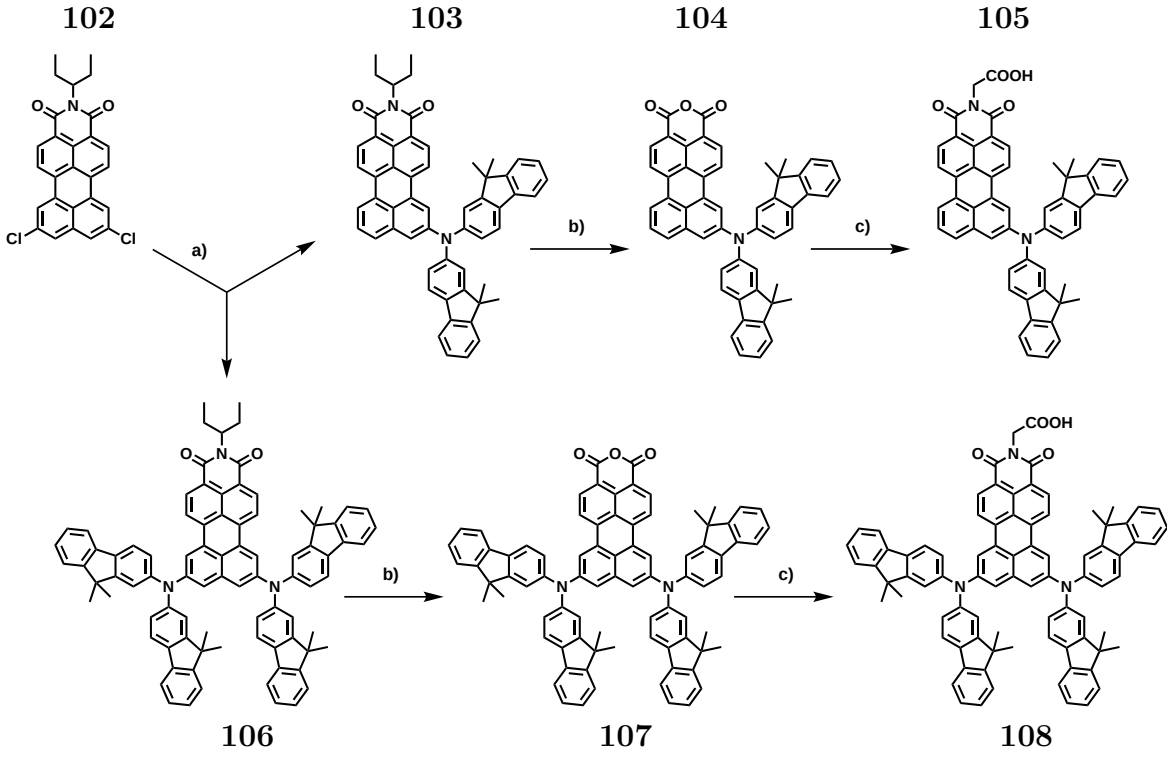

a) Bis-(9,9-dimethylfluorene-2-yl)-amine, caesium carbonate, $Pd_2(dba)_3$, BINAP, toluene, 100°C, 16 h; yield: 15 % (**103**), 5 % (**106**); b) KOH, 2-methyl-2-butanol, 1,4-dioxane, reflux, overnight, yield (crude): 96 % (**104**); 94 % (**107**); g) glycine, imidazole, 140°C, overnight, yield: 87 % (**105**); 85 % (**108**)

Figure 4.8: Synthesis of the 8- and 8,11-donor functionalised sensitisers **105** and **108**

.

The 8,11-functionalised perylene monoimide was synthesised according to the scheme presented in figure 4.8. Compound **102** prepared by [redacted][3] was reacted under Buchwald conditions with the fluorenyl-amine donor to give **106**. As a side product, mono-functionalised perylene monoimide **103** was obtained. The yields of 5 and 15 % are rather low. This is due to the unexpected 9- and 8,10-functionalised side products (figure 4.9 on the next page) which will be discussed in more depth further on. After isolation of **106** and **103** via column chromatography on silica gel and gel permeation chromatography the two compounds were saponified individually. As both compounds showed very low solubility, 1,4-dioxane was added to the 2-methyl-2-butanol in a ratio

[3]Details on the synthesis will be presented in his forthcoming thesis

of (1:2). In the following imidisation step the anchoring group was introduced. Overall, 80 mg of **105** and 45 mg of **108** were synthesised for device testing.

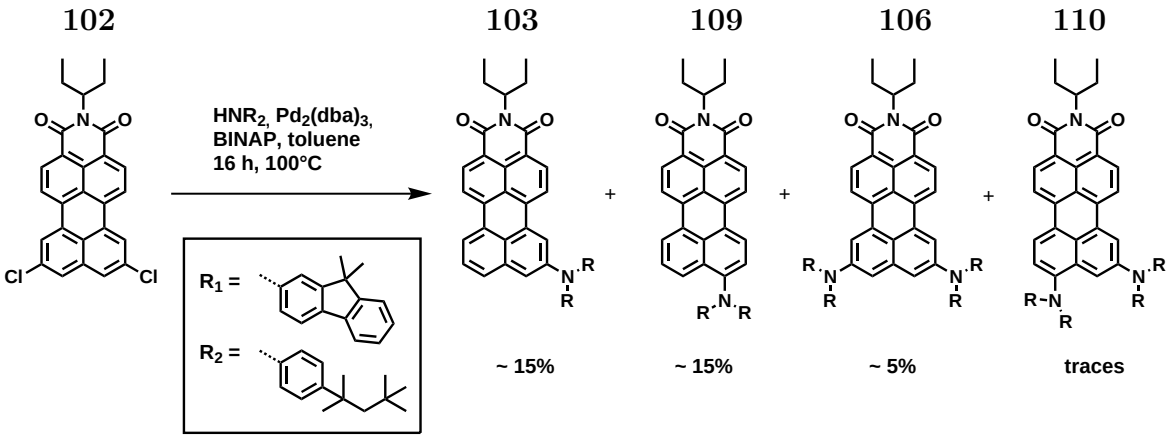

Figure 4.9: Direct coupling of 8,11-dichloro-perylene monoimide leads to functionalisation of the 8-, 8,11-, 9- and 8,10-position (**103**-**110**)

One step towards a slimmer molecule is the synthesis of the 8,10-difunctionalised perylene monoimide (**110**), also bearing the advantage of having one donor group in a *peri*-position and hence in strong conjugation with the perylene core. One way to a 8,10-functionalised perylene monoimide was the already above mentioned unexpected side reaction of a 8,11-dichloro-perylene monoimide[4] **102** with bis-(9,9-dimethylfluorene-2-yl)-amine under Buchwald conditions shown in figure 4.9. Here, formation of the 8,10- (**110**) (see ^{1}H-NMR and ^{1}H,^{1}H-NOESY spectra of **122** in figure 4.13 on page 79 for proof of structure) and 9-functionalised (**109**) as well as 8,11- ((**106**)) and 8-functionalised (**103**) perylene monoimide could be observed. These products arise from an unexpected shift in the functionalisation position. Various 1,4-palladium induced migrations are known in literature;[117] 1,2-migrations, however, are rare.[118]

The mechanism was not fully investigated but an aryne mechanism could be supposed. It was observed, that the palladium catalyst is still playing a key role, as there is no conversion without it. However, if a dibromo-perylene monoimide is used instead of the dichloro-perylene monoimide, less shifting was observed. It may be the case, however, that bromine, being more prone to oxidative addition than chlorine, chooses mainly the first intended Buchwald mechanism whereas the chlorine derivative partially undergoes a competing aryne-based mechanism. That said, a similar aryne-based mechanism for a palladium-catalysed coupling was presented by Worlikar and Larock[118]. Moreover, reaction with bis(4-(2,4,4-trimethylpentane-2-yl)phenyl)amine instead of the bis-(9,9-dimethylfluorene-2-yl)-amine showed higher shares of the shifted products, suggesting, that the size of the amine may also play a role. Without addition of the palladium catalyst, the reaction does not start at all, confirming that the

[4]Details will be presented in the forthcoming thesis of [redacted].

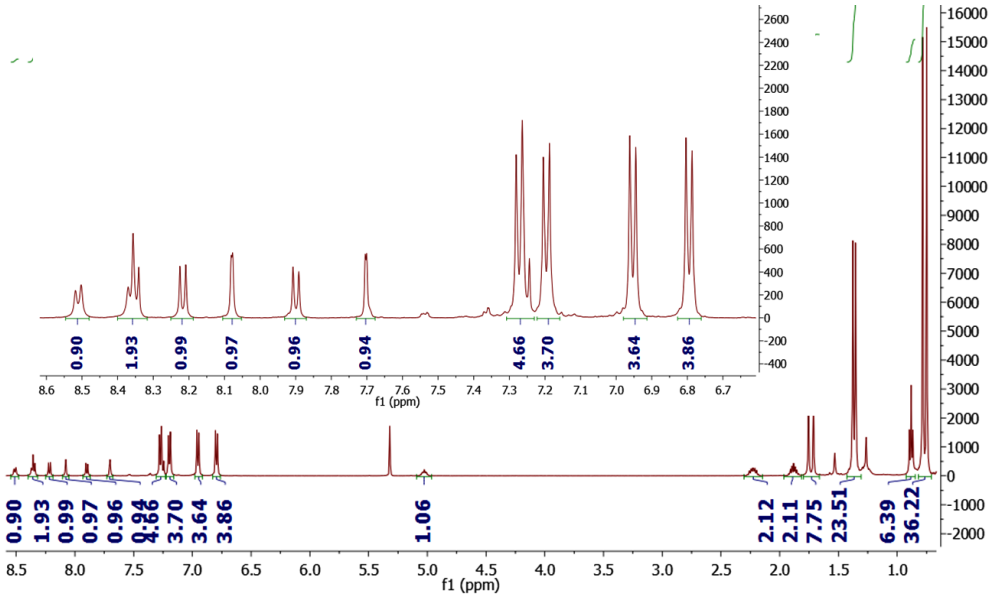

500 MHz, DCM, 298 K

Figure 4.10: ^{1}H-NMR of **122**

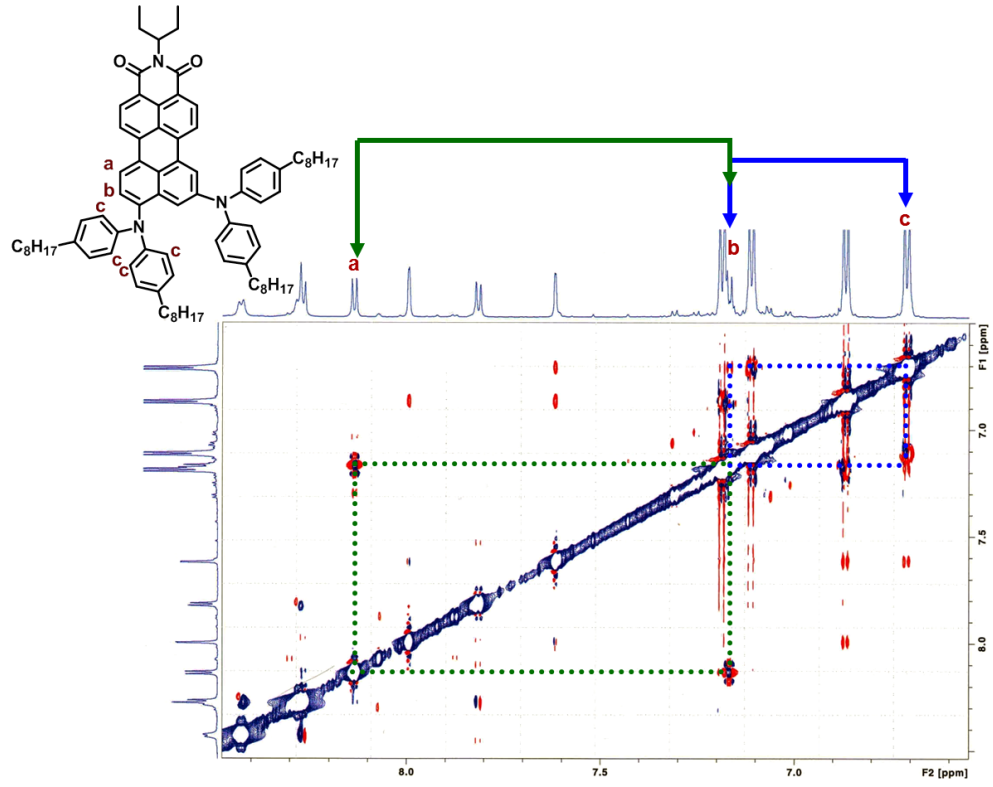

500 MHz, DCM, 298 K

Figure 4.11: ^{1}H,^{1}H-NOESY of **122**

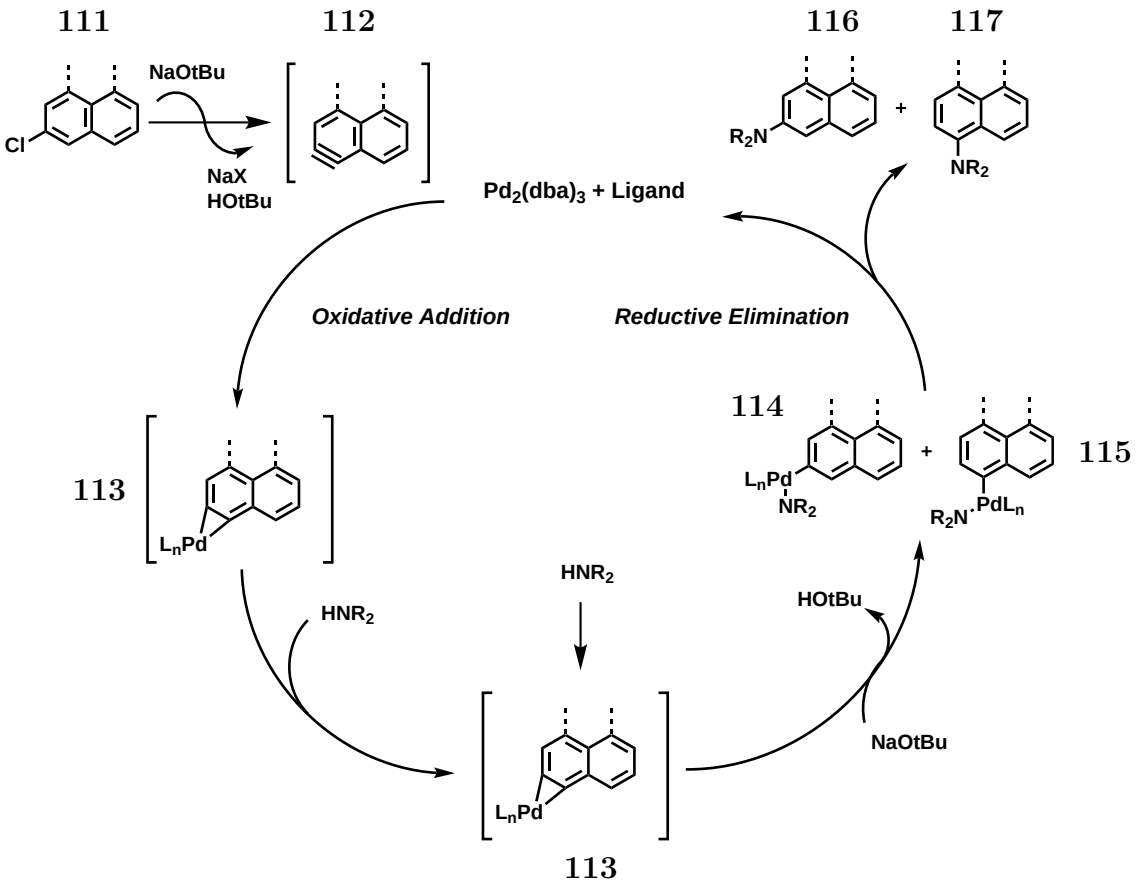

Figure 4.12: Suggested aryne-mechanism for a palladium-catalysed reaction inducing 1,2-migration

catalyst must be involved in the mechanism.

The suggested aryne-Buchwald mechanism described in figure 4.12 starts with the abstraction of HCl due to the base sodium NaO*t*Bu, forming HO*t*Bu and NaCl and leaving an aryne-type bond on the perylene core (**112**). This step is followed by insertion of the palladium forming a three-membered cycle with the former aryne carbon atoms (**113**). The mechanism described so far follows that described by Worlikar and Larock[118]. However, at this point in the process, the generally known Buchwald mechanism proceeds instead of a halogen insertion. The lone pair of the amine coordinates with the palladium and then may break either bond of the three-membered cycle (**114** and **115**), leading to two isomeric products (**116** and **117**) after reductive elimination. This *shift reaction* leads to four different products (**103**-**110**) which may be separated only with great effort, and yield only a small amount of the asymmetric double-donor perylene monoimide.

Another way to build up the 8,10-functionalised perylene monoimide (**122**) deliberately is by borylating the 11-position (*edge*-position) of a 9-functionalised perylene monoimide to yield (**120**), substitution with bromo (**121**) and a subsequent Buchwald coupling. This route, though considerably longer, is much simpler in its purification of the desired 8,10-functionalised compound **122**. Moreover, this stepwise synthesis route

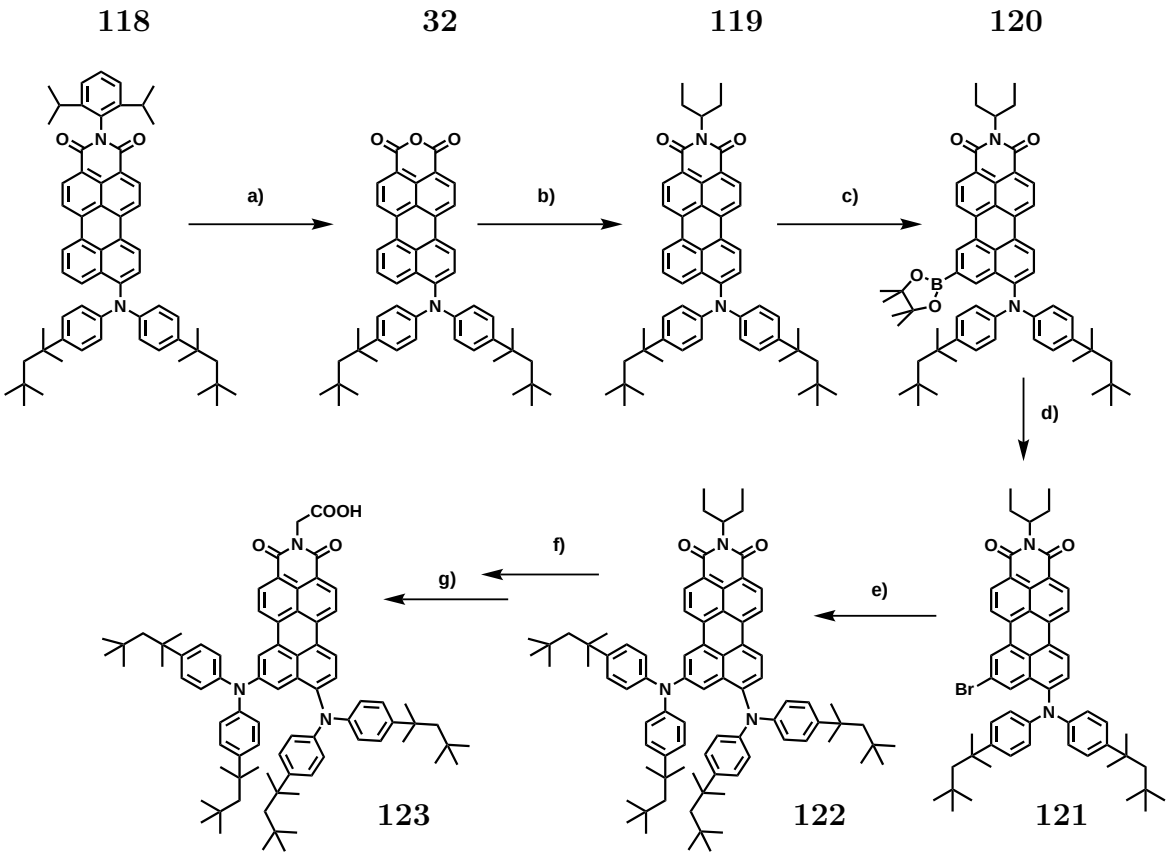

a) KOH, 2-methyl-2-butanol, reflux, overnight, yield: 96 %; b) pentan-3-amine, imidazole, 140°C, overnight, yield: 91 %; c) $[Ir(OMe)COD]_2$, dtbpy, THF (dry), 60°C, overnight, conversion: approx. 50 %; d) $CuBr_2$, dioxane, methanol, water, 120°C, overnight; e) bis-(4-(2,4,4-trimethylpentane-2-yl)phenyl)-amine, NaO*t*Bu, $Pd_2(dba)_3$, tri-*tert*-butylphosphine, toluene, 80°C, overnight; yield: approx. 35 % f) KOH, 2-methyl-2-butanol, reflux, overnight, yield (crude): 93 %; g) glycine, imidazole, 140°C, overnight, yield: 90 %

Figure 4.13: Route to build up an 8,10-functionalised perylene monoimide (**123**)

also bears the great advantage of allowing the introduction of different donor groups in the two positions. An important prerequisite in general for the second iridium-catalysed borylation is the absence of another reactive site for borylation on the donor and imide structure, nameley a sterically unhindered proton with neighbouring protons in the α- and α'-position.

The borylation step is the bottleneck of the synthesis, not so much due to major side reactions but because of rather low conversion (about 50 %). In order to achieve good solubility of the perylene monoimide in the reaction mixture, tetrahydrofuran was used as the solvent. Ishiyama et al. who presented this borylation reaction on smaller aromatic systems reached yields of up to 90 %. Moreover, they state, that the polarity of the solvent has a strong influence on the reaction speed, unpolar solvents leading to a higher reactivities.[119,120] Maybe by changing the solvent to a less polar one, better conversion could be reached despite a loss in solubility. In fact, the borylation of the

naked perylene monoimide in both *edge*-position shows nearly quantitative conversion[5]. The non-borylated compound, however, does not interfere with the next two steps and can be retrieved in the purification step after the Buchwald reaction. The conversion to bromo was done without separation of starting material and product. In the conversion reaction to bromo deborylation is the main risk, which can be confined by using excess $CuBr_2$ (5 equivalents). This step was purified only roughly by column chromatography. Due to very similar retention of the brominated compound **121** and the initial starting material **118** full separation would have been rather inefficient. After the subsequent Buchwald amination, **118** could be separated from the product **122** via column chromatography on silica gel with a mixture of dichloromethane:petrol ether (2:1). As the starting material was a mixture of **118** and **121**, the yield for this step can only be estimated and is about 35 %. On thin layer chromatography, however, no other major side product besides **118** could be detected. Saponification and imidisation to obtain the final product **123** were carried out according to the established protocol without any difficulties and an overall yield of 84 % for the two steps.

Using the route described in 4.13 on the previous page, 95 mg of the final sensitiser **123** were prepared, the overall yield of the route being approximately 10-15 %. Optimisation of the borylation step as described above would certainly leverage this route.

The absorption spectra of both **123** and **108** are shown in figure 4.14 on page 82. For comparison, the absorption spectra of **33** as a 9-functionalised and of **105** as an 8-functionalised dye have been added. The different donor groups only affect the absorption in the short wavelength region up to 400 nm. As the designated application of these compounds are dye-sensitised solar cells, the light between approximately 300 and 400 nm will be absorbed by the titanium dioxide, meaning the impact of the donor groups can be neglected in this discussion.

The rather broad intramolecular charge transfer (ICT) band with a maximum at 580 nm and a molar extiction coefficient (ϵ) of 20.942 $M^{-1}cm^{-1}$ visible in **33** is hardly recognisable for the 8-functionalised perylene monoimide **105**, only a shoulder of low intensity reaching out to 650 nm can be detected. Instead compound **105** shows a more blue shifted intense band which can be assigned to the π-π*-transition with a maximum at 484 nm molar ϵ of 26.991 $M^{-1}cm^{-1}$. In this range, **33** shows only weak absorption. The absorption range of this short-wavelength band for **105**, as well as the weakly developed fine structure, resemble the unsubstituted perylene monoimide (λ_{max} = 507 nm, ϵ = 35.000 $M^{-1}cm^{-1}$, see figure 2.3 on page 35 and 3.2 on page 61). This is not surprising as the *edge*-positions are only in weak conjugation with the acceptor system due to the *meta*-analogue postion. The tailing of the absorption in the range of 550-650 nm, however, can be attributed to some charge transfer within the molecule. This weak

[5]Details will be provided in the forthcoming thesis of [redacted].

Dye	Structure	HOMO	LUMO	
105	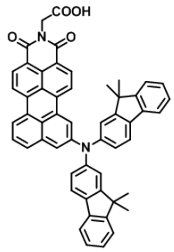	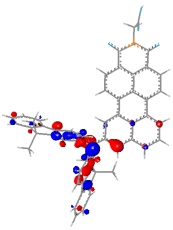	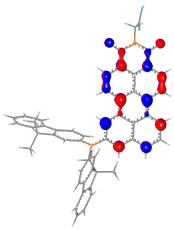	IP: 5.29 EA: 3.20 S1: 691 nm S2: 496 nm f1: 0.02 f2: 0.62
108	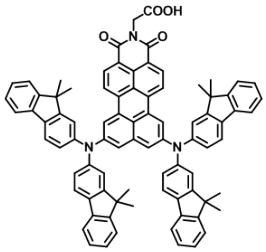	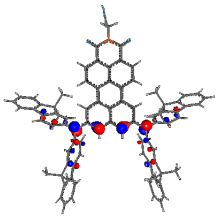	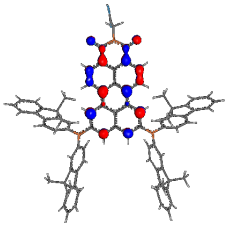	IP: 5.16 EA: 3.22 S1: 697 nm S2: 682 nm S3: 495 nm f1: 0.05 f2: 0.03 f3: 0.59
123	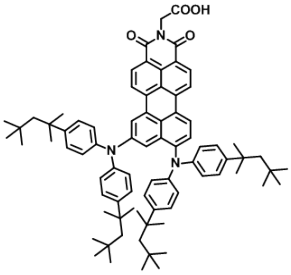	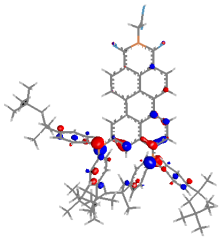	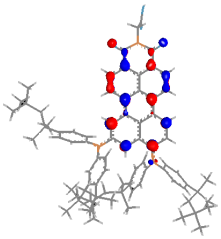	IP: 5.10 EA: 3.15 S1: 676 nm S2: 595 nm f1: 0.24 f2: 0.21
33	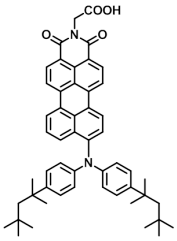	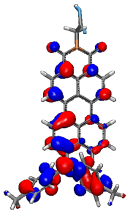	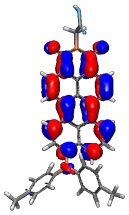	IP: 5.52 EA: 3.21 S1: 602 nm S2: 465 nm f1: 0.52 f2: 0.25
129	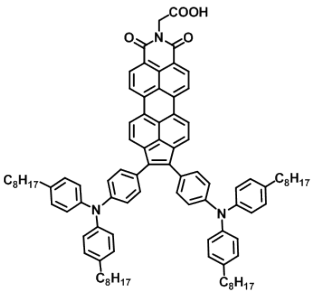	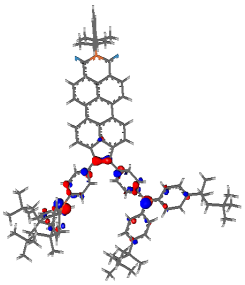	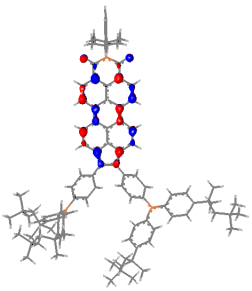	IP: 4.89 EA: 3.46 S2: 772 nm S4: 537 nm f2: 0.34 f4: 0.76

(DFT; performed by BASF SE)

Table 4.1: Calculated orbital surfaces, ionisation potential (IP), electron affinity (EA), transitions (S) and oscillator strengths (f) of compound **105**, **108**, **123**, **33**, and **129**

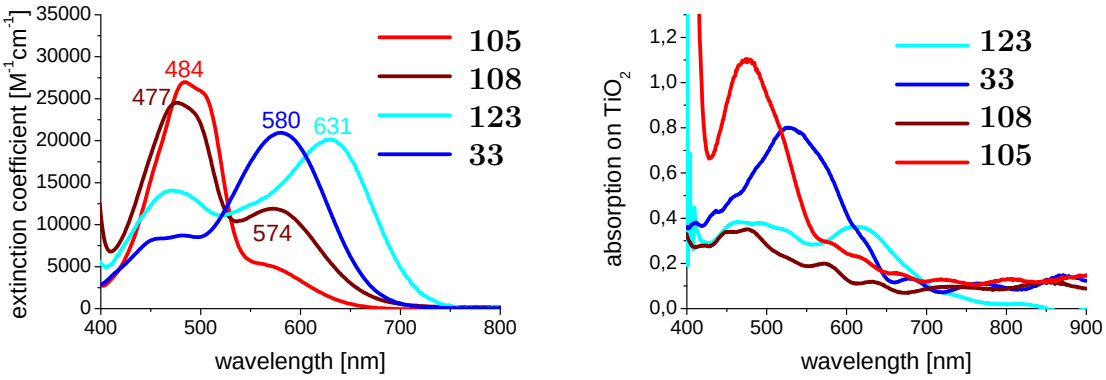

(a) Solution absorption (b) TiO_2 absorption

Figure 4.14: Absorption spectra of the 9-, 8-, 8,11-, and 8-10-functionalised perylene monoimides (**33**, **105**, **108**, and **123**) in dichloromethane (a) and on titanium dioxide (b)

communication between the donor in the *edge*-position and the perylene monoimide core is confirmed in the localisation of the HOMO and LUMO coefficients according to DFT-calculations which show strong orbital partitioning (table 4.1 on the previous page). As already discussed in chapter 2 on page 31, the HOMO and LUMO of **33** are strongly coupled. The predicted spectrum of **105** is, in general, in agreement with the experimental one. The low intensity band can be assigned to the bathochromic S1 transition, the high intensity to the S2 transition around 496 nm. With an f1 of 0.02, however, the calculation underestimates the charge transfer intensity. As discussed in chapter 2 on page 31, the predictions for **33** are very close to the experimental results.

Introduction of an additional donor in the second *edge*-position (**108**) shows an even stronger hypsochromic shift to λ_{max} at 477 nm and a decrease of the intensity of the π-π^*-transition-band (ϵ = 24.517), with the fine structure now blurred. The charge transfer band is, however, considerably more intense, with a local maximum at 574 nm and ϵ of 11.904 $M^{-1}cm^{-1}$. The double functionalisation, though not showing a strong red-shift leads to a noticeable broadening of the spectrum, which is desirable for the application in organic photovoltaics. The growth of the CT-band is not due to stronger coupling of HOMO and LUMO, but due to the second donor group delivering its share of charge transfer. Like for **105**, the DFT calculations underestimate that charge transfer predicting only a transition at around 495 nm with an intensity of f3: 0.59 (table 4.1 on the preceding page).

A similar bathochromic shift was achieved by the 9-functionalised perylene monoimide **33**, first presented by Li in his PhD thesis in 2008 [87] and discussed in the course of chapter 2 on page 31. Comparing the 8,11-functionalised perylene monoimide (**108**) with **33**, the strong conjugation of the *peri*-position with the acceptor is striking. Not only reaches **33** with a λ_{max} of 580 nm a slightly stronger red-shift but with an ϵ of

Dye	λ_{max} [nm] / ϵ [$M^{-1}cm^{-1}$]	LUMO [eV]	HOMO [eV]	bandgap [eV]
105	484 / 26,991	-3.7	-5.0	1.2
108	574 / 11,904	-3.5	-5.1	1.6
	477 / 24,517			
123	631 / 20,194	-3.5	-5.0	1.5
33	580 / 20,942	-3.7	-5.2	1.5
129	519 / 31,961	-3.8	-5.0	1.2

Absorption measured in DCM; HOMO and LUMO determined by cyclic voltammetry in DCM

Table 4.2: Optical and electrochemical properties of the dyes

20.942 $M^{-1}cm^{-1}$ a much higher extinction, harvesting a lot more light in the longer wavelength region. It is nevertheless missing out in the shorter wavelength region, as the perylene monoimide (π-π*-transition) absorption band is almost completely vanished, another indication for a strong donor-acceptor coupling and charge transfer in **33**.

The 8,10-functionalised perylene monoimide **123** exhibits an even stronger bathochromic shift of additional 51 nm compared to **33**, with a λ_{max} at 631 nm with an ϵ of 20.194 $M^{-1}cm^{-1}$. This extinction coefficient of **123** is comparable to that of **33**, in the long wavelength region, but **123** has the added feature of a satisfactory extinction of up to around 13.000 $M^{-1}cm^{-1}$ in the shorter wavelength region. This compound can be understood as a combination of **33** and **105**, however, the strong charge transfer through the *peri*-position is dominant. The absorption bands are well predicted by DFT-calculations, though at slightly longer wavelengths than experimentally determined: a strong S1 transition around 676 nm and an almost equally pronounced transition at 595 nm. Moreover, the different qualities of charge transfer of *edge*- and *peri*-donor are well visible in the prediction of HOMO and LUMO coefficients. Regarding the absorption in solution, the 8,10-functionalised perylene monoimide **123** is the most promising for the application in dye-sensitised solar cells.

The photovoltaic performance of the three new compounds is listed in 4.3 on the following page and compared to the results of **33** already presented in chapter 2 on page 31. Regarding efficiency, the 8,10-functionalised perylene monoimide **123** with an η of 3.3 % still cannot reach the performance of **33** ($\eta = 4.4$ %). However, it should be noted that the results for the three new dyes derive from a first testing whereas **33** has been the subject of optimisation for approximately four years. For a more equal comparison, first photovoltaic performance presented by Li[87] showed an efficiency of only $\eta = 2.2$ %, while the latest published results demonstrated an η of 3.2 %[79]. Looking at the the other performance indicators of both dyes, **123** lags behind **33** both in EQE and short-circuit current but shows a better fill factor.

Dye	EQE_{max} [%]	V_{OC} [mV]	I_{SC} [$mAcm^{-2}$]	FF [%]	η [%]
105	50	740	-4.63	60	2.1
108	22	580	-1.59	55	0.5
123	34	800	-5.82	71	3.3
33	51	800	-7.91	66	4.4
129	–	640	-0.13	70	0.1

Table 4.3: Photovoltaic performance of **105**, **108**, **123**, **33**, and **129**

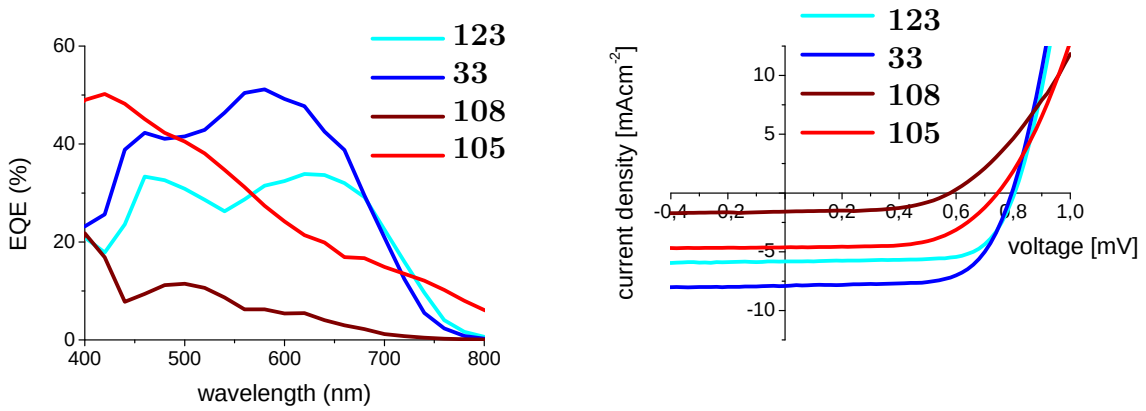

(a) EQE (b) IV

Figure 4.15: EQE (a) and IV (b) of the 9-, 8-, 8,11-, and 8-10-functionalised perylene monoimides

EQE and short-circuit current results are generally connected and even though they are rather low for **123**, an excellent interal quantum efficiency can be suspected, because not only the EQE curve is rather flat (EQE_{max} = 34 %) but also the absorptivity on titanium dioxide reaches only values of around 0.4 compared to values of up to 0.8 for **33** (figure 4.15). This indicates that the dye molecules adsorbed on the titanium dioxide surface are efficiently contributing to the EQE.

Good extinction in dichloromethane solution but low extinction on titanium dioxide and thus less dye concentration on the surface are probably caused by steric hindrance due to the 8-functionalisation. An even lower extinction on titanium dioxide and EQE can be observed in the double-*edge*-functionalised **108**. As the titanium dioxide substrates used were prepared by screen printing in large batches, they can be considered to have the same layer thickness. This is why, for dyes with similar extinction coefficient in solution, a much lower extinction on the titanium dioxide hints at lower dye concentration. For **108** the extinction on titanium dioxide is only between 0.2-0.4 in the short wavelength and even lower in the long wavelength region, the EQE being even lower, resulting in an extremely low current of just -1.59 $mAcm^{-2}$. **105** manages, however, a high absorptivity on titanium dioxide and EQE especially in the short-wavelength region. This may be possible through a somewhat staggered

arrangement of the dye on the titanium dioxide-surface as it does not bear a second donor group and can therefore compensate the generally high steric demand of the *edge*-position. **105** yields, however, rather low current and in the end with 2.1 % only moderate efficiency.

Regarding their LUMO levels critical for the electron injection into the titanium dioxide, all dyes seem to be in an acceptable range (table 4.2 on page 83). Though with an energy of -3.7 eV, the LUMO of **105** is rather low but comparable to that of **33**. Introduction of a second donor moiety could improve the LUMO level energies. As desired, the LUMO is elevated for both double donor dyes (**123** and **108**) to -3.5 eV according to the reduction potential determined by cyclic voltammetry.

A hoped-for benefit from functionalising the *edge*-position was less aggregation minimising the unwanted dye-to-dye recombination reaction. Minimising aggregation and maximising dye concentration in order to achieve a high EQE is of course always a trade-off, which in this case seems to have narrowed the EQE and current considerably. One option for optimisation of the 8,10-functionalised **123** could be keeping a bulky donor in the *peri*-position but introducing a smaller donor moiety in the *edge*-position (figure 4.24 on page 93). This way, hopefully, the concentration of the dye on the surface, the extinction of the dye on titanium dioxide, the EQE and also the current could be improved without losing voltage or achieving a lower FF – hence overall leading to higher power conversion efficiency.

Figure 4.16: Solutions of **105**, **33**, **108**, **123** and **129** (from left to right) in dichloromethane

4.4 Peri-Pentannulated Perylene Monoimide

Another concept explored as part of the effort to add multiple donors uses a rigid spacer, obtained by pentannulation of a perylene monoimide in the 9,10-position[121] symmetrically introducing triarylamine donor moieties. At the same time the pentanullation enlarges the core leading to an altered perylene monoimide-based chromophore. The phenylene spacer between the acceptor and donor moieties improves orbital partitioning and thus reduces unwanted back-transfer of the electrons but the five-membered ring functions to some extent also like a buffer. As shown by Lütke Eversloh et al.[121] aryl substitutents on five-membered rings achieved by pentannulation of PMI do not

partake in conjugation. Moreover it is the pentannulation that allows facile introduction of two donor groups yielding a symmetric double donor sensitiser **129**.

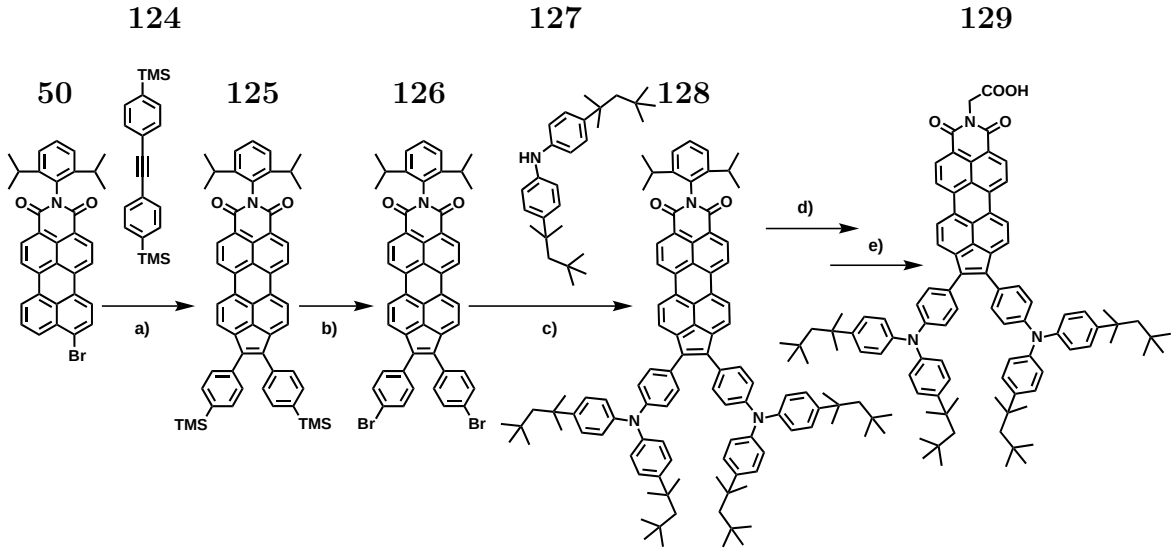

a) Pd-catalysed pentannulation; b) THF, NBS, rt → reflux, 1 week, yield: 38 %; c)$Pd_2(dba)_3$, tri-t-butylphosphine, NaOtBu, toluene, 80°C, overnight, yield: 68 %; d) 2-methyl-2-butanol, KOH, reflux, overnight, yield (crude): 76 %; e) glycine, imidazole, 140°C, overnight, yield: 82 %

Figure 4.17: Synthesis of a *peri*-pentannulated perylene monoimide, with two amine donor groups

The first step is a palladium-catalysed of **50** pentannulation reaction with TMS-tolane **124**.[6] The TMS-groups can subsequently be changed to bromine by reacting **125** with *N*-bromosuccinimide in tetrahydrofuran. Whereas the first TMS-Br exchange starts already at room temperature, the second conversion takes place only very reluctantly even under reflux. After one week, the reaction was stopped, yielding 38 % of the desired **126**, the mono-substitued compound being the main side product. If this synthesis were repeated, a faster alternative might be a TMS-I exchange with iodine monochloride. The resulting iodine PMI derivative, however, might then be more susceptible to dehalogenation in the following Buchwald amination. For the bromine-derivative **126** the palladium-catalysed Buchwald amination was carried out to yield **128** in a very satisfactory yield for a double functionalisation of 68 %. As a side product mono-amination with combined debromination occurred, which could be removed easily by gel permeation chromatography. Like for the other sensitisers the anchoring group was introduced by first saponification in 2-methyl-2-butanol and potassium hydroxide and then imidisation with glycine in imidazole giving the final product **129** with an overall yield of 62 % for the two steps and an amount of 115 mg for testing.

[6] This was carried out by [redacted], the synthetic details will be presented in his forthcoming thesis.

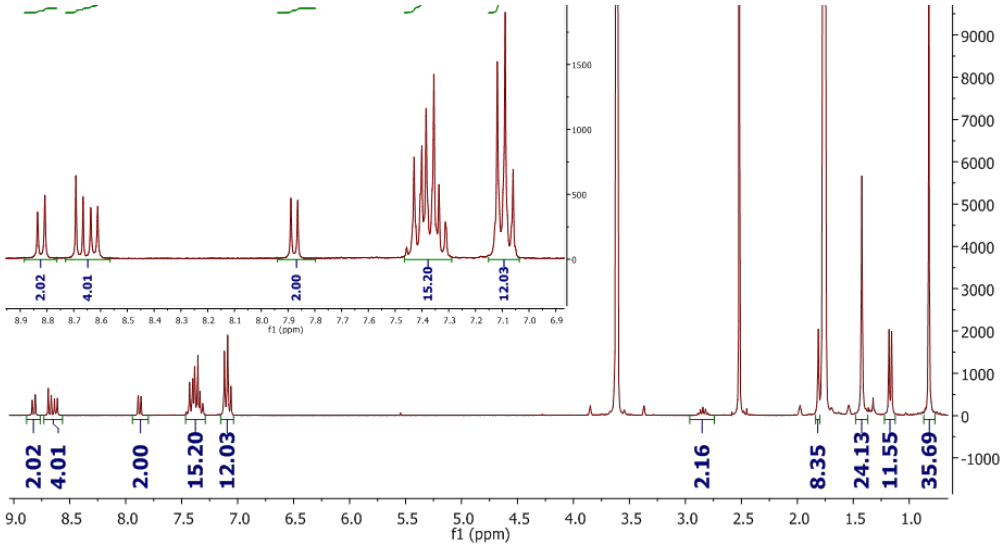

Figure 4.18: ^{1}H-NMR spectrum of **128** (300 MHz, THF, 298 K)

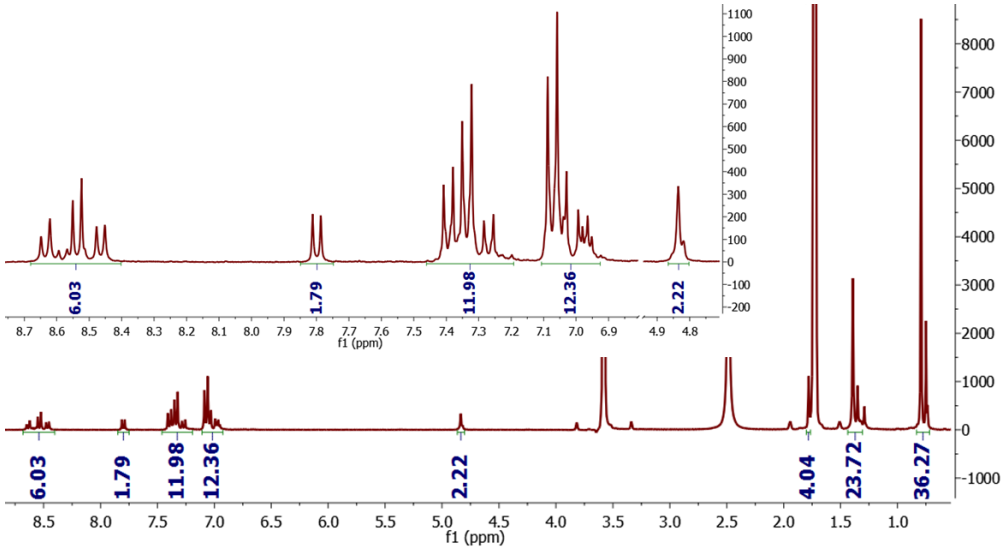

Figure 4.19: ^{1}H-NMR spectrum of **129** (300 MHz, THF, 298 K)

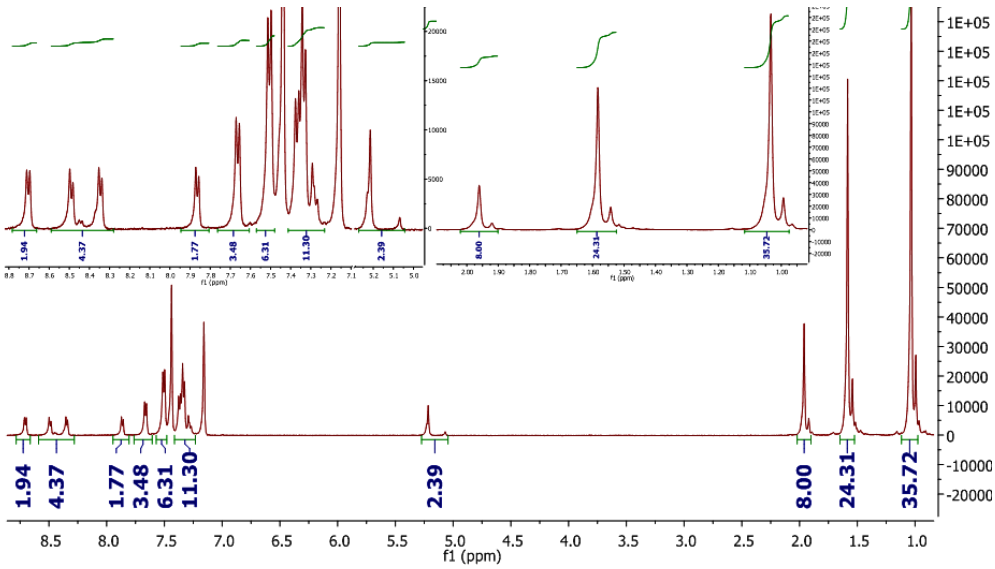

Figure 4.20: ^{1}H-NMR spectrum of **129** (500 MHz, o$C_6D_4Cl_2$, 453 K)

The ^{1}H-NMR spectrum of **129** in tetrahydrofuran is presented in figure 4.19 on the previous page (middle) and though integrating to the correct number of protons, splitting into an unexpected number of peaks can be observed. At first glance the presence of impurities could be suspected. Especially the twin peak at δ 4.85-4.9 ppm where the CH_2-signal of the anchoring group should appear as a singlet is unexpected. Residues of the anhydride precursor are not detectable on thin layer chromatography and if they were present, would only result in additional signals in the aromatic region. For comparison the ^{1}H-NMR spectrum of the *N*-(2,6-di*iso*propylphenyl)-precursor **128** also recorded in tetrahydrofuran is shown in figure 4.18 on the preceding page (top). Herein, a very neat splitting pattern of the symmetric compound is visible, especially the four doublets integrating to overall eight protons in the low field region of the spectrum belonging to the pentannulated perylene monoimide core are very clear in their appearance. This is a proof that the additional splitting in the spectrum of the final compound **129** is not caused by rotational hindrance of the donor groups as that would also have to be apparent in the *N*-(2,6-di*iso*propylphenyl)-precursor. As another option, protonation of the amines was considered, which could have occurred during the acidic work-ups after saponification and imidisation. This, however, could be excluded, as treatment of the NMR-solution with NaOD and subsequent measurements showed that the singlet peak of protonated tetrahydrofuran at δ 10.84 ppm would readily disappear but all other peaks remain steady. Protonation seemed furthermore quite improbable as all sensitisers bearing a glycine anchoring group presented in this thesis were treated the same way and never showed such behaviour.

In order to better detect the individual peaks, the compound was measured in different high-boiling solvents, i.e. dimethyl sulfoxide, tetrachloroethane, and o-dichlorobenzene on a 500 MHz NMR spectrometer. The best spectrum was obtained in *o*-dichlorobenzene at 453 K (figure 4.20 on the previous page (bottom)). Like in the spectrum of the *N*-(2,6-di*iso*propylphenyl)-precursor **128**, the four doublets can be detected in the low field of the spectrum, however, an additional small doublet appearing at around δ 8.47-8.4 ppm and the doublet at δ 8.4-8.3 ppm exhibiting a shoulder to the left. Including the additional doublet and the shoulder, the signals integrate to roughly eight protons. Due to the overlap of the solvent peaks, integration in the region between δ 7.6-7.1 ppm the integration of the peaks cannot be done to complete satisfaction; however, from the tetrahydrofuran spectrum a good fit with the expected number of protons for this compound is already established. The supposed CH_2-signal of the anchoring group is now well separated into two peaks, a singlet of low intensity at δ 5.1-5.05 ppm and another peak posessing a shoulder hinting at a doublet of much higher intensity at δ 5.25-5.2 ppm. Moreover, all three signals which can be attributed to the branched alkyl chains of the donor show an even splitting into two peaks instead of just singlets.

The splitting of the signal of an aliphatic proton adjacent to the imide nitrogen and subsequently the appearance of additional core proton signals is known for a *N*-(1-nonyldecyl)-9-(bis(4-(2,4,4-trimethylpentane-2-yl)phenyl)amino-perylene-3,4-dicarboximide (PMI-d-C9), however, in solid-state NMR measurements. Tasios et al.[68] describe different push-pull-PMI derivatives and their self-assembling behaviour, attributing the splitting of the NMR-signals to the fact that in some of the molecules the proton adjacent to the imide nitrogen undergoes hydrogen bonding and is coordinated to one of the carbonyls on either side. They additionally report that this hydrogen-bonding is not unusual for similar perylene monoimide derivatives but that those show quantitative hydrogen bonding. Seeing that the singlet peak at δ 5.1-5.05 ppm is of much lower intensity than the supposed doublet at δ 5.25-5.2 ppm, it can be presumed that the hydrogen-bonded species is predominant. Why this hydrogen-bonding could not be observed in the other perylene monoimide sensitisers is hard to say. Moreover, it is unclear whether this hydrogen bonding occurs inter- or intramolecularly. If it were intermolecularly, then one reason for this phenomenon might be that this sensitiser is symmetric with a rather large flat core favouring π-π-stacking. In case of **108** – the only other symmetric sensitiser presented in this work – the bulky fluorene donor groups might prevent similar behaviour.

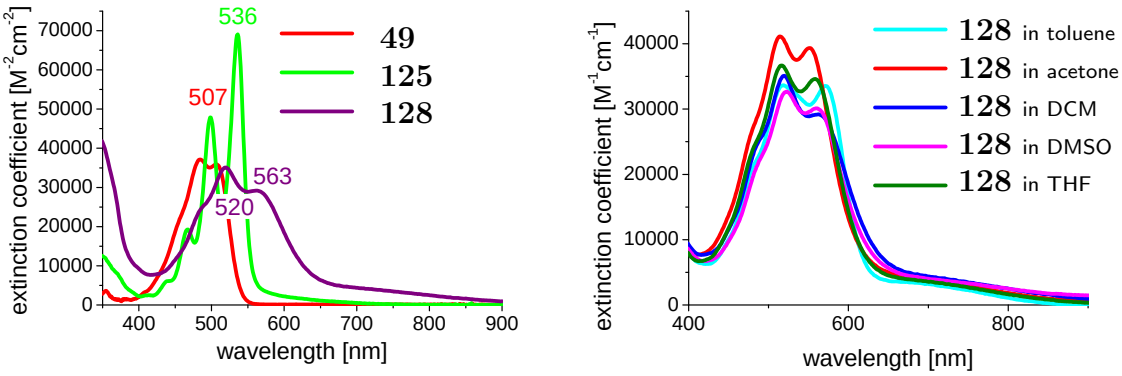

(a) UV Absorption (b) UV Absorption

Figure 4.21: Change in absorption in dichloromethane during synthesis (a) and absorption of **128** in different solvents (b).

The absorption spectra of the first synthesis steps is presented in figure 4.21. The pentannulation induces a dramatic change in the optical properties, resulting in i) a pronounced fine structure with three distinct bands (not unexpected for such a large stiff core), ii) a bathochromic shift of nearly 30 nm, from λ_{max} = 507 nm for perylene monoimide to λ_{max} = 536 nm for the pentannulated perylene monoimide, and iii) an extinction coefficient of 70.000 $M^{-1}cm^{-1}$, which is almost twice as high as for the precursor **125**. Introduction of the donor moieties leads again to a decrease of the extinction coefficient and blurring of the fine structure. The three bands are consider-

ably broadened and bathochromically shifted, the highest extinction at $\lambda = 520$ nm, but a second local maximum at 560 nm with a tail reaching 900 nm, hinting at charge transfer.

The absorption of **128** was measured in dichloromethane, tetrahydrofuran, acetone, DMSO, and toluene (figure 4.21 on the previous page) to see whether the different polarities of the solvents would have an influence on the absorption. A strong solvatochromic behaviour would have been strong evidence for assigning the tailing band to charge transfer but only little variation can be observed in band shape and extinction.

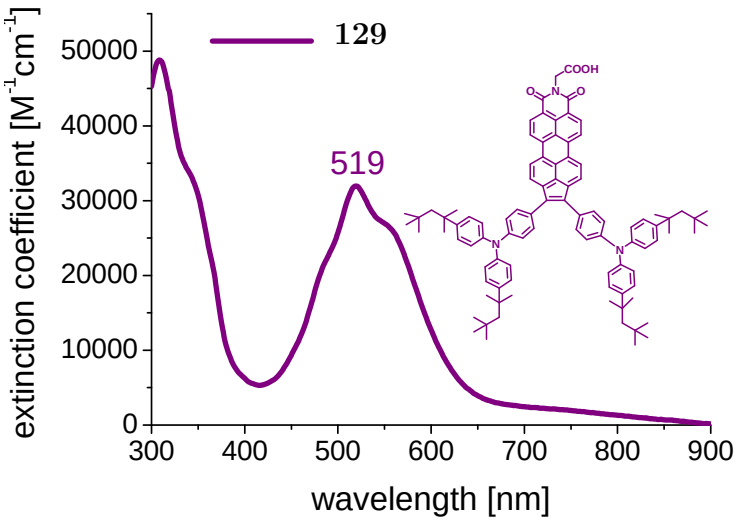

Figure 4.22: Absorption spectrum of the *peri*-pentannulated perylene monoimide

The final compound with its anchoring group shows as expected a very similar absorption spectrum with a λ_{max} at 519 nm and an extinction coefficient of approximately 32.000 $M^{-1}cm^{-1}$. The experimentally determined absorption is in good agreement with the DFT-calculation data presented in table 4.1 on page 81. An S1 transition band in the near-infrared region ($\lambda = 1018$ nm) is predicted with an intensity of 0.06[7] and in fact, the most bathochromically shifted visible band is the S2 transition of low intensity (f2 = 0.34) at 772 nm corresponding to the broad and flat presumed CT-band reaching out to 900 nm. The very intense band with its λ_{max} at 519 nm is predicted as the S4 transition ($\lambda = 537$ nm, f4 = 0.76).

The localisation of the HOMO/LUMO coefficients shows almost complete separation of the orbitals with little communication via the five-membered ring. This as well corresponds to the absorption spectrum showing only a very weak CT-band and mainly absorption in the perylene monoimide region.

Sensitiser **129** was processed and measured in a DSSC under the same conditions as compounds **108**, **123**, and **33** and exhibited with 0.1 % efficiency together with **108**

[7]For clarity only the most important values are listed in the table.

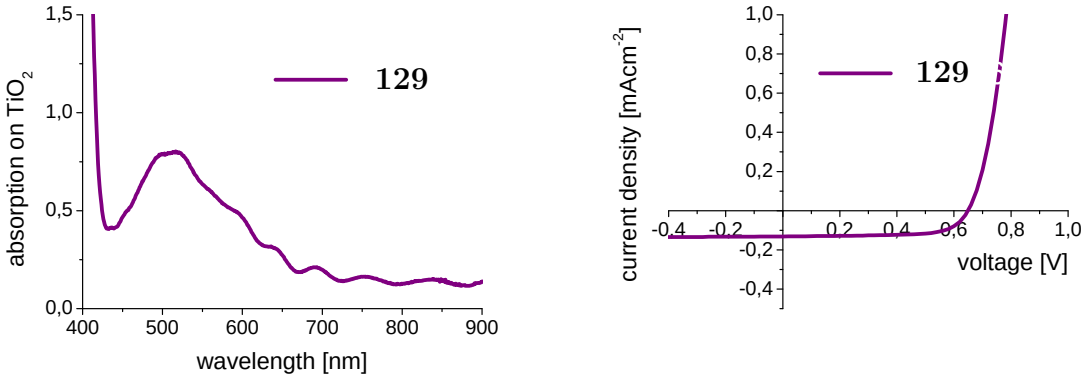

(a) EQE (b) IV

Figure 4.23: Absorption on titanium dioxide (a) and IV-curve of **129** (b)

by far the worst photovoltaic performance of all sensitisers presented within this thesis. Whereas for **108** unsuitable sterics, i. e. bulkiness of the molecule, are suspected to be the main reason for the poor efficiency, the case of **129** is different. Though also bearing two large donor groups, these donor groups are not attached in the *edge*-positions but in the extended *peri*-positions and the aryl amine with branched alkyl chains are less bulky than the bis(fluorenyl)amine-donor. The absorption on titanium dioxide with values of up to 0.8 comparable to those of **33** confirms that a reasonable dye concentration is achieved on the substrate (figure 4.23). An EQE curve, however, was due to poor response not measurable. This is also reflected in the very low short-curcuit current of -0.13 $mAcm^{-2}$ (figure 4.23). The reason for the feeble performance of **129** can be found in the low lying LUMO (table 4.2 on page 83). DFT-calculations also suggest a much lower LUMO level for this dye by predicting a considerably higher electron affinity than for the other dyes (table 4.1 on page 81). Lütke Eversloh et al.[121] also observed that with increasing number of peri-pentannulated rings on perylene, the LUMO level drops. With an energy level of approximately -3.8 eV, the LUMO lies 0.1 eV lower than that of **33**. Sensitiser **33** possesses in a titanium dioxide-based cell just about the driving force needed for efficient injection.[79] At the same time Boschloo et al.[122] suggest that the acceptor states of titanium dioxide are relevant for the injection rather than the conduction band, therefore efficient injection is still possible for sensitisers with low lying LUMO, e. g. **33**. With -3.8 eV for the LUMO energy of **129** a cut-off point seems to be reached where electron injection is suppressed.

4.5 Conclusion

Unfortunately, the first intended 9,10-functionalised perylene monoimide could not yet be achieved. However, functionalisation of the *edge*-positions and especially the

asymmetric 8,10-functionalisation have brought us closer to the presumably ideal 9,10-functionalised double donor. The attempts to synthesise this target by tetrabromination or coupling have demonstrated, that a functionalisation of those two positions in a perylene monoimide or terrylene monoimide is in principle possible. The coupling reaction could, if conditions can be optimised, make the realisation of the 9,10-functionalisation accomplishable. Another possibility is using the described side reaction via an aryne mechanism inducing a shift of both functinalities in 8- and 11-positions towards the *peri*-positions. The only chance achieving this would be by using a very small amine. But if the high degree of dehalogenation cannot be prevented, the yield will be far from sufficient. Besides the herein described attempts it will, of course, always be possible and desirable that other fresh routes will be developed by successive researchers, one example being the conversion of carboxylic acid in the *peri*-positions to bromo moieties. The di-carboxylic-acid-functionalised perylene monoimide has already been achieved.[123,124,125,126] The conversion of these acid groups to a halogen can by achieved by the Hunsdiecker reaction[127] in which silver salts are degraded under elimination of carbon dioxide in order to give bromine- and chlorine-substituted substrates. The Hunsdiecker reaction is mainly used for aliphatic compounds but several variations suitable for aromatic system have been described in literature.[128,129,130,131]

Besides attaching two donors directly to the perylene monoimide core, also other double-donor concepts introducing different kind of spacer moieties have been investigated. One of these concepts - the double donor via introduction of a branched terthiophene spacer - has already been presented in the last chapter. These two compounds, the perylene monoimide **83** and the naphthalene monoimide **84** link the concept of spacer introduction of the first chapter with the double donors of the current chapter.

Of all sensitisers bearing two amine donor groups, the 8,10-functionalised perylene monoimide seems to be the most promising as it shows the broadest absorption, the strongest bathochromic shift, and a rather high LUMO level energy. As in other cases, steric hindrance might be the main reason for the only moderate efficiency in the cell but the concept shows great potential for improvements (figure 4.24 on the next page). One obvious possible improvement would be the replacement of the rather bulky alkylated bis-phenyl amine donor with a phenyl amine donor or even aliphatic amine. Moreover, the 10-position donor group could be bridged with a phenylene spacer, improving the orbital partitioning and thus impeding unwanted back-transfer of the electrons. A third suggestion for optimisation would be the replacement of the bis(4-(2,4,4-trimethylpentane-2-yl)phenyl)amine donor with a bis-(9,9-dimethyl fluorene-2-yl)-amine donor, as sensitisers bearing this donor have often outperformed their analougues with the alkylated bis(phenyl)amine donor. In order to prevent borylation of the donor, the 7-position of the fluorene moieties should be blocked, for example with methyl groups.

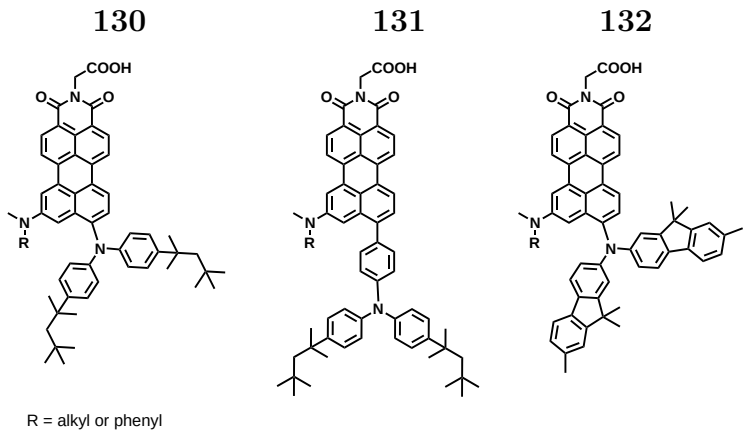

Figure 4.24: Suggestions to optimise the 8,10-donor-functionalised perylene monoimide

Another concept to achieve a double donor sensitiser was the extension of the perylene monoimide core through *peri*-pentannulation which at the same time allowed introduction of two triphenylamine donors. Though synthetically successful, the sensitiser showed very poor performance in dye-sensitised solar cells. The most likely reason for this is the low-lying LUMO of the dye – a limitation in connection with the titanium dioxide semiconductor. In a different cell set-up using another semiconductor this might be of less consequence.

Within the course of this doctoral thesis but also by my predecessor Li [87] working on this topic, many sensitiser concepts have been pursued using the perylene monoimide core, [36] leaving limited options for the future. Working on the perylene core to achieve improved chromophores seems a good way to open up alternatives for sensitiser design despite the first set-back of the *peri*-pentannulated perylene monoimide. Making use of the *Cadogan reaction* [91], another core-modification will be presented in the following chapter aiming towards new sensitisers for dye-sensitised solar cells but also for a new chromophore class in general.

Chapter 5

Enlargement of the Perylene-π-System: Cadogan Chemistry Towards a Novel Class of Chromophores

5.1 Introduction to Cadogan Chemistry

One way of achieving a bathochromic shift is the enlargement of the π-system. In the past this has been done by extending the long axis from perylene to terrylene by coupling with an additional naphthalene unit, or with several units to go as far as the octarylene (in form of a octarylene diimide)[132] or as presented in the previous chapter by pentannulation of the perylene monoimide in the *peri*-positions. Another option is to extend the short axis of the perylene core. First extension along that axis leads to a hypsochromic shift as shown by Müller[116] with the synthesis of a coronene diimide. However, with further extension along the same axis, bathochromic shifts of the absorption maximum can be achieved as demonstrated by Lütke Eversloh et al.[133].

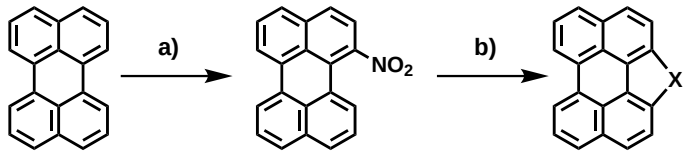

7 **133** **134**

a) fuming HNO_3/H_2O 1/1.6 (v/v), 1,4-dioxane, 60 °C, 25-30 min; b) X = NH: triethyl phosphite, reflux, 2h; X = Se: selenium powder, 180°C, 5h; X = S: sulfur powder, NMP, 180°C, 5h

Figure 5.1: Fusion of a *bay*-nitro-group on perylene using *Cadogan conditions*

In this chapter a third alternative will be presented – extending the perylene core by

an indole or quinoline moiety in the *peri*-position via fusion of a nitro group following the concept of Cadogan et al.[91] leading to an assymmetric extension of the perylene core. Ever since this original publication of Cadogan et al. in the 1960s presenting the fusion of a nitro-functionalised biphenyl to a carbazole, *Cadogan Chemistry* has been widely used especially for the synthesis of various carbazoles and indoles.[134,135,136,137] However, Jiang et al.[138] have recently shown the introduction of a nitro group in the *bay*-position of the perylene and its fusion to the perylene core (figure 5.1 on the preceding page), introducing a nitrogen, sulfur or selenium into the five-membered ring and generating a blue shift in absorption, as known for *bay*-extensions of perylene (s. above). Their work is the first use of *Cadogan Chemistry* on perylenes and suggested the application of the resulting materials in organic electronics.

Introduction of a heteroatom, especially an electron-rich one like nitrogen, is favourable in achieving a bathochromic shift. If it is placed well away from the accepting unit, push-pull character can be induced and the nitrogen can be considered a donor, the impact of this donor depending on the conjugation pathway towards the acceptor moiety.

5.2 Indole-Extended Perylene Monoimide

A first attempt towards extension via *Cadogan Chemistry* was made on a perylene monoimide introducing a nitrophenyl in the 9-position of the perylene via Suzuki coupling and subsequent fusion to yield (**136**). The synthesis route is presented in figure 5.2 on the next page. An attempt to couple 4,4,5,5-tetramethyl-2-(2-nitrophenyl)-1,3,2-dioxaborolane (**138**) with 9-bromo-perylene monoimide (**50**) failed. Aryl halides in proximity of an electron-withdrawing group are known to be more activated for oxidative addition.[139] Thus, the bromo functionality of the perylene monoimide was converted into a boronic ester (**51**) and Suzuki coupling with 1-bromo-2-nitrobenzene (**135**) was achieved in yields of up to 70%. The following fusion was first carried out using triethylphosphite as per Cadogan et al.[91]. Fusion occurred, but a byproduct of similar colour and a mass corresponding to the suggested structure **139** was formed – an intermediate with the phosphite still attached to the nitrogen on the fused ring. The purple colour indicates that fusion has taken place, the greater retention factor (0.8 for the byproduct / 0.35 for the product in dichloromethane) speaks for a tertiary amine rather than a secondary amine as secondary amines show much stronger interactions with the silica on a thin layer chromatography plate. In order to prevent the formation of this byproduct, the fusion was carried out in *ortho*-dichlorobenzene using triphenylphosphine as suggested by Du et al.[136]. Reaction in the microwave showed no major byproducts leading to a crude yield of around 70%, the product (**137**) directly precipitating from the reaction mixture.

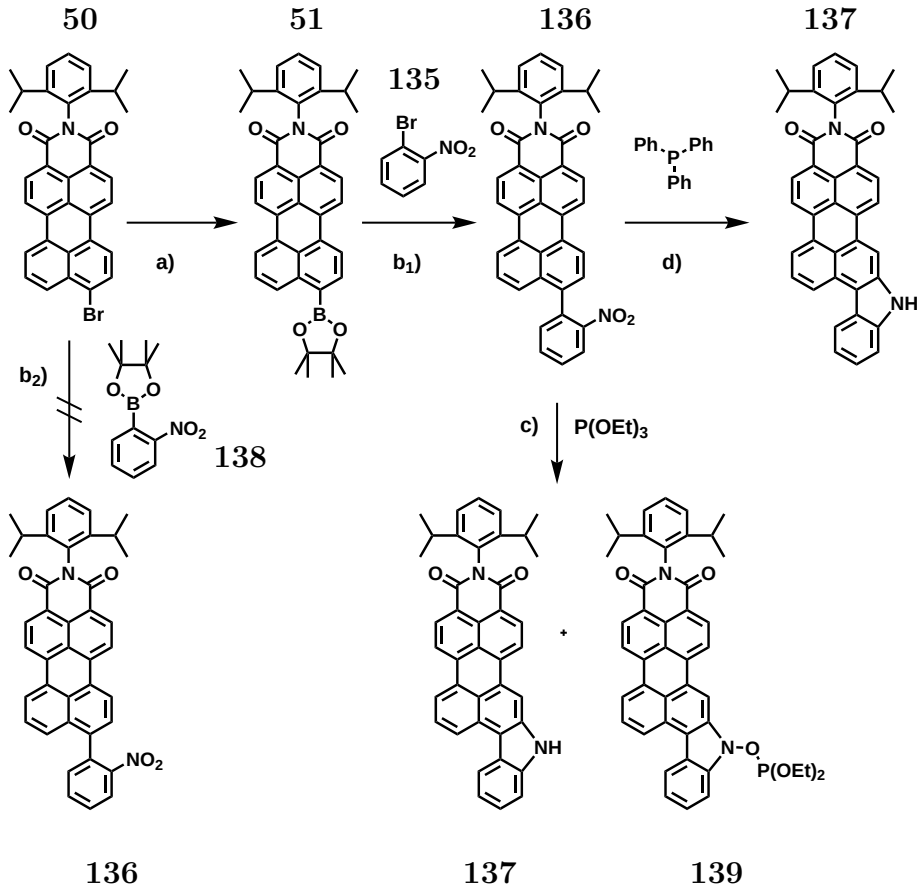

a) Bispinacolatodiboron, potassium acetate, $Pd(dppf)Cl_2$, dioxane, 80°C, 15h, yield: 85 %; b_1) K_2CO_3, $Pd(PPh_3)_4$, toluene, water, ethanol, 80 °C, 24h, yield: 70 %; b_2) K_2CO_3, $Pd(PPh_3)_4$, toluene, water, ethanol, 80 °C, overnight, no conversion; c) triphenylphosphine, o-dichlorobenzene, microwave (300 W, 182°C, 8h), yield: 56 %; d) triethylphosphite, microwave (300 W, 160°C, 1h), no yield determined

Figure 5.2: Synthesis route of an indole-extended perylene monoimide **137** via *Cadogan Chemistry*

Using the crude product **137**, alkylation of the indole-nitrogen was pursued using sodium hydride and the alkyl bromide to yield 53 % of **140** (figure 5.3 on the following page). The reasons for this alkylation were i) enhancement of solubility of the compound, ii) easier handling in the course of the following reaction steps, iii) indroducing a barrier in order to weaken aggregation in the solar cell device, and iv) improvement of the stability of the dye by functionalising this reactive site.

Like all former sensitisers, the *N*-(2,6-di*iso*propylphenyl)-perylene monoimide **140** was saponified to give the anhydride **141** and imidised with glycine to introduce the anchor for the adsorption on titanium dioxide. Compared to the former sensitisers compound **142** showed only very poor solubility in dichloromethane and also much lower solubility in tetrahydrofuran. The low solubility adding to the difficulty of the strong adhesion of the carboxylic acid group to the silica gel caused great challenges in the purification of the final product and is the main reason for the rather low yield of the imidisation of only 56 %. Therefore, only 50 mg of the final product – but well

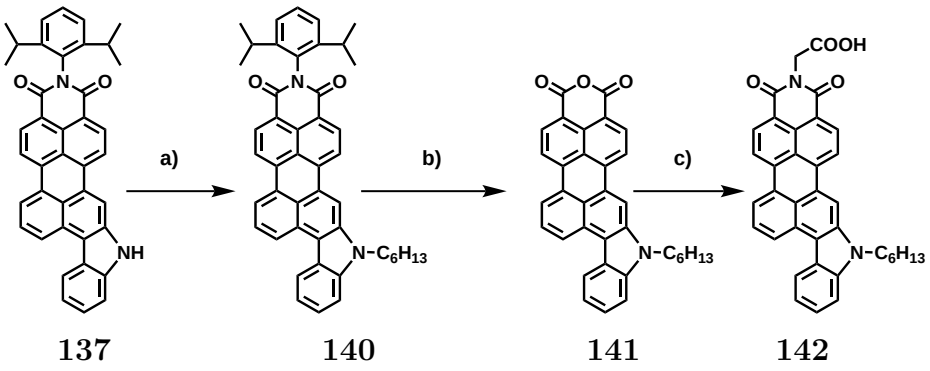

a) NaH, hexylbromide, DMF (anhydrous), rt, yield: 53 %; b) KOH, 2-methyl-2-butanol, reflux, overnight, yield (crude): 96 %; c) glycine, imidazole, 140°C, overnight, yield: 56 %

Figure 5.3: Alkylation, saponification and imidisation of an indole-extended perylene monoimide **142**

enough for device testing – were obtained.

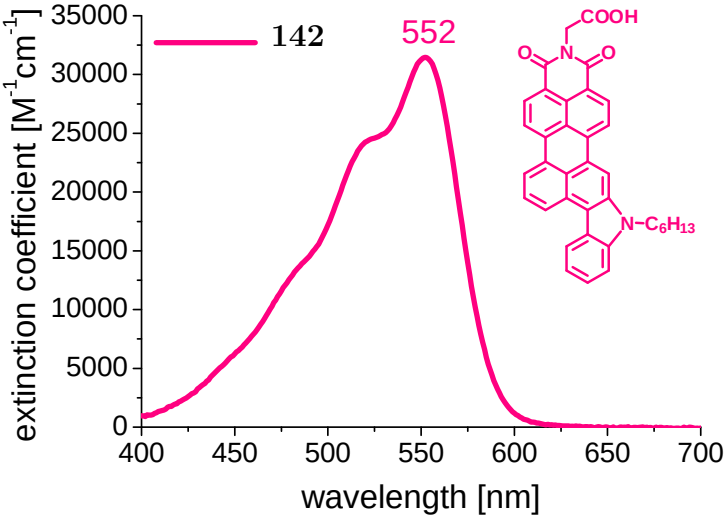

Figure 5.4: Absorption spectrum of an indole-extended perylene monoimide

The absorption spectrum in tetrahydrofuran is shown in figure 5.4. The absorption maximum at 552 nm ($\epsilon = 31.469\ \mathrm{M^{-1}cm^{-1}}$) is about 50 nm red-shifted compared to the *N*-(2,6-di*iso*propylphenyl)-perylene monoimide. The shape of the absorption is rather sharp – typical for larger rigid π-systems and reminiscent of the absorption of perylene diimide.[46] The bathochromic shift in absorption derives from the core-extension rather than strong intramolecular charge transfer, therefore **142** is certainly not a push-pull dye.

5.3 Introduction of a Donor in the Extended Peri-Position

The indole nitrogen has little donor character and cannot compensate for the push observed in other sensitisers, for example **33**, mentioned in the previous chapters. Hence, to achieve the desired push-pull effect, an additional donor moiety must be introduced, preferably in a well conjugated position. As can be seen in figure 5.5 this was done in the extended *peri*-position, thus well conjugated with the imide acceptor and as far away as possible from it to keep a strong dipole over the whole molecule.

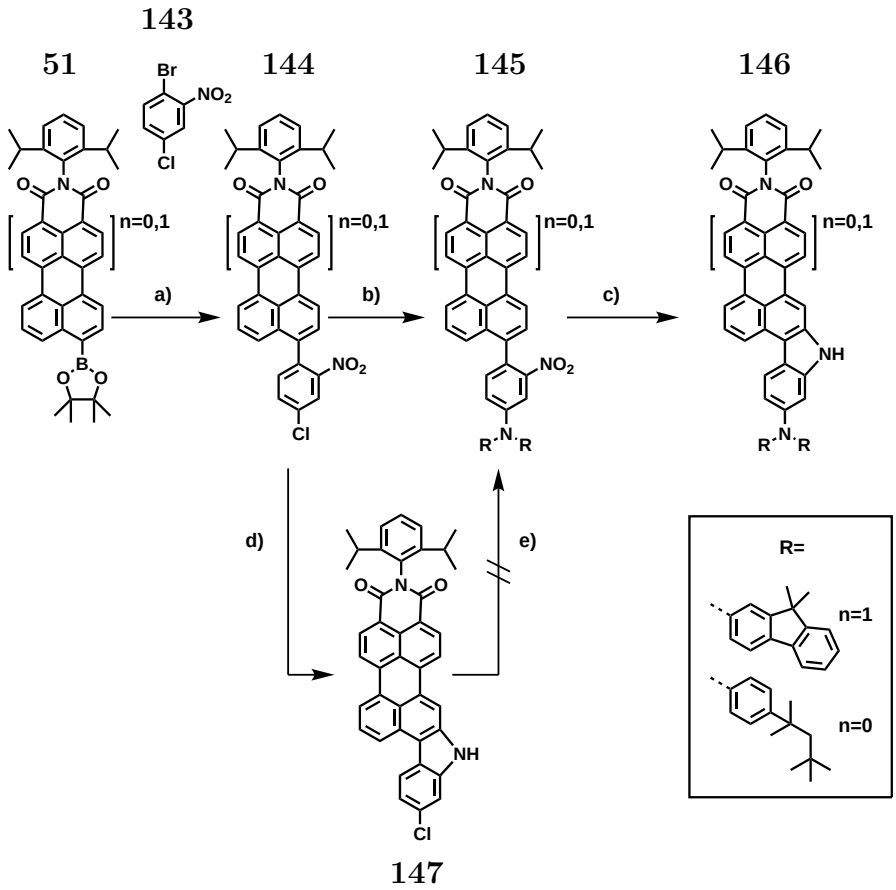

a) K_2CO_3, $Pd(PPh_3)_4$, toluene, water, ethanol, 80 °C, 36 h (n=1) / 60 h (n=0), yield: 79 % (n=1), 32 % (n=0); b) n=1: bis-(9,9-dimethylfluorene-2-yl)-amine, caesium carbonate, $Pd_2(dba)_3$, BINAP, toluene, 100°C, 16h, yield: 65 %; n=0: (*p*-2,4,4-trimethylpentane-2-yl-phenyl)amine, caesium carbonate, $Pd_2(dba)_3$, BINAP, toluene, 100°C, 16h, yield: 64 % c) triphenylphosphine, o-dichlorobenzene, microwave (300 W, 182°C, 8h), yield: 62 % (n=1), 82 % (n=0); d) triphenylphosphine, o-dichlorobenzene, microwave (300 W, 182°C, 8h); e) bis-(9,9-dimethylfluorene-2-yl)-amine, caesium carbonate, $Pd_2(dba)_3$, BINAP, toluene, no conversion

Figure 5.5: Synthesis route of an indole-extended donor-functionalised perylene monoimide **146** and naphthalene monoimide analogue via *Cadogan Chemistry*

Synthetically this functionalisation could be achieved by using 1-bromo-4-chloro-2-nitrobenzene **143** for the Suzuki coupling **147**, followed by a Buchwald reaction with an amine donor to give **145** and subsequent fusion in *ortho*-dichlorobenzene with

triphenylphosphine yielding **146**. In order to achieve a more flexible building block, an attempt was made to first establish the five-membered ring and later on introduce the donor functionality. Wheras the fusion proceeded, the successive reaction under standard Buchwald conditions ($Pd_2(dba)_3$, BINAP and caesium carbonate, toluene, 100°C) failed. Heterocyclic halides containing basic nitrogens are known to be hindered in amination due to interaction of the basic nitrogen with the palladium.[140] This may have been the reason why no conversion took place in the Buchwald amination of **147**. In the presence of caesium carbonate, the proton of the indole moiety of **147** might have been abstracted, leaving a negative and hence basic nitrogen which then disabled the palladium catalyst. One way to prove this would be to alkylate **147** before Buchwald amination.

In this case, the naphthalene as well as the perylene derivative were prepared to compare the effect of the indole nitrogen on both homologues. In case of the perylene derivative, an excellent yield of 79 % could be achieved for the first Suzuki coupling introducing **143**. For the naphthalene monoimide, the reaction yielded only 32 %, rather little for a Suzuki coupling. Here, similar conditions were used for the napthhthalene as for the perylene. Generally both reactions proceed very slowly. Whereas most Suzuki couplings are completed after one night, they had to be left for 36 h (perylene) and 60 h (naphthalene) until all starting material was consumed. For the next step, introduction of the amine donors via Buchwald amination, the yields of both naphthalene and perylene derivative were both around 65 %. In the fusion step, with 82 % a much higher yield could be reached for the naphthalene derivative than for the perylene monoimide (62 %). Main reason for this was not so much higher conversion but better solubility of the naphthalene derivative facilitating column chromatography on silica gel.

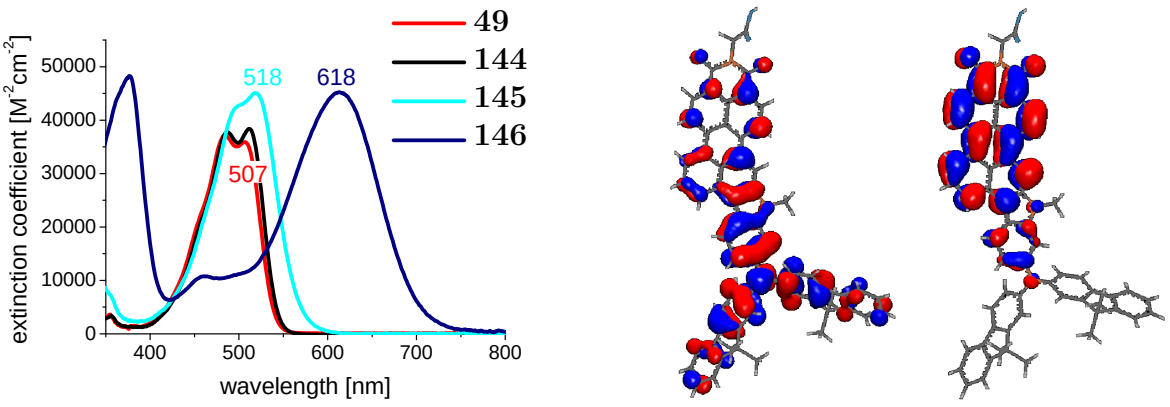

(a) UV Absorption

(b) HOMO and LUMO of **149**

DFT; performed by BASF SE

Figure 5.6: Change in absorption in dichloromethane during synthesis (a) and HOMO and LUMO of **149** (b)

The absorption spectra of the first, colour-determining syntheses steps are presented in figure 5.6 on the preceding page. The introduction of the chloro-nitrophenyl-group has practically no influence on the extinction nor the absorption maximum or the shape of the band (compound (**144**)). It is the introduction of the donor (**145**) which enhances the absorptivity and gives a first moderate broadening of the absorption band, shifting λ_{max} around 10 nm to longer wavelengths and generating a higher extinction ($\epsilon \approx 45.000\ M^{-1}cm^{-1}$). At this stage it is comparable to compound **62** of the π-spacer compounds presented in chapter 2 on page 31. The blue-shifted λ_{max} for **145** compared to **62** is probably a result of the electron-pulling nitro-group on the spacer as well as a presumably stronger twist and orbital separation due to the steric hindrance of the nitro-substituent. Fusion under *Cadogan conditions* then induces a tremendous bathochromic shift of 100 nm (λ_{max} = 518 nm to λ_{max} = 618 nm) without losing extinction. This absorption band can be attributed to a charge transfer transition in the dye. Upon flattening (**146**) and at the same time extension of the core, the donor is now well coupled with the acceptor as can be seen in the pictures of the HOMO and LUMO coefficients (figure 5.6 on the preceding page, compound **149**). Vertical extension of the π-system results in higher extinction,[115,46] compensating for the expected loss of absorptivity owing to the now established intramolecular charge transfer from the donor to the imide acceptor along the long axis of the molecule.

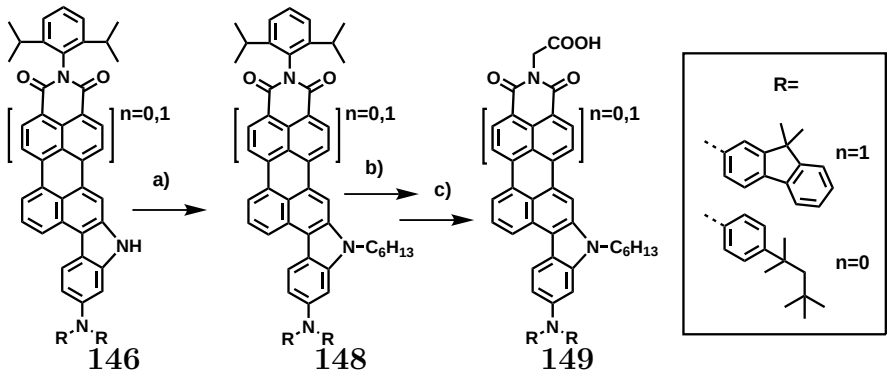

a) NaH, hexylbromide, DMF (anhydrous), rt, yield: 92 % (n=1), 71 % (n=0) ; b) KOH, 2-methyl-2-butanol, reflux, overnight, yield (crude): 94 % (n=1), 95 % (n=0); c) glycine, imidazole, 140°C, overnight, yield: 59 % (n=1), 87 % (n=0)

Figure 5.7: Alkylation, saponification and imidisation of an indole-extended donor-functionalised perylene monoimide (**149**) and naphthalene monoimide (**150**)

Like in the above described case, the fusion was followed by alkylation, saponification and imidisation yielding **149**, now applicable for solid-state dye-sensitised solar cells. The synthesis was carried out the same way for the naphthalene analogue (**150**) only varying the donor from a bis-flurenylamine donor in the case of the perylene to a bis-phenylamine donor for the naphthalene. In the case of the perylene derivative,

in a scale of 120 mg, alkylation proceeded in an excellent yield of 92 %. For the naphthalene derivative, working in a scale of 350 mg, only 71 % of the alkylated product were yielded. No side reactions were observed but conversion of the starting material remained limited, though excess of both base and hexylbromide were used. This decrease in yield with increasing scales was observed in follow-up syntheses. After saponification, both naphthalene and perylene derivative were used for the imidisation step directly after work-up. After purification, 87 % could be yielded of the naphthalene **149** (n=0) but only 59 % of the perylene **149** (n=1). Like in the case of compound **142**, this comparatively low yield was not because of low conversion but rather due to very low solubility of the compound, making the column chromatography on silica gel more difficult. A total of 100 mg of the final perylene derivative **149** (n=1) and 75 mg of the naphthalene derivative **150** were made for testing in sDSSCs.

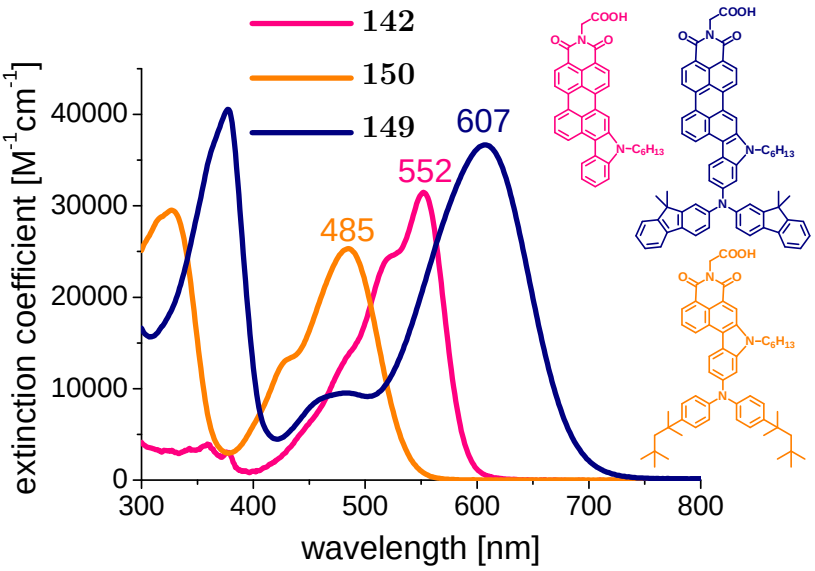

Figure 5.8: Absorption spectra of indole-extende perylene monoimides with and without donor and naphthalene monoimide with donor

Compared to the indole-extended perylene monoimide without donor, the one with donor (**149**) and of course even more so the smaller naphthalene derivative with a more flexible donor group (**150**) show better solubility in dichloromethane. The absorption spectra in comparison to **142** are presented in figure 5.8. As expected, the introduction of a donor group in the extended *peri*-position results in a large red-shift of around 55 nm, leading to an absorption maximum of 607 nm (624 nm in dichloromethane) and a tail reaching out to 730 nm. What is remarkable, however, is an additional increase in extinction of around 5.000 $M^{-1}cm^{-1}$ to 36.675 $M^{-1}cm^{-1}$. Usually introduction of a donor moiety directly connected to the accepting core broadens the charge-transfer band but lowers the extinction. As mentioned before the reason for this absorbance increase is the vertically extended π-system, now similar to terrylene monoimide.

The experimentally determined absorption spectra are in good agreement with the

DFT-predictions (table 5.1 on the next page) suggesting just one strong absorption band for **142** at around 535 nm. The HOMO and LUMO coefficients are both localised on the extended perylene core system, confirming that the bathochromic shift compared to perylene monoimide derives from core extension rather than strong intramolecular charge transfer.

For **149** and even more pronounced for **150**, however, orbital partitioning can be observed, the HOMO coefficients mainly localised on the donor and the LUMO coefficients on the acceptor, the new indole-extended perylene monoimide core. This reinforces the presumption that both dyes are classic push-pull systems. Moreover, according to the DFT-calculations two strong transitions, a bathochromic CT- and a π-π*-transition are predicted. The predicted absorption bands, however, are red-shifted relative to those detected experimentally. The absorption band of the naphthalene derivative is blue shifted compared to **142**, absorbing with a λ_{max} at 485 nm (502 nm in dichloromethane) in the range of perylene monoimide. With the shortest π-system, it consequently shows the lowest extinction coefficient (ϵ = 25.320 $M^{-1}cm^{-1}$). It is, however, only slightly lower than the extinction coefficient of most of the π-spacer sensitisers and higher than the extinction of **33** or the 8,10- and 8,11-double donor-PMIs (**123** and **108**) presented in the preceding chapter.

Figure 5.9: Solutions of *Cadogan NMI* with donor, *Cadogan PMI*, and *Cadogan PMI* with donor (from left to right) in THF

All three *Cadogan dyes* (**142**, **150**, and **149**) were applied as sensitisers in solid-state dye-sensitised solar cells and their photovoltaic performance measured. Different additives and solvents were used for the three dyes in order to find the best individual conditions for each dye to yield the highest power conversion efficiency. Therefore, the different spectra shown in figure 5.10 on page 105 and figure 5.11 on page 106 should not be used for direct comparison. What can be compared, however, are the top power conversion efficiencies for the dyes, **149** being the most successful with an η of 3.8%, followed by **150** with an η of 3.2%, leaving **142** the least efficient, with an η of 2.6%. The naphthalene derivative outperforming the perylene sensitiser **142** is on first glance very remarkable, as perylenes usually show much better light harvesting

Dye	Structure	HOMO	LUMO	
150	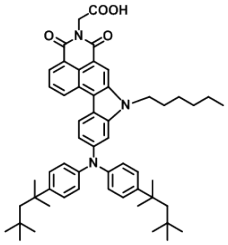	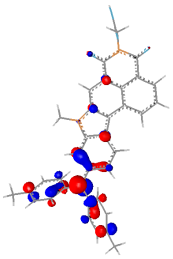	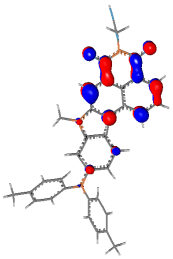	IP: 5.33 EA: 3.10 S1: 526 nm S2: 411 nm f1: 0.39 f2: 0.58
142	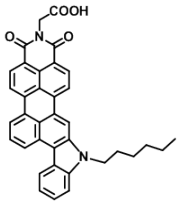	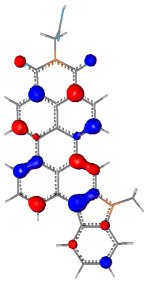	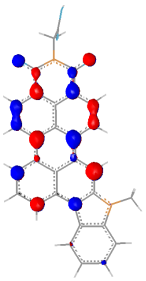	IP: 5.74 EA: 3.17 S1: 535 nm S2: 473 nm f1: 0.70 f2: 0.09
149	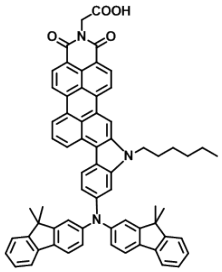	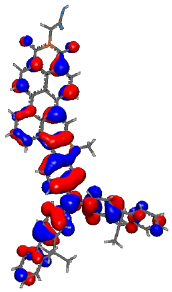	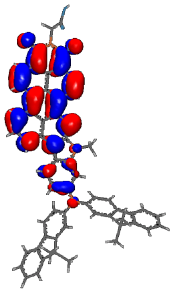	IP: 5.10 EA: 3.14 S1: 676 nm S2: 509 nm f1: 0.68 f2: 0.45
151	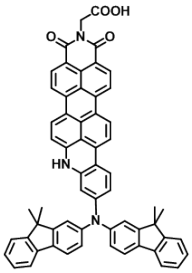	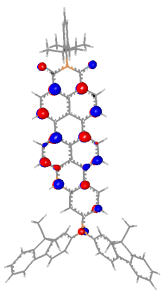	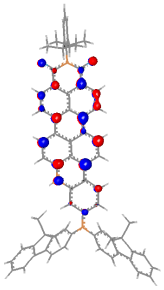	IP: 5.06 EA: 2.87 S1: 606 nm S2: 498 nm f1: 1.21 f2: 0.00

(DFT; performed by BASF SE)

Table 5.1: Calculated orbital surfaces, ionisation potential (IP), electron affinity (EA), transitions (S) and oscillator strengths (f) of compound **150**, **142**, **149**, and **151**

due to their larger conjugated core. In this case, however, the naphthalene derivative is a push-pull system with a broad absorption and a strong bathochromic shift of the absorption maximum into the visible region. Moreover it shows higher extinction on titanium dioxide than the perylene monoimide **142** and an excellent EQE of up to 50 %. Another advantage with respect to processing is its higher solubility, leaving more choices regarding solvents.

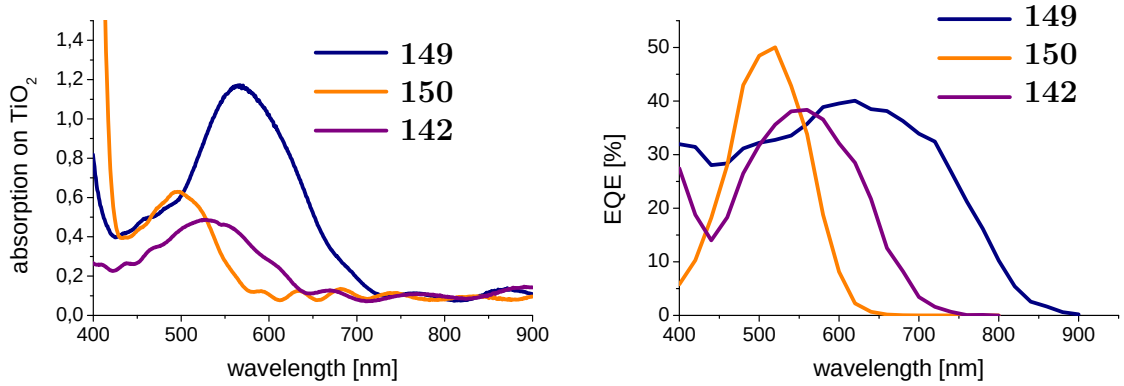

(a) TiO_2 absorption (b) EQE

Figure 5.10: Absorption on TiO_2 (a) and EQE-curves (b) of the *Cadogan dyes*

Not only is the naphthalene derivative **150** outperforming **142** in respect to power conversion efficiency, but it is also reaching almost the efficiency of the comparable perylene push-pull sensitiser **149**. This high performance likely derives from the exceptionally high voltage obtained obtained for **150** and shown in the I-V curve (figure 5.11 on the following page).

Looking at the absorption of the dyes on titanium dioxide in figure 5.10, the absorption of **150** and **142** compared to **149** looks rather poor, but this may derive from the different processing conditions employed. Whereas the two sensitisers with the donor group, **150** and **149**, were processed from dichloromethane solution, tetrahydrofuran had to be used for the poorly soluble **142**. As cells in which the dyes were processed from tetrahydrofuran solution compared to toluene or dichloromethane solution usually lead to lower efficiency results, tetrahydrofuran is only used in cases when the dye cannot be solved in the other solvents. Though **150** and **149** were both processed in the same solvent, top efficiency results were achieved with different additives. As described in the introduction and chapter 3, additives interact with the semiconductor surface, e.g. increasing its polarity, and are used to tune the energy level of the conduction band to optimise the driving force for injection. As the cyclic voltammetry measurements imply, the two dyes possess very different LUMO energy levels. Especially the rather high LUMO level energy of **150** allows to use an additive raising the energy level of the conduction band. This leads to an increased open-circuit voltage

(nearly 1 V for **150**, by far the highest value presented in this thesis), whilst still being able to inject efficiently into the titanium dioxide. At the same time additives take up space on the titanium dioxide surface, decreasing the dye concentration. This effect can differ for different additives and dyes and may have been stronger in the case of the additive used for **150** than the additive used for **149** and **142**. Last but not least, **150** possesses the lowest extinction coefficient of the three dyes in solution, which of course affects also the absorbance on titanium dioxide. However, with regard to the EQE (figure 5.11), **142** reaches a similar value as **149**, while **150** shows even higher intensities, indicating a rather high internal quantum efficiency for **150**. In broadness, however, the spectra of **142** and **150** are clearly inferior to **149**, which exceeds **142** by around 200 nm and **150** by 300 nm in the long wavelength region. In the short wavelength region, **150** outclasses **149** in its EQE intensity, suggesting potential to further optimise **149** towards additional light harvesting, which will be discussed in the following subchapter.

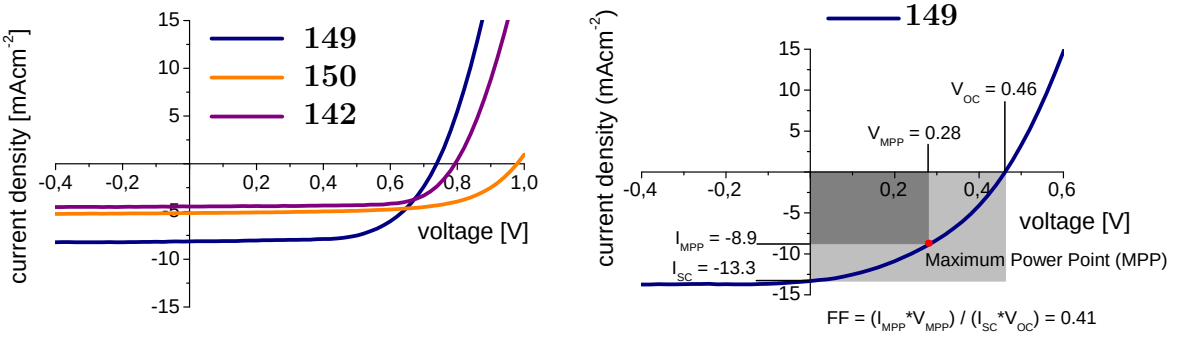

(a) IV - top efficiencies

(b) IV - top current

Figure 5.11: IV-curves of the top efficiency measurements of the dyes (a) and IV-curve of the top current measurement of **149** (b)

Another remarkable characteristics of **149** is the short-circuit current of 13.3 $mAcm^{-2}$ that can be achieved (figure 5.11) by choosing an additive which lowers the conduction band of the semiconductor, similar to the approach taken for sensitiser **83** in chapter 3 on page 57. This is to the best of knowledge an unprecedented value for perylene sensitisers in sDSSCs. Using additives boosting the current by lowering the titanium dioxide conduction band will, however, always have a negative influence on the open-circuit voltage, leading to a decreased energy difference between the conduction band of the semiconductor and the valence band of the hole transporting material. In fact, the open-circuit voltage of 460 mV in this measurement was only a little more than half of the top-efficiency measurement. In addition to these two values, the fill factor, strongly dependent on the shape of the I-V curve, is of similar importance. Here, the fill factor of 0.41 is a rather low value (figure 5.11). Combined with the low open-circuit

Dye	λ_{max} [nm] / ϵ [$M^{-1}cm^{-1}$]	LUMO [eV]	HOMO [eV]	bandgap [eV]
150	485 / 25,320	-3.1	-4.8	1.7
142	522 / 31,469	-3.5*	-5.6**	2.1
149	607 / 36,675	-3.5	-5.0	1.5

Absorption measured in tetrahydrofuran, HOMO and LUMO determined by cyclic voltammetry in dichloromethane; *determined by cyclic voltammetry in tetrahydrofuran due to solubility problems in dichloromethane; **HOMO estimated via optical bandgap as the oxidation could not be clearly detected by cyclic voltammetry.

Table 5.2: Optical and electrochemical properties of the *Cadogan dyes*

Dye	EQE_{max} [%]	V_{OC} [mV]	I_{SC} [$mAcm^{-2}$]	FF [%]	η [%]
142	38	800	-4.5	72	2.6
149	40	740	-8.1	64	3.8
150	50	980	-5.2	64	3.2

Table 5.3: Photovoltaic performance of the *Cadogan dyes*

voltage, this may be a second reason for the low efficicency of 2.5% despite the high current.

5.4 Additional Light Harvesting

Compared to the sensitisers with rigid π-spacers, e. g. **60** with an an efficiency of up to 4.5 %, the efficiency of the *Cadogan perylene monoimide* with donor η 3.8 % is a little lower. All dyes, however, need individual treatment upon processing, so in a system optimised for the spacer dyes of chapter 2 on page 31, 3.8 % is a very respectable first result, which can be considered in the same range as the spacer dyes. This new dye (**149**) shows several remarkable features including a strong red-shift in absorption, leading to an unprecedented bathochromic EQE curve for perylene sensitisers reaching out to 900 nm, and an exceptionally high current of 13.3 $mAcm^{-2}$. A third outstanding feature is that these values are reached by a dye showing a large absorption gap in the high energy region of 400-600 nm, leaving an enormous potential for further optimisation.

Filling this absorption gap might be achieved by two strategies. One is in the sphere of device making, namely using dye-cocktails of complementary absorbing dyes or building tandem cells. Here, the naphthalene monoimide **150**, with donor absorbing mainly in the desired short-wavelength region and having the benefit of a high current, might be a suitable partner for the perylene monoimide **150**. The second strategy relies on synthetic chemistry, introducing an additional chromophore, filling the absorption gap and capable of transferring this energy via Förster resonance energy transfer (FRET) to the indole-extended perylene core.

In case of **149**, there are two possible sites to achieve such a bichromophore system. One is the donor which could be varied, the other is the indole nitrogen. In the case of donor variation, only chromophores without an additional acceptor moiety are advisable. A second acceptor moiety on the donor would weaken the molecular dipole and lead to deteriorated charge transfer to the perylene. Sensitisers with stronger ICT character exhibit improved injection efficiency, leading to higher currents. Moreover, more polarised dyes are also known to show higher open-circuit voltage.[66] In case of introduction of a second chromophore on the indole nitrogens, an alkyl chain could be used to bridge the indole-perylene core to a second chromophore, which could be either polar or apolar. The introduction of a chromophore bearing its own anchoring group is also imaginable, such a compound would be a hybrid of the bichromophore and dye-cocktail with a fixed dye-ratio. The short-wavelength absorbing chromophore could either transfer the energy via FRET to the perylene system, or directly inject electrons into the titanium dioxide conduction band. This direct injection could also take place without an anchor, if the short-wavelength absorbing dye remains close to the titanium dioxide.

Bichromophoric Systems for Energy Transfer Because of the high degree of flexibility in chromophore choice, the concept of introduction of a second chormophore on the indole nitrogen was pursued as a first step towards additional light harvesting. This was carried out in cooperation with Zagranyarsky who synthesised and introduced two chromophores on the indole nitrogen of the *Cadogan perylene monoimide* with donor - a tetrathiophene (**156**) having no dipole and a push-pull naphthalene imide derivative (**167**). The syntheses and final structures are shown in figure 5.12 on the next page and 5.13 on page 110.

The introduction of a tetrathiophene was achieved by alkylation of the indole nitrogen with 2-bromo-5-(bromomethyl)thiophene in tetrahydrofuran using sodium hydride as the base at room temperature. Subsequently, a linear terthiophene boronic ester was coupled under Suzuki conditions. In order to introduce the anchoring group the bichromophoric system was saponified in basic conditions and imidised with glycine in imidazole. Handling of this compound proved to be rather difficult due to low solubility and a tendency of the thiophene chain to easily cleave.

The *push-pull* naphthalene derivative was built up from a 4-bromo-naphthalene monoanhydride which was first reacted with benzene-1,2-diamine in acetic acid in a condensation reaction with nearly quantitative yield; however, giving two different conformational isomers. The donor was prepared in parallel by reacting 1,6-dibromohexane with aniline and sodium hydride in acetonitrile at 60°C for four hours, unfortunately yielding only 17 %. The two building blocks were joined via a Buchwald coupling to give the push-pull naphthalene derivatives (**164**/**165**) with a bromo-terminated C_6-

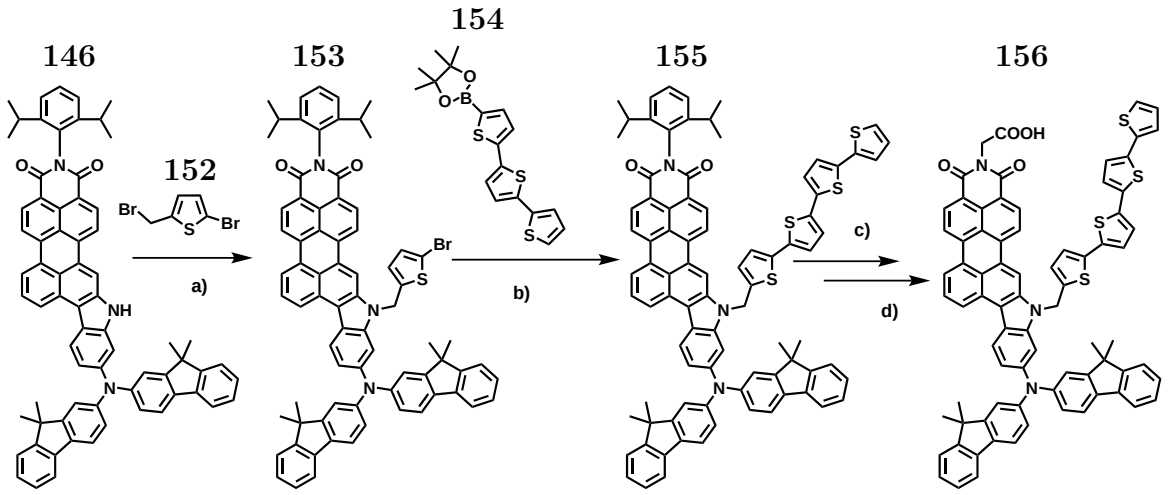

Synthesis carried out by [redacted].
a) NaH, THF, 3h, rt, yield: 94 %; b) $Pd(PPh_3)_4$, K_2CO_3 (1M), 1,4-dioxane, 85°C, 5h yield: 83 %; c) KOH, 2-methyl-2-butanol, 1,4-dioxane, reflux, overnight, yield (crude): 90 %; d) glycine, imidazole, 140°C, overnight

Figure 5.12: Introduction of a tetrathiophene on the indole nitrogen of the *Cadogan perylene monoimide* with donor

chain. Under alkylation conditions the naphthalene derivative was introduced at the indole nitrogen and the resulting bichromophore was saponified and imidised under the established conditions. Compared to the previously described sensitiser **156**, the compound was much better soluble and stable.

The normalised absorption spectra of the bichromophoric systems are compared to that of **149** in figure 5.14 on page 111. Both, the tetrathiophene and the naphthalene chromophore manage to improve the absorption between 400 and 500 nm, although still lacking in intensity compared to the bathochromic CT-band deriving from the perylene push-pull system. For the naphthalene chromophore, the spectra of the isomer mixture (red curve) and the pure isomer **167** (black curve) were recorded, with little difference noted between the two.

Looking at the absorption on titanium dioxide (figure 5.14 on page 111), however, the bichromophoric systems show relatively poor absorbance. Without quantifying the amounts of adsorbed dye, this comparison can be made as the same type of substrates with a titanium dioxide layer thickness of 1.8 μm were used. The intensity in the short wavelength region is similar to the intensity in the long wavelength region. The poor extinction on titanium dioxide could be due to the poor solubility of the bichromophoric systems in dichloromethane or the different additive used during the processing compared to **149**. A third and very likely reason may be the size of the molecule resulting in a poor dye loading due to steric hindrance.

A similar picture can be detected in the EQE spectrum in figure 5.15 on page 111. The bichromophoric systems show an acceptable EQE of up to 30% in the region from

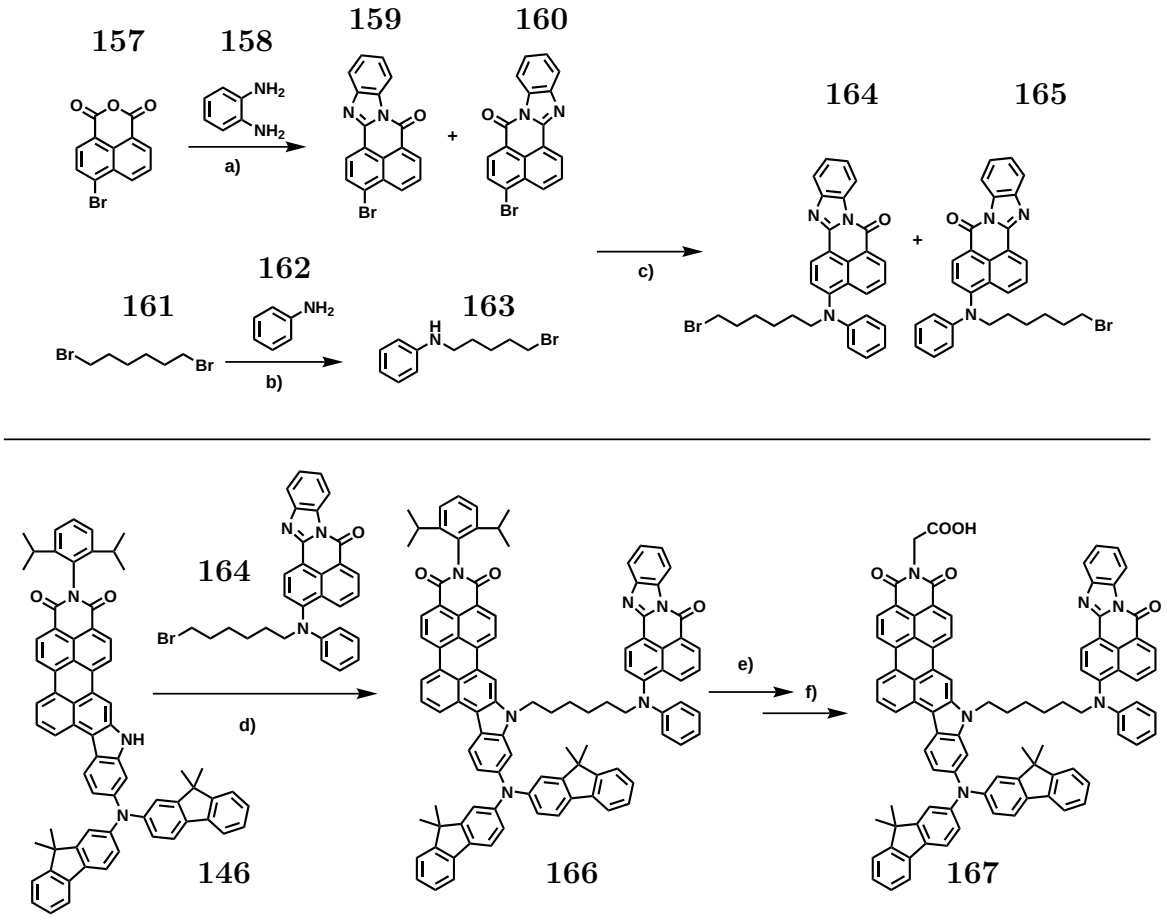

Synthesis carried out by [redacted].
a) acetic acid, yield: 98 %; b) NaH, acetonitrile, 60°C, 4h, yield: 17 %; c) NaO*t*Bu, $Pd_2(dba)_3$, tri-*t*-butylphosphine, toluene, 90°C, 2h, yield: 60 %; d) K_2CO_3, 18-crown-6, o-xylene, reflux, 20h, yield: 69 %; e) KOH, 2-methyl-2-butanol, reflux, overnight, yield (crude): 89 %; f) glycine, imidazole, 140°C, overnight, yield: 55 %

Figure 5.13: Synthesis of a push-pull naphthalene derivative (a) and its introduction on the indole nitrogen of the *Cadogan perylene monoimide* with donor (b)

Dye	EQE_{max} [%]	V_{OC} [mV]	I_{SC} [$mAcm^{-2}$]	FF [%]	η [%]
156	29	700	-4.7	58	1.9
167 + Isomer	32	800	-4.7	61	2.3

Table 5.4: Photovoltaic performance of the bichromophoric systems

450-500 nm but at long wavelengths this drops to a relatively poor EQE of only 10-20%. This long wavelength value is roughly half of what **149** shows; however, only the orders of magnitude can be compared because of the differences in processing due to the distinct needs of each dye.

The I-V curves reflect this proportion in the EQE curves. With comparable open circuit voltage – especially between **149** and **156** – the bichromophoric systems reach only a little over half the short circuit current of **149**. The short circuit current is

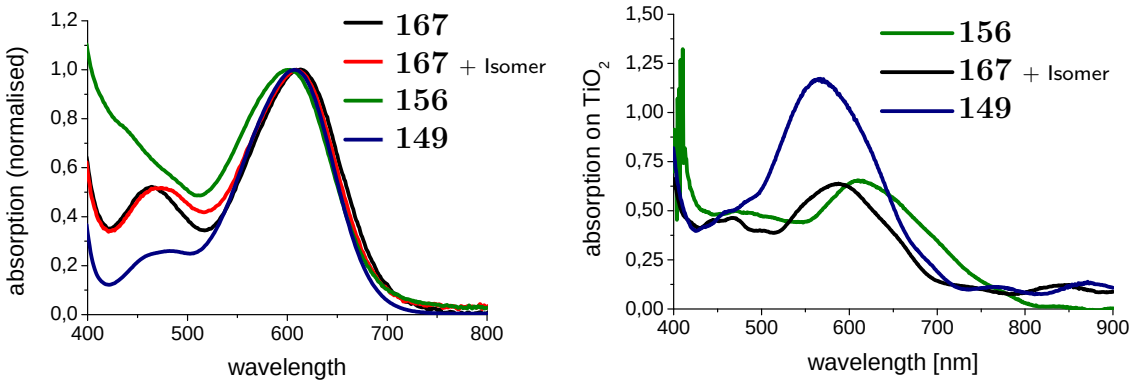

(a) Solution absorption (b) TiO_2 absorption

Figure 5.14: Absorption spectra of indole-functionalised bichromophoric systems in comparison with the *Cadogan perylene monoimide* with donor in solution (a) and on TiO_2 (b)

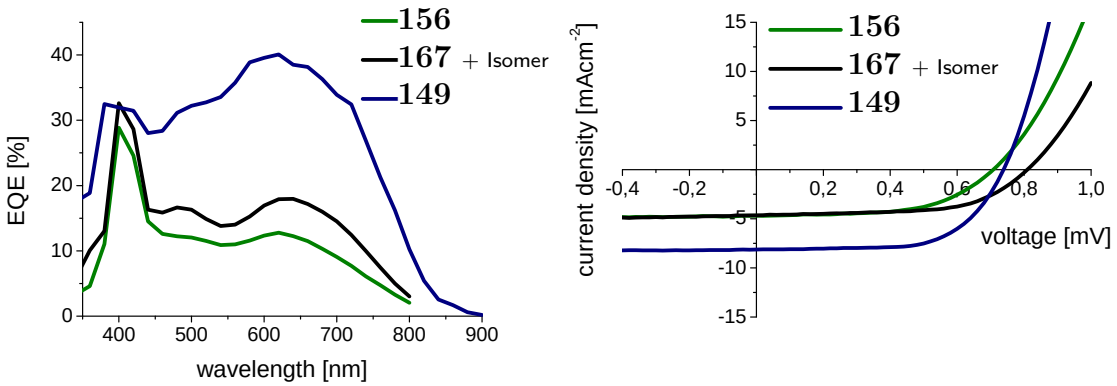

(a) EQE (b) IV

Figure 5.15: EQE-curves (a) and IV-curves (b) of the indole-functionalised bichromophoric systems in comparison with the *Cadogan perylene monoimide*

in general strongly connected to the broadness and intensity of the EQE curve which is in itself strongly influenced by the absorbance spectrum on titanium dioxide. The initial success in intensifying the absorption in the short-wavelength region, which could be demonstrated in the solution absorption spectrum, could unfortunately not be transferred onto the titanium dioxide. This in turn resulted in a loss of efficiency. Neither of the bichromophoric sensitisers could reach efficiency values of more than 2.3%.

The above mentioned introduction of a second chromophore for light harvesting purpose on the donor seems after the drawbacks of the indole-functionalised systems a promising alternative for the future. Main benefit would be that the original slim rod-like shape of the molecule could be preserved, hopefully allowing better adsorption on titanium dioxide. For this reason, a rather small chromophore should be chosen.

Moreover it should have a low dipole moment in itself in order not to disturb the push-pull nature of the molecule. Pyrene has already in the spacer series of chapter 2 on page 31 proven to be an outstanding chromophore for short wavelength light harvesting, the bis-pyrenylamine donor to be an excellent donor moiety. Hence, for the *Cadogan perylene monoimide* optimisation, use of the bis-pyrenylamine donor seems a promising option.

Dye-Cocktails A common concept to increase the photoresponse of a cell is combining two dyes which possess complementary absorption spectra. This can be done either by loading one dye after the other on the titanium dioxide or by mixing the two dyes in one solution to adsorb. Cid et al.[141] for example used the sequential adsorption process with the phthalocyanine dye **TT1** and 2-cyanoacrylic acid-4-(bis-dimethylfluoreneaniline)dithiophene (**JK2**) whereas Ogura et al.[142] directly mixed an organic (**D131**) with a ruthenium-based dye (**black dye**). In both cases, increased efficiencies could be achieved for the cocktail cells compared to the cells containing the individual dyes and also the current record of 12.3 % in liquid DSSCs presented in the introduction was achieved by a co-sensitisation concept.[16] However, the increase in efficiency compared to the better performing dye of the cocktail is usually moderate. For Cid et al.[141] the efficiency of **JK2** of 7.08 % was improved to 7.74 % by co-sensitisation with **TT1**, and from 7.00 % to 7.43 % with a sqaraine dye **SQ1**[143]. In the case of Ogura et al.[142] the efficiency of 10.0 % of the **black dye** could be enhanced to 11.0 % in a cocktail with **D131**.[1] Main driver for the increased efficiency is the improved current, closely connected to the spectral response. Wheras the short-circuit currents of cocktail cells are generally higher than the short-circuit currents of the individual sensitiser cells, the open circuit voltage tends to be a compromise of the ones measured in the individual cells. The only moderate increase in efficiencies which could be demonstrated so far, is a main drawback of the co-sensitisation concept because at the same time the complexity of the system is considerably increased: two sensitisers have to be synthesised and especially in case of stepwise adsorption, the device making process is more complicated.

Compound **149** was tested together with a naphthalene-based sensitiser (**ID741**), which was synthesised by BASF.[2] The solution absorption spectra of **149** and **ID741** are presented in figure 5.16 on the next page. In solution **ID741**, with its rather low extinction coefficient, is only able to fill a small part of the absorption gap left by **149**. Looking at the absorption of the dyes on titanium dioxide, the desired additional absorption in the short-wavelength region of the spectrum can be detected; unfortunately

[1] The high efficiency cocktail systems described here were applied in liquid DSSCs.

[2] While its structure cannot be disclosed here, the main purpose of this section is to show the principle of light harvesting optimisation of **149** with **ID741** in a dye-cocktail. Consequently, more relevant than the structure of **ID741** are its optical properties.

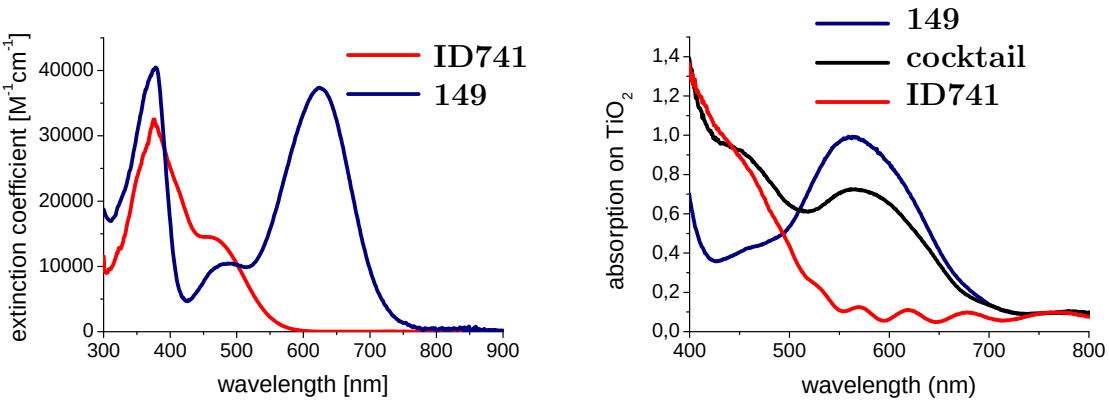

(a) Solution absorption (b) TiO_2 absorption

cocktail: **149** + **ID741**

Figure 5.16: Solution absorption (a) and absorption on titanium dioxide (b) of **149** and its dye-cocktail partner **ID741**

combined with a decreased extinction in the region of 500-700 nm. This is not surprising as now both dyes have to "share the space" on the titanium dioxide-surface for anchoring, another reason why efficiencies of individual cells are usually not additive in a cocktail cell.

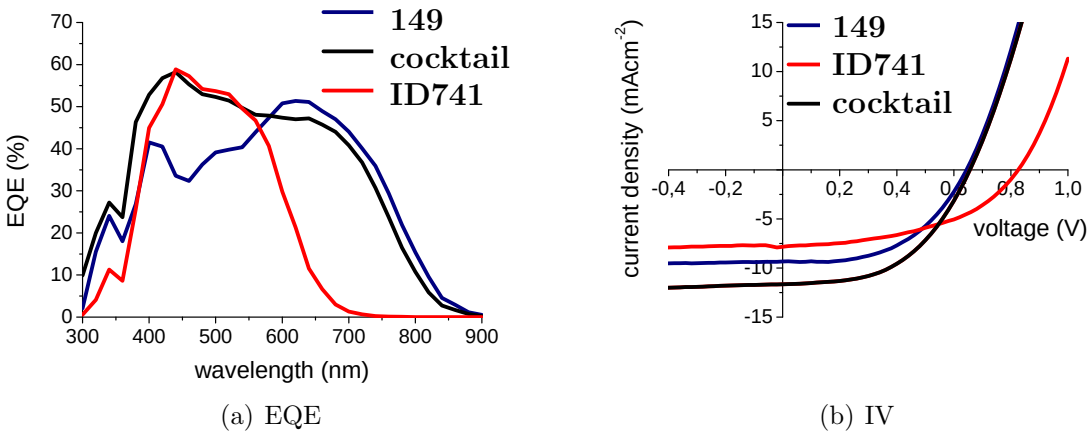

(a) EQE (b) IV

cocktail: **149** + **ID741**

Figure 5.17: EQE-curves (a) and IV-curves (b) of **ID741**, **149** and their cocktail cell

The EQE spectra of the individual dyes and the cocktail are presented in figure 5.17. For the cocktail the curve shows high intensities at shorter wavelengths like the EQE spectrum of the individual **ID741** cell. In the longer wavelength region the contribution of **149** leads to a high EQE as well, again similar in intensity to the one of the individual **149** cell. At first glance this may seem surprising as the absorbance on titanium dioxide

Dye	EQE_{max} [%]	V_{OC} [mV]	I_{SC} [$mAcm^{-2}$]	FF [%]	η [%]
149	51	640	-9.34	52	3.0
ID741	59	820	-7.83	47	3.0
cocktail	58	660	-11.77	51	4.0

Table 5.5: Photovoltaic performance of **149**, **ID741**, and the two dyes in a dye-cocktail

was lower in case of the cocktail but like the additives, the addition of **ID741** might have supressed aggregation of **149** and prevented unwanted recombination reactions between the dye molecules. Aggregation of **149** molecules could also be the reason for the slightly broader EQE of the **149** cell towards the NIR.

The broadened EQE spectrum of the cocktail cell compared to the ones of the individual dyes is directly reflected in the improved current of 26 % compared to the individual **149** cell and even 50 % compared to the **ID741** cell. Regarding open-circuit voltage, however, the cocktail cell could reach only about the same open-circuit voltage (660 mV) as the cell of **149** (640 mV). It could thus not profit from the high open-circuit voltage of **ID741** (820 mV). Nevertheless, with an overall power conversion efficiency of $\eta = 4\%$ compared to $\eta = 3\%$, the cocktail cell shows an increase of 25% in efficiency compared to the single dye cells. This increase is in good agreement with the 26 % current increase compared to the individual **149** cell on the one hand and the strong current increase (50 %) combined with the voltage loss (22 %) in the individual **ID741** cell. Admittedly, **149** does not reach its top current or voltage values[3] in this testing series but an $\eta = 4\%$ could not be reached using **149** alone.

The first attempt of using **149** in a dye-cocktail was successful and proved the concept of being able to harvest additional short-wavelength light, improving the current and overall power conversion efficiency of the cell. Employing dye-cocktails, however, increases the complexity of the cell system and therefore in most cases also the costs. Therefore, an only small performance improvement is not enough to justify the additional effort. If, however, a better matching partner can improve the efficiency considerably reaching an overall efficiency well beyond 5%, therefore outperforming the *spacer dyes* (chapter 2 on page 31), then the use of dye cocktails is certainly an attractive option towards highly efficient devices. This will need careful matching of the dyes regarding their spectral properties and open-circuit voltage. Regarding the absorption, **150** would certainly be an interesting partner. Looking at the solution spectra (figure 5.8 on page 102), **150** fits much better into the absorption gap of **149** and is itself with efficiencies over 3 % a well working sensitiser. However, the good performance results mainly from its very high voltage which again, like in the case of **ID741**, might be lost in a cocktail with the lower voltage dye **149**. Regarding voltage,

[3]The top values presented in table 5.3 on page 107

a perylene sensitiser, maybe even one of the spacer dyes, e.g. **57** with its open-circuit voltage of 760 mV but stronger current properties and absorption maximum at 512 nm might be a better cocktail partner for **149**.

5.5 Six-Membered Rings and Double Cadogan Reactions – An Outlook

Besides the above reported indole extension of the perylene core through the *peri*-position, the *Cadogan reaction* offers more options for interesting chemical modifications, three of which shall be briefly presented in this chapter: six-memeberd ring formation via *Cadogan chemistry*, five-six-membered double ring formation, and two times *Cadogan ring fusion* on perylene monoimide. All three projects are in an early stage of investigation, only preliminary tests and observations have been made up until now. The following will not be a success story of new sensitisers but an account of three attempts to broaden the application of the perylene monoimide *Cadogan chemistry* in three different directions. Their presentation in this context should be regarded as an outlook.

Six-Membered Ring Formation The first modification, the six-membered ring formation is a side product (**151**) of the above described reaction leading to **149**. After the fusion step under Cadogan conditions, next to the blue target compound **146**, a green side product with a smaller retention factor on thin layer chromatography could be spotted and isolated via preparative thin layer chromatography. The compound possesses the same mass[4] as the precursor of **149** but a much more bathochromic absorption spectrum with an impressive shift of λ_{max} from 618 to 737 nm, thus roughly 120 nm (figure 5.18 on the following page), leading to the educated guess that it is in fact the product of the, according to Cadogan et al.[91], less favoured six-ring formation yielding **151**.

DFT-calculations suggest a more hypsochromic λ_{max} for **151** than for the isomer **146** and the prediction of the HOMO/LUMO coefficient localisation suggest, that **151** shows almost no orbital partitioning like **142**. Here the DFT-predictions seem to have failed, clearly underestimating the influence of the donor group in the extended *peri*-position which is visible in the experimentally obtained absorption spectrum.

Unfortunately, a number of peaks in the ^{1}H-NMR spectrum are broad making a clear interpretation impossible. Even high temperature measurements in tetrachloroethane could not improve the resolution of the peaks. The best results were achieved on a 700 MHz spectrometer in tetrahydrofuran at 298 K as shown in 5.19 on page 117. The

[4]FD Mass Spectrum (8kV): m/z = 968.5 (100 %)[M^+] (calc. 969.4)

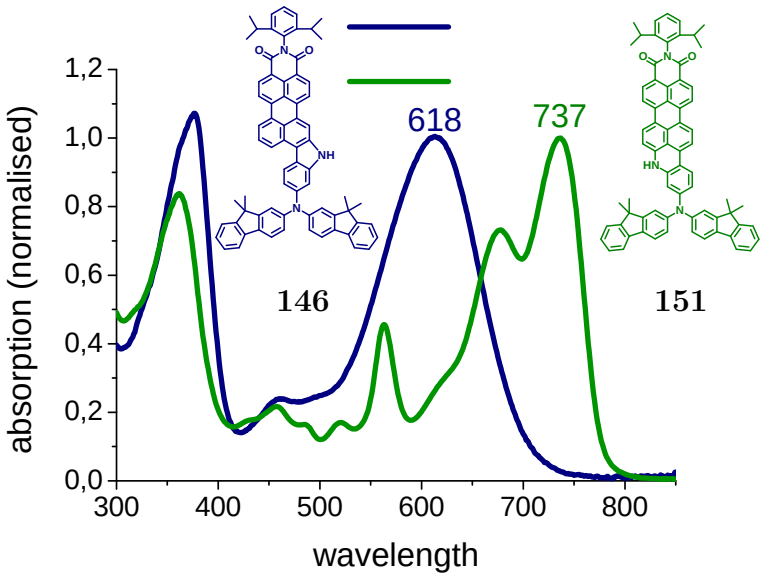

Figure 5.18: Absorption spectra of perylene monoimides enlarged by an indole (**146**) and quinoline (**151**) moiety

proton on the nitrogen within the new formed ring, however, can be assigned and clearly distinguished from the proton on the nitrogen of the five-membered ring in the case of the precursor of **149** by its shift (figure 5.19 on the facing page). Integrating this peak and defining its integration value as 1 leaves the rest of the peaks with an overall integration of roughly 28 as expected for the six-membered ring isomer.

Interestingly, not all signals in the ^{1}H-NMR spectrum of the presumed **151** are broad; the high field region of the spectrum is rather sharp. These must be the signals belonging to the donor and imide group as they are well known from other compounds bearing the same groups. The protons of the core, however, are all broad, suggesting a high degree of aggregation which is in good agreement with the lower solubility of this green derivative compared to **146** and the large flat core of the six-membered ring.

Besides the broad peaks, the purity of the six-membered ring compound seems worse than the one of the five-membered ring. Purification of the compound proved to be very difficult due to the compounds strong interaction with the silica gel during column chromatography and though less soluble than the five-membered ring **146**, precipitation or crystallisation of **151** was not successful. An attempt to alkylate **151** using the same conditions (NaH, hexlybromide, DMF (anhydrous), rt, 3 h) as for the five-membered ring compounds failed as well as an attempt to introduce a phenyl-substituent in an Ullmann reaction (iodobenzene, potassium carbonate, CuI, 2,2'-bipyridine, *o*-dichlorobenzene, reflux, 24h). In both cases no conversion occured. Introduction of an aryl or alkyl group would have increased the solubility of the compound and simplified the purification of it.

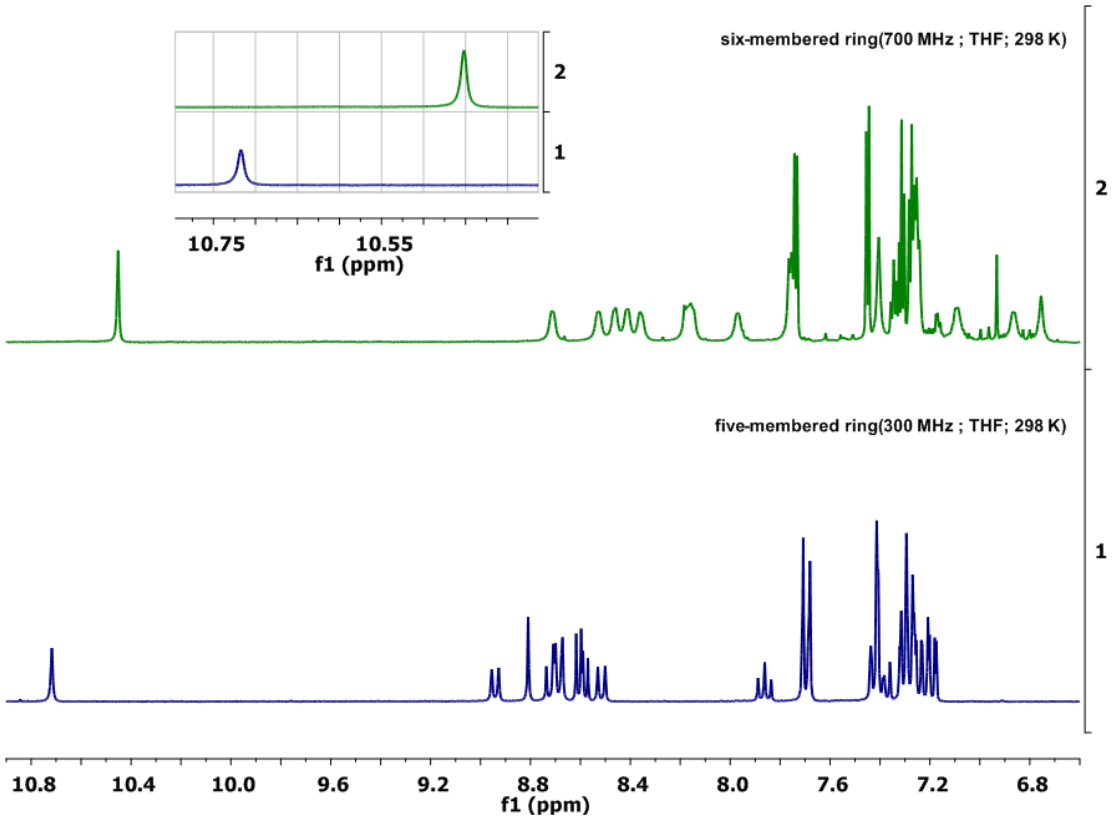

Figure 5.19: Comparison of the ^{1}H-NMR aromatic regions of the five-membered ring and six-membered ring Cadogan perylene monoimide with donor.

Double Cadogan Reaction on Perylene Monoimide A second synthesis opportunity is the combination of the five- and six-membered ring in a double *Cadogan reaction* (**172**). This was attempted on a perylene monoimide as demonstrated in figure 5.20 on the next page. Via Suzuki coupling 4-bromo-3,5-dinitroaniline **168** was introduced in the *peri*-position of *N*-(2,6-di*iso*propylphenyl)perylene monoimide. The amino-group was subsequently reacted with 1-bromo-4-(*tert*-butyl)benzene **170** in order to enhance the solubility of the compound before ring fusion. A bottleneck of this synthetic route is the Suzuki coupling, as the dinitroaniline is sterically hindered. However, a similar sterically hindered Suzuki coupling to synthesise 2,6-dinitro-1,1'-biphenyl had been achieved before, yielding 45 %.[144] Different conditions (a) $Pd(PPh_3)_4$ (10 %), K_2CO_3 (1 M), dioxane, water, ethanol, 90°C, overnight; b) $Pd(PPh_3)_4$ (15 %), K_2CO_3 (0.5 M), toluene, water, ethanol, 100°C (microwave), 1h) were tried but led in the first case only to deborylation and homo-coupling of **51** and in the second case only to traces of the desired product **169**. A combination of the conditions – lower base concentration, increased amount of catalyst, high temperature and short reaction time ($Pd(PPh_3)_4$ (0.15 M), K_2CO_3 (0.5 M), dioxane, water, ethanol, 100°C for 1.5 hours) showed better conversion. Both reactions containing product were united and purified via column

chromatography on silica with dichloromethane yielding alltogehter 11%[5] (27 mg) of **169**, relatively little compared to other Suzuki coupling reactions which achieve yields of up to 80%. The homo-coupled perylene monoimide, the open form of quaterylene diimide, which is usually known to be a small side product, is the main product of the reaction. Reason for this can be found in the steric hindrance of the two nitro groups but also in their strong electron withdrawing nature. In the previous cases, when the 1-bromo-4-chloro-2-nitrobenzene or the 1-bromo-2-nitrobenzene had been introduced, the reaction had with reaction times of 24-36 hours proceeded much slower than in other cases.

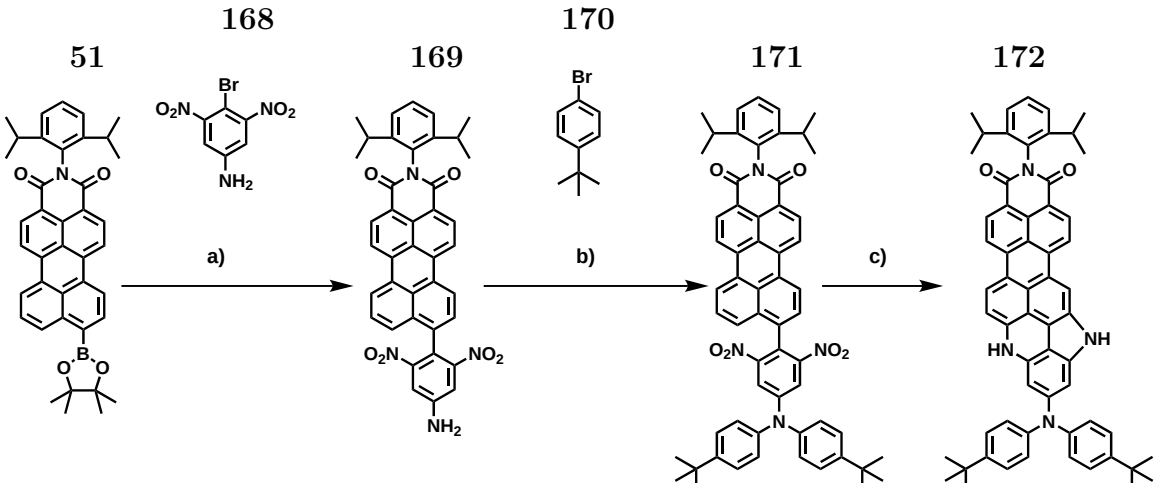

a) $Pd(PPh_3)_4$ (15 %), K_2CO_3 (0.5 M), dioxane, water, ethanol, 100°C, 1h, yield: > 11 %; b) $Pd_2(dba)_3$, tri-*t*-butylphosphine, NaOtBu, toluene, 80°C, overnight, yield: 37 %; c) triphenylphosphine, *o*-dichlorbenzene, 182°C, 300 W, 6h, conversion could not be proved

Figure 5.20: Synthesis attempt to achieve a *double Cadogan reaction* on perylene monoimide.

The desired intermediate **171** was identified via FD-mass spectrometry and ^{1}H-NMR spectroscopy. The ^{1}H-NMR spectrum of **169** is presented in figure 5.21 on the facing page clearly showing the characteristic singlet with the integration value of 2 belonging to the two protons adjacent to the nitro-groups on the *N,N*-bis(4-(tert-butyl)phenyl)-3,5-dinitroaniline moiety.

After introduction of two aryl groups on the amine functionality via Buchwald coupling yielding 14 mg (37 %) of **171**, a first attempt to fuse the dinitro intermediate in order to achieve **172** was made, leading to unclear results: after two hours the FD-mass spectrum showed primarily the mass of the one-times fused compound with still the second nitro group on the molecule, the one-times fused without the second nitro group but also the mass of a potentially two-times fused compound which could be the desired product **172**. After six hours, only the mass of **172** could be identified in the

[5]The individual yields were not determined. As the first reaction showed only traces of product, the yield of the improved conditions must have been in the range of 15-20 %.

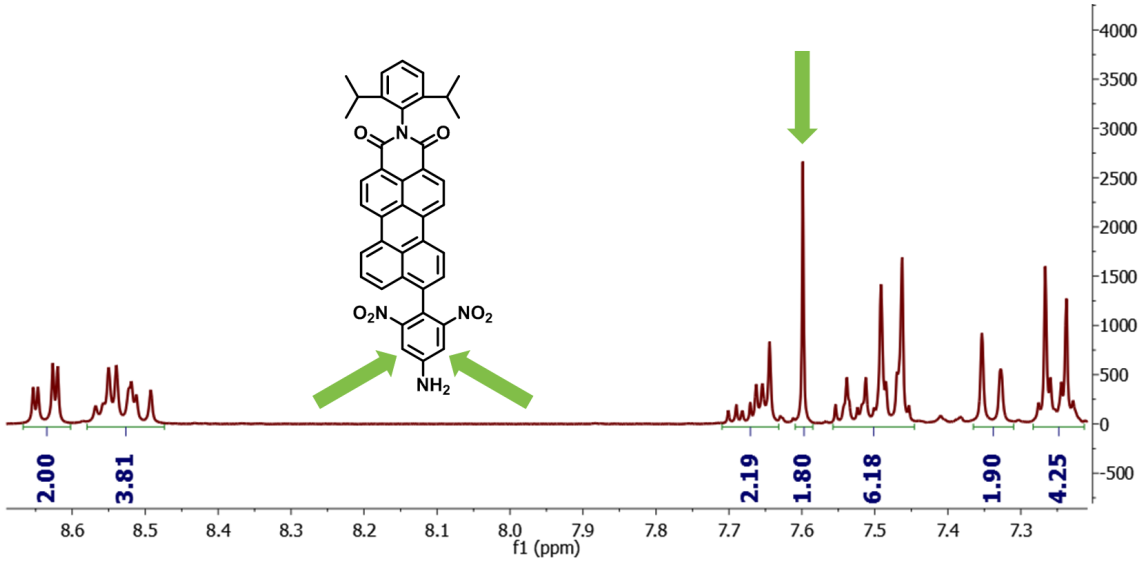

Figure 5.21: Aromatic region of the ^{1}H-NMR spectrum of the dinitro intermediate.

FD-mass spectrum besides various other peaks of either very low (m/z = 339, 538) or very high molecular weight (m/z = 1126) which could not be assigned. Unfortunately, the target compound **172** could not be isolated.

Only 14 mg of **171** had been available for the fusion reaction. In order to make stirring possible, a minimum amount of solvent had to be added. The reduced concentration of the starting material compared to prior fusions might have been a reason for lower conversion. On the other hand, the two-times fused product the must suffer from a greater deal of strain than the one-times fused derivatives. This strain might also hinder the formation of the desired product. However, as Jiang et al.[138] had shown the formation of **134** in a similarly rigid system, so it should generally be possible to yield **172**. It is disappointing that no clear conclusion could be drawn from this first experiment. The FD-mass spectrum results are, however, promising, so a larger scale reaction might be able to successfully explore this option of a *double Cadogan reaction*.

Two Times Cadogan Reaction on Perylene Monoimide Still aiming at the double donor in the two *peri*-positions described in chapter 4 on page 67, the new functionalisation option in the *edge*-positions combined with the *Cadogan fusion* seems another alternative to achieve this long desired compound.

If two nitro-benzene moieties are introduced by Suzuki coupling in the 8,11-position, three possible isomers could be formed upon fusion. Both indoles could fuse into the

7,12-positions of the perylene monoimide, one could fuse up in the 7-position, the other one down in the 10-position or both could fuse down into the 9,10-position to form a double-*peri*-donor-functionalised perylene monoimide. All three products could be formed in yields according to their statistic probability, or some kind of selectivity for one or the other position might be observed.

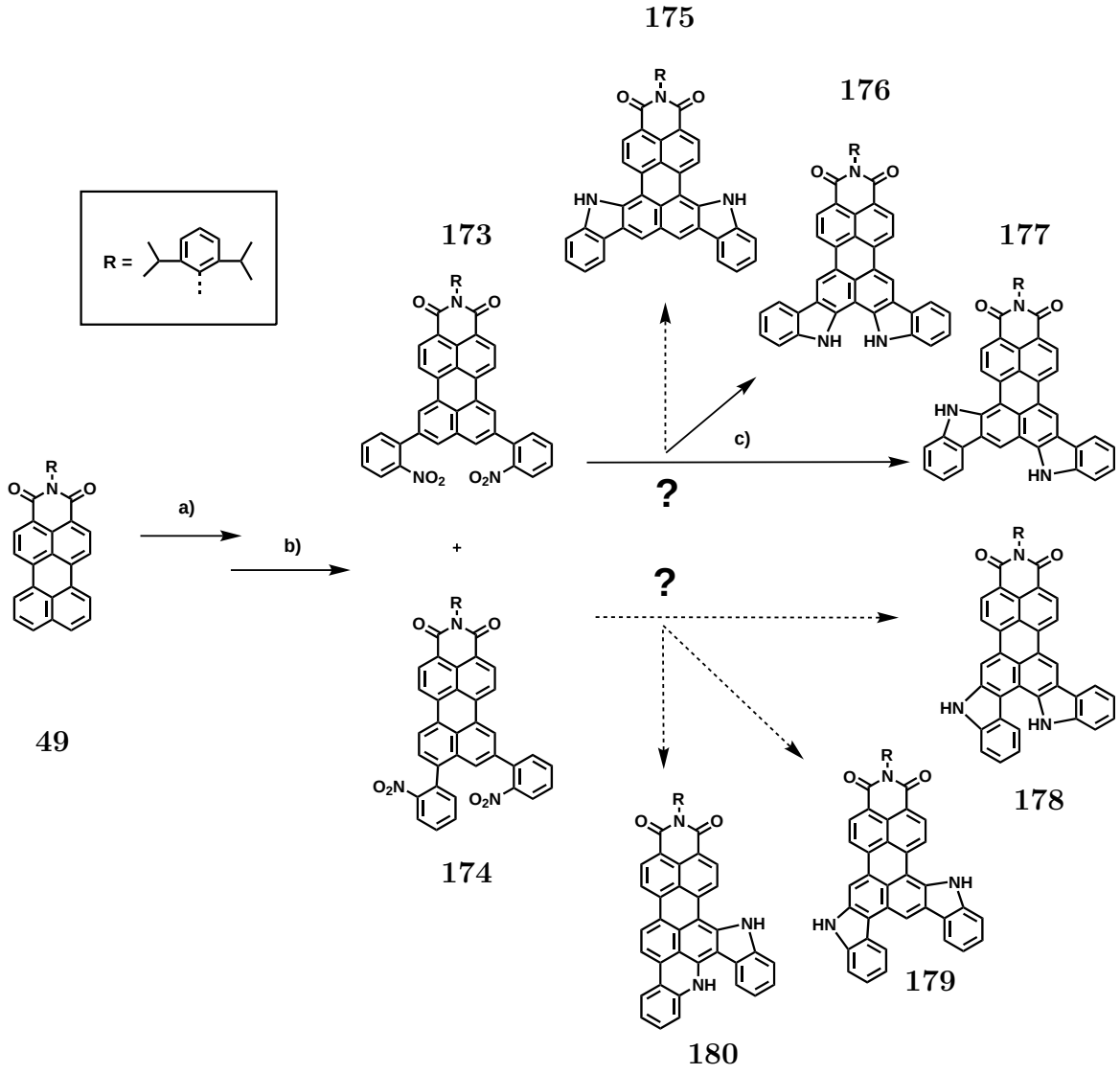

Figure 5.22: Synthesis attempt to achieve a double-donor in the *peri*-positions of perylene monoimide via *edge*-functionalisation and *Cadogan fusion*.

The synthesis was carried out as demonstrated in figure 5.22. After iridium-catalysed borylation of perylene monoimide (synthesis carried out by [redacted] and will be described in his forthcoming thesis), Suzuki coupling was performed on 500 mg of the crude borylation intermediate. The reaction lead to mono-, di- and even

tri-functionalised[6] product. What was not anticipated at the time was, that like in the *edge*-functionalisations described in chapter 4 on page 67, a mixture of 8,10- and 8,11-functionalised perylene monoimide was obtained. As the borylation and Suzuki coupling were carried out as a tandem reaction without purification of the intermediate, it is uncertain which step led to the asymmetric by-product. Via recycling gel permeation chromatography a small fraction (30 mg) of di-substituted compound could be isolated but it still contained two different starting materials (**173** and **174**) for the *Cadogan fusion*. The behaviour of the constitutional isomers is in the case of silica column chromatography as well as gel permeation chromatography too similar for them to be separated in larger quantities. If, however, the shifting mechanism can be understood and controlled, this challenge could be overcome.

The mixture of **173** and **174** is certainly not a desirable starting position for a successful and efficient synthesis. However, for proof of concept, whether this twofold fusion would be possible and whether some selectivity for either fusion to the *peri*- or fusion to the *bay*-position would be observed, the mixture was sufficient. *Cadogan fusion* was carried out in a scale of 30 mg. The possible products of this fusion are shown in 5.22 on the facing page. In general, formation of the six-membered ring is less favoured as established in literature and confirmed in the case of the perylene monoimide with donor above. Hence, isomer **180** is the least probable or expected to be formed only in negligible yields. A clean 8,11-substituted symmetrical starting material would reduce the number of possible isomers to three (**175**, **176**, **177**).

The FD-mass spectrum showed the peaks of one times as well as two times fusion upon *Cadogan conditions*. The reaction mixture was purified via two preparative thin layer chromatography plates (a) dichloromethane; b) petrol ether, dichloromethane, tetrahydrofuran, methanol). The first purification enabled separation of the one times fused from the two times fused products; the second enabled separation and isolation of the two main isomers in very small amounts (both <5 mg). Their molecular structures could be identified by means of nuclear magnetic resonance spectroscopy (figure 5.25 on the next page and 5.28 on page 123). The main product, blue to the eye as a solid, purple in tetrahydrofuran solution is the symmetrical compound **176**. The minor product, turquoise to the eye as solid and light blue in tetrahydrofuran solution, is the asymmetrical isomer **177**. It should be noted that the fact that only the two isomers **176** and **177** were isolated does not mean that the formation of the other compounds **175**, **178**, **179**, and **180** did not occur.

^{1}H-NMR, ^{1}H,^{1}H-COSY, and ^{1}H,^{1}H-NOESY spectra of the symmetrical compound **176** are presented in figure 5.25 on the next page. The ^{1}H-NMR spectrum clearly shows the two singlets and five doublets all integrating to two protons as expected for the symmetrical isomers. One of the triplets of the indole moieties can also be identified,

[6]Deriving from borylation of the *N*-(2,6-di*iso*propylphenyl)-moiety

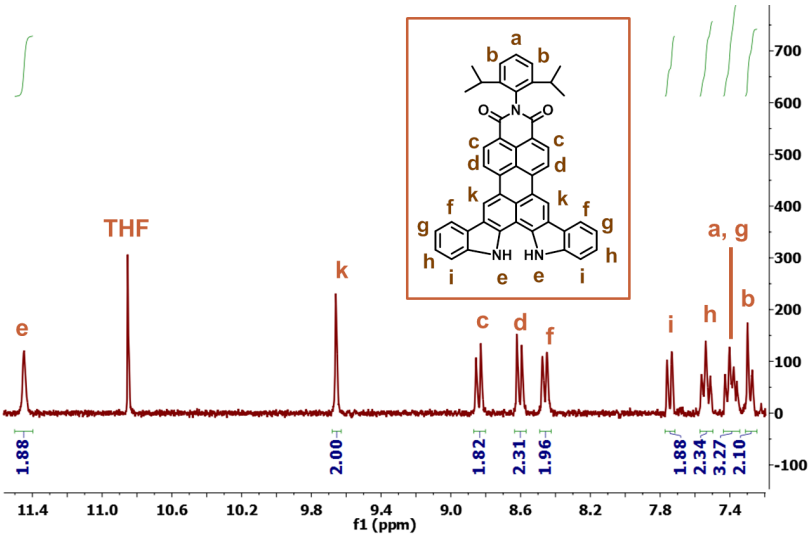

Figure 5.23: ^{1}H-NMR spectrum of the symmetric isomer **176** (300 MHz, THF, 298 K)

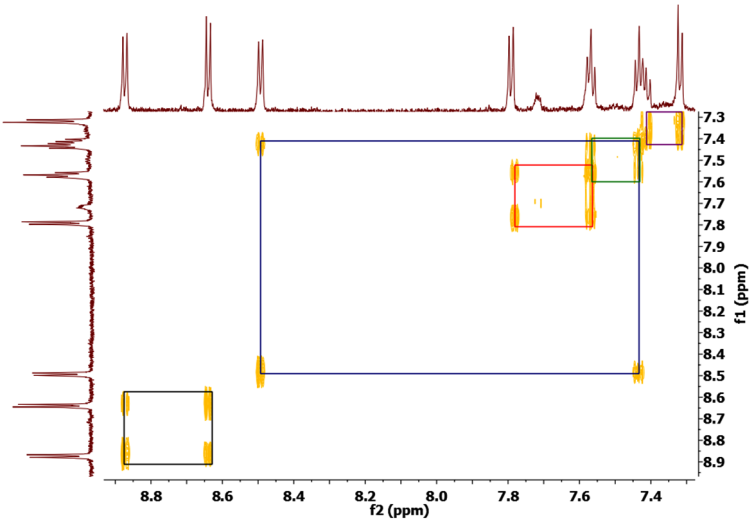

Figure 5.24: ^{1}H,^{1}H-COSY spectrum of the symmetric isomer **176** (700 MHz, THF, 298 K)

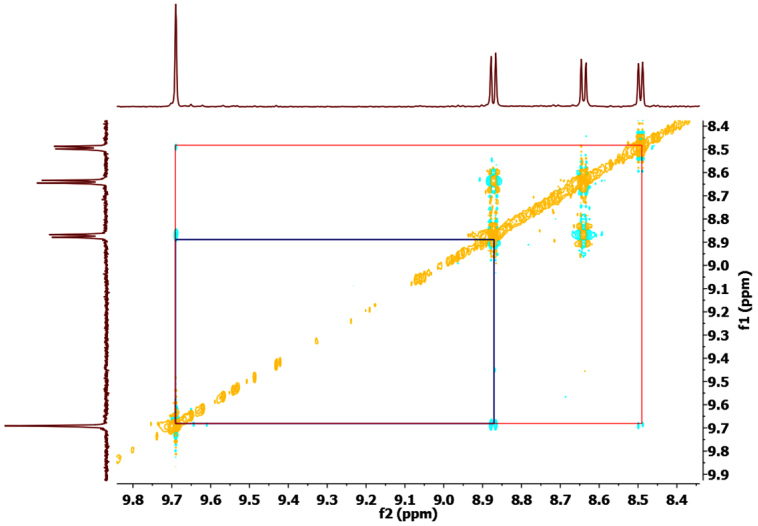

Figure 5.25: ^{1}H,^{1}H-NOESY spectrum of the symmetric isomer **176** (700 MHz, THF, 298 K)

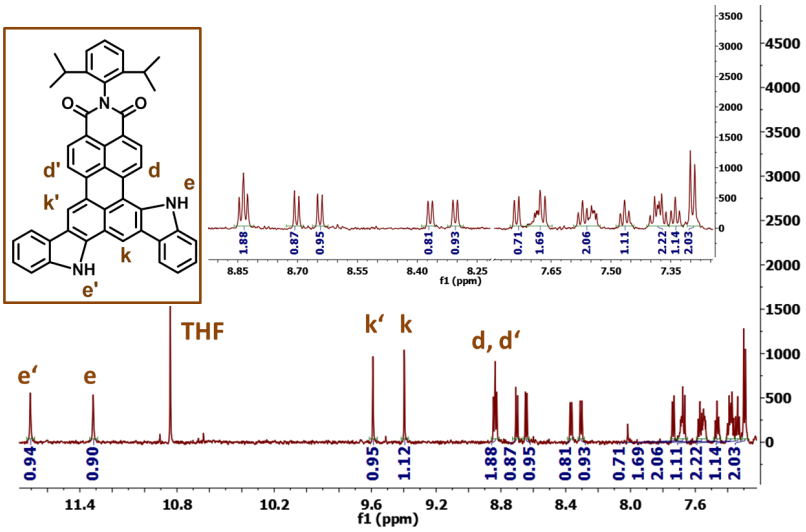

Figure 5.26: ^{1}H-NMR spectrum of the asymmetric isomer **177** (700 MHz, THF, 298 K)

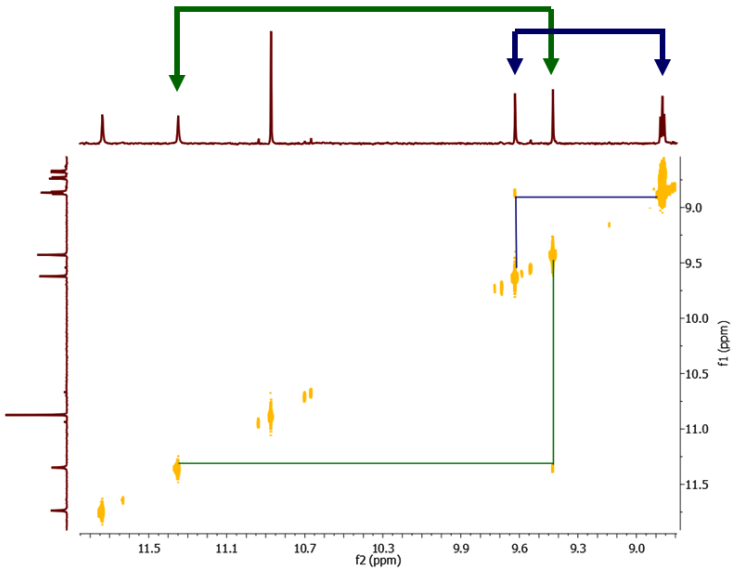

Figure 5.27: ^{1}H,^{1}H-COSY spectrum of the asymmetric isomer **177** (700 MHz, THF, 298 K)

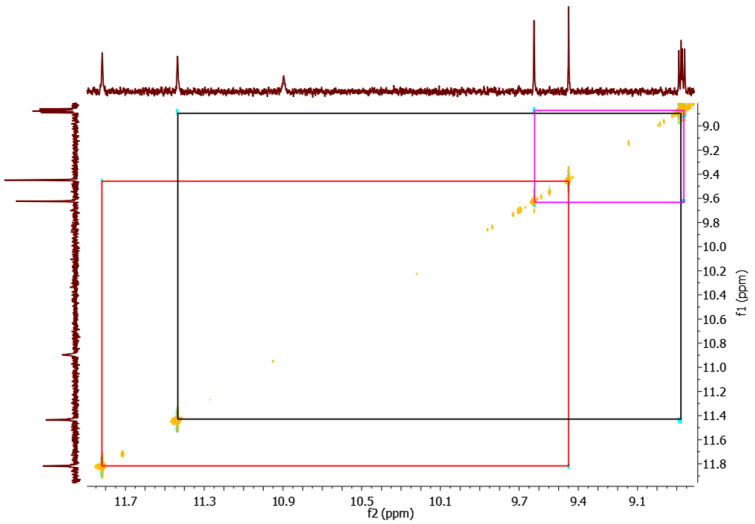

Figure 5.28: ^{1}H,^{1}H-NOESY spectrum of the asymmetric isomer **177** (700 MHz, THF, 298 K)

the other one is overlaid by the triplet of the *N*-(2,6-di*iso*propylphenyl)-moiety. The additional singlet at δ 10.84 ppm does not belong to the compound but is the signal of the protonated tetrahydrofuran, here strongly visible due to the low concentration of the product in the solution. The singlet furthest shifted to the low field can be assigned to the protons on the nitrogens of the indole moiety. This lowfield shift of the NH proton could already be observed for the *Cadogan perylene monoimide* with donor described. The ^{1}H,^{1}H-COSY spectrum helps identifying the protons c and d on the core and the *N*-(2,6-di*iso*propylphenyl)-moiety. In the ^{1}H,^{1}H-NOESY spectrum, a coupling of the singlet belonging (k) to the perylene core to the d protons is visible, now clearly proving that the singlet protons on the core are situated in the *bay*- not the *peri*-position, hence confirming that fusion occurred in the two *peri*-positions (9,10-position). Another proof is the coupling of the singlet (k) to the f protons, which are located at a distance of only approximately 2.2 Å[7]. The ^{4}J-coupling of k and d could already be detected in the ^{1}H,^{1}H-COSY spectrum, again affirming that the singlet k belongs to the protons on the perylene core, not on the indole nitrogen.

^{1}H-NMR, ^{1}H,^{1}H-COSY, and ^{1}H,^{1}H-NOESY spectra of the symmetrical compound **177** are presented in figure 5.28 on the preceding page. The splitting of the peaks, especially of the characteristic singlets belonging to the protons attached to the nitrogen and on the perylene core, make the asymmetry of the molecule evident. Having already assigned the signals of the symmetric isomer **176** helps with the set of peaks important for the identification of the isomer. Looking at the ^{1}H,^{1}H-NOESY spectrum, coupling of one of the NH-protons (e') with one of the core singlets (k) can be observed as well as coupling between the other core singlet (k') with one of the two doublets of the AB-system on the core. This already is strong evidence that one nitrogen was fused into the *bay*-, the other one into the *peri*-position. Additionally interactions between the NH-proton e with the other doublet of the AB-system on the core, a little more low-field shifted, can be observed, supporting the ealier structural suggestion. Last but not least, the ^{1}H-COSY spectrum shows ^{5}J-coupling of the NH-proton e with the core singlet k and core singlet k' with the doublet d' of the AB-system on the core.

The solution absorption as well as fluorescence emission spectra in tetrahydrofuran of both isomers are presented in figure 5.29 on the next page. The asymmetric isomer **177** shows a more bathochromic λ_{max} at 629 nm compared to the symmetric compound **176** with a λ_{max} at 595 nm. The symmetric isomer, however, exhibits an additional more bathochromic band with a local maximum at 699 nm which can be attributed to the charge transfer arising from the push of the nitrogens in both *peri*-positions. Both compounds were excited at shorter wavelengths than their absorption maxima, as for both dyes the absorption maxima are overlaid by the emission. The dyes were thus excited at their second maximum in the excitation spectrum. Both dyes possess an

[7] estimated by 3D ChemBioOffice

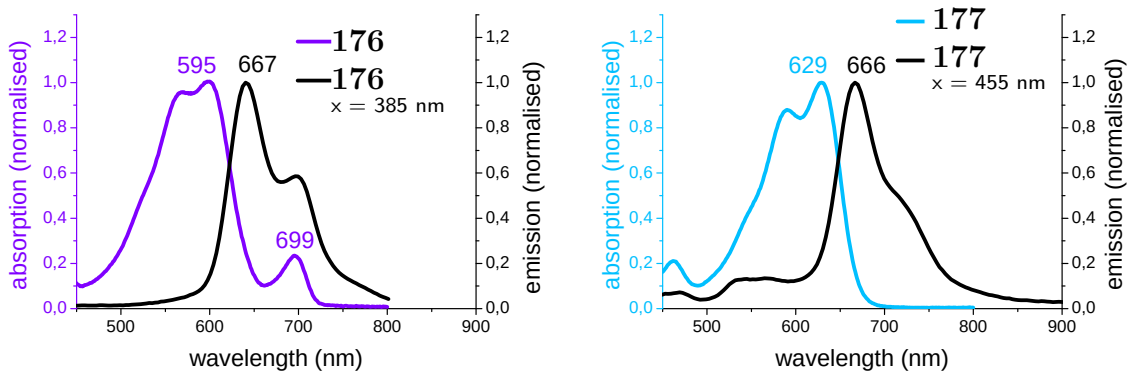

(a) **176** (symmetric) (b) **177** (asymmetric)

Figure 5.29: Solution absorption and emission of the symmetric isomer **176** (a) and the asymmetric (b) isomer **177** after two times *Cadogan fusion* on perylene monoimide.

emission maximum at 666/667 nm. Considering the more bathochromic λ_{max} of isomer **177**, this results in a rather small Stokes shift, known for asymmetric compounds. A second emission band at around 700 nm can be detected in the emission spectrum of the symmetric isomer **176**, in the asymmetric case **177** only appearing as a shoulder.

Main interest of this investigation was the fusion behaviour of the 8,11-functionalised perylene monoimide **173** and though the set-up of the experiment was not ideal, needing improvisation along the snyhtesis route, the main questions could be answered: a) two times fusion into the desired 9,10-positions is possible and b) there is a selectivity for the 9,10-fusion and not for the 7,12- or the asymmetric 7,10-fusion.

One way to force the fusion into the 9,10-positions could be by blocking the undesired 7,12-positions. A similar strategy was carried out by Curiel et al.[145], who recently published a two times fusion in the 1,8-positions of the napthtalene by previously blocking the 3,6-positions. Blocking these positions in case of the perylene monoimide bears additional synthetic challenges. It would have to be carried out after borylation or the Suzuki coupling. Whereas the 7,12-positions are available for functionalisation in the perylene diimide together with the other *bay*-positions (1,6-positions). In perylene monoimide these positions are up to now the only positions which cannot be addressed selectively. If control can be gained over the 8,10- and 8,11-functionalisation, this selectivity should be sufficient to synthesise larger scales of the double donor-functionalised perylene monoimide in the two *peri*-positions.

5.6 Conclusion

Indole extension of the aromatic core of perylene is a powerful means to enter new classes of chromophores. Using a bromo-chloro-nitrophenyl for this extension gives

an additional opportunity of introducing a second functionality. In this work the additional functionality was a donor, but for other purposes acceptor groups or a second chromophore might also be interesting.

Introducing an additional donor group and therefore introducing strong push-pull character into the naphthalene monoimide **150** and the perylene monoimide **149** leads to two very interesting new sensitisers for sDSSC – **150** being an excellent high-voltage short-wavelength dye, whereas **150** enabled light harvesting into the NIR and with its absorption dip in the near UV region still leaves room for improvement, for example to introduce a stronger short-wavelength absorbing donor group or finding a better cocktail partner than **ID741**.

A twofold fusion has already been shown on the perylene monoimide. The symmetric compound **176** that was formed could be an interesting ligand for metal complexes.

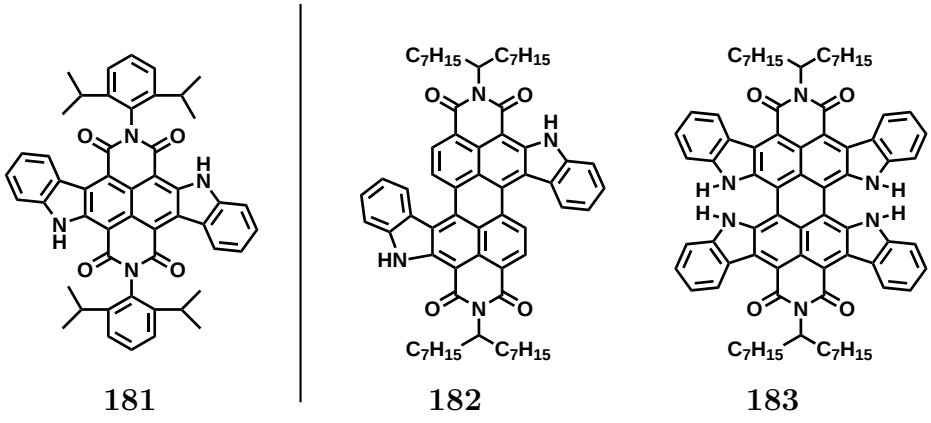

Figure 5.30: Naphthalene diimide derivative **181**[3] and possible perylene diimides **182** and **183** for the future via *Cadogan chemistry*

In this chapter the indole extension was performed only on naphthalene and perylene monoimide. In the future, also the extension of perylene diimides either via the two *bay*-positions or as lately made possible by Teraoka et al.[55] and Battagliarin et al.[56] also the four *ortho*-positions (figure 5.30) would be an interesting target in order to tune the optical, electronic and morphological properties of perylene diimides for applications in organic electronics, e. g. photovoltaics or OFETs. A similar indole extended naphthalene diimide **181** (figure 5.30), has been recently presented by Suraru et al.[3], and has been used as a p-channel semiconductor in an organic thin-film transistor with a mobility of 0.56 $cm^2V^{-1}s^{-1}$ and an current on/off ratio of 10^6. Suraru et al.[3] achieved this indole extension by a palladium-catalysed coupling of dibromonaphthalene diimide and 2-bromoaniline followed by nucleophilic substitution of the bromine at the naphthalene core. This synthesic route, however afforded a rather low yield of only 12%, whereas for the Suzuki-Cadogan sequences presented in this chapter yields of up to 50%[8] are possible. The core-extended naphthalene diimide exhibits al-

[8] 80% for the Suzuki coupling and 60% for the *Cadogan fusion*

ready a λ_{max} of 491 nm ($\epsilon = 38.600\ M^{-1}cm^{-1}$) and a second local maximum at 622 nm ($\epsilon = 24.200\ M^{-1}cm^{-1}$) in dichloromethane,[3] showing great promise for the perylene derivatives.

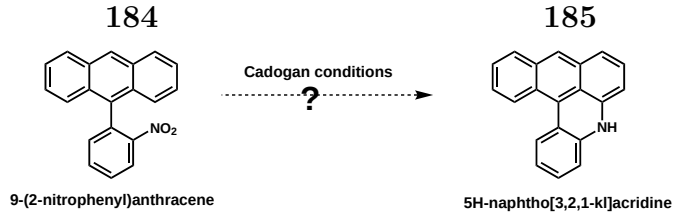

Figure 5.31: Suggested *Cadogan reaction* on 9-(2-nitrophenyl)anthracene to form 5H-naphtho[3,2,1-kl]acridine.

The topic of six-membered ring formation has been briefly explored via the investigation of a by-product in case of the *Cadogan perylene monoimide* with donor (**149**). This possibility of six-membered ring formation via the *Cadogan reaction* may offer many opportunities, especially in the case, where no five-membered ring but only a six-membered ring can be formed. A proof of concept of this hypothesis might be made by synthesising 9-(2-nitrophenyl)anthracene **184** which could only form the six-membered ring to yield 5H-naphtho[3,2,1-kl]acridine **185** (figure 5.31). If such six-membered rings could be formed easily, then this chemistry would open-up new promising paths for heterocyclic chemistry, e. g. for the synthesis of heterocoronenes.

Chapter 6

Perylene Diimide Colour Tuning

The previous chapters have focused on different approaches for the preparation of push-pull PMIs with distinct optical properties, mainly for the use in sDSSCs. This chapter will present a series of terthiophene *bay*-substituted perylene diimides. At first glance, this may look like a disruption of the general theme of this thesis. Many of the approaches presented for the perylene monoimides, however, can also be applied to the perylene diimides (PDIs), for example the attachment of the terthiophene dendron used as a π-spacer in chapter 3 on page 57. In the following, a terthiophene-PDI series along the lines of *Light Harvesting and Orbital Tuning* will be presented .

Perylene diimides are known as sensitisers in dye-sensitised solar cells and as n-type semiconductors in bulk heterojunction and flat heterojunction devices.[36] For years, research groups all over the world have been working on new PDI derivatives tuning their optical, electronic and morphological properties in order to achieve improved materials for organic photovoltaics or other organic electronics applications like OFETs or sensors.[146,43,147,148,149]

In this chapter three *N,N'*-bisoctyl perylene diimide (PDI) derivatives (compound **190-192**, figure 6.1 on page 131) with terthiophene moieties on the perylene core including the terthiophene dendron from chapter 3 on page 57 will be presented. The results of this chapter have already been presented in literature.[108]

Thiophene-based materials are well-known as both organic p-type and n-type semiconductors, and exhibit extraordinary charge transport properties that find broad application in optoelectronic devices.[150] Whereas the focus of other research groups so far has mainly been variation of the chain length of the thiophene moiety,[151,152] this work will explore three PDIs bearing terthiophene units of different architectures in the 1,7(*bay*)-positions of the perylene core (figure 6.1 on page 131). While these terthiophene-PDIs all have the same molecular weight, as they all consist of a PDI and six thiophene units, they are of distinctly different colour, i.e. bluish green, purple, and dark green, respectively, indicating a strong impact of the architecture on the electronic properties. By coupling two terthiophenes as electron-donating groups in the

1,7-position of PDI, *bay*-functionalised PDI compounds for which the first oxidation potential is shifted considerably into the negative direction compared to unsubstituted PDI could be achieved. This was the first report varying the colour of perylene dyes by only changing the arrangement of the thiophenes attached to the 1,7-positions of the perylene core.

All three compounds were prepared by Suzuki couplings of the *N,N'*-bisoctyl-1,7-dibromo-perylene-3,4:9,10-tetracarboxylic acid diimide[1] **186** with the three different terthiophene moieties (5'-(4,4,5,5-tetramethyl-[1,3,2]dioxaborolan-2-yl)-5,5"-bistrimethylsilyl)-2,2':3',2"-terthiophene[153,154] (**78**), 3'-(4,4,5,5-tetramethyl-[1,3,2]dioxaborolan-2-yl)-5,5"-bistrimethylsilyl)-2,2':5',2"-terthiophene (**187**), and 5-(4,4,5,5-tetramethyl-[1,3,2]dioxaborolan-2-yl)-2,2':5',2"-terthiophene (**154**), respectively), followed by removal of the trimethylsilyl groups with tetra-n-butylammonium fluoride (TBAF) in the cases of compound **190** and **192** (figure 6.1 on the next page). 86 mg of **190**, 45 mg of **192**, and 120 mg of **191** were obtained.

The three terthiophene moieties (**78**, **187**, **154**) were synthesised and kindly provided by Dr. Chang-Qi Ma and Martina A. Gatys, members of the group of Prof. Bäuerle at the University of Ulm. Detailed information on the synthesis can be found in the above mentioned publication.[108]

Both compounds **191** and **192** consist of linear terthiophenes based on α-α connection of the three thiophene units. For **191**, the terthiophene and the PDI core are joined via the α-position of the terminal thiophene. In compound **192**, however, it is the middle thiophene unit of the terthiophene chain which is linked to the PDI core via its β-position. In contrast to **191** and **192**, compound **190** is comprised of two branched terthiophenes containing an α-α and an α-β connection of the thiophene units within the terthiophene building block. The terthiophene itself is α-linked to the PDI core at the middle thiophene unit.

To investigate the differences in the intramolecular charge transfer (ICT) characters caused by the terthiophene architecture, the absorption and fluorescence emission spectra of compound **190**-**192** were measured and are displayed in figure 6.2 on page 132. Going from **192** $\rightarrow$ **190** $\rightarrow$ **191**, a monotonic decrease of the absorption coefficient and a red-shift of the absorption onset are observed, which indicates varying donor strength due to the different architectures of the three terthiophenes. Whereas the branched terthiophene compound (**190**) and the linear α-connected terthiophene compound (**191**) both show broad, structureless, and intense low-energy charge transfer absorption bands (transition from the ground state S0 to the excited charge transfer singlet state S1) with a maxima at $\lambda = 591$ nm and 610 nm respectively, this S0 $\rightarrow$ S1 band has almost vanished in the linear β-connected terthiophene compound (**192**).[155,156] These effects can be explained by the the decreasing length of the α-

[1] pure regioisomer of the 1,7-brominated perylene diimide available in the group

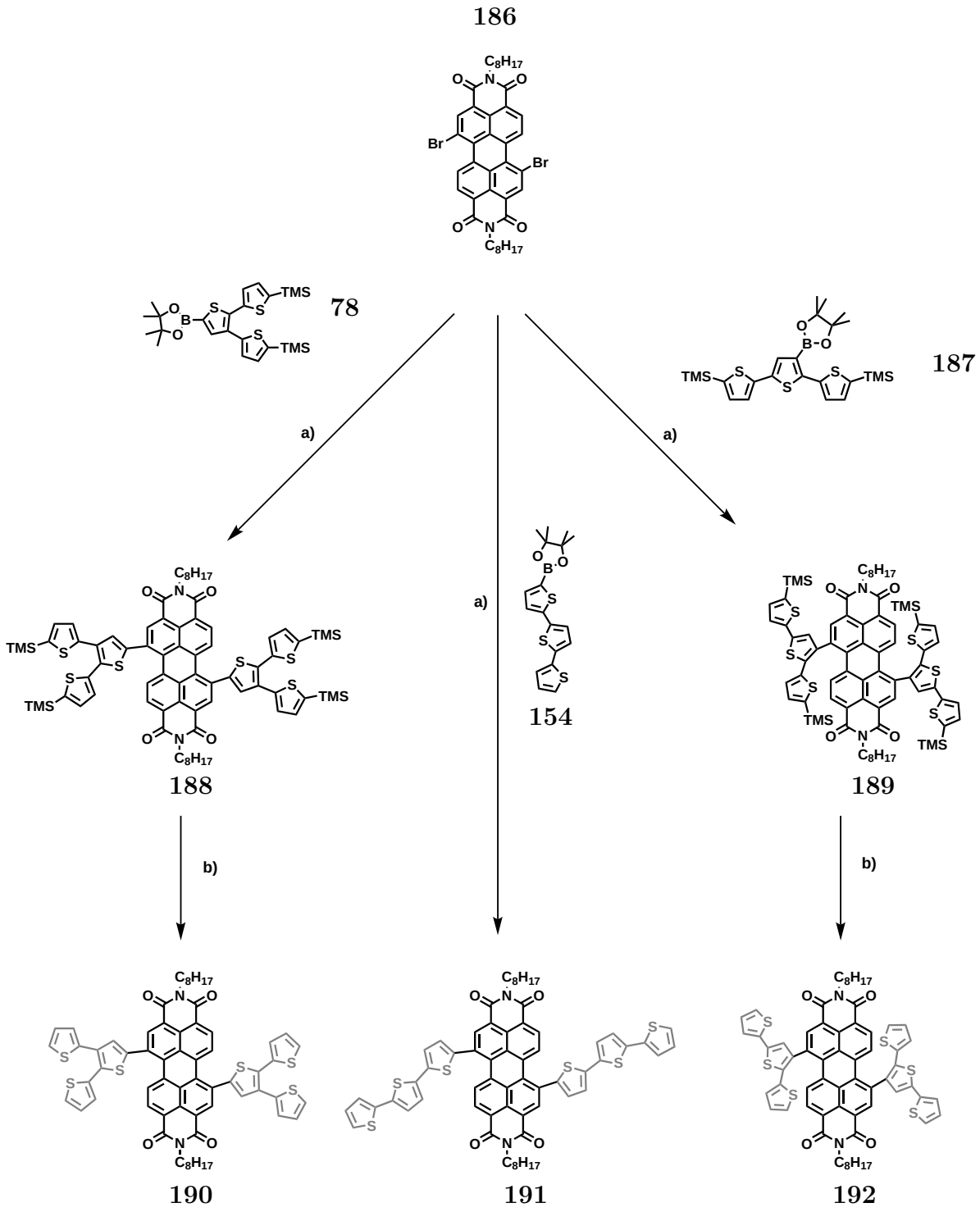

a) $Pd(PPh_3)_4$, K_2CO_3, toluene, H_2O, ethanol, 80°C, 3 days; yields: 47%, 30%, 44% respectively b) TBAF, tetrahydrofuran, 30-40 min, RT-40°C; yield: 78%

Figure 6.1: Synthesis scheme of the terthiophene substituted perylene dicarboximides **190-192**

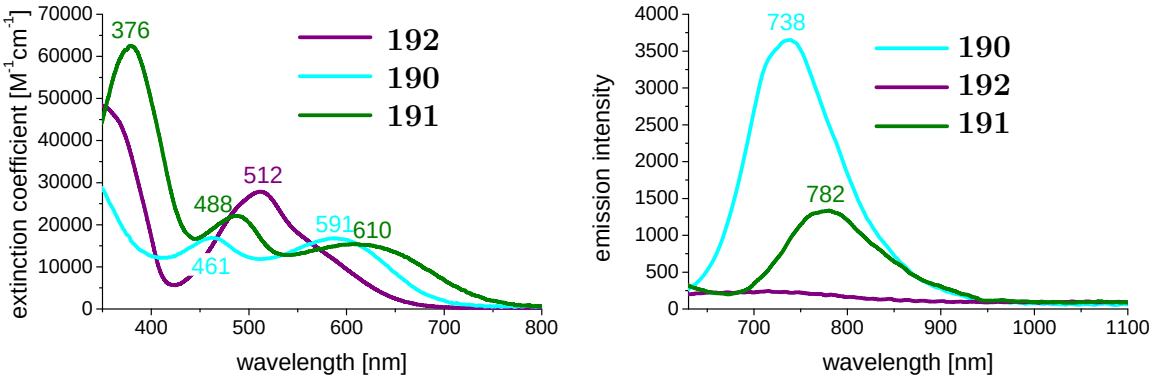

(a) Absorption of **190-192** in dichloromethane (b) Fluorescence of **190-192** in toluene

Figure 6.2: Absorption of **190-192** in dichloromethane (a) and fluorescence emission of **190-192** in toluene (b)

conjugated oligothiophene around the PDI core (**191** > **190** > **192**). Compound **191** possesses three α-connected thiophenes resulting in the longest conjugation, which is reflected in the largest bathochromically shifted absorption maximum, relative to the underivatised PDI. This red-shift is noticeably smaller for compound **190**, which contains only two α-conjugated thiophenes around the PDI core. Compound **192** with the β-connected terthiophene on the other hand shows a hypsochromic shift (λ_{max} = 512 nm), due to lack of conjugation (β-connected with PDI core) between the PDI core and the terthiophene moiety. This hypsochromic shifted absorption maximum of **192** compared to a naked PDI (λ_{max} = 526 nm for *N,N'*-bis(1-heptyloctyl)3,4:9,10-perylene tetracarboxdicarboximide.)[95], however, results from the electronic S0 → S2 transition.

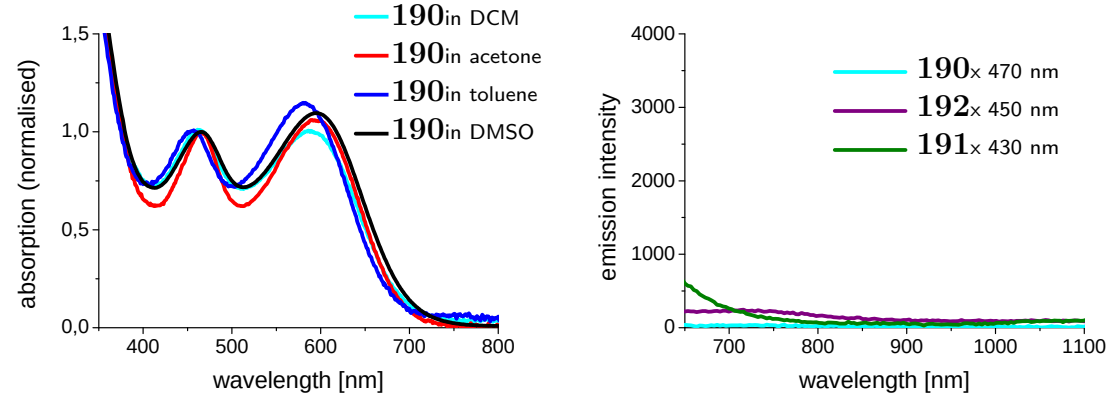

(a) Absorption of **190** in different solvents (b) Fluorescence of **190-192** in DMSO

Figure 6.3: Absorpton of compound **190** in different solvents (a) and complete fluorescence quenching of **190-192** in DMSO (b)

Regarding the fluorescence (figure 6.2), compound **190** and **191** show emission bands at λ_{max} = 738 nm and 782 nm, respectively. As the emission bands are in

Dye	HOMO/LUMO$_{CV}$ [eV]	BG$_{CV}$ [eV]	BG$_{opt}$ [eV]	λ_{maxAbs} [nm]	λ_{maxEm} [nm]	MALDI-TOF before/after sunlight irradiation*
190	-5.7/-3.9	1.8	1.8	593	739	1107/1103
191	-5.4/-3.9	1.5	1.6	608	782	1107/1107
192	-5.5/-3.9	1.6	1.9	509	–	1107/decomposed

Absorption and emission mesured in toluene; *no further purification

Table 6.1: HOMO and LUMO levels, band gap (BG), absorption and fluorescence maxima, and MALDI-TOF data for **190**-**192**

the near infrared region and very broad, without the typical PDI fine structure, these emission bands can be assigned to an intramolecular charge transfer between the terthiophene donor and the PDI acceptor.[157] Moreover both compounds possess large Stokes shifts (147 nm and 172 nm respectively). Compared to the S1 → S0 emission band in compound **190**, the one in compound **191** is bathochromically shifted. This red-shift in emission results just like the red-shift in absorption from the longer conjugation. Compound **192** does not show any significant fluorescence. This indicates that the charge-transfer state of **192** could be quenched by electron transfer and thus supports the presence of a photoinduced electron transfer (PET) fluorescence quenching mechanism. The emission intensity of compound **191** is much lower than the one of compound **190**. A similar fluorescence quenching in the presence of a thiophene donor was detected by Huang et al. for dithienothiophene PDI copolymers[158]. Moreover, a decrease in the fluorescence quantum yield correlated to an increasing number of α-connected thiophene units in the 1,7-position of PDI was observed.[151,152] Correspondingly, the quantum yields of compound **190** and **191** could be determined as 16% and 8%, respectively, using cresyl violet ($\Phi = 54\%$[159]) as a reference.

Contrary to the absorption where only weak solvent sensitivity is observed (figure 6.3 on the facing page shows the normalised absorption of compound **190** in dichloromethane, acetone, toluene, and DMSO), the fluorescence of compound **190** and **191** is thoroughly quenched in DMSO (figure 6.3 on the preceding page). This solvent effect confirms the assumption that these low energy emission bands result from charge transfer. As all three compounds are symmetrical and according to quantum mechanical calculations (figure 6.2 on page 138) exhibit no strong dipole (0.82, 1.86, and 2.45 debye for **191**, **192**, **190**, respectively), it is reasonable that no obvious solvatochromic absorption is observed. Fluorescence quenching in more polar solvents can be explained by a higher thermodynamic driving force helping the photoinduced electron transfer from the donor to the acceptor moiety.[154]

The HOMO and LUMO energy levels of the three terthiophene-PDI compounds

were determined via cyclovoltammetry using the onset (table 6.1 on the previous page). Moreover, the bandgaps deduced from the cyclovoltammetric results were compared with the optical bandgaps inferred from the onsets of the longest wavelength absorption bands. In general, we can see good agreement of the electrochemical and optical results with the exception of compound **192** which shows a much smaller electrochemical than optical bandgap. The LUMO level is mainly determined by the PDI core and resembles the LUMO level of *bay*-unsubstituted PDI (LUMO: -3.8 eV; HOMO: -5.8 eV for *N,N'*-bis(1-ethylpropyl)-3,4,9,10-perylenetetracarboxylic acid diimide[159]). In contrast, the HOMO is strongly influenced by the donor and the donor-acceptor interactions. Because of the β-connection of the terthiophene and a strong twist of the donor (D, terthiophene) with respect to the acceptor (A, perylene) plane around the D-A bond, the donor is decoupled in compound **192** and the HOMO in the D-A compound is mainly determined by the high HOMO of the terthiophene itself. DFT calculations carried out by Bouzinne et al. found a HOMO level energy of -5.18 eV for a linear terthiophene.[160] It is the same decoupling effect which determines the large optical bandgap, as for the orbital partitioning between the HOMO and LUMO, the intensity of the intramolecular charge transition is very low. Hence no clear ICT absorption band can be observed.[2]

For conjugated thiophene-PDI-D-A-systems previously investigated, the bandgap diminished with every additional thiophene unit (bandgaps for N,N'-Di(2-ethylhexyl)-perylene-3,4,9,10-tetracarboxylic acid diimide and its thiophene(T)-substituted derivatives: PDI: 2.31 eV; 1T-PDI-1T: 1.97 eV; 2T-PDI-2T: 1.73 eV; 3T-PDI-3T: 1.63 eV).[152] The decreasing electrochemical band gaps and corresponding bathochromic shift in the absorption maximum (optical band gap) observed for **190** and **191** agree with this trend. The small electrochemical, but not optical, band gap seen in **192** is the result of the decoupling effects. Thus decoupling and increase in conjugation length – which on first glance seem to be contrary effects – can both result in a decrease in band gap.

As mentioned above, compound **190** and **191** show substantial charge transfer whereas compound **192** exhibits strong photoinduced electron transfer. These characteristics can also influence the photochemical stability of the three compounds. In order to investigate their photochemical stability, solutions in toluene were exposed to sunlight for several days and interestingly all three compounds show different behaviour as presented in figure 6.4 on the facing page. Compound **191** is stable and shows the same mass in MALDI-TOF (figure 6.5 on the next page) and the same absorption bands as before irradiation (figure 6.4 on the facing page). In contrast, compound **192** changes colour from purple to yellow, and according to both MALDI-TOF and absorption measurements, is completely decomposed. Most interesting is compound **190**, which undergoes a colour change from green to red and shows a decrease in mass of 4 accord-

ing to MALDI-TOF (figure 6.5). The colour as well as the loss of mass indicate the loss of four hydrogens and photoinduced fusion of the terthiophene moiety, which is known in literature for various branched terthiophenes. According to Jayasuriya et al.[161] the 2,2'3',2"-terthiophene always fuses to the benzo[1,2-b:3,4-b':6,5-b"]trithiophene in an isomerically pure fashion. We therefore suggest the formation of compound **193** according to the structure shown in figure 6.5. The fusion of the branched terthiophene leads to a new and more stable chromophore donor which strongly affects the optical properties.

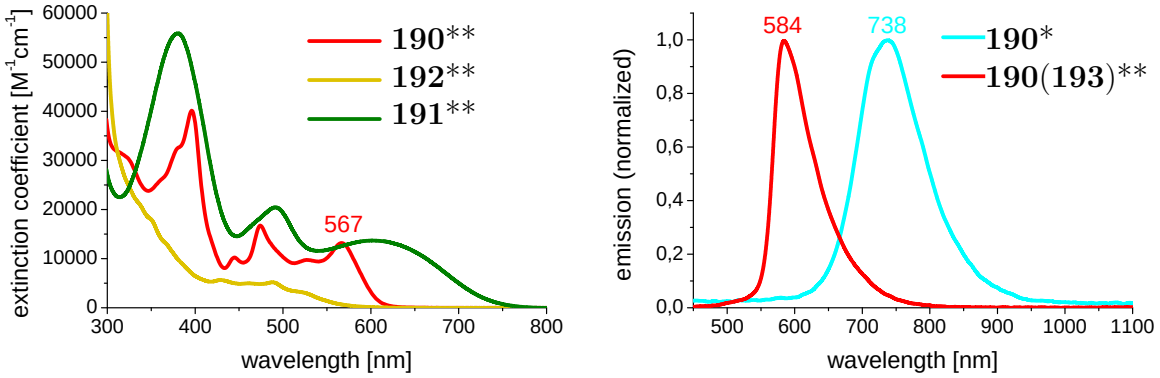

(a) Absorption (**190-192**) after sunlight irradiation

(b) Emission (**190**) before and after sunlight irradiation

Figure 6.4: Absorption of **190-192** in toluene after sunlight irradiation (a) and fluorescence emission spectra in toluene of **190** before and after sunlight irradiation (b)

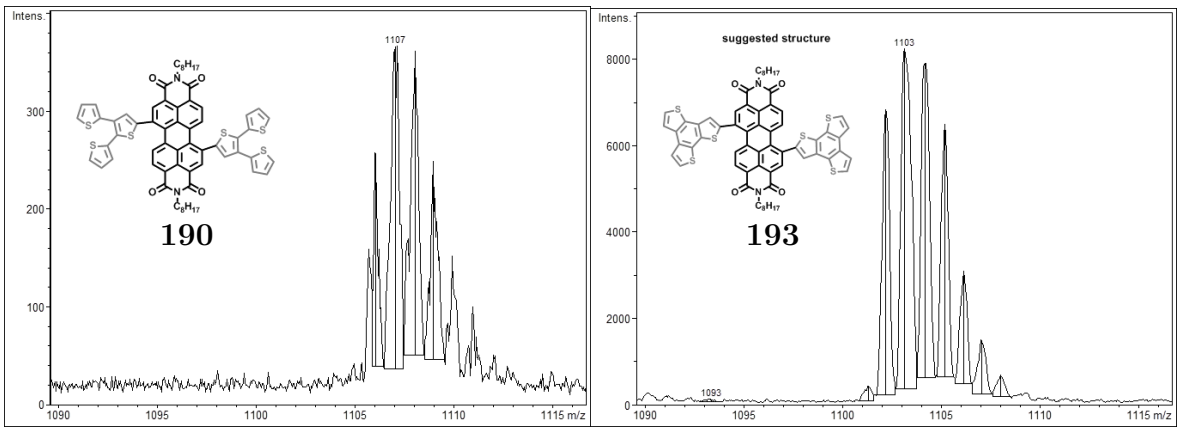

(a) Maldi-TOF before fusion

(b) Maldi-TOF after fusion

Figure 6.5: Maldi-TOF spectrum of compound **190** before (a) and compound **193** (suggested structure) after (b) sunlight irradiation

Upon fusion compound **190** experiences a strong hypsochromic shift of the absorption, the longest wavelength absorption band occuring at a λ_{max} of only 567 nm (figure 6.4). A similar blue shift of 154 nm can also be observed in the fluorescence with

a $\lambda_{max} = 584\,\text{nm}$ (figure 6.4 on the preceding page), in the fluorescence range of PDI. This hypsochromic shift in absorption indicates a rather large bandgap. The LUMO in the fused product of compound **190** should remain unchanged as the PDI core is not altered. Hence a larger bandgap should correspond to a lower HOMO level energy. Quantum mechanical calculations (table 6.2 on page 138) show a strong twist of the fused donor and the PDI acceptor in **193**, the two planes being almost perpendicular to each other (approximately 97°), which leads to a stronger decoupling of the donor from the acceptor. A similar case, enhanced by the β-connection, is compound **192** in which we found a strong influence of the donor moiety on the HOMO level energy. DFT calculations by Taerum et al.[162] predict the HOMO of terthienobenzene, the proposed donor moiety in **193**, to be as low as -5.93 eV. This is consistent with the larger optical bandgap observed.

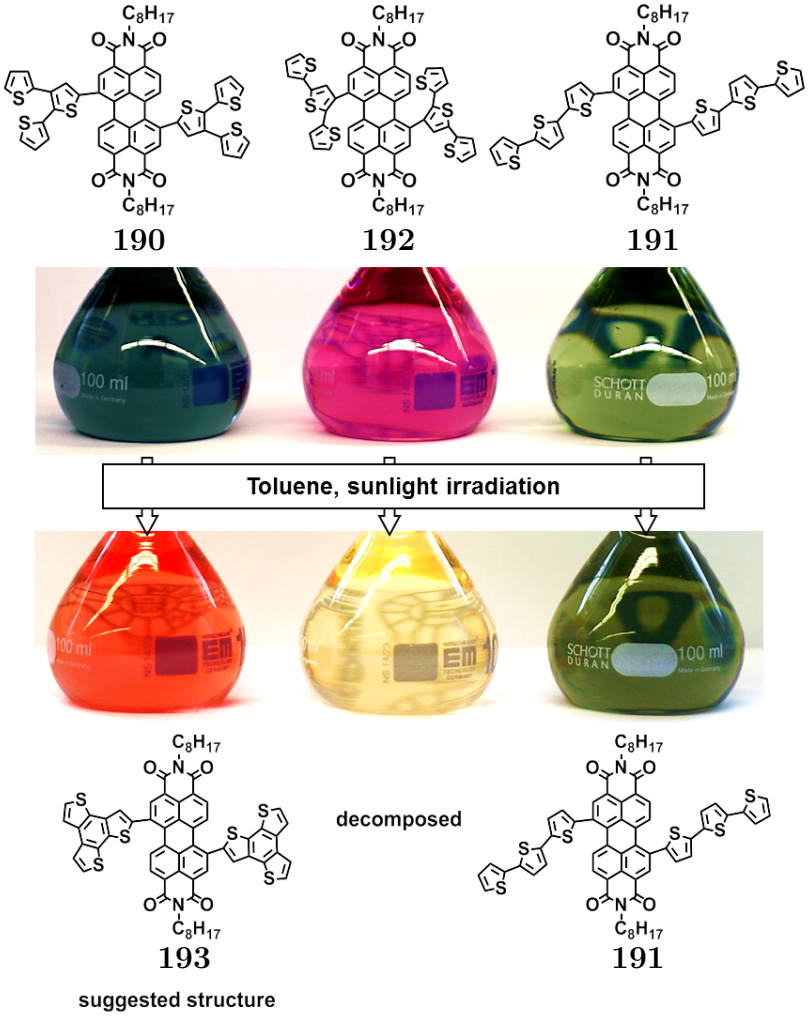

Figure 6.6: Solution colours (in toluene) and molecular structures of **190-192** before and after light irradiation (suggested structure **193**)

In summary, it was shown how different terthiophene architectures can influence optical and photochemical properties of D-A-terthiophene PDIs. The syntheses of

three different *bay*-substituted donor-acceptor terthiophene PDIs were presented. The target compounds were characterised by UV-Vis absorption, fluorescence, as well as cyclovoltammetric measurements and their photochemical stability was tested. The optical properties showed that the colour can be adjusted and energy levels tuned by variation of conjugation, assembly and connection of the thiophene moieties within the terthiophene and towards the PDI core. The photochemical stability varies strongly and photoinduced fusion of the branched terthiophene moiety offers a way to synthesise new chromophores. The tuning of colour and energy levels of these terthiophene PDIs is of vital interest for the potential application in organic electronics, especially for organic photovoltaics as they show promising absorption in their broadness in the UV-Vis region (especially **190** and **191**) and their high absorption coefficients (especially **192**). The terthiophene PDIs **190**, **192**, and **191** all possess suitable energy levels for the application as the acceptor component in bulk heterojunction cells in combination with P3HT (LUMO: -3,2 eV; HOMO: -5.2 eV).

Just recently this concept of energy level tuning by using different conjugation pathways was taken up by Balaji et al.[163] who synthesised oligothiophene-PDI D-A-D compounds, one with β-linkage (like **192**) and another with α-linkage (like **191**). In these systems they observed that both compounds exhibit an ambipolar redox behaviour but different charge transport properties, i. e. the β-linked predominantly hole transporting, the α-linked electron transporting properties.

Dye	Structure	HOMO	LUMO
190	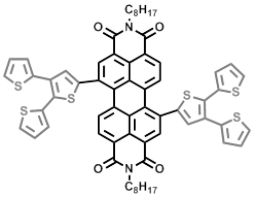	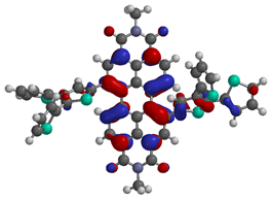	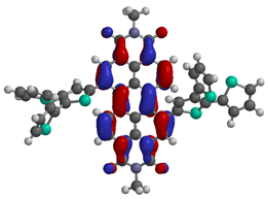
191	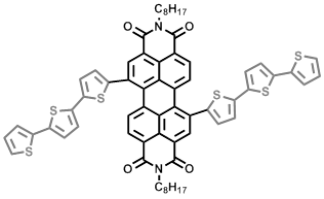	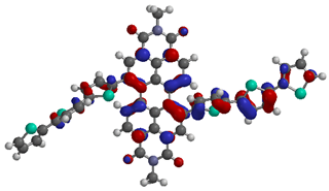	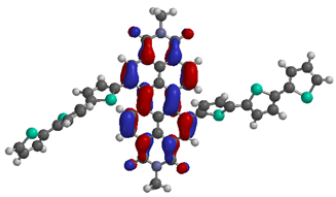
192	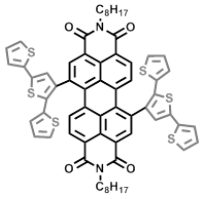	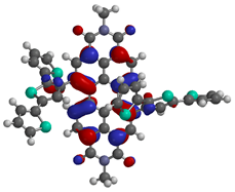	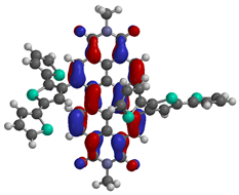
193	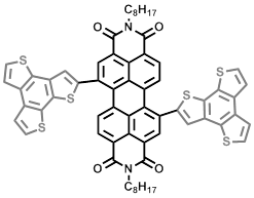	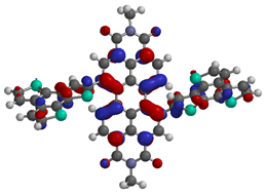	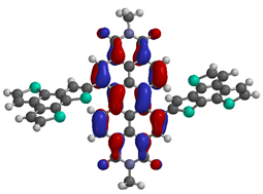

(Spartan, Hatree-Fock, 3-21G(*))

Table 6.2: Orbital surfaces of compound **190** , **192**, **191**, and **193**

Chapter 7

Conclusion

The starting point and motivation for this thesis was the very promising sensitiser **33** (**ID176**) with its small "fault" of a somewhat too low LUMO energy. New concepts of perylene sensitiser design were needed. A major difficulty was maintaining other performance indicators such as broad absorption and high absorptivity, while tuning the HOMO and LUMO levels. In order to achieve a good balance of all the sensitiser requirements, several new approaches were pursued(figure 7.1).

The rigid π-spacer-concept demonstrated how energy level tuning by decoupling took place at the cost of broad absorption. It did, however, also show that narrow but strongly absorbing sensitisers with suitable HOMO and LUMO levels can compete with broad absorbing sensitisers like **33**. Adjusting the spacer length and the addition of a pyrene donor to achieve additional absorption made it possible to outperform **33** regarding cell efficiency and, in fact, all other sensitisers presented in this work. With **69** a record efficiency of nearly 5% for perylene dyes in s-DSSCs was achieved.

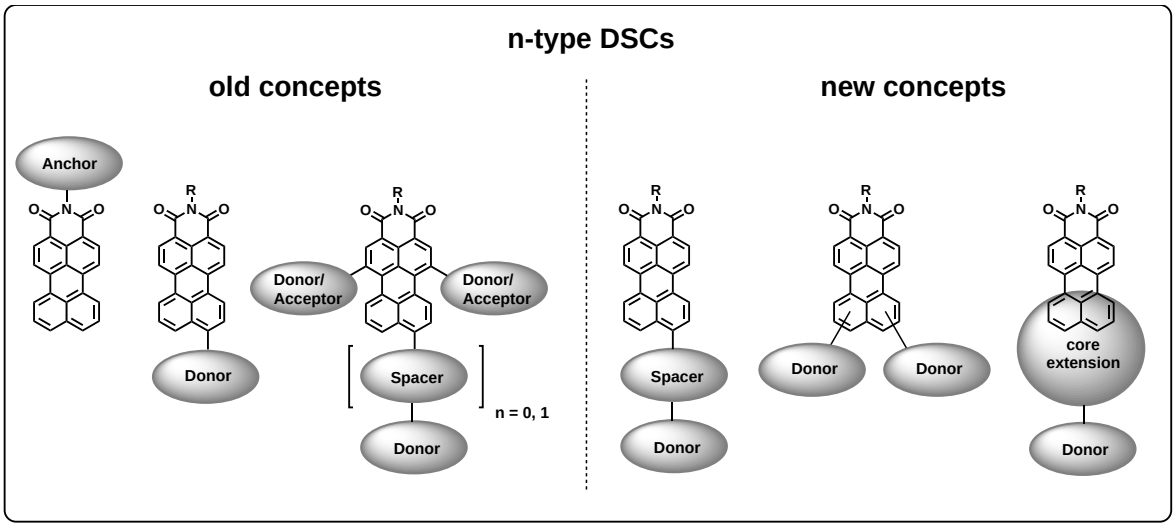

Figure 7.1: Old and new design concepts of PMIs for n-type DSSCs

The second concept probed was the use of double donor-functionalisation (figure 7.1

on the previous page), the two sensitisers **83** and **84** with the flexible thiophene dendron spacer presented in chapter 3 on page 57 are a hybrid between the spacer functionalisation and double donors. The double donor approach is certainly the most structurally diverse of this work, from the symmetrical **105** to the assymmetrical donor **123** to the pentannulated perylene monoimide sensitiser **129**. Three major findings were gained from these different approaches: i) orbital tuning and broad absorption *as well as* good absorptivity can be achieved with compounds such as **123**; ii) functionalisation of the *edge*-position typically leads to decreased adsorption on titanium dioxide, as observed in **123** and even more so in **108**;[1] iii) a lower LUMO than that of **33** will inhibit the electron injection and make power conversion nearly impossible, as seen for **129**. Besides the use of these dyes as sensitisers in sDSSCs, all double donors are new substitution patterns on perylene monoimides which may become more important in the future of our group. Here, I would like to again acknowledge the work of [redacted] and [redacted], who made these substitutions available. Unfortunately the long desired double-*peri*-functionalisation could not be achieved via a 9,10-halogenated building block. However, two amines in both *peri*-positions (**176**) could be achieved by exploring the potential of *Cadogan chemistry* (chapter 5 on page 95).

The indole extensions of the perylene core prepared via *Cadogan chemistry* represent a new class of chromophores, with strong bathochromic shifts of their lowest energy absorption as a result of their extended π-system compared to the parent naphthalene or perylene imide. This extension of the perylene core is the third and last new design concept for sDSSC sensitisers explored in this work (figure 7.1 on the preceding page). Donor-functionalisation of these systems allowed for the synthesis of a sensitiser (**149**) with an EQE reaching out into the desired NIR region. The rather low solubility of the π-extended perylene derivatives presents a great challenge for purification and DSSC processing but will hopefully be tackled in the future, allowing higher power conversion efficiencies to be reached.

Within the new sensitiser concepts higher LUMO levels and more bathochromic absorption were of major importance. The 8,10-double donor perylene monoimide (**123**) showed a very broad and bathochromic absorption, but the *Cadogan*-derived perylene monoimide with an additional donor (**149**) was the only sensitiser reaching into the NIR. The even more bathochromic absorbing quinoline-extended isomer holds promise as well, but unfortunately was not yet tested in DSSCs[2]. Higher LUMO levels could be reached in all new sensitiser concepts with one exception: the *peri*-pentannulated perylene monoimide (**129**). This sensitiser uniting the concepts of core extension, decoupling, and double donor funcionalisation possesses an even lower LUMO than that

[1] This qualitative conclusion could be drawn from considerably reduced absorbance of the *edge*-functionalised compared to the *peri*-functionalised senisitisers on titanium dioxide-layers of the same thickness despite comparable extinction of the dyes in solution.

[2] due to too small amounts and failed alkylation

of **33**, and clearly demonstrated that too low a LUMO will prohibit efficient electron injection from the LUMO of the dye into the titanium dioxide. The cut-off point for the LUMO level is situated somewhere between the LUMO level energies of **33** and **129**.

The indole-extension of the perylene or naphthalene core, however, is not only interesting for the DSSC application. Besides the development and realisation of new sensitiser concepts, a second major motive of this thesis was to contribute to perylene chemistry in general. Regarding the *Cadogan chemistry*, the product of the double fusion in the two *peri*-positions **176** should be mentioned here as an interesting candidate for metal complexation. In addition to the indole extension, the isomeric six-membered ring could be achieved. Hopefully this quinoline-extension can be used more widely to facilitate the synthesis of other heterocyclic compounds. Thus besides striving for more bathochromic DSSC sensitisers, the different variants *Cadogan chemistry* performed on perylene should be understood as exploring the options of an established synthesis and extending its application.

Another more general contribution within this thesis was the investigation of the 1,2-migration of the palladium-catalysed couplings in the *edge*-positions and the development of the base-induced aryne-mechanism. By introducing boronic ester groups, bromines and chlorines, [redacted] provided the most important building blocks for further functionalisation. The Buchwald-Hartwig and Suzuki coupling reactions in chapter 4 on page 67 and 5 on page 95 were the first experiences with functionalisation of these to-date untouched *edge*-positions. Unfortunately, full proof of the mechanism by either isolation of intermediates and the absence of migration in base-free coupling reactions, e. g. Stille or Ullmann coupling was not undertaken in the course of this thesis. These exciting preliminary results, however, are a great opportunity to explore the reaction conditions and the mechanism more thoroughly in order to gain control over the migration to either induce or prevent it. Asymmetric products, even double *peri*-functionalised perylenes might be achieved or *edge*-connected donor-acceptor polymers.

The perylene diimide colour tuning was one example to transfer concepts of perylene monoimide DSSC sensitisers (terthiophene dendron π-spacer, chapter 3 on page 57) to perylene diimides. At the same time the small architectural changes in the terthiophene donor moieties demonstrated how sensitive colour and orbital tuning is. Another promising concept to be transferred from perylene monoimides to perylene diimides would be the indole-extension with help of the *Cadogan chemistry*. Two or four times indole fusion via the *bay*- or *ortho*-positions of perylene diimide as proposed in chapter 5 on page 95 could also lead to interesting new perylene diimide derivatives for organic electronics.

It was be demonstrated, that absorption as well as energy level tuning can be

performed at will. However, regarding the application in sDSSCs, this tuning has only led to small improvements in overall performance. Liquid DSSCs have shown, that efficiencies of 12% and higher can be reached[16]; efficiencies that are also required by the market in order to compete with current thin film technologies. Solid-state DSSCs with a power conversion efficiency of around 7% in general and perylene monoimide-sensitised sDSSCs with an η of around 5%, however, still lag behind. This obviously leads to the question whether it is worth continuing research in this field. The many advantages, such as stability and versatility regarding functionalisation and colour tuning, have already been presented in the introduction. In fact, perylene monoimide-based sensitisers fulfill all requirements of broad and strong absorption to generate charges and good energy level tuning to ensure efficient injection and regeneration within the system.

The current bottleneck of the solid-state DSSCs is the low conductivity of the state-of-the-art hole conductor spiro-MeOTAD. With only 10^{-5}S/cm after doping[164] its conductivity is considerably lower than that of most liquid electrolytes. A better conducting hole transporting material would allow to build thicker cells (like in liquid DSSCs), profit from the excellent light harvesting properties of the sDSSC sensitisers and improve efficiencies with the current generation of sensitisers. That this is in general possible, has just been demostrated by Chung et al.[17] who have employed an inorganic whole conductor ($CsSnI_3$) with a conductivity of up to 60 S/cm, yielding around 10 % efficiency in a 10 μm thick cell (thus more than five times as thick as the standard sDSSCs) with the ruthenium-based sensitiser N719. Currents of up to 20 mA/cm^2 were generated and conducted efficiently, the η of 10 % being close the record values of 10-11 % of the dye in a liquid cell.[165] In the liquid cell, however, titanium dioxide-layers as thick as 16 μm were used to achieve comparable currents.

The recent results of Chung et al.[17] can be considered as a break-through for the solid-state DSSCs, demonstrating their equality in efficiency to the parent liquid technology. Ruthenium sensitisers suffer from lower extinction than most metal-free dyes, especially towards longer wavelengths[166], so it is not far-fetched that the herein presented strongly absorbing perylene sensitisers (e. g. the *Cadogan perylene monoimide* with donor **149** yielding a current of nearly 14 mA/cm^2 already in a 1.8 μm cell) might reach similar or even higher efficiencies in a similarly thick cell. Whether this inorganic hole conductor or a new organic hole conductor will later on fulfill all requirements for a stable and highly efficient cell, the dyes will have to be optimised to interact well with the new material. Dye-donor-HTM[3] match needs to be considered[103] in order to get good pore filling and charge transport. After many years of absorption and orbital tuning, the future challenge will be identifying an improved state-of-the-art hole conductor following spiro-MeOTAD and modify the dyes accordingly towards a new

[3]HTM: hole transporting material

generation of high efficient and mature sDSSCs.

Chapter 8

Experimental Part

8.1 General Methods

8.1.1 Chemicals and Solvents

Unless otherwise noted, all reagents were obtained from commercial suppliers (e. g. Acros, Aldrich, Fluka, Strem). *N*-(2,6-Di*iso*propylphenyl)-perylene-3,4-dicarboximide and bis(9,9-dimethyl-9*H*-fluorene-2-yl)amine were kindly supplied by BASF SE.

8.1.2 Chromatography

Preparative column chromatography was performed on silica gel 60 (0.063-0.2 mm/70-230 mesh ASTM) from Machery Nagel. For analytical thin layer chromatography (TLC) aluminium plates with 0.2 mm silica-gel coating with fluorescent indicator (ALUGRAM® SIL G/UV_{254} from Machery Nagel) were used. Automated recycling gel permeation chromatography was performed on a JAI LC-9101 (Recycling Preparative HPLC) on two consecutive Ultrastyragel® THF 103 Å columns (19 x 300 mm). Preparative gel permeation chromatography was carried out on Bio-Beads^{TM} S-X1 Beads (200-400 Mesh) from BIO-RAD.

8.1.3 NMR Spectroscopy

^{1}H-NMR and ^{13}C-NMR as well as the ^{1}H,^{1}H-COSY and ^{1}H,^{1}H-NOESY spectra were recorded with a Bruker DPX-250, Bruker AMX-300, Bruker DRX-500 or Bruker DPX-700 spectrometer by using the residual proton resonance of the solvent or the carbon signal of the deuterated solvent as the internal standard. Chemical shifts are reported in parts per million.

8.1.4 Mass Spectrometry

FD mass spectra were recorded with a VG Instruments ZAB 2-SE-FPD, Maldi-TOF mass spectra on a Bruker Reflex II-TOF spectrometer using a 337 nm nitrogen laser. High resolution mass spectra (ESI) were measured as a service of the Institute of Organic Chemistry, Johannes-Gutenberg-Universität, Mainz.

8.1.5 IR Spectroscopy

Infrared spectra were recorded on a Nicolet FT-IR 730 with an ATR unit (Zn-Se crystal).

8.1.6 UV-Vis and Fluorescence Spectroscopy

UV-Vis spectra in solution were recorded on a Perkin-Elmer Lambda 40 and Perkin-Elmer Lambda 9 spectrometers. UV-Vis spectra on titanium dioxide were provided by the Joint Innovation Lab (BASF SE). Fluorescence emission spectra were recorded on a J & M Tidas spectrometer.

8.1.7 Elemental Analysis

Elemental analysis of solid samples was carried out on a Foss Heraeus Vario EL as a service of the Institute for Organic Chemistry, Johannes-Gutenberg-Universität, Mainz.

8.1.8 Quantum Chemical Calculations

Density functional theory (DFT) calculations were performed by BASF SE with the Turbomole program suite version 5.10.[167] Geometry optimisations were carried out with the BP86 functional[168,169] making use of the RI approximation.[170] The HOMO (LUMO) potential was derived from the geometry-optimised positively (negatively) charged radical cation of the dye molecule. The def-SV(P) basis set was applied in all geometry optimisations.[171] To arrive at actual ionisation potentials, the medium was taken into account by single point calculations with a continuum dielectric model[171] using a dielectric constant of 4.5, typical for organic materials as spiro-MeOTAD.

8.1.9 Electrochemical Characterisation

Cyclic voltammetry for spectroelectrochemistry experiments were carried out by [redacted] with an EG&G Princeton Applied Research potentiostat, model 273. The working electrode consisted of an palladium-carbon electrode (1.5 mm diameter) that was polished on a felt pad with 0.05 μm alumina and washed with milli-Q water before each experiment. A platinum wire was used as the counter electrode and an Ag wire as

the reference electrode. The measurements were calibrated with ferrocene/ferrocenium (Fc/Fc^+). The CV measurements were carried out in a solution of Bu_4NPF_6 (0.1 M) in dry dichloromethanewith a scan rate of 50 mV $s^{-}1$ at room temperature under argon.

Coversion of energy on the absolute vacuum scale to the normal hydrogen electrode (NHE) was performed as follows:

$E^0 = E_{abs}$ -4.44

where E^0 corresponds to the Energy vs. NHE and E_{abs} to the energy on the absoute vacuum scale.

8.1.10 Fabrication and Characterisation of sDSSCs

Solid-state dye-sensitised solar cells layers were prepared by BASF SE as follows[1]: First a TiO_2 blocking layer was prepared on a FTO-covered glas substrate by spray pyrolysis.[172] Following, a TiO_2 paste (Dyesol), diluted with terpineol, was applied by screen printing, resulting in a film thickness of 1.8 μm. All films were then sintered for 1 h at 450°C, followed by a 30 min treatment in a 40 mM aqueous solution of $TiCl_4$ at 65°C, followed by another sintering step. The electrodes were then dyed in 0.5 mM dye solution in dichloromethane, toluene or tetrahydrofuran[2]. The dye coated TiO_2 electrodes with both dyes contain an organic coadditive (BASF additives). Spiro-MeOTAD was applied by spin-coating from a solution in chlorobenzene also containing 20 mM $Li(CF_3SO_2)_2N$. Device fabrication was completed by evaporation of 200 nm of silver as the counter electrode. The active area of the solid-state DSSCs was defined by the size of these contacts (0.13 cm^2), and the cells were masked with an aperture of the same area for measurements. Current-voltage characteristics at 1000 W/m^2 under AM 1.5G conditions and the incident photon to current conversion efficiency (IPCE)/external quantum efficiency (EQE) spectra were measured for all cells.

The cells were assembled manually, however, in some steps using apparatuses which allow the treatment of several substrates at the same time, minimising the error due to manual inaccuracies within one testing series. The titanium dioxide-substrates for example were made in large batches by screen printing in order to achieve the same layer thickness for the substrates and the back electrode can be vapour deposited on 10-16 substrates at the same time. In order to reduce measuring errors, two substrates of the same additive-solvent combination with four cells each were tested. The effiencies presented here are an average of the cell results. Cells, which did not reach 70 % efficiency of the top cell amongst the eight cells, were expected to have a major defect and were not included in the avarage. Still, cell results can vary. With help of one standard dye, which has been included in all measurement series for several years now,

[1] See also Wonneberger et al.[63]

[2] In parrallel experiments, different solvents were used to find the best solvent for each dye. In most cases, this was toluene

the error of a cell measurement could be estimated over the past years and is roughly +/-0.2 in efficiency.

8.2 Material Synthesis: Synthetic Procedures and Characterisation (SPC)

Some of the syntheses described in the following were repeated several times in different scales. The conditions reported here were ususally the ones that had led to the best results.

8.2.1 SPC: Decoupling via Introduction of Rigid pi-Spacers in Donor-Acceptor Systems

N-(2,6-Diisopropylphenyl)-9-(5-chloro-3-methylbenzo[b]thiophene-2-yl)perylene-3,4-dicarboximide

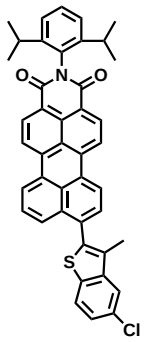

1g of *N*-(2,6-di*iso*propylphenyl)-9-(4,4,5,5-tetramethyl-1,3,2-dioxaborolane-2-yl)-3,4-perylene-dicarboxylic acid monoimide (1.64 mmol) and 643 mg of 2-bromo-5-chloro-3-methylbenzo[*b*]thiophene (2.46 mmol) were dissolved in 100 mL of toluene in a Schlenk tube. 2.25 g of potassium carbonate (16.3 mmol) in 10 mL of water and 1 mL of ethanol were added and the solution was purged with argon for 30 minutes. After addition of 95 mg of tetrakis(tri-phenylphosphine)palladium (0.085 mmol) the solution was again purged with argon for 30 minutes and stirred at 80 °C overnight. The reaction mixture was extracted with dichloromethane and dried over magnesium sulfate. The solvent was evaporated under reduced pressure and the resulting solid was purified roughly by column chromatography on silica gel with dichloromethane.

Yield: 630 mg red solid (58%)

^{1}H-NMR (300 MHz, CD_2Cl_2, 298 K):
δ [ppm]: 8.71 - 8.64 (m, 2H), 8.63 - 8.54 (m, 4H), 7.93 - 7.81 (m, 3H), 7.77 (d, J = 7.8, 1H), 7.71 - 7.63 (m, 1H), 7.55 - 7.47 (m, 1H), 7.42 (dd, J = 2.0, 8.5, 1H), 7.36 (d, J = 7.6, 2H), 2.85 - 2.70 (m, 2H), 2.25 (s, 3H), 1.15 (d, J = 6.9, 12H).

^{13}C-NMR (75 MHz, CD_2Cl_2, 298 K):
δ [ppm]: 164.6, 146.7, 142.3, 138.5, 138.0, 137.7, 137.5, 135.1, 133.9, 132.5, 132.4, 132.1, 131.7, 131.1, 131.0, 130.9, 130.4, 130.0, 129.9, 129.6, 128.8, 128.2, 127.4, 125.6, 124.8, 124.6, 123.9, 123.7, 122.5, 121.9, 121.7, 121.2, 29.7, 24.3, 13.1.

IR spectrum (ATR):
ν_{max} [cm^{-1}] = 2961, 2928, 2868, 1700, 1660, 1590, 1576, 1569, 1354, 1290, 1243, 1077, 862, 832, 752.

UV-Vis spectrum (CD_2Cl_2):
λ_{max} [nm] (ϵ [$M^{-1}cm^{-1}$])= 518 (40,902).

High Resolution Mass (ESI):
$[M+H]^+$: calculated: 662.1921, found: 662.1964, discrepancy: 2.5 ppm.

Elemental analysis ($C_{43}H_{34}ClNO_2$):
calculated: 77.99% C, 4.87% H, 2.12% N, 4.84% S
found: 77.64% C, 5.15% H, 2.13% N, 4.85% S

(a) N-(2,6-Diisopropylphenyl)-9-(8-bromodibenzo[b,d]thiophene-2-yl)perylene-3,4-dicarboximide;
(b) N-(2,6-Diisopropylphenyl)-9-(6-bromo-9-ethyl-9H-carbazole-3-yl)perylene-3,4-dicarboximide;
(c) N-(2,6-Diisopropylphenyl)-9-(6-bromo-9-phenyl-9H-carbazole-3-yl)perylene-3,4-dicarboximide;
(d) N-(2,6-Diisopropylphenyl)-9-(7-bromo-9-ethyl-9H-carbazole-2-yl)perylene-3,4-dicarboximide

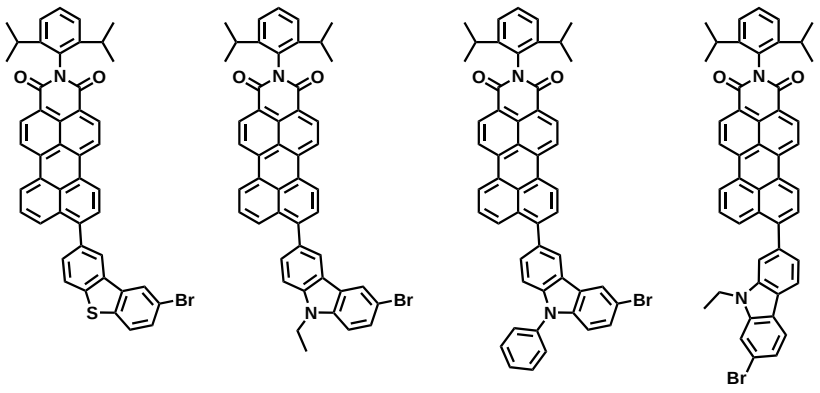

Synthesis of a:
1g of *N*-(2,6-di*iso*propylphenyl)-9-(4,4,5,5-tetramethyl-1,3,2-dioxaborolane-2-yl)-3,4-perylene-dicarboxylic acid monoimide (1.64 mmol)and 840 mg of 2,8-dibromodibenzo[*b,d*]thiophene (2.47 mmol) were dissolved in 80 mL of toluene in a Schlenk tube. 1.6 g of potassium carbonate (11.6 mmol) in 8 mL of water, 0.8 mL of ethanol were added and the solution was purged with argon for 30 minutes. After addition of 360 mg of tetrakis(triphenylphosphine)palladium (0.322 mmol) the solution was again purged with argon and stirred at 80 °C overnight. The reaction mixture was extracted with dichloromethane and dried over magnesium sulfate. The solvent was evaporated under reduced pressure and the product was roughly isolated by column chromatography on silica gel with dichloromethane, giving a mixture of the product and its debrominated analogue (about 60% yield (crude)). This mixture was directly used for the following reactions, generally lowering the yield of the subsequent Buchwald aminations. Several batches of compound a were made, the ratio of brominated to debrominated species probably not identical. Therefore the yields of the subsequent Buchwald aminations vary between approximately 20-60 %.

Synthesis of b, c, and d:
Compounds b, c, and d were prepared accordingly using the respective dibromocarbazoles achieving similar yields. For all compounds the mixture of brominated and debrominated species was used directly for the next step.

N-(2,6-Diisopropylphenyl)-9-(4-aminophenyl)perylene-3,4-dicarboximide

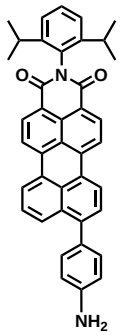

1 g of *N*-(2,6-di*iso*propylphenyl)-9-(4,4,5,5-tetramethyl-1,3,2-dioxaborolane-2-yl)-3,4-perylene-dicarboxylic acid monoimide (1.65 mmol), 580 mg of *tert*-butyl (4-bromophenyl)carbamate (2.14 mmol) were dissolved in 70 mL of toluene in a Schlenk tube. 1.4 g of potassium carbonate (10.1 mmol) in 7 mL of water, 0.7 mL of ethanol were added and the solution was purged with argon for 30 minutes. After addition of 367 mg of tetrakis(triphenylphosphine)palladium (0.329 mmol) the solution was again purgend with argon and stirred at 80 °C overnight. The reaction mixture

was extracted with dichloromethane and dried over magnesium sulfate. The solvent was evaporated under reduced pressure and the product was isolated by column chromatography on silica gel with dichloromethane. Main side product was the free amine (*N*-(2,6-Di*iso*propylphenyl)-9-(4-aminophenyl)perylene-3,4-dicarboximide).

Yield: 546 mg pink solid (49%)

520 mg of the solid were dissolved in tetrahydrofuran and the solution purged with HCl gas (from concentrated H_2SO_4/HCl) for about 20 minutes to cleave the Boc-protection group. The solvent was removed under reduced pressure. Methanol was added and the resulting precipitate filtered.

Yield: 410 mg purple solid (93%)

The two-step procedure described here was a method established in the group, but could probably be carried out without the column purification after the first step as the main side product is the deprotected compound aimed for. An alternative synthesis procedure can be found in literature[173].

N-(2,6-Diisopropylphenyl)-9-(8-(bis(4-(2,4,4-trimethylpentane-2-yl)phenyl)amino)dibenzo[b,d]thiophene-2-yl)perylene-3,4-dicarboximide

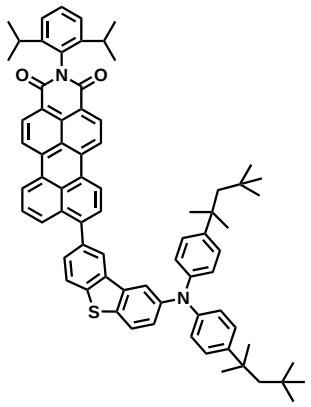

280 mg of *N*-(2,6-di*iso*propylphenyl)-9-(8-bromodibenzo[*b*,*d*]thiophene-2-yl)perylene-3,4-dicarboximide, 150 mg of bis(*p*-2,4,4-trimethylpentane-2-yl-phenyl)amine, 37 mg sodium *tert*-butoxide 70 mg tris(dibenzylideneacetone)dipalladium(0) and 35 mg tri-*tert*-butyl-phosphine were dissolved in 6 mL of dry toluene under argon and stirred overnight at 80°C. The reaction mixture was purified via column chromatography on silica with dichloromethane.

Yield[3]: 170 mg pink solid (43%)

^{1}H-NMR (250 MHz, THF, 298 K):
δ [ppm]: 8.76 - 8.56 (m, 6H), 8.13 - 7.94 (m, 3H), 7.88 - 7.76 (m, 2H), 7.71 - 7.55 (m, J = 8.1, 10.7, 13.3, 3H), 7.44 - 7.22 (m, 8H), 7.02 (d, J = 8.7, 4H), 2.90 - 2.69 (m, J = 6.5, 13.1, 2H), 1.69 (s, 4H), 1.38 - 1.27 (m, 12H), 1.14 (d, J = 6.8, 12H), 0.69 (d, J = 10.9, 18H).

^{13}C-NMR (176 MHz, THF, 298 K):
δ [ppm]: 167.71, 164.4, 147.2, 146.9, 146.5, 145.2, 144.1, 141.2, 138.6, 138.4, 137.5, 137.4, 136.77, 134.3, 134.0, 133.7, 132.8, 132.5, 131.6, 131.5, 130.6, 130.1, 129.7, 129.6, 129.5, 129.4, 128.2, 128.0, 128., 125.3, 125.1, 124.8, 124.4, 124.3, 124.2, 123.9, 123.8, 122.4, 122.3, 121.7, 121.4, 117.4, 65.8, 57.9, 38.9, 33.0, 32.2, 32.0, 31.6, 30.7, 30.0, 24.3, 20.1, 14.1.

IR spectrum (ATR):
ν_{max} [cm^{-1}] = 3042, 2951, 2900, 2682, 1702, 1664, 2594, 1573, 1508, 1475, 1353, 1323, 1290, 1241, 1192, 1175, 1016, 889, 811, 750.

UV-Vis spectrum (CH_2Cl_2):
λ_{max} [nm] (ϵ [M^{-1}cm^{-1}])= 519 (36,172).

High Resolution Mass (ESI):
$[M]^+$: calculated: 1054.5471, found: 1054.5480, discrepancy: 0.9 ppm.
The triphenylamine moiety is losing an electron to form $[M]^+$ as well as $[M+H]^+$.

Elemental analysis ($C_{74}H_{74}N_2O_2S$):
calculated: 84.21% C, 7.07% H, 2.65% N, 3.04% S
found: 84.16% C, 7.00% H, 2.64% N, 3.09% S

[3]As the starting material was contaminated with the debrominated species, the product yield in the coupling is relatively low compared to other Buchwald amination reactions.

9-(8-(Bis(4-(2,4,4-trimethylpentane-2-yl)phenyl)amino)dibenzo[b,d]thiophene-2-yl)perylene-3,4-dicarboxy monoanhydride

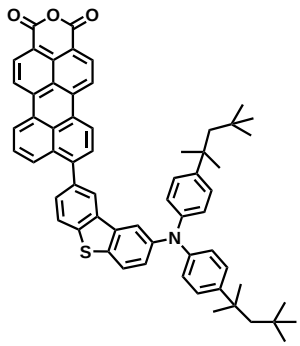

160 mg of *N*-(2,6-di*iso*propylphenyl)-9-(8-(bis(4-(2,4,4-trimethylpentane-2-yl)phenyl)amino)dibenzo[*b,d*]thiophene-2-yl)perylene-3,4-dicarboximide were dissolved in 11 mL of 2-methyl-2-butanol. 340 mg of potassium hydroxide were added, the reaction mixture desoxygenated and refluxed under argon overnight. The reaction mixture was poured into an ice water/acetic acid mixture (10:2). The precipitate was filtered, washed with water and after drying dissolved in dichloromethane. 1-2 mL of acetic acid were added and the solution was stirred for 1-2 days. After removal of the dichloromethane under reduced pressure, methanol was added. The precipitate was filtered and washed with methanol. The crude compound was purified by column chromatography on silica with dichloromethane. The obtained anhydride was precipitated from tetrahydrofuran into methanol.

Yield: 110 mg pink solid (80%)

^{1}H-NMR (250 MHz, THF, 298 K):
δ [ppm]: 8.70 - 8.53 (m, 4H), 8.50 - 8.41 (m, 2H), 8.08 (dd, J = 4.8, 6.8, 2H), 7.98 (d, J = 8.3, 1H), 7.86 (d, J = 2.1, 1H), 7.80 (d, J = 8.7, 1H), 7.70 - 7.54 (m, J = 6.1, 11.0, 18.0, 3H), 7.31 - 7.22 (m, 5H), 7.01 (d, J = 8.6, 4H), 1.68 (s, 4H), 1.29 (d, J = 12.8, 12H), 0.65 (s, 18H).

^{13}C-NMR (126 MHz, THF, 298 K):
δ [ppm]: 161.3, 147.3, 146.6, 145.3, 144.7, 141.2, 139.4, 139.2, 137.6, 137.3, 136.9, 134.5, 134.0, 133.7, 133.4, 130.8, 130.3, 129.8, 129.6, 129.5, 129.4, 128.3, 128.1, 127.8, 125.7, 125.2, 124.5, 124.4, 124.1, 124.0, 121.9, 121.6, 118.7, 118.6, 117.6, 58.0, 39.0, 33.1, 32.3, 32.1.

IR spectrum (ATR):
ν_{max} [cm^{-1}] = 2951, 1761, 1726, 1570, 1506, 1474, 1365, 1339, 1283, 1147, 1131, 1023,

1002, 810, 763, 742, 689.

UV-Vis spectrum (CH_2Cl_2):
λ_{max} [nm] (ϵ [$M^{-1}cm^{-1}$])= 511 (35,659).

High Resolution Mass (ESI):
$[M]^+$: calculated: 895.4059, found: 895.4074, discrepancy: 1.7 ppm.
The triphenylamine moiety is losing an electron to form $[M]^+$ as well as $[M+H]^+$.

N-Carboxymethyl-9-(8-(bis(4-(2,4,4-trimethylpentane-2-yl)phenyl)amino) dibenzo[b,d]thiophene-2-yl)perylene-3,4-dicarboximide

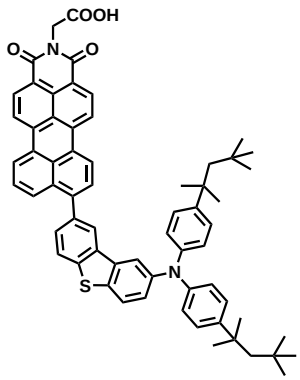

90 mg of *N*-(2,6-Di*iso*propylphenyl)-9-(8-(bis(4-(2,4,4-trimethylpentane-2-yl)phenyl)-amino)dibenzo[*b,d*]thiophene-2-yl)perylene-3,4-dicarboxylic acid monoanhydride, 2 g of glycine, and 3 g of imidazole were mixed in a Schlenk tube and stirred under argon at 140 °C overnight. After cooling down dilute hydrochloric acid was added. The precipitate was filtered, washed with water and afterwards dissolved in tetrahydrofuran and precipitated in methanol.

Yield: 85 mg pink solid (90%)

^{1}H-NMR (250 MHz, THF, 298 K):
δ [ppm]: 8.66 - 8.41 (m, 6H), 8.13 - 8.02 (m, 2H), 7.94 (d, J = 8.3, 1H), 7.88 (d, J = 2.1, 1H), 7.80 (d, J = 8.7, 1H), 7.70 - 7.50 (m, 3H), 7.32 - 7.21 (m, 5H), 7.01 (d, J = 8.6, 4H), 4.84 (s, 2H), 1.68 (s, 4H), 1.31 (s, 12H), 0.65 (s, 18H).

^{13}C-NMR (126 MHz, THF, 298 K):
δ [ppm]: 169.7, 163.8, 147.2, 146.6, 145.3, 144.0, 141.1, 138.4, 138.2, 137.7, 137.6, 136.9, 134.5, 133.9, 132.2, 131.0, 130.6, 130.1, 129.7, 129.4, 128.2, 128.1, 127.7, 125.2, 124.7, 124.5, 124.4, 124.1, 123.9, 122.0, 121.9, 121.5, 121.3, 117.6, 58.0, 41.6, 39.0,

33.2, 32.6, 32.1, 30.9, 30.8, 30.5.

IR spectrum (ATR):
ν_{max} [cm^{-1}] = 2950, 1693, 1655, 1592, 1570, 1506, 1474, 1366, 1319, 1291, 1245, 1171, 1072, 1017, 977, 810, 756, 721.

UV-Vis spectrum (CH_2Cl_2):
λ_{max} [nm] (ϵ [$M^{-1}cm^{-1}$])= 512 (28,382).

High Resolution Mass (ESI):
$[M+H]^+$: calculated: 953.4352, found: 953.4346, discrepancy: -0.6 ppm.

N-(2,6-Diisopropylphenyl)-9-(8-(bis(4-(octyloxy)phenyl)amino)dibenzo[b,d]thiophene-2-yl)perylene-3,4-dicarboximide

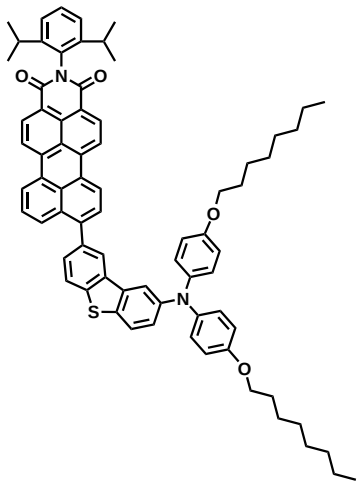

250 mg of *N*-(2,6-di*iso*propylphenyl)-9-(8-bromodibenzo[b,d]thiophene-2-yl)perylene-3,4-dicarboximide, 150 mg of bis(4-(octyloxy)phenyl)amine, 37 mg of sodium-*tert*-butoxide, 70 mg of tris(dibenzylideneacetone)dipalladium(0), and 35 mg tri-*tert*-butyl-phosphine were dissolved in 6 mL of dry toluene under argon and stirred overnight at 80°C. The reaction mixture was purified via silica column chromatography with dichloromethane and petrol ether (3:1).

Yield[4]: 130 mg pink solid (36%)

^{1}H-NMR (500 MHz, THF, 298 K):

[4]As the starting material was contaminated with the debrominated species, the product yield in the coupling is relatively low compared to other Buchwald amination reactions.

δ [ppm]: 7.97 - 7.85 (m, 4H), 7.81 (d, J = 8.0, 2H), 7.38 (d, 1H), 7.24 (d, J = 8.1, 1H), 7.17 (d, J = 8.4, 1H), 7.06 (d, J = 2.0, 1H), 6.94 (t, J = 7.5, 1H), 6.89 (t, J = 7.5, 1H), 6.81 (t, J = 7.9, 2H), 6.62 - 6.56 (m, 1H), 6.49 (d, J = 7.8, 2H), 6.35 (dd, J = 2.2, 8.8, 1H), 6.21 (d, J = 8.9, 4H), 5.99 (d, J = 8.9, 4H), 3.07 (t, J = 6.4, 4H), 2.05 - 1.94 (m, 2H), 0.69 - 0.37 (m, 30H), 0.34 (d, J = 6.8, 12H).

^{13}C-NMR (126 MHz, THF, 298 K):
δ [ppm]: 164.7, 156.8, 148.2, 147.2, 144.5, 142.6, 141.3, 138.9, 137.8, 137.6, 137.2, 134.28, 133.4, 133.1, 132.8, 130.8, 129.9, 129.7, 129.6, 128.4, 128.3, 127.1, 125.5, 125.1, 124.6, 124.4, 124.2, 124.1, 124.0, 122.6, 122.5, 121.9, 121.7, 116.3, 115.6, 69.0, 33.1, 31.0, 30.7, 30.6, 30.3, 27.4, 24.6, 23.9, 14.8.

IR spectrum (ATR):
ν_{max} [cm^{-1}] = 3038, 2923, 2850, 1701, 1662, 1592, 1574, 1504, 1468, 1356, 1235, 1016, 810, 759, 713.

UV-Vis spectrum (CH_2Cl_2):
λ_{max} [nm] (ϵ [M^{-1}cm^{-1}])= 518 (38,351).

High Resolution Mass (ESI):
$[M]^+$: calculated: 1086.5369, found: 1086.5360, discrepancy: -0.9 ppm.
The triphenylamine moiety is losing an electron to form $[M]^+$ as well as $[M+H]^+$.

Elemental analysis ($C_{74}H_{74}N_2O_4S$):
calculated: 81.73% C, 6.86% H, 2.58% N, 2.95% S
found: 81.70% C, 6.98% H, 2.58% N, 3.05% S

N-Carboxymethyl-9-(8-(bis(4-(octyloxy)phenyl)amino)dibenzo[b,d]thiophene-2-yl)perylene-3,4-dicarboximide

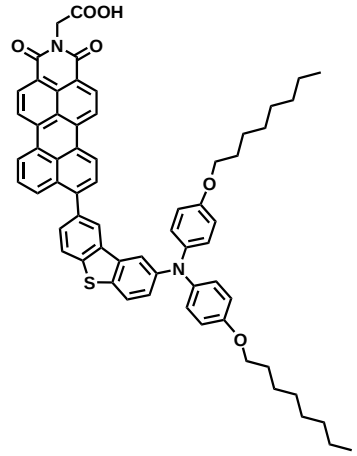

100 mg of *N*-(2,6-di*iso*propylphenyl)-9-(8-(bis(4-(octyloxy)phenyl)amino)dibenzo-[*b,d*]thiophene-2-yl)perylene-3,4-dicarboximide (0.092 mmol) were dissolved in 7 mL of 2-methyl-2-butanol. 206 mg of potassium hydroxide (3.68 mmol) were added, the reaction mixture desoxygenated and refluxed under argon overnight. The reaction mixture was poured into an ice water/acetic acid mixture (10:2). The precipitate was filtered, washed with water and after drying dissolved in dichloromethane. 1-2 mL of acetic acid were added and the solution was stirred for 1-2 days. After removal of the dichloromethane under reduced pressure, methanol was added. The precipitate was filtered and washed with methanol. The crude mixture was used directly for the next step.

Yield (crude): 80 mg red solid (94%)

80 mg of 9-(8-(bis(4-(octyloxy)phenyl)amino)dibenzo[*b,d*]thiophene-2-yl)perylene-3,4-dicarboxy monoanhydride, 1.8 g of glycine (0.024 mol) and 3 g of imidazole (0.044 mol) were mixed in a Schlenk tube and stirred under argon at 140 °C overnight. After cooling down dilute hydrochloric acid was added. The precipitate was filtered and washed with water. The crude product was purified by column chromatography on silica gel with dichloromethane, tetrahydrofuran, and acetic acid.

Yield: 75 mg pink solid (88%)

^{1}H-NMR (250 MHz, THF, 298 K):
δ [ppm]: 8.45 - 8.15 (m, 7H), 8.03 (d, J = 8.2, 1H), 7.96 (d, J = 2.1, 1H), 7.87 (d, J = 8.3, 1H), 7.74 (d, J = 8.7, 1H), 7.64 (dd, J = 1.5, 8.2, 1H), 7.56 (d, J = 7.8, 1H), 7.48

(t, J = 8.0, 1H), 7.16 (dd, J = 2.2, 8.7, 1H), 7.00 (d, J = 8.9, 4H), 6.75 (d, 4H), 4.83 (s, 2H), 3.80 (t, J = 6.4, 4H), 1.25 (d, J = 20.2, 23H), 0.94 - 0.74 (m, 8H).

^{13}C-NMR (126 MHz, THF, 298 K):
δ [ppm]: 169.8, 163.6, 156.5, 148.0, 143.8, 142.2, 140.9, 137.9, 137.7, 137.6, 137.4, 137.0, 133.6, 132.9, 131.8, 131.7, 130.5, 130.1, 129.9, 129.5, 129.2, 128.9, 127.8, 127.2, 126.9, 124.8, 124.4, 124.0, 123.6, 123.5, 121.5, 121.4, 121.0, 120.8, 116.0, 115.3, 68.7, 41.5, 32.8, 30.7, 30.4, 30.2, 27.0, 23.5, 14.5.

IR spectrum (ATR):
ν_{max} [cm^{-1}] = 3043, 2920, 2855, 1690, 1663, 1594, 1567, 1502, 1468, 1365, 1236, 1171, 1068, 1024, 972, 815, 757.

UV-Vis spectrum (CH_2Cl_2):
λ_{max} [nm] (ϵ [M^{-1}cm^{-1}])= 514 (32,537).

High Resolution Mass (ESI):
[M]$^+$: calculated: 984.4172, found: 984.4183, discrepancy: 1.1 ppm.
The triphenylamine moiety is losing an electron to form [M]$^+$ as well as [M+H]$^+$.

Elemental analysis ($C_{64}H_{60}N_2O_6S$):
calculated: 78.02% C, 6.14% H, 2.84% N, 3.25% S
found: 77.49% C, 6.64% H, 2.75% N, 3.20% S

N-(2,6-Diisopropylphenyl)-9-(8-(bis(9,9-dimethyl-9H-fluorene-2-yl)amino)dibenzo[b,d]thiophene-2-yl)perylene-3,4-dicarboximide

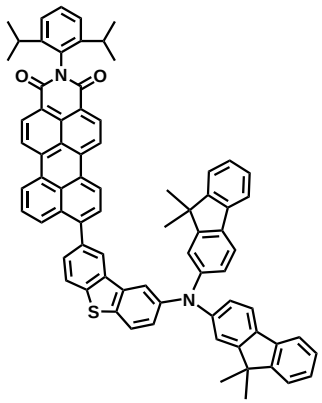

300 mg of *N*-(2,6-di*iso*propylphenyl)-9-(8-bromodibenzo[*b,d*]thiophene-2-yl)perylene-3,4-dicarboximide (0.405 mmol), 320 mg of bis(9,9-dimethyl-9*H*-fluorene-2-yl)amine

(0.798 mmol), 78 mg of sodium *tert*-butoxide (0.813 mmol), 98 mg of tris(dibenzylidenaceton)dipalladium(0) (0.107 mmol), and 49 mg of tri-*tert*-butylphosphine (0.242 mmol) were dissolved in 10 mL of dry toluene under argon and stirred at 80°C overnight. The reaction mixture was purified by silica column chromatography with dichloromethane and a subsequent gel permeation chromatography with chloroform.

Yield[5]: 252 mg pink solid (59%)

^{1}H-NMR (250 MHz, THF, 298 K):
δ [ppm]: 8.76 - 8.63 (m, 4H), 8.58 (d, J = 8.1, 2H), 8.32 (d, J = 1.3, 1H), 8.20 (d, J = 2.0, 1H), 8.09 (d, J = 8.2, 1H), 7.99 (d, J = 8.5, 1H), 7.90 (t, J = 4.3, 2H), 7.72 - 7.53 (m, 7H), 7.44 - 7.33 (m, J = 4.3, 4.9, 6H), 7.31 - 7.15 (m, 5H), 7.10 (dd, J = 2.0, 8.2, 2H), 2.87 - 2.69 (m, J = 6.8, 13.5, 2H), 1.38 (s, 12H), 1.12 (d, J = 6.8, 12H).

^{13}C-NMR (176 MHz, THF, 298 K):
δ [ppm]: 164.3, 156.1, 154.4, 148.8, 146.9, 146.8, 144.1, 141.0, 134.0, 138.5, 138.3, 138.2, 137.8, 137.6, 136.8, 135.4, 135.2, 133.9, 132.8, 132.5, 132.4, 131.5, 130.5, 130.0, 129.7, 129.6, 129.3, 128.0, 127.9, 127.8, 127.3, 126.3, 126.0, 125.2, 124.7 124.3, 124.2, 123.8, 123.7, 123.2, 122.3, 122.2, 121.6, 121.4, 120.1, 119.1, 118.7, 47.6, 35.2, 30.8, 30.0, 29.9, 27.4, 24.3.

IR spectrum (ATR):
ν_{max} [cm^{-1}] = 3050, 2957, 2921, 2863, 1698, 1660, 1595, 1570, 1447, 1354, 1293, 1273, 1244, 1025, 810, 755, 732.

UV-Vis spectrum (CH_2Cl_2):
λ_{max} [nm] (ϵ [$M^{-1}cm^{-1}$])= 351 (46,240); 513 (38,993).

High Resolution Mass (ESI):
$[M]^+$: calculated: 1062.4219, found: 1062.4225, discrepancy: 0.6 ppm.
The triphenylamine moiety is losing an electron to form $[M]^+$ as well as $[M+H]^+$.

Elemental analysis ($C_{76}H_{58}N_2O_2S$):
calculated: 85.84% C, 5.50% H, 2.63% N, 3.02% S
found: 85.70% C, 5.54% H, 2.51% N, 3.09% S

[5]As the starting material was contaminated with the debrominated species, the product yield in the coupling is relatively low compared to other Buchwald amination reactions.

N-Carboxymethyl-9-(8-(bis(9,9-dimethyl-9H-fluorene-2-yl)amino)dibenzo[b,d]-thiophene-2-yl)perylene-3,4-dicarboximide

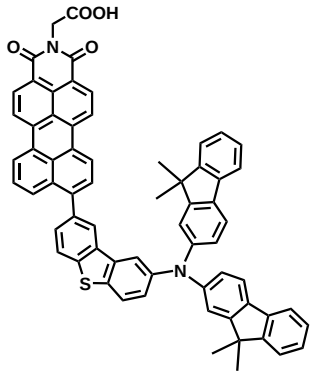

200 mg of *N*-(2,6-diisopropylphenyl)-9-(8-(bis(9,9-dimethyl-9*H*-fluorene-2-yl)amino)-dibenzo[*b,d*]thiophene-2-yl)perylene-3,4-dicarboximide (0.188 mmol) were dissolved in 14 mL of 2-methyl-2-butanol. 420 mg potassium hydroxide (7.5 mmol) were added, the reaction mixture desoxygenated and refluxed under argon overnight. The reaction mixture was poured into an ice water/acetic acid mixture (10:2). The precipitate was filtered, washed with water and after drying dissolved in dichloromethane. 1-2 mL of acetic acid were added and the solution was stirred for 1-2 days. After removal of the dichloromethane under reduced pressure, methanol was added. The precipitate was filtered and washed with methanol. The crude mixture was used directly for the next step.

Yield (crude): 155 mg pink solid (90%)

120 mg of 9-(8-(bis(9,9-dimethyl-9*H*-fluorene-2-yl)amino)dibenzo[*b,d*]thiophene-2-yl)perylene-3,4-dicarboxylic acid monoanhydride (0.133 mmol), 3 g of glycine (0.04 mol), and 4 g of imidazole (0.058 mol) were mixed in a Schlenk tube and stirred under argon at 140 °C overnight. After cooling down dilute hydrochloric acid was added. The purple precipitate was filtered and washed with water. The crude product was purified by column chromatography on silica gel with dichloromethane, tetrahydrofuran, and acetic acid.

Yield: 107 mg pink solid (84%)

^{1}H-NMR (300 MHz, CD_2Cl_2, 289 K):
δ [ppm]: 8.53 (t, J = 8.4, 2H), 8.45 - 8.31 (m, 4H), 8.09 - 7.93 (m, 4H), 7.82 (d, J = 8.7, 1H), 7.65 - 7.49 (m, 7H), 7.42 - 7.20 (m, 9H), 7.11 (dd, J = 2.1, 8.2, 2H), 4.98 (s, 2H), 1.40 (s, 12H).

^{13}C-NMR (126 MHz, CD_2Cl_2, 289 K):
δ [ppm]: 169.7, 163.7, 156.1, 154.5, 148.9, 146.9, 143.9, 141.0, 140.1, 138.1, 138.0, 137.9, 137.6, 136.8, 135.3, 133.7, 132.1, 131.9, 130.8, 130.4, 129.9, 129.5, 129.2, 128.0, 127.9, 127.5, 127.4, 126.2, 125.0, 124.6, 124.5, 124.3, 123.8, 123.3, 121.8, 121.7, 121.4, 121.2, 120.2, 119.2, 118.7, 47.7, 41.5, 30.8, 27.4.

IR spectrum (ATR):
ν_{max} [cm^{-1}] = 3043, 2951, 2923, 2854, 1697, 1659, 1596, 1568, 1448, 1366, 1278, 1240, 1070, 1023, 811, 758, 736.

UV-Vis spectrum (CH_2Cl_2):
λ_{max} [nm] (ϵ [M^{-1}cm^{-1}])= 350 (42,575); 513 (33,743).

High Resolution Mass (ESI):
$[M]^+$: calculated: 960.3022, found: 960.3046, discrepancy: 2.5 ppm.
The triphenylamine moiety is losing an electron to form $[M]^+$ as well as $[M+H]^+$.

Elemental analysis ($C_{66}H_{44}N_2O_4S$):
calculated: 82.48% C, 4.61% H, 2.91% N, 3.34% S
found: 81.88% C, 4.82% H, 2.51% N, 3.33% S

N-(2,6-Diisopropylphenyl)-9-(8-(bis(4-(5'-hexyl-[2,2'-bithiophene]-5-yl)phenyl)-amino)dibenzo[b,d]thiophene-2-yl)perylene-3,4-dicarboximide

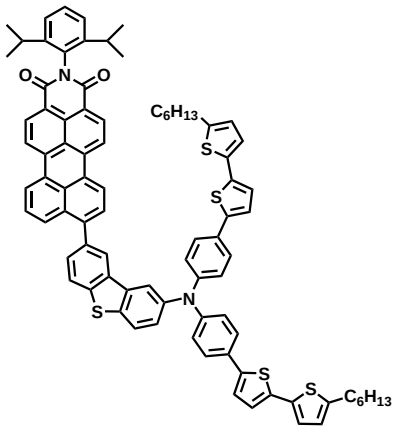

170 mg of *N*-(2,6-di*iso*propylphenyl)-9-(8-bromodibenzo[*b,d*]thiophene-2-yl)perylene-3,4-dicarboximide (0.229 mmol), 190 mg of bis(4-(5'-hexyl-[2,2'-bithiophene]-5-yl)-phenyl)amine (0.286 mmol), 33 mg of sodium *tert*-butoxide (0.344 mmol), 42 mg of tris(dibenzylidenaceton)dipalladium(0) (0.046 mmol), and 21 mg of tri-*tert*-butylphos-

phine (0.104 mmol) were dissolved in 10 mL of dry toluene under argon and stirred at 80°C overnight. The reaction mixture was purified via silica column chromatography with dichloromethane.

Yield[6]: 155 mg red solid (51%)

^{1}H-NMR (700 MHz, CD_2Cl_2, 298 K):
δ [ppm]: 8.59 - 8.57 (m, 2H), 8.47 - 8.41 (m, 4H), 8.14 (d, J = 1.4, 1H), 8.04 (d, J = 8.4, 1H), 8.00 - 7.96 (m, 2H), 7.85 (d, J = 8.8, 1H), 7.65 - 7.61 (m, 2H), 7.57 - 7.54 (m, 1H), 7.50 (t, J = 7.9, 1H), 7.46 (d, J = 8.7, 4H), 7.36 - 7.34 (m, 3H), 7.13 (d, J = 8.7, 4H), 7.09 (d, J = 3.7, 2H), 7.00 (d, J = 3.7, 2H), 6.94 (d, J = 3.5, 2H), 6.67 (dt, J = 0.9, 3.5, 2H), 2.79 - 2.74 (m, 6H), 1.68 - 1.63 (m, 4H), 1.39 - 1.29 (m, 12H), 1.14 (dd, J = 4.3, 6.8, 12H), 0.90 - 0.87 (m, 6H).

^{13}C-NMR (176 MHz, CD_2Cl_2, 298 K):
δ [ppm]: 164.4, 147.3, 146.5, 146.0, 145.1, 143.4, 142.3, 140.4, 138.1, 137.9, 137.1, 137.0, 136.7, 135.9, 135.3, 135.1, 133.1, 132.2, 132.0, 130.9, 129.7, 129.6, 129.3, 129.1, 129.0, 128.9, 128.7, 127.5, 127.2, 126.8, 125.6, 125.2, 124.5, 124.4, 124.2, 124.0, 123.6, 123.5, 123.3, 121.3, 121.2, 120.8, 120.6, 118.4, 100.4, 32.0, 31.2, 30.5, 29.5, 29.1, 24.1, 23.0, 14.2.

IR spectrum (ATR):
ν_{max} [cm^{-1}] = 3062, 2954, 2924, 2851, 1701, 1661, 1591, 1567, 1500, 1477, 1433, 1356, 1320, 1279, 1246, 1175, 1058, 1021, 958, 928, 901, 810, 784, 753.

UV-Vis spectrum (CH_2Cl_2):
λ_{max} [nm] (ϵ [$M^{-1}cm^{-1}$])= 402 (67,062), 512 (44,409).

High Resolution Mass (ESI):
$[M]^+$: calculated: 1326.4354, found: 1326.4332, discrepancy: -1.7 ppm.
The triphenylamine moiety is losing an electron to form $[M]^+$ as well as $[M+H]^+$.

Elemental analysis ($C_{86}H_{74}N_2O_2S_5$):
calculated: 77.79% C, 5.62% H, 2.11% N, 12.07% S
found: 77.48% C, 6.05% H, 2.05% N, 11.47% S

[6]As the starting material was contaminated with the debrominated species, the product yield in the coupling is relatively low compared to other Buchwald amination reactions.

N-Carboxymethyl-9-(8-(bis(4-(5'-hexyl-[2,2'-bithiophene]-5-yl)phenyl)amino)dibenzo[b,d]thiophene-2-yl)perylene-3,4-dicarboximide

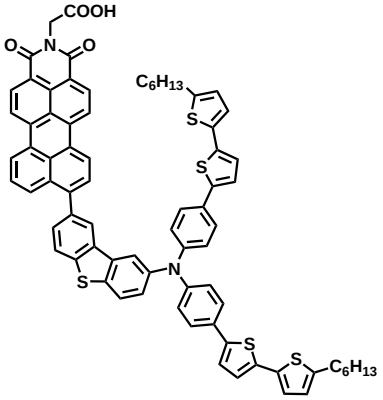

130 mg *N*-(2,6-di*iso*propylphenyl)-9-(8-(bis(4-(5'-hexyl-[2,2'-bithiophene]-5-yl)phenyl)amino)dibenzo[*b,d*]thiophene-2-yl)perylene-3,4-dicarboximide (0.083 mmol) were dissolved in 9 mL of 2-methyl-2-butanol. 220 mg potassium hydroxide (3.92 mmol) were added, the reaction mixture desoxygenated and refluxed under argon overnight. The reaction mixture was poured into an ice water/acetic acid mixture (10:2). The precipitate was filtered, washed with water and after drying dissolved in dichloromethane. 1-2 mL of acetic acid were added and the solution was stirred for 1-2 days. After removal of the dichloromethane under reduced pressure, methanol was added. The precipitate was filtered and washed with methanol. The crude mixture was used directly for the next step.

Yield (crude): 100 mg red solid (88%)

100 mg of 9-(8-(bis(4-(5'-hexyl-[2,2'-bithiophene]-5-yl)phenyl)amino)dibenzo[*b,d*]-thiophene-2-yl)perylene-3,4-dicarboxylic acid monoanhydride (0.086 mmol), 2 g of glycine (0.03 mol), and 3 g of imidazole (0.04 mol) were mixed in a Schlenk tube and stirred under argon at 140 °C overnight. After cooling down dilute hydrochloric acid was added. The purple precipitate was filtered and washed with water. The crude product was purified by column chromatography on silica gel with dichloromethane, tetrahydrofuran, and acetic acid.

Yield: 80 mg red solid (83%)

^{1}H-NMR (250 MHz, THF, 298 K):
δ [ppm]: 8.53 - 8.18 (m, 8H), 8.08 (d, J = 8.1, 1H), 7.92 (d, J = 8.6, 2H), 7.73 - 7.45 (m, 7H), 7.38 (d, J = 8.5, 1H), 7.22 - 7.08 (m, 6H), 6.96 (d, J = 3.8, 2H), 6.90 (d,

J = 3.5, 2H), 6.62 (d, J = 3.6, 2H), 4.82 (s, 2H), 2.74 (t, J = 7.5, 4H), 1.70 - 1.55 (overlapped by solvent, m, 4H), 1.44 - 1.22 (m, 12H), 0.89 (t, J = 6.5, 6H).

^{13}C-NMR (126 MHz, THF, 298 K):
δ [ppm]: 169.7, 148.1, 145.9, 145.8, 143.7, 142.9, 140.9, 138.1, 138.0, 137.8, 137.7, 137.4, 136.8, 136.0, 135.8, 133.6, 131.9, 131.8, 131.6, 130.7, 130.3, 129.9, 129.8, 129.6, 129.5, 129.1, 127.9, 127.2, 125.8, 124.9, 124.8, 124.7, 124.6, 123.9, 121.6, 121.5, 121.2, 120.9, 119.3, 65.8, 41.5, 32.6, 31.6, 30.8, 30.7, 29.7, 23.5, 20.1, 14.5, 14.1.

IR spectrum (ATR):
ν_{max} [cm^{-1}] = 2951, 2924, 2852, 1730, 1692, 1655, 1592, 1569, 1503, 1435, 1368, 1318, 1279, 1245, 1171, 1073, 831, 791, 756.

UV-Vis spectrum (CH_2Cl_2):
λ_{max} [nm] (ϵ [M^{-1}cm^{-1}])= 397 (46,574), 508(30,833).

High Resolution Mass (ESI):
[M]$^+$: calculated: 1224.3157, found: 1224.3206, discrepancy: 4.0 ppm.
The triphenylamine moiety is losing an electron to form [M]$^+$ as well as [M+H]$^+$.

N-(2,6-Diisopropylphenyl)-9-(6-(bis(4-(2,4,4-trimethylpentane-2-yl)phenyl)amino)-9-ethyl-9H-carbazole-3-yl)perylene-3,4-dicarboximide

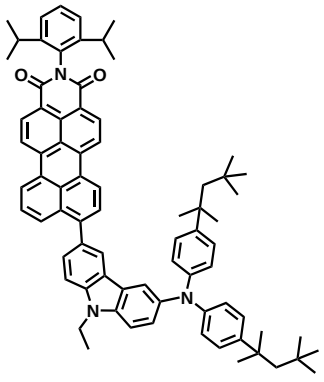

500 mg of *N*-(2,6-di*iso*propylphenyl)-9-(6-bromo-9-ethyl-9*H*-carbazole-3-yl)perylene-3,4-dicarboximide (0.663 mmol), 390 mg of bis(p-2,4,4-trimethylpentane-2-yl-phenyl)amine (0.992 mmol), 95 mg of sodium-*tert*-butoxide (0.990 mmol), 120 mg of tris(dibenzylidenaceton)dipalladium(0) (0.131 mmol) and 60 mg of tri-*tert*-butylphosphine (0.297 mmol) were dissolved in 12 mL dry toluene under argon and stirred at 80°C overnight. The reaction mixture was purified via silica column chromatography with dichloromethane.

Yield[7]: 230 mg purple solid (32%)

^{1}H-NMR (500 MHz, THF, 298 K):
δ [ppm]: 8.67 (d, J = 8.0, 1H), 8.63 (dd, J = 4.2, 8.2, 3H), 8.58 (dd, J = 3.1, 8.0, 2H), 8.17 (d, J = 1.2, 1H), 8.10 (d, J = 8.5, 1H), 7.92 (d, J = 2.0, 1H), 7.71 - 7.65 (m, 2H), 7.63 (dd, J = 1.6, 8.4, 1H), 7.59 - 7.54 (m, 1H), 7.52 (d, J = 8.8, 1H), 7.41 - 7.36 (m, 1H), 7.32 - 7.27 (m, 3H), 7.21 (d, J = 8.8, 4H), 6.97 (d, J = 8.8, 4H), 4.56 - 4.48 (m, 2H), 2.85 - 2.75 (m, 2H), 1.72 (overlaid with solvent, s, 4H) 1.51 (t, J = 7.1, 3H), 1.33 (s, 12H), 1.14 (dd, J = 1.1, 6.8, 12H), 0.76 (s, 18H).

^{13}C-NMR (126 MHz, THF, 298 K):
δ [ppm]: 163.4, 146.3, 145.9, 144.5, 142.7, 140.4, 140.2, 137.7, 137.6, 137.5, 133.0, 131.8, 131.5, 131.4, 130.5, 130.4, 129.6, 129.3, 128.6, 128.4, 127.9, 127.7, 126.9, 126.7, 126.6, 125.4, 124.0, 123.8, 123.3, 123.1, 121.9, 121.1, 1209, 120.4, 120.0, 118.2, 109.5, 108.6, 56.9, 37.8, 37.4, 32.0, 31.2, 31.0, 29.7, 29.0, 23.3, 13.3.

IR spectrum (ATR):
ν_{max} [cm^{-1}] = 3042, 2955, 2925, 2990, 1701, 1658, 1593, 1572, 1507, 1485, 1350, 1291, 1245, 1227, 1196, 1174, 1128, 814, 752.

UV-Vis spectrum (CH_2Cl_2):
λ_{max} [nm] (ϵ [M^{-1}cm^{-1}])= 525 (37,271).

High Resolution Mass (ESI):
$[M]^+$: calculated: 1065.6172, found: 1065.6141, discrepancy: -2.9 ppm.
The triphenylamine moiety is losing an electron to form $[M]^+$ as well as $[M+H]^+$.

[7]As the starting material was contaminated with the debrominated species, the product yield in the coupling is relatively low compared to other Buchwald amination reactions.

N-Carboxymethyl-9-(6-(bis(4-(2,4,4-trimethylpentane-2-yl)phenyl)amino)-9-ethyl-9H-carbazole-3-yl)perylene-3,4-dicarboximide

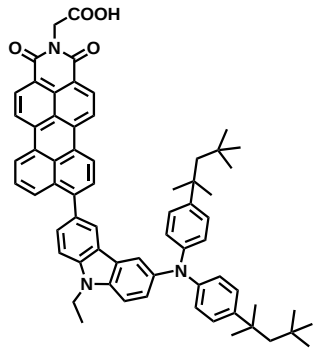

190 mg of *N*-(2,6-di*iso*propylphenyl)-9-(6-(bis(4-(2,4,4-trimethylpentane-2-yl)phenyl)amino)-9-ethyl-9*H*-carbazole-3-yl)perylene-3,4-dicarboximide (0.178 mmol) were dissolved in 15 mL of 2-methyl-2-butanol. 400 mg of potassium hydroxide (7.14 mmol) were added, the reaction mixture desoxygenated and refluxed under argon overnight. The reaction mixture was poured into an ice water/acetic acid mixture (10:2). The precipitate was filtered, washed with water and after drying dissolved in dichloromethane. 1-2 mL of acetic acid were added and the solution was stirred for 1-2 days. After removal of the dichloromethane under reduced pressure, methanol was added. The precipitate was filtered and washed with methanol. The crude mixture was used directly for the next step.

Yield (crude): 150 mg purple solid (80%)

110 mg of 9-(6-(bis(4-(2,4,4-trimethylpentane-2-yl)phenyl)amino)-9-ethyl-9*H*-carbazole-3-yl)perylene-3,4-dicarboxy monoanhydride (0.121 mmol), 2 g of glycine (0.03 mol), and 3 g of imidazole (0.04 mol) were mixed in a Schlenk tube and stirred under argon at 140 °C overnight. After cooling down dilute hydrochloric acid was added. The precipitate was filtered and washed with water. The crude product was purified by column chromatography on silica gel with dichloromethane, tetrahydrofuran, and acetic acid.

Yield: 95 mg purple solid (82%)

^{1}H-NMR (300 MHz, CD_2Cl_2, 298 K):
δ [ppm]: 8.58 - 8.34 (m, 6H), 8.16 - 8.06 (m, 2H), 7.85 (d, J = 1.9, 1H), 7.70 - 7.51 (m, 4H), 7.44 (d, J = 8.7, 1H), 7.32 (dd, J = 2.1, 8.7, 1H), 7.21 (d, J = 8.7, 4H), 6.96 (d, J = 8.6, 4H), 4.98 (s, 2H), 4.45 (q, J = 7.1, 2H), 1.68 (s, 4H), 1.51 (t, J = 7.1, 3H), 1.32 (s, 12H), 0.73 (s, 18H).

^{13}C-NMR (126 MHz, THF, 298 K):
δ [ppm]: 169.6, 163.6, 147.3, 145.2, 143.6, 141.3, 141.2, 138.5, 138.2, 138.1, 133.8, 131.9, 131.5, 130.7, 130.5, 130.2, 129.5, 129.2, 128.8, 128.7, 127.6, 127.5, 127.4, 126.4, 125.9, 124.9, 124.8, 124.6, 124.0, 122.9, 122.8, 121.5, 121.3, 121.0, 120.7, 119.4, 110.5, 109.5, 57.8, 41.4, 38.7, 38.4, 33.0, 32.2, 32.0, 30.7, 14.3.

IR spectrum (ATR):
ν_{max} [cm^{-1}] = 2951, 2899, 2872, 1737, 1694, 1658, 1593, 1568, 1507, 1486, 1366, 1289, 1227, 1129, 1070, 1017, 976, 809, 756.

UV-Vis spectrum (CH_2Cl_2):
λ_{max} [nm] (ϵ [M^{-1}cm^{-1}])= 526 (34,806).

High Resolution Mass (ESI):
$[M]^+$: calculated: 963.4975, found: 963.4981, discrepancy: 0.6 ppm.
The triphenylamine moiety is losing an electron to form $[M]^+$ as well as $[M+H]^+$.

N-(2,6-Diisopropylphenyl)-9-(6-(bis(4-(2,4,4-trimethylpentane-2-yl)phenyl)amino)-9-phenyl-9H-carbazole-3-yl)perylene-3,4-dicarboximide

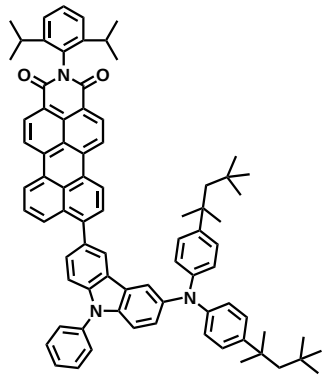

300 mg of *N*-(2,6-di*iso*propylphenyl)-9-(6-bromo-9-phenyl-9*H*-carbazole-3-yl)perylene-3,4-dicarboximide (0.374 mmol), 220 mg of bis(p-2,4,4-trimethylpentane-2-yl-phenyl)amine (0.559 mmol), 54 mg of sodium *tert*-butoxide (0.559 mmol), 50 mg of tris(dibenzylidenaceton)dipalladium(0) (0.055 mmol), and 25 mg of tri-*tert*-butylphosphine (0.124 mmol) were dissolved in 8 mL dry toluene under argon and stirred at 80°C overnight. The reaction mixture was purified via silica column chromatography with dichloromethane.

Yield[8]: 90 mg purple solid (22%)

^{1}H-NMR (700 MHz, CD_2Cl_2, 298 K):
δ [ppm]: 8.63 (d, J = 7.9, 2H), 8.58 - 8.49 (m, 4H), 8.18 - 8.11 (m, 2H), 7.88 (s, 1H), 7.72 - 7.66 (m, 5H), 7.63 - 7.55 (m, 3H), 7.55 - 7.48 (m, 2H), 7.40 (d, J = 8.9, 1H), 7.35 (d, J = 7.9, 2H), 7.29 - 7.21 (m, 5H), 7.00 (d, J = 8.2, 4H), 2.81 - 2.74 (m, 2H), 1.70 (s, 4H), 1.34 (s, 12H), 1.15 (dd, J = 1.0, 6.8, 12H), 0.74 (s, 18H).

^{13}C-NMR (176 MHz, CD_2Cl_2, 298 K):
δ [ppm]: 164.7, 146.7, 146.5, 144.9, 144.2, 142.2, 141.6, 138.5, 138.4, 133.5, 132.5, 132.4, 132.3, 132.0, 131.2, 130.6, 130.5, 129.8, 129.3, 129.0, 128.8, 128.5, 128.2, 127.6, 127.5, 124.7, 124.6, 124.4, 124.0, 122.9, 122.4, 121.4, 121.2, 120.9, 120.6, 117.9, 111.3, 110.5, 57.5, 38.6, 32.8, 32.0, 31.8, 29.6, 24.3.

IR spectrum (ATR):
ν_{max} [cm^{-1}] = 3031, 2955, 2897, 2867, 1699, 1666, 1593, 1571, 1504, 1483, 1465, 1355, 1276, 1245, 1224, 1196, 1178, 1026, 901, 816, 755, 697.

UV-Vis spectrum (CH_2Cl_2):
λ_{max} [nm] (ϵ [$M^{-1}cm^{-1}$])= 522 (37,045).

High Resolution Mass (ESI):
$[M]^+$: calculated: 1113.6172, found: 1113.6155, discrepancy: -1.6 ppm.
The triphenylamine moiety is losing an electron to form $[M]^+$ as well as $[M+H]^+$.

Elemental analysis ($C_{80}H_{81}N_3O_4$):
calculated: 86.21% C, 7.14% H, 3.77% N, –% S
found: 85.70% C, 7.38% H, 3.70% N, –% S

[8]As the starting material was contaminated with the debrominated species, the product yield in the coupling is relatively low compared to other Buchwald amination reactions.

N-Carboxymehtyl-9-(6-(bis(4-(2,4,4-trimethylpentane-2-yl)phenyl)amino)-9-phenyl-9H-carbazole-3-yl)perylene-3,4-dicarboximide

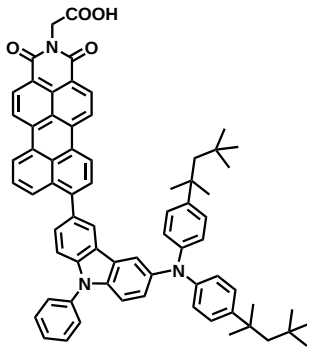

70 mg of *N*-(2,6-di*iso*propylphenyl)-9-(6-(bis(4-(2,4,4-trimethylpentane-2-yl)phenyl)-amino)-9-phenyl-9*H*-carbazole-3-yl)perylene-3,4-dicarboximide (0.063 mmol) were dissolved in 6 mL of 2-methyl-2-butanol. 140 mg of potassium hydroxide (2.51 mmol) were added, the reaction mixture desoxygenated and refluxed under argon overnight. The reaction mixture was poured into an ice water/acetic acid mixture (10:2). The precipitate was filtered, washed with water and after drying dissolved in dichloromethane. 1-2 mL of acetic acid were added and the solution was stirred for 1-2 days. After removal of the dichloromethane under reduced pressure, methanol was added. The precipitate was filtered and washed with methanol. The crude mixture was used directly for the next step.

Yield (crude): 53 mg purple solid (88%)

53 mg of 9-(6-(bis(4-(2,4,4-trimethylpentane-2-yl)phenyl)amino)-9-phenyl-9*H*-carbazole-3-yl)perylene-3,4-dicarboxylic acid monoanhydride (0.055 mmol), 1 g of glycine (0.013 mol), and 2 g of imidazole (0.029 mol) were mixed in a Schlenk tube and stirred under argon at 140 °C overnight. After cooling down dilute hydrochloric acid was added. The purple precipitate was filtered and washed with water. The crude product was purified by column chromatography on silica gel with dichloromethane, tetrahydrofuran, and acetic acid.

Yield: 48 mg purple solid (86%)

^{1}H-NMR (500 MHz, THF, 298 K):
δ [ppm]: 8.61 - 8.51 (m, 2H), 8.51 - 8.40 (m, 4H), 8.24 (s, 1H), 8.06 (d, J = 8.4, 1H), 7.99 (d, J = 2.0, 1H), 7.74 - 7.64 (m, 5H), 7.61 - 7.50 (m, 4H), 7.40 (d, J = 8.8, 1H), 7.27 - 7.20 (m, 5H), 6.99 (d, J = 8.7, 4H), 4.84 (s, 2H), 1.33 (s, 12H), 0.75 (s, 18H).

^{13}C-NMR (126 MHz, THF, 298 K):
δ [ppm]: 169.8, 163.9, 147.3, 145.1, 144.0, 142.7, 142.1, 139.3, 138.8, 138.5, 138.4, 134.0, 132.9, 132.2, 132.1, 131.1, 131.0, 130.5, 129.7, 129.4, 129.3, 129.2, 128.7, 128.0, 127.9, 127.8, 127.7, 126.6, 125.5, 125.1, 124.8, 124.7, 123.2, 123.1, 121.8, 121.6, 121.4, 121.1, 119.1, 111.7, 110.8, 58.0, 41.7, 38.9, 33.2, 32.3, 32.1.

IR spectrum (ATR):
ν_{max} [cm^{-1}] = 2951, 2903, 2870, 1695, 1659, 1593, 1569, 1502, 1485, 1464, 1366, 1319, 1225, 810, 756, 699.

UV-Vis spectrum (CH_2Cl_2):
λ_{max} [nm] (ϵ [M^{-1}cm^{-1}])= 521 (30,219).

High Resolution Mass (ESI):
$[M]^+$: calculated: 1011.4975, found: 1011.4990, discrepancy: 1.5 ppm.
The triphenylamine moiety is losing an electron to form $[M]^+$ as well as $[M+H]^+$.

N-(2,6-Diisopropylphenyl)-9-(7-(bis(4-(2,4,4-trimethylpentane-2-yl)phenyl)amino)-9-ethyl-9H-carbazole-2-yl)perylene-3,4-dicarboximide

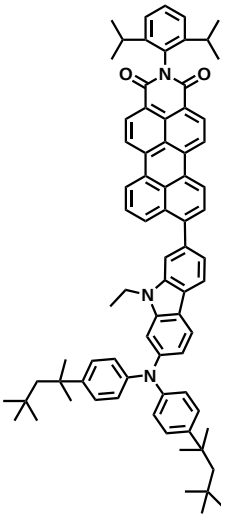

500 mg of *N*-(2,6-di*iso*propylphenyl)-9-(7-bromo-9-ethyl-9*H*-carbazole-2-yl)perylene-3,4-dicarboximide (0.663 mmol), 350 mg of bis(p-2,4,4-trimethylpentane-2-yl-phenyl)amine (0.890 mmol), 95 mg of sodium *tert*-butoxide (0.990 mmol), 120 mg of tris(dibenzylidenacetone)dipalladium(0) (0.131 mmol), and 60 mg of tri-*tert*-butylphosphine (0.297 mmol) were dissolved in 12 mL of dry toluene under argon and stirred at 80°C overnight. The reaction mixture was purified via silica column

chromatography with dichloromethane.

Yield[9]: 215 mg purple solid (30%)

^{1}H-NMR (700 MHz, THF, 298 K):
δ [ppm]: 8.75 (d, J = 7.9, 1H), 8.73 - 8.67 (m, 3H), 8.61 (dd, J = 3.2, 7.9, 2H), 8.18 - 8.11 (m, 2H), 8.00 (d, J = 8.3, 1H), 7.76 (d, J = 7.6, 1H), 7.66 - 7.60 (m, 2H), 7.42 - 7.34 (m, 2H), 7.34 - 7.27 (m, 6H), 7.13 (s, 1H), 7.07 (d, J = 8.6, 4H), 6.99 (d, J = 8.3, 1H), 4.27 (q, J = 7.0, 2H), 2.84 - 2.76 (m, 2H), 1.78 (s, 4H), 1.39 (s, 12H), 1.30 (t, J = 7.2, 3H), 1.14 (d, J = 6.8, 12H), 0.80 (s, 18H).

^{13}C-NMR (176 MHz, THF, 298 K):
δ [ppm]: 164.5, 148.4, 147.0, 146.9, 145.8, 145.0, 142.9, 141.7, 138.8, 138.7, 137.6, 134.3, 132.9, 132.7, 132.6, 131.7, 130.8, 130.6, 129.8, 129.7, 129.6, 129.4, 128.2, 128.0, 125.3, 124.9, 124.6, 124.5, 124.1, 122.4, 122.2, 121.8, 121.6, 121.4, 120.4, 119.2, 117.5, 111.0, 104.9, 58.1, 39.1, 38.1, 33.3, 32.4, 32.2, 30.2, 25.9, 25.8, 24.5, 14.2.

IR spectrum (ATR):
ν_{max} [cm^{-1}] = 3031, 2954, 2899, 2868, 1700, 1660, 1592, 1571, 1506, 1454, 1352, 1290, 1244, 1229, 1195, 1176, 1133, 908, 831, 813, 754.

UV-Vis spectrum (CH_2Cl_2):
λ_{max} [nm] (ϵ [$M^{-1}cm^{-1}$])= 370 (27,365), 526 (38,506.

High Resolution Mass (ESI):
$[M]^+$: calculated: 1065.6172, found: 1065.6177, discrepancy: 0,4 ppm.
The triphenylamine moiety is losing an electron to form $[M]^+$ as well as $[M+H]^+$.

[9]As the starting material was contaminated with the debrominated species, the product yield in the coupling is relatively low compared to other Buchwald amination reactions.

N-Carboxymethyl-9-(7-(bis(4-(2,4,4-trimethylpentane-2-yl)phenyl)amino)-9-ethyl-9H-carbazole-2-yl)perylene-3,4-dicarboximide

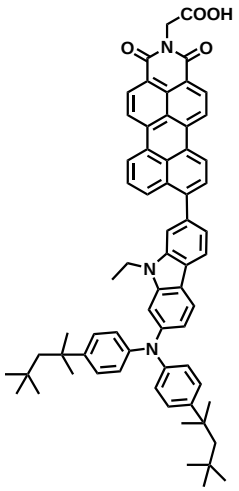

160 mg of *N*-(2,6-di*iso*propylphenyl)-9-(7-(bis(4-(2,4,4-trimethylpentane-2-yl)phenyl)amino)-9-ethyl-9*H*-carbazole-2-yl)perylene-3,4-dicarboximide (0.150 mmol) were dissolved in 12 mL of 2-methyl-2-butanol. 336 mg of potassium hydroxide (6.0 mmol) were added, the reaction mixture desoxygenated and refluxed under argon overnight. The reaction mixture was poured into an ice water/acetic acid mixture (10:2). The precipitate was filtered, washed with water and after drying dissolved in dichloromethane. 1-2 mL of acetic acid were added and the solution was stirred for 1-2 days. After removal of the dichloromethane under reduced pressure, methanol was added. The precipitate was filtered and washed with methanol. The crude mixture was used directly for the next step.

Yield (crude): 135 mg purple solid (99%)

135 mg of 9-(7-(bis(4-(2,4,4-trimethylpentane-2-yl)phenyl)amino)-9-ethyl-9*H*-carbazole-2-yl)perylene-3,4-dicarboxy monoanhydride (0.149 mmol), 2 g of glycine (0.03 mol), and 3 g of imidazole (0.04 mol) were mixed in a Schlenk tube and stirred under argon at 140 °C overnight. After cooling down dilute hydrochloric acid was added. The purple precipitate was filtered and washed with water. The crude product was purified by column chromatography on silica gel with dichloromethane, tetrahydrofuran, and acetic acid.

Yield: 105 mg purple solid (70%)

^{1}H-NMR (700 MHz, THF, 298 K):
δ [ppm]: 8.47 (d, J = 7.2, 1H), 8.41 (d, J = 6.6, 1H), 8.38 - 8.25 (m, 4H), 8.14 (d, J =

7.7, 1H), 8.07 (d, J = 8.2, 1H), 8.00 (d, J = 8.3, 1H), 7.73 (s, 1H), 7.68 (d, J = 7.5, 1H), 7.54 (t, J = 7.7, 1H), 7.40 - 7.29 (m, 5H), 7.14 (s, 1H), 7.08 (d, J = 8.5, 4H), 6.99 (d, J = 8.1, 1H), 4.84 (s, 2H), 4.39 - 4.29 (m, 2H), 1.78 (s, 4H), 1.42 - 1.33 (m, 15H), 0.81 (s, 18H).

^{13}C-NMR (176 MHz, THF, 298 K):
δ [ppm]: 169.6, 163.6, 148.1, 146.7, 145.3, 144.7, 142.6, 141.6, 138.0, 137.9, 137.4, 133.7, 131.8, 131.7, 130.6, 130.4, 130.0, 129.4, 129.0, 128.9, 127.8, 127.6, 127.3, 124.8, 124.4, 123.8, 122.1, 121.6, 121.4, 121.2, 121.0, 120.7, 120.1, 119.0, 117.2, 111.0, 104.7, 57.9, 41.4, 38.8, 38.0, 33.0, 32.2, 32.0, 25.7, 25.6, 14.1.

IR spectrum (ATR):
ν_{max} [cm^{-1}] = 3030, 2953, 2898, 2866, 1762, 1694, 1695, 1595, 1566, 1505, 1457, 1370, 1315, 1293, 1251, 1235, 1126, 1071, 978, 827, 811, 754.

UV-Vis spectrum (CH_2Cl_2):
λ_{max} [nm] (ϵ [M^{-1}cm^{-1}])= 526 (35,621).

High Resolution Mass (ESI):
$[M]^+$: calculated: 963.4975, found: 963.4931, discrepancy: -4.6 ppm.
The triphenylamine moiety is losing an electron to form $[M]^+$ as well as $[M+H]^+$.

N-(2,6-Diisopropylphenyl)-9-(5-(bis(4-(2,4,4-trimethylpentane-2-yl)phenyl)amino)-3-methylbenzo[b]thiophene-2-yl)perylene-3,4-dicarboximide

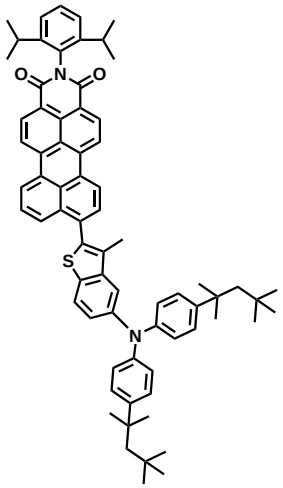

300 mg of *N*-(2,6-di*iso*propylphenyl)-9-(5-chloro-3-methylbenzo[*b*]thiophene-2-yl)-perylene-3,4-dicarboximide (0.454 mmol), 267 mg of bis(p-2,4,4-trimethylpentane-2-yl-phenyl)amine (0.677 mmol), 294 mg of caesium carbonate (0.903 mmol), 41

mg of tris(dibenzylideneacetone)dipalladium(0) (0,045 mmol), and 56 mg of 2,2´-bis(diphenylphosphino)-1,1´-binaphthyl (0.090 mmol) were dissolved in 12 mL of dry toluene under argon and stirred for 16 h at 100°C. The reaction mixture was purified via silica column chromatography with dichloromethane and petrol ether (1:3).

Yield: 240 mg red solid (52%)

^{1}H-NMR (300 MHz, THF, 298 K):
δ [ppm]: 8.80 - 8.70 (m, 4H), 8.67 - 8.60 (m, 2H), 7.95 (d, J = 8.7, 1H), 7.78 (dd, J = 8.2, 12.8, 2H), 7.71 - 7.64 (m, 1H), 7.45 - 7.36 (m, 2H), 7.36 - 7.27 (m, 6H), 7.23 (dd, J = 2.1, 8.6, 1H), 7.05 (d, J = 8.7, 4H), 2.86 - 2.73 (m, 2H), 2.06 (s, 3H), 1.77 (s, 3H), 1.39 (s, 12H), 1.14 (d, J = 6.8, 12H), 0.79 (s, 18H).

^{13}C-NMR (75 MHz, THF, 298 K):
δ [ppm]: 164.5, 147.0, 146.8, 145.1, 142.8, 138.4, 138.1, 136.9, 136.1, 135.1, 134.6, 132.8, 132.7, 131.6, 131.5, 131.4, 131.0, 130.8, 130.1, 129.8, 129.4, 128.7, 128.1, 125.5, 124.5, 124.3, 123.7, 122.8, 122.7, 122.0, 118.3, 58.1, 39.1, 33.3, 32.4, 32.2, 30.1, 24.5, 13.0.

IR spectrum (ATR):
ν_{max} [cm^{-1}] = 2957, 2867, 1702, 1664, 1592, 1577, 1507, 1447, 1356, 1292, 1246, 917, 834, 808, 753.

UV-Vis spectrum (CH_2Cl_2):
λ_{max} [nm] (ϵ [M^{-1}cm^{-1}])= 519 (45,911).

High Resolution Mass (ESI):
$[M]^+$: calculated: 1018.5471, found: 1018.5467, discrepancy: -0.4 ppm.
The triphenylamine moiety is losing an electron to form $[M]^+$ as well as $[M+H]^+$.

Elemental analysis ($C_{71}H_{74}N_2O_2S$):
calculated: 83.65% C, 7.32% H, 2.75% N, 3.14% S
found: 82.92% C, 7.25% H, 2.71% N, 3.07% S

N-Carboxymethyl-9-(5-(bis(4-(2,4,4-trimethylpentane-2-yl)phenyl)amino)-3-methylbenzo[b]thiophene-2-yl)perylene-3,4-dicarboximide

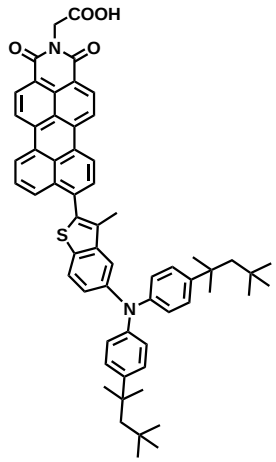

190 mg of *N*-(2,6-di*iso*propylphenyl)-9-(5-(bis(4-(2,4,4-trimethylpentane-2-yl)phenyl)amino)-3-methylbenzo[*b*]thiophene-2-yl)perylene-3,4-dicarboximide (0.186 mmol) were dissolved in 15 mL of 2-methyl-2-butanol. 420 mg of potassium hydroxide (7.5 mmol) were added, the reaction mixture desoxygenated and refluxed under argon overnight. The reaction mixture was poured into an ice water/acetic acid mixture (10:2). The precipitate was filtered, washed with water and after drying dissolved in dichloromethane. 1-2 mL of acetic acid were added and the solution was stirred for 1-2 days. After removal of the dichloromethane under reduced pressure, methanol was added. The precipitate was filtered and washed with methanol. The solvent was removed under reduced pressure. The crude mixture was used directly for the next step.

Yield (crude): 140 mg red solid (88%)

140 mg of 9-(5-(bis(4-(2,4,4-trimethylpentane-2-yl)phenyl)amino)-3-methylbenzo-[*b*]thiophene-2-yl)perylene-3,4-dicarboxylic acid monoanhydride (0.163 mmol), 2 g of glycine (0.03 mol), and 3 g of imidazole (0.04 mol) were mixed in a Schlenk tube and stirred under argon at 140°C overnight. After cooling down dilute hydrochloric acid was added. The precipitate was filtered and washed with water. The crude product was purified by column chromatography on silica gel with dichloromethane, tetrahydrofuran, and acetic acid.

Yield: 103 mg red solid (69%)

^{1}H-NMR (300 MHz, THF, 298 K):
δ [ppm]: 8.65 - 8.43 (m, 6H), 7.91 (d, J = 8.3, 1H), 7.80 (d, J = 8.7, 1H), 7.71 (d, J =

7.8, 1H), 7.67 - 7.58 (m, 1H), 7.44 (d, J = 2.0, 1H), 7.32 (d, J = 8.7, 4H), 7.22 (dd, J = 2.1, 8.6, 1H), 7.05 (d, J = 8.7, 4H), 4.85 (s, 2H), 2.06 (s, 3H), 1.77 (overlaid with solvent, s, 4H), 1.36 (d, J = 18.1, 12H), 0.78 (s, 18H).

^{13}C-NMR (126 MHz, THF, 298 K):

δ [ppm]: 169.7, 163.8, 147.0, 146.8, 145.0, 142.8, 138.2, 137.9, 136.9, 136.0, 135.2, 134.5, 132.3, 131.5, 131.3, 131.0, 130.8, 130.0, 129.3, 128.6, 128.1, 127.8, 125.3, 124.3, 123.7, 1224, 122.3, 121.8, 118.3, 58.1, 55.1, 41.6, 39.1, 33.3, 32.4, 32.2, 30.8, 12.9.

IR spectrum (ATR):

ν_{max} [cm^{-1}] = 2949, 2891, 2866, 1694, 1661, 1592, 1571, 1505, 1447, 1367, 1248, 1168, 1092, 1066, 809, 758.

UV-Vis spectrum (THF):

λ_{max} [nm] (ϵ [M^{-1}cm^{-1}])= 510 (32,115).

High Resolution Mass (ESI):

[M]$^+$: calculated: 916.4274, found: 916.4297, discrepancy: 2.5 ppm.
The triphenylamine moiety is losing an electron to form [M]$^+$ as well as [M+H]$^+$.

N-(2,6-Diisopropylphenyl)-9-(3-bis(7-(tert-butyl)pyrene)aminobenzyl)perylene-3,4-dicarboximide

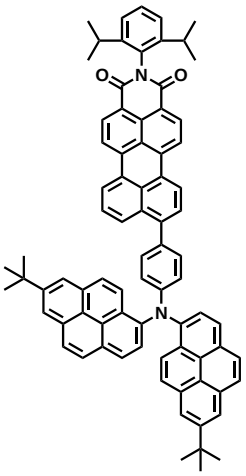

250 mg *N*-(2,6-diisopropylphenyl)-9-(3-aminobenzyl)perylene-3,4-dicarboximide (0.436 mmol), 147 mg of 1-bromo-7-(*tert*-butyl)pyrene (0.436 mmol), 55 mg of sodium *tert*-butoxide (0.567 mmol), 60 mg of tris(dibenzylideneacetone)dipalladium(0) (0.066 mmmol) and 30 mg of tri-*tert*-butylphosphine (0.148 mmol) were dissolved in 10 mL of dry toluene under argon and stirred overnight at 80°C. After cooling down 147

mg 1-bromo-7-(tert-butyl)pyrene (0,436 mmol), 55 mg of sodium *tert*-butoxide (0,567 mmol), 60 mg of tris(dibenzylideneacetone)dipalladium(0) (0,066 mmmol), and 30 mg tri-*tert*-butylphosphine (0,148 mmol) were added under argon and again stirred overnight at 80°C. The solvent was evaporated under reduced pressure and the reaction mixture purified via column chromatography on silica gel with dichloromethane. Main side product was the mono-substituted derivative.

Yield: 150 mg purple solid (32%)

^{1}H-NMR (700 MHz, CD_2Cl_2, 298 K):
δ [ppm]: 8.61 (dd, J = 5.4, 8.0, 2H), 8.53 - 8.45 (m, 4H), 8.43 (d, J = 9.2, 2H), 8.28 (d, J = 1.4, 2H), 8.23 (d, J = 1.2, 2H), 8.20 (d, J = 8.4, 1H), 8.13 (d, J = 8.3, 2H), 8.09 - 8.00 (m, 6H), 7.92 (d, J = 8.2, 2H), 7.66 - 7.60 (m, 2H), 7.50 (t, J = 7.9, 1H), 7.36 (dd, J = 8.3, 12.4, 4H), 6.96 (d, J = 8.4, 2H), 2.80 - 2.71 (m, 2H), 1.58 (s, 18H), 1.14 (d, J = 6.8, 12H).

^{13}C-NMR (176 MHz, CD_2Cl_2, 298 K):
δ [ppm]: 164.5, 151.2, 150.2, 146.5, 143.9, 142.1, 138.3, 138.2, 133.0, 132.3, 132.2, 132.1, 131.6, 131.3, 131.0, 130.1, 129.6, 128.8, 128.5, 128.2, 127.6, 127.5, 127.3, 126.7, 126.4, 126.1, 124.5, 124.4, 124.3, 123.7, 123.5, 123.1, 122.9, 121.2, 120.9, 120.7, 120.4, 120.0, 35.5, 32.0, 29.4, 24.1.

IR spectrum (ATR):
ν_{max} [cm^{-1}] = 3037, 2954, 2926, 2904, 2864, 1703, 1660, 1591, 1567, 1496, 1453, 1415, 1354, 1285, 1247, 1178, 931, 872, 838, 812, 755, 715, 682.

UV-Vis spectrum (CH_2Cl_2):
λ_{max} [nm] (ϵ [$M^{-1}cm^{-1}$])= 539 (38,482).

High Resolution Mass (ESI):
$[M]^+$: calculated: 1084.4968, found: 1084.4915, discrepancy: -4.9 ppm.
The triphenylamine moiety is losing an electron to form $[M]^+$ as well as $[M+H]^+$.

N-Carboxymethyl-9-(3-bis(7-(tert-butyl)pyrene)aminobenzyl)perylene-3,4-dicarboximide

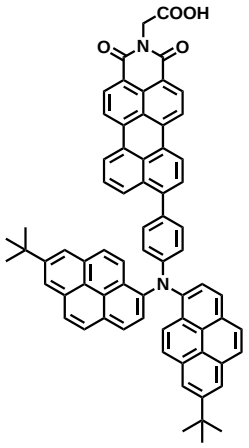

120 mg *N*-(2,6-di*iso*propylphenyl)-9-(3-bis(7-(*tert*-butyl)pyrene)aminobenzol)perylene-3,4-dicarboximide (0.111 mmol) were dissolved in 15 mL of 2-methyl-2-butanol. 248 mg of potassium hydroxide (4.42 mmol) were added, the reaction mixture desoxygenated and refluxed under argon overnight. The reaction mixture was poured into an ice water/acetic acid mixture (10:2). The precipitate was filtered, washed with water and after drying dissolved in dichloromethane. 1-2 mL of acetic acid were added and the solution was stirred for 1-2 days. After removal of the dichloromethane under reduced pressure, methanol was added. The precipitate was filtered and washed with methanol. The solvent was removed under reduced pressure. The crude mixture was used directly for the next step.

Yield (crude): 100 mg purple solid (98%)

100 mg 9-(3-bis(7-(*tert*-butyl)pyrene)aminobenzyl)perylene-3,4-dicarboxylic acid monoanhydride (0.108 mmol), 2 g of glycine (0.03 mol), and 3 g of imidazole (0.04 mol) were mixed in a Schlenk tube and stirred under argon at 140°C overnight. After cooling down dilute hydrochloric acid (water:acid (5:1)) was added. The precipitate was filtered and washed with water. The crude product was purified by column chromatography on silica gel with dichloromethane, tetrahydrofuran, and acetic acid.

Yield: 96 mg purple solid (90%)

^{1}H-NMR (300 MHz, THF, 298 K):
δ [ppm]: 8.53 - 8.40 (m, 4H), 8.40 - 8.22 (m, 8H), 8.20 - 8.00 (m, 9H), 7.91 (d, J = 8.2, 2H), 7.62 - 7.51 (m, 2H), 7.40 (d, J = 8.7, 2H), 6.98 (d, J = 8.6, 2H), 4.82 (s, 2H), 1.58 (s, 18H).

^{13}C-NMR (126 MHz, THF, 298 K):
δ [ppm]: 169.8, 163.7, 151.8, 150.4, 143.9, 142.9, 138.1, 137.9, 133.3, 133.1, 132.5, 132.2, 132.0, 131.9, 131.8, 130.6, 130.4, 130.2, 130.0, 129.2, 129.1, 128.8, 128.2, 128.0, 128.0, 127.7, 127.3, 127.2, 127.0, 126.8, 124.9, 124.7, 124.3, 124.2, 123.5, 123.4, 121.5, 121.2, 121.0, 120.7, 120.6, 41.5, 36.0, 32.3.

IR spectrum (ATR):
ν_{max} [cm^{-1}] = 3038, 2955, 2902, 2866, 1757, 1697, 1659, 1594, 1564, 1499, 1369, 1292, 1242, 1224, 1168, 1067, 973, 878, 837, 810, 756.

UV-Vis spectrum (CH_2Cl_2):
λ_{max} [nm] (ϵ [M^{-1}cm^{-1}])= 335 (35,859), 410 (28,794), 539 (36,565).

High Resolution Mass (ESI):
$[M]^+$: calculated: 982.3771, found: 982.3791, discrepancy: 2.1 ppm.
The triphenylamine moiety is losing an electron to form $[M]^+$ as well as $[M+H]^+$.

8.2.2 SPC: Flexible pi-Spacer for Improved Light Harvesting and Introduction of a Second Donor

N-(2,6-Diisopropylphenyl)-9-(5,5”-bis(trimethylsilyl)-[2,2’:3’,2”-terthiophene]-5’-yl)-perylene-3,4-dicarboximide

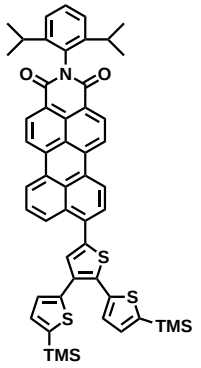

300 mg of *N*-(2,6-di*iso*propylphenyl)-9-bromo-perylene-3,4-dicarboximide (0.534 mmol), 300 mg of (5’-(4,4,5,5-tetramethyl-1,3,2-dioxaborolan-2-yl)-[2,2’:3’,2”-terthiophene]-5,5”-diyl)bis(trimethylsilane) (0.579 mmol) and were dissolved in 30 mL of toluene in a Schlenk tube. 750 mg of potassium carbonate (5.435 mmol) in 3 mL of water and 0.3 mL of ethanol were added. The solution was purged with argon for about 30 minutes. After addition of 90 mg of tetrakis(triphenylphosphine)palladium (0.081 mmol) the solution was again purged for about 30 minutes with argon and stirred under argon at 80 °C overnight. The reaction mixture was extracted with dichloromethaneand dried over magnesium sulfate. The solvent was evaporated under reduced pressure and the resulting solid was purified by column chromatography on silica gel with dichloromethane.

Yield: 360 mg purple solid (77%)

^{1}H-NMR (250 MHz, CD_2Cl_2, 298 K):
δ [ppm]: 8.50 (dd, J = 1.1, 8.1, 2H), 8.40 (d, J = 8.5, 1H), 8.36 - 8.23 (m, 4H), 7.68 - 7.52 (m, 2H), 7.48 - 7.40 (m, 1H), 7.37 - 7.26 (m, 3H), 7.25 - 7.09 (m, 4H), 2.83 - 2.60 (m, 2H), 1.10 (d, J = 6.8, 12H), 0.30 - 0.24 (m, 18H).

^{13}C-NMR (75 MHz, CD_2Cl_2, 298 K):
δ [ppm]: 164.66, 146.84, 140.33, 137.96, 137.76, 137.55, 135.11, 133.64, 133.40, 132.89, 132.40, 132.34, 131.60, 131.01, 130.04, 129.86, 129.66, 129.58, 129.39, 128.99, 128.97, 128.18, 128.07, 128.01, 127.97, 127.74, 127.30, 126.64, 124.82, 124.75, 123.96, 121.67, 121.10, 120.99, 29.90, 24.49, 2.29.

IR spectrum (ATR):
ν_{max} [cm^{-1}] = 3057, 2960, 2869, 1701, 1662, 1591, 1568, 1503, 1449, 1408, 1354, 1292, 1247, 1091, 1024, 986, 835, 802, 752.

UV-Vis spectrum (CD_2Cl_2):
λ_{max} [nm] (ϵ [$M^{-1}cm^{-1}$])= 525 (40,329).

High Resolution Mass (ESI):
$[M+H]^+$: calculated: 872.2542, found: 872.2528, discrepancy: -1.6 ppm.

N-(2,6-Diisopropylphenyl)-9-(5,5"-bis[4-N,N-diphenylaniline]-[2,2':3',2"-terthiophene]-5'-yl)-perylene-3,4-dicarboximide

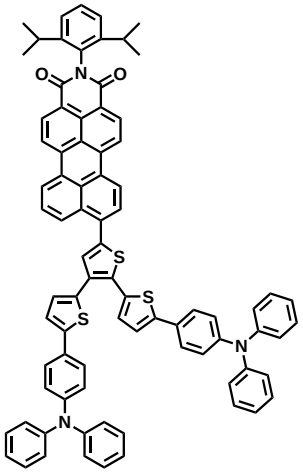

315 mg *N*-(2,6-di*iso*propylphenyl)-9-(5,5"-bis(trimethylsilyl)-[2,2':3',2"-terthiophene]-5'-yl)-perylene-3,4-dicarboximide (0.360 mmol) were dissolved in tetrahydrofuran and cooled to 0°C. Under argon 128 mg of *N*-bromosuccinimide (0.721 mmol) dissolved in tetrahydrofuran were added dropwise. The solution was stirred under argon at room temperature for 24 h. The solvent was evaporated under reduced pressure and the resulting solid was purified by column chromatography on silica gel with first pure toluene and later pure dichloromethane. The crude product was used directly for the next step.

Yield (crude): 262 mg purple solid (82 %)

400 mg of *N*-(2,6-di*iso*propylphenyl)-9-(5,5"-dibromo-[2,2':3',2"-terthiophene]-5'-yl)-perylene-3,4-dicarboximide (0.451 mmol) and 390 mg of 4-(diphenylamino)phenyl)boronic acid (1.349 mmol) were dissolved in 40 mL toluene in a Schlenk tube.

800 mg of potassium carbonate (5.797 mmol) in 4 mL of water and 0.4 mL of ethanol were added. The solution was purged with argon for about 30 minutes. After addition of 200 mg of tetrakis(triphenylphosphine)palladium (0.179 mmol) the solution was again purged for about 30 minutes with argon and stirred under argon at 80°C overnight. The reaction mixture was extracted with dichloromethane and dried over magnesium sulfate. The solvent was evaporated under reduced pressure and the resulting solid was purified roughly by column chromatography on silica gel with dichloromethane followed by a more thorough purification over a recycling gel permeation chromatography with chloroform to seperate the product from the mono-functionalised by-product.

Yield: 235 mg dark purple solid (43%)

^{1}H-NMR (300 MHz, CD_2Cl_2, 298 K):
δ [ppm]: 8.60 (d, J = 8.0, 2H), 8.56 - 8.35 (m, 5H), 7.84 - 7.62 (m, 2H), 7.59 - 6.98 (m, 36H), 2.89 - 2.68 (m, 2H), 1.17 (d, J = 6.8, 12H).

^{13}C-NMR (126 MHz, CD_2Cl_2, 298 K):
δ [ppm]: 164.6, 148.3, 148.1, 148.0, 147.9, 146.7, 146.4, 145.1, 140.2, 138.0, 137.6, 136.1, 135.1, 133.4, 133.3, 133.0, 132.9, 132.4, 132.2, 131.5, 131.0, 129.9, 129.8, 129.7, 129.5, 129.4, 129.0, 128.7, 128.6, 128.2, 128.1, 127.31, 127.0, 125.2, 125.1, 124.9, 124.6, 124.0, 123.9, 123.8, 123.1, 123.0, 121.6, 121.1, 121.0, 29.7, 24.3.

IR spectrum (ATR):
ν_{max} [cm^{-1}] = 3060, 3030, 2960, 2978, 2868, 1700, 1661, 1589, 1487, 1468, 1408, 1354, 1326, 1272, 1244, 1193, 1778, 1025, 938, 834, 809, 794, 750, 693.

UV-Vis spectrum (CD_2Cl_2):
λ_{max} [nm] (ϵ [$M^{-1}cm^{-1}$])= 366 (50,066), 526 (45,055).

High Resolution Mass (ESI):
$[M]^+$: calculated: 1213.3769, found: 1213.3795, discrepancy: 2.1 ppm.
The triphenylamine moiety is losing an electron to form $[M]^+$ as well as $[M+H]^+$.

Elemental analysis ($C_{82}H_{59}N_3O_2S_3$):
calculated: 81.09% C, 4.90% H, 3.46% N, 7.92% S
found: 80.57% C, 4.99% H, 3.45% N, 7.97% S

9-(5,5"-Bis[4-N,N-diphenylaniline]-[2,2':3',2"-terthiophene]-5'-yl)-perylene-3,4-dicarboxyanhydride

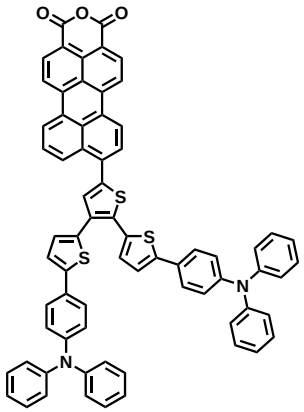

200 mg of *N*-(2,6-di*iso*propylphenyl)-9-(5,5"-bis[4-*N,N*-diphenylaniline]-[2,2':3',2"-terthiophene]-5'-yl)-perylene-3,4-dicarboximide (0.165 mmol) were dissolved in 14 mL of 2-methyl-2-butanol. 370 mg of potassium hydroxide (6.6 mmol) were added and the reaction mixture desoxygenated and refluxed under argon overnight. The reaction mixture was poured into an ice water/acetic acid mixture (10:2). The precipitate was filtered, washed with water and after drying dissolved in dichloromethane. 1-2 mL of acetic acid were added and the solution was stirred for 1-2 days. After removal of the dichloromethane under reduced pressure, methanol was added. The precipitate was filtered and washed with methanol. The crude compound was purified by column chromatography on silica with dichloromethane. The obtained anhydride was precipitated from tetrahydrofuran into methanol.

Yield: 155 mg dark purple solid (90%)

^{1}H-NMR (700 MHz, THF, 298 K):
δ [ppm]: 8.72 - 8.67 (m, 2H), 8.63 (dd, J = 2.4, 8.2, 2H), 8.56 (d, J = 8.7, 1H), 8.51 (dd, J = 3.1, 7.9, 2H), 7.86 (d, J = 7.8, 1H), 7.77 (dt, 1H), 7.58 (s, 1H), 7.53 - 7.48 (m, 4H), 7.30 (d, J = 3.7, 1H), 7.29 - 7.21 (m, 11H), 7.11 - 7.06 (m, 8H), 7.05 - 6.99 (m, 8H).

^{13}C-NMR (126 MHz, THF, 298 K):
δ [ppm]: 161.4, 149.1, 148.9, 148.8, 147.3, 145.9, 140.9, 139.3, 138.9, 136.7, 136.0, 134.0, 133.9, 133.8, 133.6, 133.4, 132.3, 130.7, 130.5, 130.3, 129.8, 129.6, 129.5, 129.2, 129.0, 127.9, 127.7, 127.6, 126.2, 125.8, 125.7, 125.4, 124.8, 124.7, 124.4, 124.3, 123.9, 123.7, 122.3, 122.2, 119.0.

IR spectrum (ATR):

ν_{max} [cm^{-1}] = 3059, 3029, 2923, 1758, 1723, 1588, 1566, 1486, 1272, 1130, 1011, 805, 793, 749, 738, 692.

UV-Vis spectrum (CH_2Cl_2):
λ_{max} [nm] (ϵ [$M^{-1}cm^{-1}$])= 364 (53,083), 526 (42,102).

High Resolution Mass (ESI):
$[M]^+$: calculated: 1054.2358, found: 1054.2323, discrepancy: -3.3 ppm.
The triphenylamine moiety is losing an electron to form $[M]^+$ as well as $[M+H]^+$.

Elemental analysis ($C_{70}H_{42}N_2O_3S$):
calculated: 79.67% C, 4.01% H, 2.65% N, 9.12% S
found: 79.15% C, 3.85% H, 2.64% N, 9.07% S

N-Carboxymethyl-9-(5,5"-bis[4-N,N-diphenylaniline]-[2,2':3',2"-terthiophene]-5'-yl)-perylene-3,4-dicarboximide

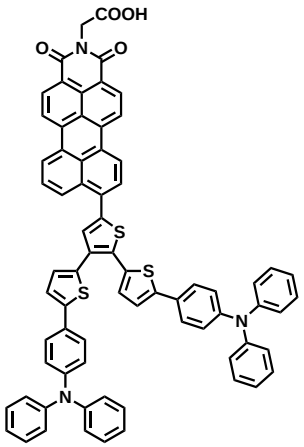

110 mg of 9-(5,5"-bis[4-*N,N*-diphenylaniline]-[2,2':3',2"-terthiophene]-5'-yl)-perylene-3,4-dicarboxianhydride (0.104 mmol), 2 g of glycine (26.7 mmol), and 3 g of imidazole (44.1 mmol) were mixed in a Schlenk tube and stirred under argon at 140°C overnight. After cooling down dilute hydrochloric acid was added. The purple precipitate was filtered and washed with water. The crude product was purified by column chromatography on silica gel with dichloromethane, tetrahydrofuran, and acetic acid.

Yield: 103 mg of a dark purple solid (89 %)

^{1}H-NMR (700 MHz, THF, 298 K):
δ [ppm]: 8.68 - 8.62 (m, 2H), 8.60 (d, J = 8.1, 2H), 8.56 - 8.50 (m, 3H), 7.84 (d, J = 7.8, 1H), 7.74 (t, J = 7.9, 1H), 7.57 (s, 1H), 7.51 (dd, J = 6.8, 8.6, 4H), 7.30 (d,

J = 3.7, 1H), 7.28 - 7.23 (m, 11H), 7.10 - 7.06 (m, 8H), 7.05 - 6.99 (m, 8H), 4.86 (s, 2H).

^{13}C-NMR (126 MHz, THF, 298 K):
δ [ppm]: 169.9, 163.7, 148.8, 148.7, 148.6, 147.0, 145.6, 141.1, 137.7, 137.3, 136.7, 135.0, 133.9, 133.8, 133.3, 133.1, 131.9, 131.8, 130.5, 130.4, 130.3, 130.2, 129.9, 129.6, 129.4, 129.1, 128.5, 127.5, 127.4, 127.2, 125.6, 125.5, 125.2, 124.7, 124.6, 124.3, 124.2, 124.1, 123.7, 123.6, 121.8, 121.7, 121.5, 121.3, 41.6.

IR spectrum (ATR):
ν_{max} [cm^{-1}] = 3059, 3032, 1694, 1656, 1589, 1566, 1487, 1368, 1315, 1272, 1171, 1131, 1071, 964, 807, 749.

UV-Vis spectrum (CH_2Cl_2):
λ_{max} [nm] (ϵ [M^{-1}cm^{-1}])= 365 (41,033), 527 (34,881).

High Resolution Mass (ESI):
$[M]^+$: calculated: 1111.2572, found: 1111.2545, discrepancy: -2.5 ppm.
The triphenylamine moiety is losing an electron to form $[M]^+$ as well as $[M+H]^+$.

N-(2,6-Diisopropylphenyl)-5-5,5”-dibromo-[2,2’:3’,2”-terthiophene]-5’-yl)-naphthalene-1,8-dicarboximide

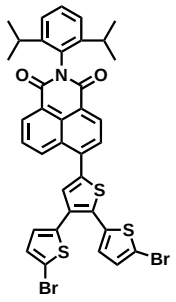

400 mg of *N*-(2,6-di*iso*propylphenyl)-1-bromo-naphthalene-4,5-dicarboximide (0.917 mmol) and 523 mg (5’-(4,4,5,5-tetramethyl-1,3,2-dioxaborolan-2-yl)-[2,2’:3’,2”-terthiophene]-5,5”-diyl)bis(trimethylsilane) (1.001 mmol) (7.246 mmol) were dissolved in 40 mL of toluene in a Schlenk tube. 1 g of potassium carbonate in 4 mL of water and 0.4 mL of ethanol were added. The solution was purged with argon for 30 minutes. After addition of 200 mg of tetrakis(triphenylphosphine)palladium (0.179 mmol) the solution was again purged with argon for 30 minutes and stirred at 80°C overnight. The reaction mixture was extracted with dichloromethane and dried over magnesium sulfate. The solvent was evaporated under reduced pressure and the resulting solid was purified by column chromatography on silica gel with toluene. The crude mixture

was used without further purification for the next step.

Yield (crude): 630 mg yellow solid (92%)

500 mg of*N*-(2,6-di*iso*propylphenyl)-1-(5,5"-bis(trimethylsilyl)-[2,2':3',2"-terthiophene]-5'-yl)-naphthalene-4,5-dicarboximide (0.668 mmol) were dissolved in tetrahydrofuran and cooled to 0°C. Under argon 238 mg of *N*-bromosuccinimide (0.133 mmol) dissolved in tetrahydrofuran were added dropwise. The solution was stirred under argon at room temperature for 24 h. The solvent was evaporated under reduced pressure and the resulting solid was purified by column chromatography on silica gel with first toluene and later dichloromethane.

Yield: 425 mg yellow solid (84 %)

^{1}H-NMR (500 MHz, CD_2Cl_2, 298 K):
δ [ppm]: 8.81 (d, J = 8.5, 1H), 8.71 (d, J = 7.2, 1H), 8.66 (d, J = 7.6, 1H), 7.94 (d, J = 7.6, 1H), 7.92 - 7.87 (m, 1H), 7.50 (t, J = 7.8, 1H), 7.42 (s, 1H), 7.35 (d, J = 7.8, 2H), 7.11 - 7.04 (m, 3H), 6.99 (d, J = 3.8, 1H), 2.81 - 2.68 (m, 2H), 1.13 (d, J = 6.9, 12H).

^{13}C-NMR (126 MHz, CD_2Cl_2, 298 K):
δ [ppm]: 164.8, 164.5, 146.6, 139.7, 138.6, 138.5, 135.8, 133.8, 132.9, 132.5, 131.8, 131.5, 131.1, 130.9, 130.6, 130.1, 130.0, 129.5, 129.2, 128.4, 128.2, 124.6, 123.6, 123.0, 114.9, 113.5, 29.7, 24.2.

IR spectrum (ATR):
ν_{max} [cm^{-1}] = 2961, 2927, 2867, 1707, 1665, 1586, 1359, 1237, 1193, 1132, 968, 900, 835, 782, 754.

UV-Vis spectrum (CH_2Cl_2):
λ_{max} [nm] (ϵ [$M^{-1}cm^{-1}$])= 399 (16,249).

High Resolution Mass (ESI):
$[M+H]^+$: calculated: 759.9649, found: 759.9651, discrepancy: 0.3 ppm.

Elemental analysis ($C_{36}H_{27}Br_2NO_2S_3$):
calculated: 56.77% C, 3.57% H, 1.84% N, 12.63% S
found: 56.19% C, 3.70% H, 1.91% N, 12.51% S

N-(2,6-Diisopropylphenyl)-5-(5,5"-bis[4-N,N-diphenylaniline]-[2,2':3',2"-terthiophene]-5'-yl)-naphthalene-1,8-dicarboximide

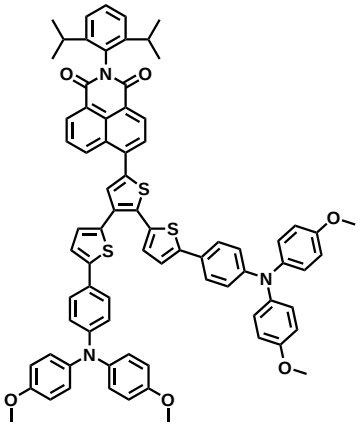

400 mg of *N*-(2,6-di*iso*propylphenyl)-1-(5,5"-dibromo-[2,2':3',2"-terthiophene]-5'-yl)-naphthalene-4,5-dicarboximide (0.524 mmol) and 680 mg of 4-methoxy-*N*-(4-methoxyphenyl)-*N*-(4-(4,4,5,5-tetramethyl-1,3,2-dioxaborolan-2-yl)phenyl)aniline (1.578 mmol) were dissolved in 40 mL toluene in a Schlenk tube. 800 mg of potassium carbonate (5.797) in 4 mL of water and 0.4 mL of ethanol were added. The solution was purged with argon for 30 minutes. After the addition of 230 mg of tetrakis(triphenylphosphine)palladium (0.207 mmol) the solution was again purged with argon for 30 minutes and stirred at 80°C overnight. The reaction mixture was extracted with dichloromethane and dried over magnesium sulfate. The solvent was evaporated under reduced pressure and the resulting solid was purified roughly by column chromatography on silica gel with dichloromethane followed by a more thorough purification over a recycling gel permeation chromatography with chloroform.

Yield: 120 mg orange-brown solid (19 %)

^{1}H-NMR (250 MHz, CD_2Cl_2, 298 K):
δ [ppm]: 8.89 (d, J = 8.6, 1H), 8.74 - 8.63 (m, 2H), 8.00 - 7.86 (m, 2H), 7.56 - 7.46 (m, 2H), 7.45 - 7.35 (m, 5H), 7.33 (d, J = 2.7, 1H), 7.24 (d, J = 3.8, 1H), 7.21 - 7.13 (m, 3H), 7.12 - 7.01 (m, 8H), 6.92 - 6.80 (m, 12H), 3.79 (d, J = 0.7, 12H), 2.85 - 2.68 (m, 2H), 1.13 (d, J = 6.8, 12H).

^{13}C-NMR (176 MHz, CD_2Cl_2, 298 K):
δ [ppm]: 164.8, 164.6, 156.9, 156.8, 149.3, 149.1, 147.0, 146.7, 145.7, 141.0, 140.9, 139.2, 138.7, 135.2, 134.6, 133.2, 132.4, 132.1, 131.9, 131.6, 130.5, 130.1, 129.9, 129.0, 128.8, 128.1, 127.5, 127.4, 126.9, 126.8, 126.4, 126.0, 124.6, 123.6, 122.7, 122.5, 122.4, 120.6, 120.5, 115.3, 115.3, 56.0, 29.7, 24.2.

IR spectrum (ATR):
ν_{max} [cm^{-1}] = 2960, 2832, 1708, 1667, 1586, 1501, 1460, 1359, 1235, 1033, 825, 797, 782, 574, 521.

UV-Vis spectrum (CH_2Cl_2):
λ_{max} [nm] (ϵ [$M^{-1}cm^{-1}$])= 383 (58,579).

High Resolution Mass (ESI):
$[M]^+$: calculated: 1209.3879, found: 1209.3866, discrepancy: -1.1 ppm.
The triphenylamine moiety is losing an electron to form $[M]^+$ as well as $[M+H]^+$.

Elemental analysis ($C_{76}H_{63}N_3O_6S_3$):
calculated: 75.41% C, 5.25% H, 3.47% N, 7.95% S
found: 75.08% C, 5.43% H, 3.37% N, 8.01% S

N-Carboxymethyl-5-(5,5"-bis[4-N,N-diphenylaniline]-[2,2':3',2"-terthiophene]-5'-yl)-naphthalene-1,8-dicarboximide

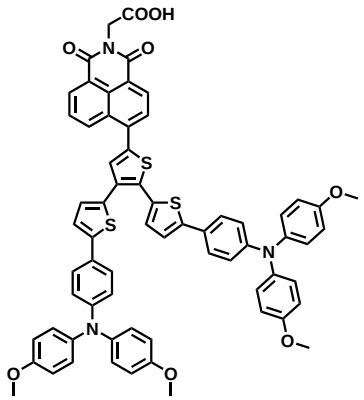

100 mg of *N*-(2,6-di*iso*propylphenyl)-1-(5,5"-bis[4-N,N-diphenylaniline]-[2,2':3',2"-terthiophene]-5'-yl)-naphthalene-4,5-dicarboximide (0.083 mmol) were dissolved in 7 mL of 2-methyl-2-butanol. 185 mg of potassium hydroxide (3.3 mmol) were added and the reaction mixture desoxygenated and refluxed under argon overnight. The reaction mixture was poured into an ice water/acetic acid mixture (10:2). The precipitate was filtered, washed with water and after drying dissolved in dichloromethane. 1-2 mL of acetic acid were added and the solution was stirred for 1-2 days. After removal of the dichloromethane under reduced pressure, methanol was added. The precipitate was filtered and washed with methanol. The compound was precipitated from tetrahydrofuran into methanol and used directrly for the next step.

Yield (crude): 80 mg orange-brown solid (92%)

80 mg of the crude anhydride (0.076 mmol), 1 g of glycine (13.4 mmol), and 2 g of imidazole (29.4 mmol) were mixed in a Schlenk tube and stirred under argon at 140°C overnight. After cooling down dilute hydrochloric acid (water:acid (5:1)) was added. The precipitate was filtered and washed with water. The crude product was purified by column chromatography on silica gel with dichloromethane, tetrahydrofuran, and acetic acid.

Yield: 77 mg orange-brown solid (91%)

^{1}H-NMR (300 MHz, THF, 298 K):
δ [ppm]: 8.85 (d, J = 8.5, 1H), 8.67 - 8.56 (m, 2H), 7.98 (d, J = 7.6, 1H), 7.95 - 7.85 (m, 1H), 7.59 (s, 1H), 7.39 (dd, J = 3.6, 8.6, 4H), 7.27 - 7.16 (m, 4H), 7.07 - 6.98 (m, 8H), 6.85 (dd, J = 2.3, 8.9, 12H), 4.84 (s, 2H), 3.75 (s, 12H).

^{13}C-NMR (75 MHz, THF, 298 K):
δ [ppm]: 169.3, 163.9, 163.6, 157.4, 157.3, 149.6, 149.4, 147.4, 145.9, 141.3, 141.2, 139.0, 138.8, 135.4, 134.3, 133.6, 132.8, 132.5, 132.3, 131.9, 131.2, 130.6, 130.2, 129.8, 129.2, 129.0, 128.3, 127.5, 127.4, 127.0, 126.9, 126.5, 123.8, 123.0, 122.8, 122.5, 120.9, 120.8, 115.4, 55.5.

IR spectrum (ATR):
ν_{max} [cm^{-1}] = 2930, 2832, 1702, 1665, 1587, 1501, 1460, 1373, 1312, 1235, 1178, 1032, 825, 781, 573.

UV-Vis spectrum (CH_2Cl_2):
λ_{max} [nm] (ϵ [M^{-1}cm^{-1}])= 378 (47,967).

High Resolution Mass (ESI):
$[M]^+$: calculated: 1107.2682, found: 1107.2720, discrepancy: 3.4 ppm.
The triphenylamine moiety is losing an electron to form $[M]^+$ as well as $[M+H]^+$.

8.2.3 SPC: Double Donor Systems

N-(2,6-Diisopropylphenyl)-1,2-bis(N,N-bis(4-(2,4,4-trimethylpentan-2-yl)phenyl)aniline)cyclopenta[c,d]-perylene-7,8-dicarboximide

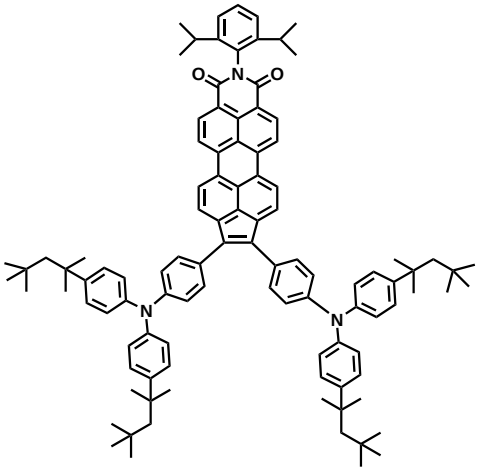

350 mg of *N*-(2,6-di*iso*propylphenyl)-1,2-bis(4-bromophenyl)cyclopenta[*c,d*]-perylene-7,8-dicarboximide (0.43 mmol), 439 mg of bis(p-2,4,4-trimethylpentane-2-yl-phenyl)amine (1.12 mmol), 107 mg of sodium *tert*-butoxide (1.12 mmol), 60 mg of tris(dibenzylideneacetone)dipalladium(0) (0.065 mmol) and 26 mg of tri-*tert*-butylphosphine (0.13 mmol) were dissolved in 20 mL of dry toluene under argon and stirred overnight at 80°C. The reaction mixture was purified via column chromatography on silica with first dichloromethane and petrol ether (2:1) and a subsequent gel permeation chromatography with dichloromethane. Main side product was the mono-substituted analogue.

Yield: 420 mg purple solid (68%)

^{1}H-NMR (250 MHz, THF, 298 K):
δ [ppm]: 8.77 (d, J = 8.1, 2H), 8.64 (d, J = 8.0, 2H), 8.57 (d, J = 7.7, 2H), 7.83 (d, J = 7.6, 2H), 7.45 - 7.26 (m, 16H), 7.11 - 7.01 (m, 11H), 2.92 - 2.72 (m, 2H), 1.75 (Überlagerung mit Lösungsmittelsignal, s, 8H), 1.39 (s, 24H), 1.14 (d, J = 6.8, 12H), 0.72 (s, 36H).

^{13}C-NMR (126 MHz, THF, 298 K):
δ [ppm]: 164.4, 148.6, 147.0, 146.0, 145.9, 143.1, 138.6, 137.2, 132.7, 132.4, 131.4, 130.8, 130.6, 129.9, 129.0, 128.1, 126.8, 125.7, 125.4, 125.2, 125.0, 124.5, 123.6, 123.4, 122.6, 101.1, 58.0, 39.2, 33.3, 32.4, 32.2, 30.8, 30.2, 24.4.

IR spectrum (ATR):

ν_{max} [cm^{-1}] = 2953, 2869, 1703, 1667, 1581, 1507, 1470, 1455, 1407, 1385, 1360, 1321, 1292, 1273, 1245, 1183, 1168, 1138, 1115, 1096, 1016, 990, 921, 829, 816, 800, 784, 753, 743.

UV-Vis spectrum (CH_2Cl_2):
λ_{max} [nm] (ϵ [$M^{-1}cm^{-1}$])= 520 (35,116).

High Resolution Mass (ESI):
$[M]^+$: calculated: 1439.9146, found: 1439.9164, discrepancy: 1.3 ppm.
The triphenylamine moiety is losing an electron to form $[M]^+$ as well as $[M+H]^+$.

N-Carboxymethyl-1,2-bis(N,N-bis(4-(2,4,4-trimethylpentan-2-yl)phenyl)aniline)cyclopenta[c,d]-perylene-7,8-dicarboximide

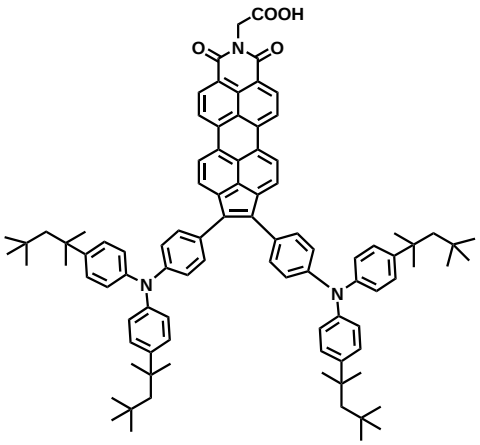

200 mg of *N*-(2,6-di*iso*propylphenyl)-1,2-bis(*N,N*-bis(4-(2,4,4-trimethylpentan-2-yl)-phenyl)aniline)cyclopenta[*c,d*]-perylene-7,8-dicarboximide were dissolved in 16 mL of 2-methyl-2-butanol and 8 mL of 1,4-dioxane. 310 mg of potassium hydroxide (5.55 mmol) were added, the reaction mixture desoxygenated and refluxed under argon overnight. The reaction mixture was poured into an ice water/acetic acid mixture (10:2). The precipitate was filtered, washed with water and after drying dissolved in dichloromethane. 1-2 mL of acetic acid were added and the solution was stirred for 1-2 days. After removal of the dichloromethane under reduced pressure, methanol was added. The precipitate was filtered and washed with methanol. The crude mixture was purfied by column chromatography on silica gel with dichloromethane petrol ether (2:1) and directly used for the next step.

Yield: 135 mg red solid (76%)

135 mg of 1,2-bis(*N,N*-bis(4-(2,4,4-trimethylpentan-2-yl)phenyl)aniline)cyclopenta-[*c,d*]-perylene-3,4-dicarboxylic acid monoanhydride (0.105 mmol), 1 g of glycine (0.013 mol) and 2 g of imidazole (0.029 mol) were mixed in a Schlenk tube and stirred under argon at 140°C overnight. After cooling down dilute hydrochloric acid was added. The brown precipitate was filtered and washed with water. The crude product was purified by column chromatography on silica gel with dichloromethane, tetrahydrofuran, and acetic acid.

Yield: 115 mg red solid (82%)

^{1}H-NMR (300 MHz, THF, 298 K):
δ [ppm]: 8.68 - 8.40 (m, 6H), 7.80 (d, J = 7.6, 2H), 7.46 - 7.19 (m, 12H), 7.11 - 6.93 (m, 12H), 4.87 - 4.80 (m, 2H), 1.78 (s, 8H, partially overlaid by solvent signal), 1.44 - 1.31 (m, J = 12.5, 24H), 0.83 - 0.72 (m, 36H).

^{13}C-NMR (126 MHz, THF, 298 K):
δ [ppm]: 163.5, 148.3, 146.1, 145.8, 145.7, 145.2, 142.5, 138.2, 136.2, 131.4, 130.3, 130.2, 129.93, 129.4, 129.0, 128.0, 127.8, 125.9, 125.3, 125.2, 124.6, 124.3, 124.0, 122.7, 122.5, 57.9, 57.8, 39.0, 38.87, 33.11, 33.04, 32.25, 32.16, 32.01..
Partial hydrogen bonding of the CH_2-group (adjacent to the imide nitrogen) to the neighbouring oxygen results in increased number of peaks in the proton- and carbon-NMR. Further details are explained in chapter 4.

IR spectrum (ATR):
ν_{max} [cm^{-1}] = 2951, 2902, 2871, 1699, 1663, 1583, 1506, 1481, 1365, 1321, 1289, 1245, 1187, 1016, 820, 804, 755.

UV-Vis spectrum (CH_2Cl_2):
λ_{max} [nm] (ϵ [$M^{-1}cm^{-1}$])= 519 (31,961).

High Resolution Mass (ESI):
$[M]^+$: calculated: 1337.7949, found: 1337.7897, discrepancy: -3.9 ppm.
The triphenylamine moiety is losing an electron to form $[M]^+$ as well as $[M+H]^+$.

N-(1'-Ethylpropyl)-8,11-bis(bis(9,9-dimethyl-9H-fluoren-2-yl)amino)perylene-3,4-dicarboximide;
N-(1'-Ethylpropyl)8-(bis(9,9-dimethyl-9H-fluoren-2-yl)amino)perylene-3,4-dicarboximide

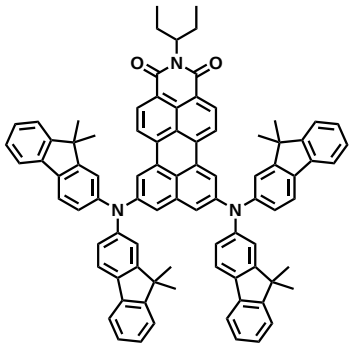

a

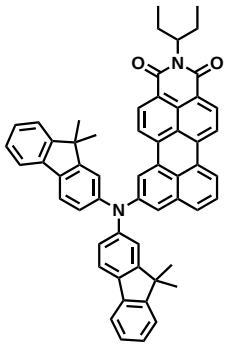

b

500 mg of *N*-(1'-ethylpropyl)-8,11-dichloro-perylene-3,4-dicarboximide (prepared by [redacted]; the procedure will be presented in his forthcoming thesis.) (1.09 mmol), 960 mg of bis-(9,9-dimethylfluorene-2-yl)-amine (2.39 mmol), 1.42 g caesium carbonate (4.34 mmol), 198 mg of tris(dibenzylideneacetone)dipalladium(0) (0.216 mmol), and 271 mg of 2,2'-bis(diphenylphosphino)-1,1'-binaphthyl (0.436 mmol) were dissolved in 30 mL of anhydrous toluene in a Schlenk tube and stirred under argon at 100°C for 16 h. Monofunctionalised (8-functionalised and 9-functionalised) and difunctionalised product (8,11-functionalised and 8,10-functionalised) was obtained. Only compound **a** (main difunctionalised product) and **b** were isolated and characterised. The reaction mixture was purified via gel permeation chromatography to seperate mono- and difunctionalised product with chloroform and via column chromatography with dichloromethane.

Yield (*compound a*; *compound b*): 50 mg brown solid (5 %); 115 mg brownish-red solid (15 %)

Compound a:

^{1}H-NMR (700 MHz, THF, 298 K):

δ [ppm]: 8.44 - 8.37 (m, 4H), 8.27 (d, J = 8.0, 2H), 7.68 (t, J = 8.5, 8H), 7.44 - 7.38 (m, 10H), 7.27 (t, J = 7.4, 4H), 7.24 - 7.18 (m, 8H), 5.06 - 4.97 (m, 1H), 2.29 - 2.18 (m, 2H), 1.89 - 1.76 (m, 2H), 1.40 (s, 24H), 0.85 (t, J = 7.4, 6H).

^{13}C-NMR (176 MHz, THF, 298 K):

δ [ppm]: 156.4, 154.6, 148.6, 148.1, 139.0, 138.8, 137.3, 136.1, 131.4, 131.0, 128.0,

127.8, 127.7, 124.5, 123.4, 122.6, 122.1, 121.9, 121.7, 120.5, 120.4, 120.0, 57.8, 47.8, 27.5, 11.8.

UV-Vis spectrum (CH_2Cl_2):
λ_{max} [nm] (ϵ [$M^{-1}cm^{-1}$])= 486 (25,828), 563 (13,369).

IR spectrum (ATR):
ν_{max} [cm^{-1}] = 3059, 3013, 2957, 2924, 2859, 1694, 1654, 1591, 1459, 1363, 1349, 1298, 1278, 1245, 1200, 1086, 826, 753, 733.

High Resolution Mass (ESI):
$[M]^+$: calculated: 1189.5546, found: 1189.5527, discrepancy: -1.6 ppm.
The triphenylamine moiety is losing an electron to form $[M]^+$ as well as $[M+H]^+$.

Compound b:
^{1}H-NMR (300 MHz, CD_2Cl_2, 298 K):
δ [ppm]: 8.48 (d, J = 8.0, 1H), 8.42 (d, J = 2.1, 1H), 8.38 - 8.30 (m, 2H), 8.22 (d, J = 7.1, 1H), 8.06 (d, J = 8.2, 1H), 7.77 - 7.67 (m, 4H), 7.62 (d, J = 8.0, 1H), 7.57 (d, J = 1.9, 1H), 7.50 (d, J = 7.7, 1H), 7.48 - 7.40 (m, 4H), 7.39 - 7.22 (m, 6H), 5.11 - 4.95 (m, 1H), 2.33 - 2.15 (m, 2H), 1.97 - 1.83 (m, 2H), 1.45 (s, 12H), 0.89 (t, J = 7.5, 6H).

^{13}C-NMR (75 MHz, CD_2Cl_2, 298 K):
δ [ppm]: 156.0, 154.3, 147.4, 147.4, 139.4, 137.2, 137.0, 136.4, 135.5, 130.8, 130.5, 130.1, 129.6, 128.0, 127.7, 127.4, 127.2, 124.9, 124.2, 123.2, 122.6, 122.4, 121.5, 120.8, 120.1, 119.7, 57.7, 47.5, 27.4, 25.6, 11.7.

UV-Vis spectrum (CH_2Cl_2):
λ_{max} [nm] (ϵ [$M^{-1}cm^{-1}$])= 477 (23,629).

IR spectrum (ATR):
ν_{max} [cm^{-1}] = 3057, 2958, 2925, 2871, 1691, 1652, 1591, 1447, 1349, 1295, 1247, 1199, 1085, 852, 798, 752, 735.

High Resolution Mass (ESI):
$[M]^+$: calculated: 790.3559, found: 790.3535, discrepancy: -3.1 ppm.
The triphenylamine moiety is losing an electron to form $[M]^+$ as well as $[M+H]^+$.

N-Carboxymethyl-8,11-bis(bis(9,9-dimethyl-9H-fluoren-2-yl)amino)perylene-3,4-dicarboximide

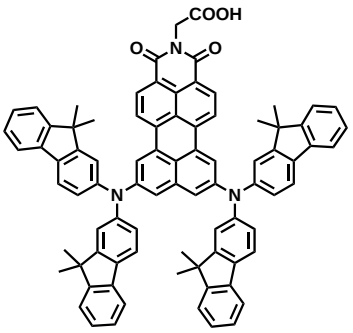

50 mg of *N*-(1'-ethylpropyl)-8,11-bis(bis(9,9-dimethyl-9*H*-fluoren-2-yl)amino)perylene-3,4-dicarboximide (0.042 mmol) were dissolved in 4 mL of 2-methyl-2-butanol and 2 mL of 1,4-dioxane. 95 mg of potassium hydroxide (1.68 mmol) were added, the reaction mixture desoxygenated and refluxed under argon overnight. The reaction mixture was poured into an ice water/acetic acid mixture (10:2). The precipitate was filtered, washed with water and after drying dissolved in dichloromethane. 1-2 mL of acetic acid were added and the solution was stirred for 1-2 days. After removal of the dichloromethane under reduced pressure, methanol was added. The precipitate was filtered and washed with methanol. The crude mixture was used directly for the next step.

Yield (crude): 45 mg red solid (94%)

45 mg of 8,11-bis(bis(9,9-dimethyl-9*H*-fluoren-2-yl)amino)perylene-3,4-dicarboxylic acid monoanhydride (0.036 mmol), 1 g of glycine (0.013 mol) and 2 g of imidazole (0.029 mol) were mixed in a Schlenk tube and stirred under argon at 140°C overnight. After cooling down dilute hydrochloric acid was added. The brown precipitate was filtered and washed with water. The crude product was purified by column chromatography on silica gel with dichloromethane, tetrahydrofuran, and acetic acid.

Yield: 40 mg red solid (85%)

^{1}H-NMR (300 MHz, THF, 298 K):
δ [ppm]: 8.35 - 8.26 (m, 4H), 8.18 (d, J = 8.2, 2H), 7.61 - 7.53 (m, 8H), 7.33 - 7.26 (m, 10H), 7.19 - 7.06 (m, 12H), 4.68 (s, 2H), 1.29 (s, 24H).

^{13}C-NMR (176 MHz, THF, 298 K):
δ [ppm]: 169.8, 164.0, 156.6, 154.9, 148.9, 148.4, 140.2, 139.0, 137.9, 136.4, 132.5, 131.5, 131.2, 128.2, 128.1, 127.9, 124.8, 123.7, 123.1, 122.5, 122.3, 122.1, 122.0, 121.0, 120.7, 120.3, 48.1, 27.7, 26.2, 26.1.

UV-Vis spectrum (CH_2Cl_2):
λ_{max} [nm] (ϵ [$M^{-1}cm^{-1}$])= 477 (24,517), 574 (11,904).

IR spectrum (ATR):
ν_{max} [cm^{-1}] = 3040, 2956, 2924, 2860, 1693, 1656, 1590, 1486, 1448, 1368, 1298, 1249, 1135, 1080, 1015, 966, 824, 777, 755, 734.

High Resolution Mass (ESI):
$[M]^+$: calculated: 1177.4819, found: 1177.4797, discrepancy: -1.8 ppm.
The triphenylamine moiety is losing an electron to form $[M]^+$ as well as $[M+H]^+$.

N-Carboxymethyl-8-(bis(9,9-dimethyl-9H-fluoren-2-yl)amino)perylene-3,4-dicarboximide

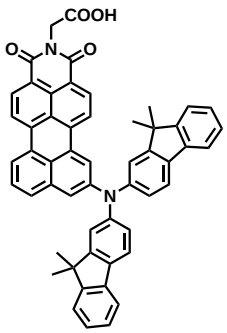

96 mg of *N*-(1'-ethylpropyl)-8-(bis(9,9-dimethyl-9*H*-fluoren-2-yl)amino)perylene-3,4-dicarboximide (0.122 mmol) were dissolved in 6 mL of 2-methyl-2-butanol and 3 mL of 1,4-dioxane. 255 mg of potassium hydroxide (4.55 mmol) were added, the reaction mixture desoxygenated and refluxed under argon overnight. The reaction mixture was poured into an ice water/acetic acid mixture (10:2). The precipitate was filtered, washed with water and after drying dissolved in dichloromethane. 1-2 mL of acetic acid were added and the solution was stirred for 1-2 days. After removal of the dichloromethane under reduced pressure, methanol was added. The precipitate was filtered and washed with methanol. The crude mixture was used directly for the next step.

Yield (crude): 85 mg red solid (96%)

85 mg of 8-(bis(9,9-dimethyl-9*H*-fluoren-2-yl)amino)perylene-3,4-dicarboxy monoanhydride (0.036 mmol), 1 g of glycine (0.013 mol) and 2 g of imidazole (0.029 mol) were mixed in a Schlenk tube and stirred under argon at 140°C overnight. After cooling down dilute hydrochloric acid was added. The precipitate was filtered and washed with water. The crude product was purified by column chromatography on silica gel with dichloromethane, tetrahydrofuran, and acetic acid.

Yield: 80 mg red solid (87%)

^{1}H-NMR (300 MHz, THF, 298 K):
δ [ppm]: 8.66 - 8.39 (m, 5H), 8.29 (d, J = 8.2, 1H), 7.77 - 7.68 (m, 5H), 7.61 (d, J = 1.8, 1H), 7.56 (t, J = 7.9, 1H), 7.49 - 7.39 (m, 4H), 7.34 - 7.18 (m, 6H), 4.81 (s, 2H), 1.43 (s, 12H).

^{13}C-NMR (126 MHz, $C_2Cl_4D_2$, 393 K):
δ [ppm]: 155.6, 153.8, 146.6, 138.6, 137.8, 135.3, 131.7, 129.9, 127.4, 126.9, 126.8, 123.7, 122.3, 122.1, 121.7, 120.9, 120.8, 120.2, 120.2, 119.5, 119.1, 46.8, 40.5, 26.9.

UV-Vis spectrum (CH_2Cl_2):
λ_{max} [nm] (ϵ [$M^{-1}cm^{-1}$])= 484 (26,991).

IR spectrum (ATR):
ν_{max} [cm^{-1}] = 3630, 3499, 3058, 2957, 2923, 2860, 1750, 1691, 1651, 1591, 1570, 1448, 1407, 1370, 1292, 1247, 1172, 1073, 1020, 970, 853, 799, 755, 736.

High Resolution Mass (ESI):
$[M]^+$: calculated: 778.2832, found: 778.2836, discrepancy: 0.6 ppm.
The triphenylamine moiety is losing an electron to form $[M]^+$ as well as $[M+H]^+$.

N-(1'-Ethylpropyl)-9-(bis(4-(2,4,4-trimethylpentane-2-yl)phenyl)amino-perylene-3,4-dicarboximide

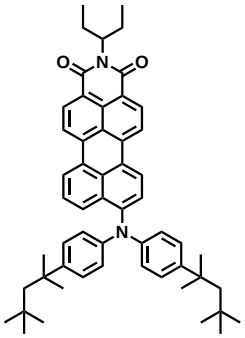

1.4 g of 9-(bis(4-(2,4,4-trimethylpentane-2-yl)phenyl)amino-perylene-3,4-dicarboxy anhydride (synthesis according to the procedure presented in the thesis of Chen Li [87], 684 mg of pentan-3-amine (7.86 mol) and 20 g of imidazole (0.29 mol) were mixed in a Schlenk tube and stirred under argon at 140°C overnight. After cooling down dilute hydrochloric acid was added. The blue precipitate was filtered and washed with water. The crude product was purified by column chromatography on silica gel with dichloromethane and petrol ether (3:2).

Yield: 1.4 g blue solid (91%)

^{1}H-NMR (300 MHz, THF, 298 K):
δ [ppm]: 8.51 - 8.36 (m, 6H), 7.88 (d, J = 8.4, 1H), 7.38 - 7.12 (m, 6H), 6.87 (d, J = 8.6, 4H), 5.05 - 4.88 (m, 1H), 2.29 - 2.07 (m, 2H), 1.88 - 1.69 (m, 2H), 1.33 - 1.16 (m, 12H), 0.78 (t, J = 7.4, 6H), 0.66 (s, 18H).

^{13}C-NMR (75 MHz, THF, 298 K):
δ [ppm]: 147.30, 146.07, 144.01, 136.81, 136.72, 131.00, 129.97, 129.86, 129.82, 127.51, 127.01, 126.49, 126.38, 126.30, 126.20, 124.65, 123.94, 122.31, 120.13, 119.77, 56.85, 56.64, 37.88, 32.07, 31.21, 30.97, 10.66.

IR spectrum (ATR):
ν_{max} [cm^{-1}] = 3034, 2953, 2874, 2691, 1652, 1593, 1566, 1500, 1457, 1349, 1268, 1246, 1197, 1085, 808, 751.

UV-Vis spectrum (CH_2Cl_2):
λ_{max} [nm] (ϵ [M^{-1}cm^{-1}])= 578 (30,907).

High Resolution Mass (ESI):

$[M]^+$: calculated: 782.481, found: 782.4789, discrepancy: -2.8 ppm.
The triphenylamine moiety is losing an electron to form $[M]^+$ as well as $[M+H]^+$.

Elemental analysis ($C_{55}H_{62}N_2O_2$):
calculated: 84.36% C, 7.98% H, 3.58% N, –% S
found: 84.25% C, 7.62% H, 3.75% N, –% S

N-(1'-Ethylpropyl)-8,10-bis(bis(4-(2,4,4-trimethylpentane-2-yl)phenyl)amino)perylene-3,4-dicarboximide

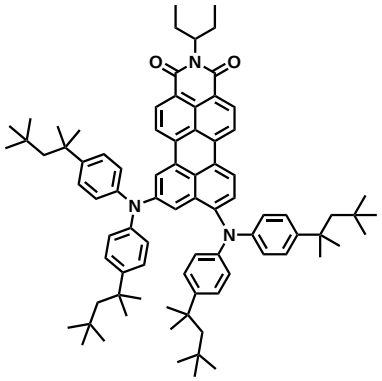

Method a:
80 mg of *N*-(1'-ethylpropyl)-8,11-dichloro-perylene-3,4-dicarboximide (prepared by [redacted]; the procedure will be presented in his forthcoming thesis.) (0.174 mmol), 960 mg of bis-(4-(2,4,4-trimethylpentane-2-yl)phenyl)-amine (0.431 mmol), 1.42 g of caesium carbonate (0.521 mmol), 20 mg of tris(dibenzylideneacetone)dipalladium(0) (0.022 mmol), and 27 mg of 2,2'-bis(diphenylphosphino)-1,1'-binaphthyl (0.0436 mmol) were dissolved in 5 mL of anhydrous toluene in a Schlenk tube and stirred under argon at 100°C for 16 h. Monofunctionalised (8-functionalised and 9-functionalised) and difunctionalised product (8,11-functionalised and 8,10-functinoalised) was obtained. Only compound **a** was isolated and characterised. The reaction mixture was purified via gel permeation chromatography to seperate mono- and difunctionalised product with chloroform and via column chromatography with dichloromethane and petrol ether (1:2).

Because of the many byproducts and only low yield (less than 5%) of the desired 8,10-functionalised product a second synthesis route was pursued (see method b). *Further details are discussed in chapter 4*

Method b:
1 g of *N*-(1'-ethylpropyl)-9-(bis(4-(2,4,4-trimethylpentane-2-yl)phenyl)amino-perylene-3,4-dicarboximide (2.28 mmol) and 360 mg of 4,4,4',4',5,5,5',5'-octamethyl-2,2'-bi(1,3,2-dioxaborolane) (1.40 mmol), 42 mg of bis(1,5-cyclooctadiene)dimethoxydiiridium (0.065 mmol), and 34 mg of 4,4'-di-*tert*-butyl-2,2'-bipyridyl (0.119 mmol) were dissolved in 70 mL of dry tetrahydrofuran under argon and stirred overnight at 60°C, however not leading to full conversion of the starting material. Both starting material and product show similar intensities on a silica thin layer chromatography plate in dichloromethane.
The solvent was removed under reduced pressure, the reaction mixture solved in dichloromethane, washed with water and dried over magnesium sulfate. It was then used without further purification for the next step.

900 mg of the mixture of *N*-(1'-ethylpropyl)-8-(4,4,5,5-tetramethyl-[1,3,2]dioxaborolan-2-yl)-10-(bis(4-(2,4,4-trimethylpentane-2-yl)phenyl)amino-perylene-3,4-dicarboximide and *N*-(1'-ethylpropyl)-9-(bis(4-(2,4,4-trimethylpentane-2-yl)phenyl)amino-perylene-3,4-dicarboximide were dissolved in 16 mL of 1,4-dioxane, 2 mL of methanol and 2 mL of water in a pressure vial. 1.1 g of copper(II)bromide (4.95 mmol) were added and the mixture was stirred overnight at 120°C.
After cooling down, the reaction mixture was roughly purified via column chromatography on silica gel with dichloromethane giving a mixture of *N*-(1'-ethylpropyl)-8-bromo-10-(bis(4-(2,4,4-trimethylpentane-2-yl)phenyl)amino-perylene-3,4-dicarboximide and *N*-(1'-ethylpropyl)-9-(bis(4-(2,4,4-trimethylpentane-2-yl)phenyl)amino-perylene-3,4-dicarboximide which was used directly for the next step.

365 mg of the mixture (approximately 2:1) of *N*-(1'-ethylpropyl)-8-bromo-10-(bis(4-(2,4,4-trimethylpentane-2-yl)phenyl)amino-perylene-3,4-dicarboximide and *N*-(1'-ethylpropyl)-9-(bis(4-(2,4,4-trimethylpentane-2-yl)phenyl)amino-perylene-3,4-dicarboximide, 65 mg of bis-(4-(2,4,4-trimethylpentane-2-yl)phenyl)-amine (0.165 mmol), 15 mg of sodium *tert*-butoxide (0.156 mmol), 21 mg of tris(dibenzylidenacetone)dipalladium(0) (0.023 mmol), and 10 mg of tri-*tert*-butylphosphine (0.050 mmol) were dissolved in 7 mL of dry toluene under argon and stirred at 80°C overnight. The reaction mixture was purified via silica column chromatography with dichloromethane and petrol ether (2:1).

Yield: 115 mg dark green solid (approx. 30 % regarding the starting material mixture)

^{1}H-NMR (700 MHz, CD_2Cl_2, 298 K):

δ [ppm]: 8.43 (d, J = 7.5, 1H), 8.30 - 8.25 (m, 2H), 8.14 (d, J = 8.2, 1H), 7.99 (d, J = 1.6, 1H), 7.82 (d, J = 8.1, 1H), 7.62 (d, J = 1.5, 1H), 7.21 - 7.15 (m, 5H), 7.11 (d, J = 8.7, 4H), 6.87 (d, J = 8.5, 4H), 6.71 (d, J = 8.6, 4H), 5.00 - 4.89 (m, 1H), 2.18 - 2.10 (m, 2H), 1.83 - 1.76 (m, 2H), 1.67 (s, 4H), 1.63 (s, 4H), 1.29 (s, 12H), 1.27 (s, 12H), 0.80 (t, J = 7.4, 6H), 0.70 (s, 18H), 0.66 (s, 18H).

^{13}C-NMR (126 MHz, CD_2Cl_2, 298 K):
δ [ppm]: 147.3, 146.7, 146.6, 146.2, 144.6, 144.3, 137.5, 137.4, 133.6, 132.1, 130.7, 130.6, 129.0, 128.1, 127.0, 127.4, 127.0, 126.7, 125.5, 122.56, 122.42, 120.48, 120.39, 119.64, 115.26, 57.61, 57.48, 57.42, 38.79, 38.61, 32.86, 32.81, 32.16, 32.14, 31.0, 31.9, 30.3, 25.6, 11.7, 1.3.

IR spectrum (ATR):
ν_{max} [cm^{-1}] = 2954, 2873, 1692, 1654, 1593, 1564, 1507, 1461, 1351, 1254, 1085, 1015, 805, 752.

UV-Vis spectrum (CH_2Cl_2):
λ_{max} [nm] (ϵ [$M^{-1}cm^{-1}$])= 612 (18,891).

High Resolution Mass (ESI):
$[M]^+$: calculated: 1173.8050, found: 1173.8015, discrepancy: -3.0 ppm.
The triphenylamine moiety is losing an electron to form $[M]^+$ as well as $[M+H]^+$.

N-Carboxymethyl-8,10-bis(bis(4-(2,4,4-trimethylpentane-2-yl)phenyl)amino)perylene-3,4-dicarboximide

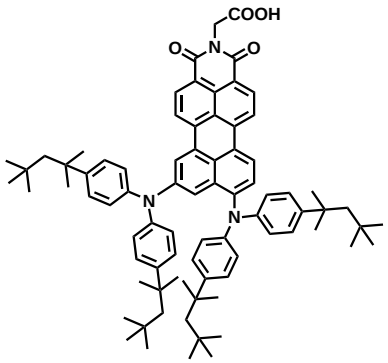

115 mg of *N*-(1'-ethylpropyl)-8,10-bis(bis(4-(2,4,4-trimethylpentane-2-yl)phenyl)amino)perylene-3,4-dicarboximide (0.097 mmol) were dissolved in 8 mL of 2-methyl-2-butanol and 4 mL of 1,4-dioxane. 219 mg of potassium hydroxide (3.92 mmol) were added, the reaction mixture desoxygenated and refluxed under argon overnight. The

reaction mixture was poured into an ice water/acetic acid mixture (10:2). The precipitate was filtered, washed with water and after drying dissolved in dichloromethane. 1-2 mL of acetic acid were added and the solution was stirred for 1-2 days. After removal of the dichloromethane under reduced pressure, methanol was added. The precipitate was filtered and washed with methanol. The crude mixture was used directly for the next step.

Yield (crude): 100 mg dark green solid (93%)

100 mg of 8,10-bis(bis(4-(2,4,4-trimethylpentane-2-yl)phenyl)amino)perylene-3,4-dicarboxy acid monoanhydride (0.094 mmol), 2 g of glycine (0.026 mol) and 3 g of imidazole (0.044 mol) were mixed in a Schlenk tube and stirred under argon at 140°C overnight. After cooling down dilute hydrochloric acid was added. The brown precipitate was filtered and washed with water. The crude product was purified by column chromatography on silica gel with dichloromethane, tetrahydrofuran, and acetic acid.

Yield: 95 mg dark green solid (90%)

^{1}H-NMR (500 MHz, THF, 298 K):
δ [ppm]: 8.47 (s, 2H), 8.38 - 8.30 (m, 2H), 8.15 (d, J = 1.7, 1H), 7.97 (d, J = 8.1, 1H), 7.78 (d, J = 1.7, 1H), 7.33 - 7.20 (m, 9H), 6.96 (d, J = 8.4, 4H), 6.83 (d, J = 8.5, 4H), 4.78 (s, 2H), 1.77 (d, J = 18.4, 8H, partially overlaid by solvent signal), 1.38 (d, J = 7.9, 24H), 0.78 (d, J = 15.2, 36H).

^{13}C-NMR (126 MHz, THF, 298 K):
δ [ppm]: 163.7, 147.3, 147.0, 146.6, 145.2, 144.8, 138.0, 132.3, 131.8, 131.4, 131.0, 128.6, 128.4, 127.9, 127.6, 127.3, 126.3, 125.8, 123.7, 123.1, 122.0, 121.3, 121.1, 120.9, 58.0, 57.9, 39.2, 39.0, 33.3, 33.2, 32.5, 32.23.

IR spectrum (ATR):
ν_{max} [cm^{-1}] = 2951, 2901, 2871, 1697, 1662, 1593, 1561, 1506, 1365, 1250, 1172, 1132, 1013, 821, 755.

UV-Vis spectrum (CH_2Cl_2):
λ_{max} [nm] (ϵ [M^{-1}cm^{-1}])= 631 (20,194).

High Resolution Mass (ESI):

$[M]^+$: calculated: 1161.7323, found: 1161.7336, discrepancy: 1.2 ppm.
The triphenylamine moiety is losing an electron to form $[M]^+$ as well as $[M+H]^+$.

8.2.4 SPC: Enlargement of the Perylene-pi-System: Cadogan Chemistry Towards a Novel Class of Chromophores

N-(2,6-Diisopropylphenyl)-9-(2-nitrophenyl)-3,4-perylene dicarboximide

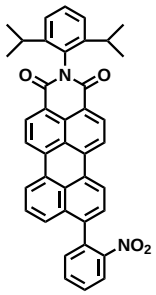

1.2 g of *N*-(2,6-di*iso*propylphenyl)-9-(4,4,5,5-tetramethyl-1,3,2-dioxaborolane-2-yl)-3,4-perylene dicarboximide (1.98 mmol), 598 mg of 1-bromo-2-nitrobenzene (2.96 mmol) were dissolved in 80 mL of toluene in a Schlenk tube. 1.6g of potassium carbonate (11.59 mmol) in 8 mL of water and 0.8 mL of ethanol were added. The solution was purged with argon for 30 minutes. After addition of 330 mg tetrakis(triphenylphosphine)palladium(0) (0.296 mmol) the solution was again purged for 30 minutes with argon. The solution was stirred at 80°C for 24 h. The reaction mixture was cooled down, washed with water and extracted with dichloromethane. The reaction mixture was purified via column chromatography on silica gel with dichloromethane.

Yield: 850 mg (70%) red solid.

^{1}H-NMR (250 MHz, THF, 289 K):
δ [ppm]: 8.83 - 8.59 (m, 6H), 8.25 (m, J = 1H), 7.84 (m, J = 2H), 7.70 - 7.56 (m, 4H), 7.49 - 7.39 (m, 1H), 7.38 - 7.29 (m, 2H), 2.84 (m, J = 2H), 1.18 (m, J = 12H).

^{13}C-NMR (176 MHz, THF, 289 K):
δ [ppm]: 164.4, 150.8, 147.0, 146.8, 139.9, 138.3, 138.1, 135.4, 133.9, 132.7, 132.5, 131.4, 130.7, 130.5, 130.4, 129.7, 129.1, 128.9, 128.5, 128.4, 127.9, 125.5, 125.2, 124.6, 124.4, 124.3, 122.5, 121.8, 121.7, 30.0, 24.4.

IR spectrum (ATR):
ν_{max} [cm^{-1}] = 2961, 2869, 1700, 1661, 1591, 1577, 1526, 1468, 1409, 1356, 1293, 1244, 1197, 1179, 1135, 1029, 932, 901, 855, 839, 810, 786.

UV-Vis spectrum (hDCM):
λ_{max} [nm] (ϵ [$M^{-1}cm^{-1}$])= 490 (36,354), 514 (38,860).

High Resolution Mass (ESI):
$[M+Na]^+$: calculated: 625.2103, found: 625.2115, discrepancy: 1.9 ppm.

N-(2,6-Diisopropylphenyl)-8,9-([b]-1-hexyl-1H-indole)-3,4-perylene dicarboximide

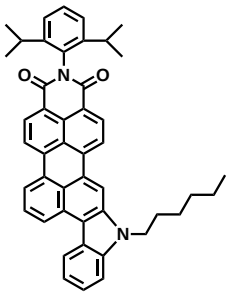

500 mg of *N*-(2,6-di*iso*propylphenyl)-9-(2-nitrobenzyl)-3,4-perylene dicarboximide (0.830 mmol) and 650 mg of triphenylphoshine (2.48 mmol) were dissolved in 15 mL of *o*-dichlorobenzene and stirred at 182 °C and 300 W in the microwave (CEM, DISCOVER-S with external pressurised air cooling) for 8h. The resulting precipitate was used without further purification for the next step.

Yield (crude): 320 mg purple solid (68%)

210 mg of *N*-(2,6-di*iso*propylphenyl)-8,9-([*b*]-1*H*-indole)-3,4-perylene dicarboximide (0.368 mmol) and 12 mg of sodium hydride (0.478 mmol) were mixed in a Schlenk tube. 15 mL of anhydrous dimethylformamide were added under argon. The solution was stirred for 30 minutes at room temperature. After a visible colour change from violet to blue, 122 mg of bromohexane (0.736 mmol) were added and the solution was stirred for another 3 h changing colour back to violet. After quenching the reaction with water, the solution was washed with water and hydrochloric acid (3:1), extracted with dichloromethaneand dried over magnesium sulfate. The crude product was purified via column chromatography on silica with dichloromethane.

Yield: 128 mg purple solid (53%)

^{1}H-NMR (250 MHz, THF, 298 K):
δ [ppm]: 8.96 (d, J = 8.2, 1H), 8.87 (s, 1H), 8.79 (d, J = 8.1, 1H), 8.73 - 8.54 (m, 5H), 7.87 (t, J = 7.9, 1H), 7.67 (d, J = 8.3, 1H), 7.52 (t, J = 7.7, 1H), 7.45 - 7.25 (m, 4H), 4.66 (t, J = 7.0, 2H), 2.91 - 2.72 (m, 2H), 2.07 - 1.89 (m, 2H), 1.55 - 1.24 (m, 6H), 1.16 (d, J = 6.8, 12H), 0.87 (t, J = 6.9, 3H).

^{13}C-NMR (126 MHz, THF, 323 K):
δ [ppm]: 164.4, 147.0, 142.1, 139.5, 139.3, 139.0, 133.0, 132.3, 132.2, 131.8, 131.6, 130.8, 129.5, 128.5, 128.2, 127.9, 127.0, 126.4, 124.3, 124.0, 123.3, 122.2, 122.1, 121.9, 121.4, 121.2, 121.1, 118.7, 110.7, 109.6, 43.5, 32.5, 30.4, 30.0, 27.7, 24.6, 23.4, 14.2.

IR spectrum (ATR):
ν_{max} [cm^{-1}] = 2961, 2926, 2867, 1693, 1654, 1593, 1575, 1570, 1465, 1354, 1284, 1245, 1196, 1176, 803, 2, 744, 730.

UV-Vis spectrum (CH_2Cl_2):
λ_{max} [nm] (ϵ [M^{-1}cm^{-1}])= 560 (35,792).

FD-MS-Spektrum (8 kV):
m/z = 654.5, calculated: 654.32

High Resolution Mass (ESI):
[M+H]$^{+}$: calculated: 655.3325, found: 655.3308, discrepancy: -2.5 ppm.

N-Carboxymethyl-8,9-([b]-1-hexyl-1H-indole)-3,4-perylene dicarboximide

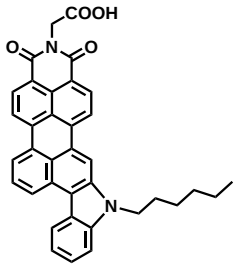

110 mg of *N*-(2,6-di*iso*propylphenyl)-8,9-([*b*]-1-hexyl-1*H*-indole)-3,4-perylene dicarboximide(0.168 mmol) were dissolved in 10 mL of 2-methyl-2-butanol. 375 mg potassium hydroxide (6.7 mmol) were added, the reaction mixture desoxygenated and refluxed under argon overnight. The reaction mixture was poured into an ice

water/acetic acid mixture (10:2). The precipitate was filtered, washed with water and after drying dissolved in dichloromethane. 1-2 mL of acetic acid were added and the solution was stirred for 1-2 days. After removal of the dichloromethane under reduced pressure, methanol was added. The precipitate was filtered and washed with methanol. The formed anhydride was used directly for the next step without further purification.

Yield (crude): 80 mg purple solid (96%)

80 mg of the crude anhydride (0.104 mmol), 1 g of glycine (13.4 mmol) and 2 g of imidazole (29.4 mmol) were mixed in a Schlenk tube and stirred under argon at 140°C overnight. After cooling down dilute hydrochloric acid (water:acid (5:1)) was added. The precipitate was filtered and washed with water. The crude product was purified by column chromatography on silica gel with tetrahydrofuran, and tetrahydrofuran:acetic acid (1:1).

Yield[10]: 50 mg (56%) purple solid.

^{1}H-NMR (300 MHz, THF, 298 K):
δ [ppm]: 8.84 (d, J = 8.1, 1H), 8.62 (s, 1H), 8.55 (d, J = 8.3, 2H), 8.50 - 8.36 (m, 4H), 7.77 (t, J = 7.9, 1H), 7.64 (d, J = 8.1, 1H), 7.52 (t, J = 7.2, 1H), 7.36 (t, J = 7.1, 1H), 5.51 (s, 2H), 4.56 (t, J = 7.2, 2H), 2.01 - 1.91 (m, 2H), 1.53 - 1.25 (m, 6H), 0.87 (t, J = 7.1, 3H).

IR spectrum (ATR):
ν_{max} [cm^{-1}] = 3223, 2927, 2856, 1736, 1688, 1649, 1593, 1573, 1366, 1327, 1285, 804, 746, 732.

UV-Vis spectrum (THF):
λ_{max} [nm] (ϵ [M^{-1}cm^{-1}])= 552 (31,469).

High Resolution Mass (ESI):
[M+H]$^+$: calculated: 553.2127, found: 553.2133, discrepancy: 1.0 ppm.

[10]The rather low yield for this step is not due to low conversion but difficult purification as the product not only shows strong interaction with silica gel but is moreover only poorly soluble.

N-(2,6-Diisopropylphenyl)-9-(4-chloro-2-nitrophenyl)-3,4-perylene dicarboximide

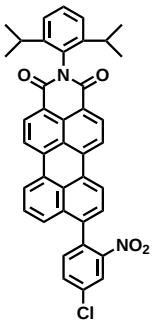

1.2 g of *N*-(2,6-di*iso*propylphenyl)-9-(4,4,5,5-tetramethyl-1,3,2-dioxaborolane-2-yl)-3,4-perylene dicarboximide (1.98 mmol), 700 mg of 1-bromo-4-chloro-2-nitrobenzene (2.96 mmol) were dissolved in 80 mL of toluene in a Schlenk tube. 1.6 g of potassium carbonate (11.59 mmol) dissolved in 8 mL of water and 0.8 mL of ethanol were added. The solution was purged with argon for 30 minutes. After addition of 330 mg tetrakis(triphenylphosphine)palladium(0) (0.296 mmol) the solution was again purged for 30 minutes with argon. The solution was stirred at 80°C for 36h. The reaction was cooled down, washed with water and extracted with dichloromethane. The reaction mixture was purified via column chromatography on silica gel with dichloromethane.

Yield: 1.0 g (79%) red solid

^{1}H-NMR (300 MHz, THF, 298 K):
δ [ppm]: 8.72 - 8.57 (m, 6H), 8.31 (d, J = 2.1, 1H), 7.90 (dd, J = 2.2, 8.2, 1H), 7.67 - 7.54 (m, 4H), 7.44 - 7.36 (m, 1H), 7.34 - 7.24 (m, 2H), 2.90 - 2.70 (m, 2H), 1.15 (t, J = 6.6, 12H).

^{13}C-NMR (176 MHz, THF, 298 K):
δ [ppm]: 164.4, 151.3, 147.1, 146.9, 138.7, 138.2, 137.9, 135.8, 135.4, 134.1, 134.1, 133.7, 132.8, 132.6, 132.5, 131.4, 130.8, 129.8, 129.2, 128.7, 128.6, 127.9, 125.7, 125.4, 124.6, 124.5, 122.7, 122.6, 121.9, 30.2, 24.5.

IR spectrum (ATR):
ν_{max} [cm^{-1}] = 3061, 2968, 2928, 2861, 1695, 1660, 1593, 1580, 1526, 1468, 1348, 1246, 836, 809, 747.

UV-Vis spectrum (CH_2Cl_2):
λ_{max} [nm] (ϵ [M^{-1}cm^{-1}])= 512 (38,386).

High Resolution Mass (ESI):
$[M+H]^+$: calculated: 637.1894, found: 637.1884, discrepancy: -1.6 ppm.

Elemental analysis ($C_{40}H_{29}ClN_2O_4$):
calculated: 75.41% C, 4.59% H, 4.40% N, –% S
found: 74.61% C, 4.76% H, 4.28% N, –% S

N-(2,6-Diisopropylphenyl)-9-(4-(bis-(9,9-dimethylfluoren-2-yl)-amin)-2-nitrophenyl)-3,4-perylene dicarboximide

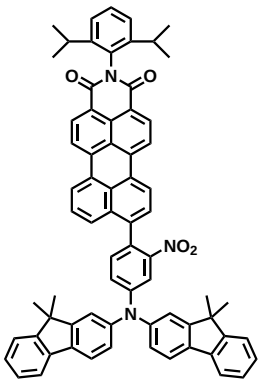

750 mg *N*-(2,6-di*iso*propylphenyl))-9-(4-chloro-2-nitrobenzyl)-3,4-perylene dicarboximide (1.18 mmol), 700 mg of bis-(9,9-dimethylfluorene-2-yl)-amine (1.75 mmol), 760 mg of caesium carbonate (2.33 mmol), 110 mg of tris(dibenzylideneacetone)dipalladium(0) (0.120 mmol), and 145 mg of 2,2´-bis(diphenylphosphino)-1,1´-binaphthyl (0.228 mmol) were dissolved in 30 mL of anhydrous toluene in a Schlenk tube and stirred under argon at 100°C for 16 h. The reaction mixture was purified via column chromatography with dichloromethane.

Yield: 770 mg red solid (65%)

^{1}H-NMR (500 MHz, THF, 298 K):
δ [ppm]: 8.73 - 8.65 (m, 4H), 8.60 (dd, J = 1.2, 8.0, 2H), 7.87 (d, J = 2.4, 1H), 7.80 (d, J = 8.2, 2H), 7.74 (dd, J = 3.5, 7.8, 3H), 7.64 (t, J = 7.9, 1H), 7.59 (d, J = 7.8, 1H), 7.52 - 7.36 (m, 7H), 7.34 - 7.24 (m, 8H), 2.87 - 2.72 (m, 2H), 1.46 (s, 12H), 1.14 (dd, J = 6.9, 9.1, 12H).

^{13}C-NMR (126 MHz, THF, 298 K):
δ [ppm]: 163.3, 155.6, 153.6, 150.5, 149.1, 146.0, 145.8, 139.1, 138.6, 137.3, 137.1, 136.2, 133.4, 133.0, 131.7, 131.4, 130.4, 129.7, 129.1, 128.1, 128.0, 127.7, 127.3, 126.9,

125.7, 124.4, 124.2, 123.7, 123.3, 122.4, 121.4, 121.0, 120.7, 120.6, 119.9, 119.5, 115.6, 46.8, 29.0, 26.3, 23.3.

IR spectrum (ATR):
ν_{max} [cm^{-1}] = 3062, 2960, 2925, 2867, 1702, 1663, 1593, 1577, 1528, 1488, 1448, 1382, 1315, 1294, 1244, 810, 754, 736.

UV-Vis spectrum (CH_2Cl_2):
λ_{max} [nm] (ϵ [$M^{-1}cm^{-1}$])= 347 (47,625), 518 (41,644).

High Resolution Mass (ESI):
$[M]^+$: calculated: 1001.4193, found: 1001.4182, discrepancy: -1.1 ppm.
The triphenylamine moiety is losing an electron to form $[M]^+$ as well as $[M+H]^+$.

Elemental analysis ($C_{70}H_{55}N_3O_4$):
calculated: 83.89% C, 5.53% H, 4.19% N, –% S
found: 83.64% C, 5.97% H, 4.17% N, –% S

N-(2,6-Diisopropylphenyl)-8,9-([b]-N,N-bis(9,9-dimethyl-9H-fluorene-2-yl)-1H-indole-6-amine)-3,4-perylene dicarboximide

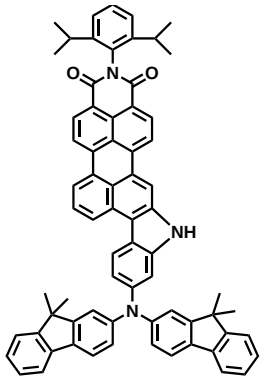

350 mg of *N*-(2,6-di*iso*propylphenyl)-9-(4-(bis-(9,9-dimethylfluorene-2-yl)-amine)-2-nitrobenzyl)-3,4-perylene dicarboximide (0.349 mmol) and 275 mg of triphenylphoshine (1.05 mmol) were dissolved in 10 mL of *o*-dichlorobenzene and stirred at 182°C and 300 W in the microwave (CEM, DISCOVER-S with external pressurised air cooling) for 8h. After removing the solvent under reduced pressure, the crude product was purified via column chromatography on silica with dichloromethane.

Yield: 210 mg blue solid (62%)

^{1}H-NMR (500 MHz, THF, 298 K):
δ [ppm]: 10.80 (s, 1H), 8.93 (d, J = 8.2, 1H), 8.80 (s, 1H), 8.75 - 8.64 (m, 3H), 8.59 (dd, J = 8.1, 11.1, 2H), 8.51 (d, J = 8.8, 1H), 7.85 (t, J = 7.9, 1H), 7.69 (d, J = 8.3, 4H), 7.45 - 7.16 (m, 15H), 2.85 - 2.74 (m, 2H), 1.43 (s, 12H), 1.14 (d, J = 6.8, 12H).

^{13}C-NMR (126 MHz, THF, 298 K):
δ [ppm]: 163.4, 155.1, 153.5, 147.8, 146.8, 145.9, 142.4, 139.0, 138.6, 138.2, 134.5, 131.9, 131.4, 130.7, 130.2, 129.7, 128.5, 127.3, 126.9, 126.8, 126.4, 126.2, 123.6, 123.4, 123.3, 122.3, 121.4, 120.9, 120.5, 120.3, 119.7, 119.2, 119.1, 118.7, 110.7, 106.1, 100.0, 94.1, 46.6, 29.0, 26.4, 23.4.

IR spectrum (ATR):
ν_{max} [cm^{-1}] = 3335, 2960, 2924, 2866, 1691, 1645, 1574, 1448, 1353, 1238, 840, 810, 755, 734.

UV-Vis spectrum (CH_2Cl_2):
λ_{max} [nm] (ϵ [M^{-1}cm^{-1}])= 377 (48,289), 618 (45,039).

High Resolution Mass (ESI):
$[M]^+$: calculated: 969.4158, found: 969.4152, discrepancy: -0.6 ppm.
The triphenylamine moiety is losing an electron to form $[M]^+$ as well as $[M+H]^+$.

N-(2,6-Diisopropylphenyl)-8,9-([b]-N,N-bis(9,9-dimethyl-9H-fluorene-2-yl)-1-hexyl-1H-indole-6-amine)-3,4-perylene dicarboximide

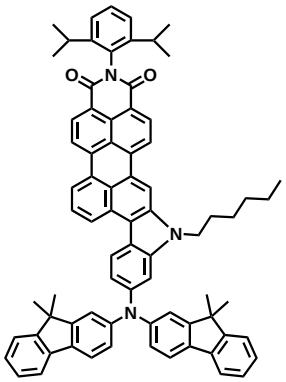

85 mg of *N*-(2,6-di*iso*propylphenyl)-8,9-([*b*]-*N,N*-bis(9,9-dimethyl-9*H*-fluorene-2-yl)-1*H*-indole-6-amine)-3,4-perylene dicarboximide (0.087 mmol) and 3 mg of sodium hydride (0.125 mmol) were mixed in a Schlenk tube. 15 mL of anhydrous dimethylformamidewere added under argon. The solution was stirred for 30 minutes at room

temperature. 60 mg of bromohexane (0.242 mmol) were added and the solution was stirred for another 3 h. After quenching the reaction with water, the solution is washed with water and hydrochloric acid (3:1), extracted with dichloromethane and dried over magnesium sulfate. The crude product was purified via column chromatography on silica with dichloromethane.

Yield: 85 mg blue solid (92%)

^{1}H-NMR (700 MHz, THF, 298 K):
δ [ppm]: 8.93 (d, J = 8.2, 1H), 8.86 (s, 1H), 8.76 (d, J = 8.2, 1H), 8.69 (d, J = 8.1, 1H), 8.65 (d, J = 7.6, 1H), 8.62 - 8.56 (m, 2H), 8.54 (d, J = 8.7, 1H), 7.84 (t, J = 7.8, 1H), 7.70 (d, J = 8.0, 4H), 7.46 - 7.40 (m, 5H), 7.39 (t, J = 7.9, 1H), 7.31 - 7.27 (m, 4H), 7.26 - 7.22 (m, 3H), 7.20 (dd, J = 2.0, 8.2, 2H), 4.53 (t, J = 7.0, 2H), 2.85 - 2.75 (m, 2H), 1.91 - 1.83 (m, 2H), 1.44 (s, 12H), 1.36 (dt, J = 7.6, 15.1, 2H), 1.27 (dt, J = 7.2, 15.3, 2H), 1.24 - 1.17 (m, 2H), 1.15 (d, J = 6.8, 12H), 0.78 (q, J = 7.5, 3H).

^{13}C-NMR (176 MHz, THF, 298 K):
δ [ppm]: 163.4, 155.1, 153.5, 147.7, 146.8, 145.9, 142.4, 139.1, 139.0, 138.6, 138.1, 134.5, 131.9, 131.4, 131.3, 130.7, 130.2, 129.8, 128.6, 127.4, 127.0, 126.8, 126.4, 126.3, 126.2, 123.5, 123.3, 123.1, 122.3, 121.4, 120.9, 120.6, 120.4, 120.3, 119.8, 119.2, 118.8, 118.7, 118.2, 118.1, 108.6, 104.5, 46.6, 42.2, 31.5, 29.4, 29.0, 26.6, 26.4, 23.3, 22.4, 13.4.

IR spectrum (ATR):
ν_{max} [cm^{-1}] = 3060, 2953, 2919, 2863, 1705, 1662, 1594, 1577, 1444, 1355, 1278, 1239, 846, 808, 756, 735.

UV-Vis spectrum (CH_2Cl_2):
λ_{max} [nm] (ϵ [M^{-1}cm^{-1}])= 379 (51,155), 623 (49,882).

High Resolution Mass (ESI):
$[M]^+$: calculated: 1053.5233, found: 1053.5226, discrepancy: -0.7 ppm.
The triphenylamine moiety is losing an electron to form $[M]^+$ as well as $[M+H]^+$.

N-Carboxymethyl-8,9-([b]-N,N-bis(9,9-dimethyl-9H-fluorene-2-yl)-1-hexyl-1H-indole-6-amine)-3,4-perylene dicarboximide

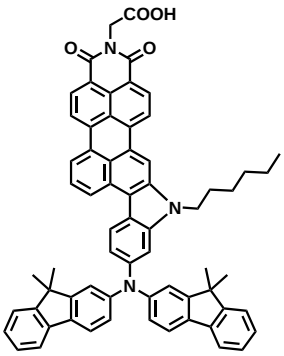

200 mg of *N*-(2,6-di*iso*propylphenyl)-8,9-([*b*]-*N,N*-bis(9,9-dimethyl-9*H*-fluorene-2-yl)-1-hexyl-1*H*-indole-6-amine)-3,4-perylene-dicarboximide (0.189 mmol) were dissolved in 15 mL of 2-methyl-2-butanol. 425 mg of potassium hydroxide (7.59 mmol) were added, the reaction mixture desoxygenated and refluxed under argon overnight. The reaction mixture was poured into an ice water/acetic acid mixture (10:2). The precipitate was filtered, washed with water and after drying dissolved in dichloromethane. 1-2 mL of acetic acid were added and the solution was stirred for 1-2 days. After removal of the dichloromethane under reduced pressure, methanol was added. The precipitate was filtered and washed with methanol. The formed anhydride was used directly for the next step without further purification.

Yield (crude): 160 mg blue solid (94%)

160 mg of the crude anhydride (0.076 mmol), 2 g of glycine (26.8 mmol), and 3 g of imidazole (44.1 mmol) were mixed in a Schlenk tube and stirred under argon at 140°C overnight. After cooling down dilute hydrochloric acid (water:acid (5:1)) was added. The precipitate was filtered and washed with water. The crude product was purified by column chromatography on silica gel with tetrahydrofuran, and tetrahydrofuran:acetic acid (1:1).

Yield: 100 mg blue solid (58%)

^{1}H-NMR (300 MHz, THF, 298 K):
δ [ppm]: 8.74 (d, J = 8.2, 1H), 8.53 (s, 1H), 8.49 - 8.26 (m, 6H), 7.68 (t, J = 7.9, 1H), 7.63 - 7.56 (m, 4H), 7.38 (d, J = 1.9, 2H), 7.35 - 7.29 (m, 3H), 7.22 - 7.09 (m, 7H), 4.65 (s, 2H), 4.37 (t, J = 7.1, 2H), 1.88 - 1.02 (m, 20H, partially overlaid with solvent), 0.67 (t, J = 7.0, 3H).

^{13}C-NMR (176 MHz, THF, 298 K):
δ [ppm]: 175.8, 164.5, 157.0, 155.5, 149.6, 144.3, 140.9, 136.4, 128.6, 128.2, 125.3, 124.8, 124.1, 122.9, 122.4, 121.7, 121.0, 120.6, 119.8, 106.1, 50.4, 48.5, 44.2, 33.2, 31.1, 28.4, 28.3, 24.2, 15.1, 10.3.

IR spectrum (ATR):
ν_{max} [cm^{-1}] = 3051, 2953, 2918, 2852, 1690, 1655, 1589, 1571, 1442, 1365, 1271, 1239, 1099, 1075, 809, 753, 732.

UV-Vis spectrum (CH_2Cl_2):
λ_{max} [nm] (ϵ [M^{-1}cm^{-1}])= 378 (40,465), 624 (37,398).

High Resolution Mass (ESI):
$[M]^+$: calculated: 951.4036, found: 951.4014, discrepancy: -2.3 ppm.
The triphenylamine moiety is losing an electron to form $[M]^+$ as well as $[M+H]^+$.

N-Cyclohexyl-4-(4-chlor-2-nitro-phenyl)-1,8-naphthalene dicarboximide

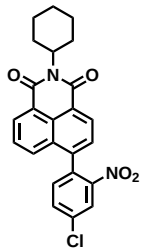

2 g of *N*-cyclohexyl-4-(4,4,5,5-tetramethyl-1,3,2-dioxaborolane-2-yl)-naphthalene-1,8-dicarboximide (4.93 mmol), 1.75 g of 1-bromo-4-chloro-2-nitrobenzene (7.40 mmol) were dissolved in 80 mL of toluene. 1.6 g of potassium carbonate (11.6 mmol) dissolved in 8 mL of water and 0.8 mL of ethanol are added. The solution was purged with argon for 30 minutes. After addition of 800 mg tetrakis(triphenylphosphine)palladium(0) (0.717 mmol) the solution was again purged for 30 minutes with argon. The solution was stirred at 80°C for 60 h. The reaction mixture was cooled down, washed with water and extracted with dichloromethane. The reaction mixture was purified via column chromatography on silica gel with dichloromethane:petrol ether (1:1).

Yield: 700 mg light-yellow solid (32%)

^{1}H-NMR (700 MHz, CD_2Cl_2, 298 K):
δ [ppm]: 8.60 - 8.55 (m, 2H), 8.23 (d, J = 2.1, 1H), 7.79 (dd, J = 2.1, 8.2, 1H), 7.74

(dd, J = 0.9, 8.4, 1H), 7.70 - 7.66 (m, 1H), 7.59 (d, J = 7.4, 1H), 7.46 (d, J = 8.2, 1H), 5.05 - 4.97 (m, 1H), 2.54 (qd, J = 3.5, 12.5, 2H), 1.90 (d, J = 13.2, 2H), 1.78 - 1.69 (m, 3H), 1.51 - 1.41 (m, 2H), 1.38 - 1.28 (m, 1H).

^{13}C-NMR (176 MHz, CD_2Cl_2, 298 K):
δ [ppm]: 164.8, 164.6, 149.8, 141.4, 136.2, 134.4, 134.1, 132.7, 131.5, 130.9, 130.7, 130.4, 128.8, 128.1, 127.5, 125.6, 124.5, 124.3, 29.7, 27.2, 26.1.

IR spectrum (ATR):
ν_{max} [cm^{-1}] = 3098, 2928, 2848, 1701, 1658, 1594, 1525, 1389, 1346, 1231, 1107, 786.

UV-Vis spectrum (CH_2Cl_2):
λ_{max} [nm] (ϵ [M^{-1}cm^{-1}])= 340 (16,888).

High Resolution Mass (ESI):
$[M+H]^+$: calculated: 435.1112, found: 435.1111, discrepancy: -0.1 ppm.

N-Cyclohexyl-4-(4-bis(p-2,4,4-trimethylpentane-2-yl-phenyl)amino-2-nitro-phenyl)-1,8-naphthalene dicarboximide

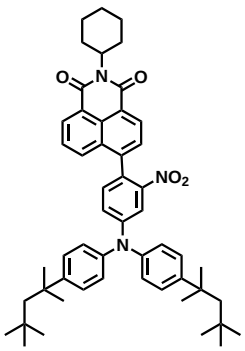

600 mg of *N*-cyclohexyl-4-(4-chloro-2-nitro-phenyl)-naphthalene-1,8-dicarboximide (1.38 mmol), 815 mg of bis(*p*-2,4,4-trimethylpentane-2-yl-phenyl)amine (2.07 mmol), 900 mg of caesium carbonate (2.76 mmol), 125 mg of tris(dibenzylideneacetone)dipalladium(0) (0.136 mmol), and 170 mg of 2,2´-bis(diphenylphosphino)-1,1´-binaphthyl (0.273 mmol) were dissolved in 30 mL of anhydrous toluene in a Schlenk tube and stirred under argon at 100°C for 16 h. The reaction mixture is purified via column chromatography with dichloromethane:petrol ether (1:1).

Yield: 640 mg yellow solid (64%)

^{1}H-NMR (700 MHz, CD_2Cl_2, 298 K):
δ [ppm]: 8.55 (d, J = 7.5, 2H), 7.93 (d, J = 8.4, 1H), 7.71 - 7.66 (m, 1H), 7.62 - 7.58 (m, 2H), 7.41 (d, J = 8.7, 4H), 7.27 (dd, J = 2.5, 8.5, 1H), 7.21 (d, J = 8.5, 1H), 7.17 (d, J = 8.6, 4H), 5.07 - 4.95 (m, 1H), 2.60 - 2.48 (m, 2H), 1.89 (d, J = 13.2, 2H), 1.80 - 1.68 (m, 7H), 1.51 - 1.23 (m, 15H), 0.76 (s, 18H).

^{13}C-NMR (176 MHz, CD_2Cl_2, 298 K):
δ [ppm]: 165.0, 164.8, 150.3, 147.9, 143.7, 143.3, 133.4, 131.5, 131.3, 130.9, 128.8, 128.4, 127.7, 125.8, 124.4, 124.2, 123.6, 123.5, 115.1, 57.6, 38.9, 32.9, 32.0, 31.8, 29.7, 27.2, 26.2.

IR spectrum (ATR):
ν_{max} [cm^{-1}] = 2949, 2867, 1700, 1661, 1593, 1532, 1504, 1397, 1343, 1336, 1233, 1183, 1111, 1015, 872, 829, 783, 762.

UV-Vis spectrum (CD_2Cl_2):
λ_{max} [nm] (ϵ [$M^{-1}cm^{-1}$])= 401 (8,583).

High Resolution Mass (ESI):
$[M]^+$: calculated: 791.4662, found: 791.4639, discrepancy: -2.9 ppm.
The triphenylamine moiety is losing an electron to form $[M]^+$ as well as $[M+H]^+$.

N-Cyclohexyl-3,4-([b]-N,N-bis(p-2,4,4-trimethylpentane-2-yl)phenyl-1-hexyl-1H-indole-6-amine)-1,8-naphthalene dicarboximide

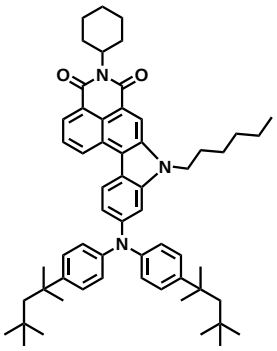

550 mg of *N*-cyclohexyl-4-(4-bis(*p*-2,4,4-trimethylpentane-2-yl)phenyl-amino-2-nitro-phenyl)-naphthalene 1,8-dicarboximide (0.694 mmol) and 545 mg of triphenylphoshine (2.08 mmol) were dissolved in 10 mL of *o*-dichlorobenzene and stirred at 182°C and 300 W in the microwave (CEM, DISCOVER-S with external pressurised air cooling) for 8h. After removing the solvent under reduced pressure, the crude product was isolated via column chromatography on silica with dichloromethane and used directly

for the next step.

Yield (crude): 430 mg orange solid (82%)

350 mg of *N*-cyclohexyl-3,4-([*b*]-*N,N*-bis(*p*-2,4,4-trimethylpentane-2-yl)phenyl-1*H*-indole-6-amine)-1,8-naphthalene dicarboximide (0.460 mmol) and 14 mg of sodium hydride (0.583 mmol) were mixed in a Schlenk tube. 15 mL of anhydrous dimethylformamidewere added under argon. The solution was stirred for 30 minutes at room temperature. 230 mg of bromohexane (1.39 mmol) were added and the solution was stirred for another 3 h. After quenching the reaction with water, the solution is washed with water and hydrochloric acid (3:1), extracted with dichloromethane and dried over magnesium sulfate. The crude product was purified via column chromatography on silica with dichloromethane.

Yield: 270 mg orange solid (71%)

^{1}H-NMR (700 MHz, THF, 298 K):
δ [ppm]: 9.08 (d, J = 8.0, 1H), 8.77 (s, 1H), 8.51 (d, J = 8.8, 1H), 8.46 (d, J = 6.8, 1H), 7.86 (t, J = 7.8, 1H), 7.35 (d, J = 8.6, 4H), 7.23 (d, J = 1.7, 1H), 7.12 (m, 5H), 5.09 (t, J = 12.1, 1H), 4.43 (t, J = 7.1, 2H), 2.73 - 2.61 (m, 2H), 1.89 (d, J = 13.1, 2H), 1.84 - 1.69 (m, 9H, partially overlaid with solvent), 1.51 - 1.24 (m, 21H), 0.88 - 0.78 (m, 21H).

^{13}C-NMR (176 MHz, THF, 298 K):
δ [ppm]: 165.7, 165.6, 149.2, 146.6, 146.1, 143.9, 139.0, 128.6, 128.5, 128.0, 125.4 124.63, 121.19, 120.94, 118.8, 116.7, 104., 58.3, 55.3, 54.5, 44.0, 39.4, 33.5, 33.0, 32.7, 32.4, 30.8, 30.4, 28.1, 28.0, 27.0, 23.8, 14.8.

IR spectrum (ATR):
ν_{max} [cm^{-1}] = 2950, 2927, 2859, 1690, 1648, 1607, 1584, 1505, 1460, 1384, 1316, 1256, 1218, 1180, 1101, 1078, 890, 826, 795, 777, 739.

UV-Vis spectrum (CH_2Cl_2):
λ_{max} [nm] (ϵ [M^{-1}cm^{-1}])= 489 (26,264).

High Resolution Mass (ESI):
[M]$^{+}$: calculated: 843.5703, found: 843.5731, discrepancy: 3.3 ppm.
The triphenylamine moiety is losing an electron to form [M]$^{+}$ as well as [M+H]$^{+}$.

Elemental analysis ($C_{58}H_{73}N_3O_2$):

calculated: 82.52% C, 8.72% H, 4.98% N, –% S
found: 81.78% C, 8.67% H, 5.07% N, –% S

N-Carboxymethyl-3,4-([b]-N,N-bis(p-2,4,4-trimethylpentane-2-yl)phenyl-1H-indole-6-amine)-1,8-naphthalene dicarboximide

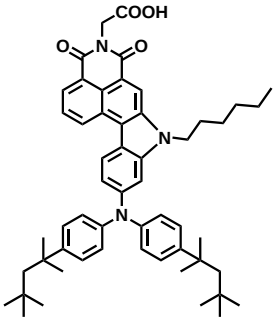

170 mg of *N*-cyclohexyl-3,4-([*b*]-*N,N*-bis(*p*-2,4,4-trimethylpentane-2-yl)phenyl-1*H*-indole-6-amine)-1,8-naphthalene dicarboximide (0.201 mmol) were dissolved in 10 mL of 2-methyl-2-butanol. 450 mg of potassium hydroxide (8.04 mmol) were added, the reaction mixture desoxygenated and refluxed under argon overnight. The reaction mixture was poured into an ice water/acetic acid mixture (10:2). The precipitate was filtered, washed with water and after drying dissolved in dichloromethane. 1-2 mL of acetic acid were added and the solution was stirred for 1-2 days. After removal of the dichloromethane under reduced pressure, methanol was added. The precipitate was filtered and washed with methanol. The formed anhydride was used directly for the next step without further purification.

Yield (crude): 145 mg red solid (95%)

80 mg of the crude anhydride (0.104 mmol), 1 g of glycine (13.4 mmol) and 2 g of imidazole (29.4 mmol) were mixed in a Schlenk tube and stirred under argon at 140°C overnight. After cooling down dilute hydrochloric acid (water:acid (5:1)) was added. The precipitate was filtered and washed with water. The crude product was purified by column chromatography on silica gel with dichloromethane, tetrahydrofuran, and acetic acid.

Yield: 75 mg orange solid (87%)

^{1}H-NMR (700 MHz, THF, 298 K):
δ [ppm]: 9.10 (d, J = 8.3, 1H), 8.72 (s, 1H), 8.50 (d, J = 8.8, 1H), 8.46 (d, J = 7.2, 1H), 7.86 (t, J = 7.8, 1H), 7.36 (d, J = 8.6, 4H), 7.23 (d, J = 1.7, 1H), 7.15 - 7.10 (m,

5H), 4.83 (s, 2H), 4.41 (t, J = 7.2, 2H), 1.83 - 1.77 (m, 6H), 1.40 (s, 12H), 1.32 - 1.24 (m, 6H), 0.88 - 0.77 (m, 21H).

^{13}C-NMR (176 MHz, THF, 298 K):
δ [ppm]: 167.0, 164.9, 164.8, 149.3, 146.6, 146.2, 144.0, 138.8, 130.5, 128.8, 128.5, 128.3, 128.0, 125.5, 125.4, 124.7, 124.4, 121.7, 119.8, 118.8, 118.7, 116.9, 104.3, 58.3, 44.1, 41.9, 39.4, 33.5, 33.0, 32.7, 32.4, 30.8, 28.1, 23.8, 14.8.

IR spectrum (ATR):
ν_{max} [cm^{-1}] = 2946, 2867, 1721, 1695, 1661, 1623, 1589, 1513, 1464, 1389, 1358, 1294, 1245, 1178, 1090, 825, 773, 738.

UV-Vis spectrum (CH_2Cl_2):
λ_{max} [nm] (ϵ [M^{-1}cm^{-1}])= 335 (26,910), 502 (25,252).

High Resolution Mass (ESI):
$[M]^+$: calculated: 819.4575, found: 819.4980, discrepancy: 0.6 ppm.
The triphenylamine moiety is losing an electron to form $[M]^+$ as well as $[M+H]^+$.

Elemental analysis ($C_{54}H_{65}N_3O_4$):
calculated: 79.08% C, 7.99% H, 5.12% N, –% S
found: 78.64% C, 8.21% H, 5.00% N, –% S

8.2.5 SPC: Perylene Diimide Colour Tuning

N,N'-Bisoctyl-1,7-bis[(5,5"-bistrimethylsilyl)-2,2':3',2"-terthien-5'-yl]-perylene-3,4:9,10-tetracarboxy acid diimide

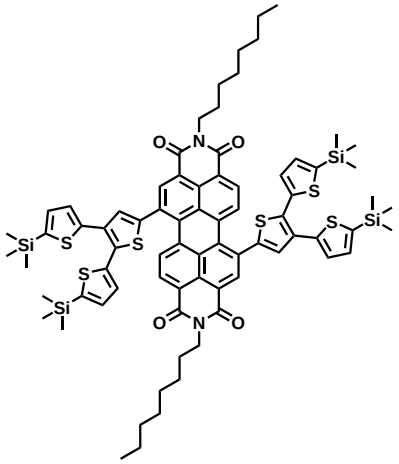

200 mg of *N,N'*-bisoctyl-1,7-dibromo-perylene-3,4:9,10-tetracarboxy diimide (0.256 mmol), 300 mg of 5'-(4,4,5,5-tetramethyl-[1,3,2]dioxaborolan-2-yl)-5,5"-bistrimethylsilyl-2,2':3',2"-terthiophene (0.578 mmol), and 1 g of potassium carbonate (7.246 mmol) were dissolved in 20 mL of toluene, 2 mL of water, and 0.2 mL of ethanol in a Schlenk tube. The solution was deoxygenated with argon, 90 mg of tetrakis(triphenylphosphine)palladium (0.081 mmol) were added and the solution was stirred under argon at 80 °C for three days. The reaction mixture was extracted with dichloromethane and dried over magnesium sulfate. The solvent was evaporated under reduced pressure and the resulting solid was purified by column chromatography on silica gel (dichloromethane/petrol ether, 3:2).

Yield: 170 mg dark green solid (47 %)

^{1}H-NMR (250 MHz, CD_2Cl_2, 298 K):
δ [ppm]: 8.63 (s, 2H), 8.39 (m, 4H), 7.48 (s, 2H), 7.31 - 7.11 (m, 8H), 4.18 (m, 4H), 1.77-1.68 (m, 4H), 1.43-1.29 (m, 19H), 0.91-0.86 (m, 7H), 0.34-0.32 (m, 36H).

^{13}C-NMR (75 MHz, CD_2Cl_2, 298 K):
δ [ppm]: 163.6, 163.4, 143.8, 142.8, 142.5, 142.0, 139.8, 135.6, 134.9, 134.9, 134.7, 134.6, 134.0, 133.3, 132.7, 130.9, 130.5, 130.00, 129.5, 128.8, 128.3, 123.0, 41.2, 32.4, 30.0, 29.8, 28.7, 27.8, 23.3, 14.5, 0.2, 0.1.

IR spectrum (ATR):

ν_{max} [cm^{-1}] = 2920, 2920, 2853, 1697, 1660, 1596, 1432, 1400, 1341, 1326, 1247, 1205, 1129, 1066, 1042, 984, 836, 811, 796, 754, 720, 696.

UV-Vis spectrum (CH_2Cl_2):
λ_{max} [nm] (ϵ [$M^{-1}cm^{-1}$])= 475 (17,631); 601(15,855).

FD-MS-Spektrum (8 kV):
m/z = 1394.9, calculated: 1394.40

Elemental analysis ($C_{76}H_{86}N_2O_4S_6Si_4$):
calculated: 65.38% C, 6.21% H, 2.01% N, 13.78% S
found: 65.62% C, 5.87% H, 2.00% N, 14.02% S

N,N'-Bisoctyl-1,7-bis(2,2':3',2"-terthien-5'-yl)-perylene-3,4:9,10-tetracarboxy diimide

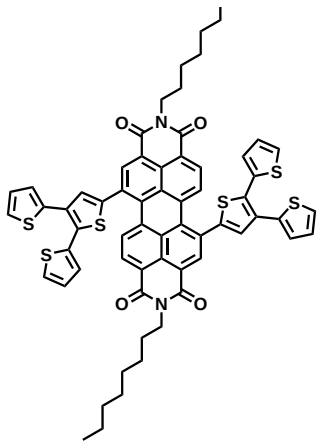

140 mg of *N,N'*-bisoctyl-1,7-bis[(5,5"-bistrimethylsilyl)-2,2':3',2"-terthien-5'-yl]-perylene-3,4:9,10-tetracarboxy diimide (0.100 mmol) were dissolved in tetrahydrofuran. A solution of 100 mg of tetra-*n*-butylammonium fluoride (0.402 mmol) in tetrahydrofuran was added dropwise under stirring at room temperature. The mixture was stirred for 30 minutes at room temperature, concentrated, and precipitated in methanol. The precipitate was then filtered and washed with methanol.

Yield: 86 mg dark green solid (78%)

^{1}H-NMR (250 MHz, CD_2Cl_2, 298 K):
δ [ppm]: 8.50 (s, 2H), 8.33 - 8.20 (m, 4H), 7.39 (s, 2H), 7.28 (ddd, J = 1.2, 5.1, 9.4, 4H), 7.15 - 7.07 (m, 4H), 6.97 (dt, J = 3.5, 5.1, 4H), 4.17 - 3.99 (m, 4H), 1.63 (m, 4H),

1.27 (m, 20H), 0.80 (m, 6H).

^{13}C-NMR (126 MHz, CD_2Cl_2, 298 K):
δ [ppm]: 163.6, 163.4, 142.9, 137.2, 135.6, 134.6, 134.2, 133.4, 132.6, 130.7, 130.5, 130.1, 129.5, 129.1, 128.3, 128.1, 128.0, 127.9, 127.7, 126.7, 123.0, 41.2, 32.4, 30.3, 30.2, 30.0, 29.8, 28.6, 27.7, 23.3, 23.2, 14.4.

IR spectrum (ATR):
ν_{max} [cm^{-1}] = 2921, 2852, 1695, 1654, 1584, 1432, 1400, 1327, 1245, 1169, 1121, 1019, 845, 810, 756, 692.

UV-Vis spectrum (CH_2Cl_2):
λ_{max} [nm] (ϵ [$M^{-1}cm^{-1}$])= 461 (16,878); 591 (16,671).

FD-MS-Spektrum (8 kV):
m/z = 1106.7, calculated: 1106.24

Elemental analysis ($C_{64}H_{54}N_2O_4S_6$):
calculated: 69.41% C, 4.91% H, 2.53% N, 17.37% S
found: 69.29% C, 5.09% H, 2.52% N, 17.55% S

N,N'-Bisoctyl-1,7-bis[(4,4"-bis-trimethylsilyl)-2,2':5'2"-terthien-3'-yl]-perylene-3,4:9,10-tetracarboxy diimide

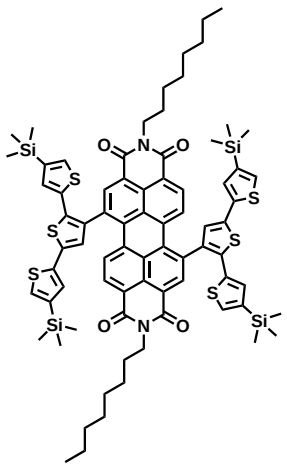

130 mg of *N,N'*-bisoctyl-1,7-dibromo-perylene-3,4:9,10-tetracarboxy diimide (0.168 mmol), 180 mg of 3'-(4,4,5,5-tetramethyl-[1,3,2]dioxaborolan-2-yl)-(5,5"-bistrimethylsilyl)-2,2':5',2"-terthiophene (0.347 mmol) and 500 mg of potassium carbonate (3.623 mmol) were dissolved in 10 mL of toluene, 1 mL of water, and 0.1

mL of ethanol in a Schlenk tube. The solution was deoxygenated with argon, 60 mg of tetrakis(triphenylphosphine)palladium (0.054 mmol) were added and the solution was stirred under argon at 80°C for three days. The reaction mixture was extracted with dichloromethane and dried over magnesium sulfate. The solvent was evaporated under reduced pressure and the resulting solid was purified by column chromatography on silica gel (dichloromethane/petrol ether, 3:2).

Yield: 70 mg dark purple solid (30%)

^{1}H-NMR (250 MHz, CD_2Cl_2, 298 K):
δ [ppm]: 8.60 (d, J = 6.1, 1H), 8.54 (d, J = 2.4, 1H), 8.35 - 8.06 (m, 4H), 7.40 - 7.06 (m, 6H), 7.02 - 6.75 (m, 3H), 6.69 - 6.58 (m, 1H), 4.29 - 3.92 (m, 4H), 1.80 - 1.61 (m, 4H), 1.31 (m, 20H), 0.86 (t, J = 4.9, 6H), 0.39 - -0.10 (m, 36H).

^{13}C-NMR (126 MHz, CD_2Cl_2, 298 K):
δ [ppm]: 163.8, 163.7, 163.6, 142.5, 142.3, 142.2, 141.8, 141.7, 141.6, 141.5, 140.6, 140.1, 140.0, 139.8, 139.4, 139.2, 139.1, 138.9, 138.8, 138.7, 136.3, 135.8, 135.7, 135.6, 135.5, 135.4, 135.3, 135.1, 134.8, 134.7, 134.6, 134.3, 133.0, 132.5, 132.3, 132.0, 130.7, 130.5, 129.6, 129.2, 128.9, 128.6, 128.3, 128.0, 127.9, 127.8, 127.7, 126.2, 125.9, 125.8, 125.6, 123.3, 123.0, 122.8, 41.1, 41.0, 40.9, 37.6, 33.3, 32.5, 32.4, 30.6, 30.3, 29.9, 29.8, 28.6, 27.9, 27.8, 27.7, 27.6, 23.3, 23.2, 20.0, 14.4, 0.1, 0.0.

IR spectrum (ATR):
ν_{max} [cm^{-1}] = 2954, 2925, 2855, 1697, 1659, 1587, 1433, 1416, 1345, 1326, 1247, 1212, 1169, 1103, 1068, 986, 921, 834, 811, 798, 751.

UV-Vis spectrum (CH_2Cl_2):
λ_{max} [nm] (ϵ [$M^{-1}cm^{-1}$])= 368 (51,319); 515 (25,340).

FD-MS-Spektrum (8 kV):
m/z = 1394.8, calculated: 1394.40

Elemental analysis ($C_{76}H_{86}N_2O_4S_6Si_4$):
calculated: 65.38% C, 6.21% H, 2.01% N, 13.78% S
found: 65.29% C, 6.63% H, 1.97% N, 13.51% S

N,N'-Bisoctyl-1,7-bis(2,2':5'2"-terthien-3'-yl)-perylene-3,4:9,10-tetracarboxy diimide

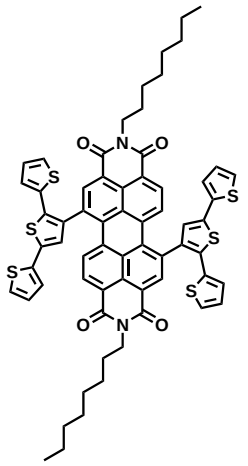

70 mg of *N,N'*-Bisoctyl-1,7-bis[(5,5"-bistrimethylsilyl)-2,2':5',2"-terthien-3'-yl]-perylene-3,4:9,10-tetracarboxy diimide (0.050 mol) were dissolved in tetrahydrofuran. A solution of 53 mg of tetra-*n*-butylammonium fluoride (0.200 mmol) in tetrahydrofuran was added dropwise under stirring at room temperature. The mixture was stirred for 30 minutes at room temperature, concentrated and precipitated from tetrahydrofuran in methanol. The precipitate was then filtered and washed with methanol

Yield: 45 mg dark purple solid (81%)

^{1}H-NMR (250 MHz, CD_2Cl_2, 298 K):
δ [ppm]: 8.57 (d, 2H), 8.42 - 8.14 (m, 4H), 7.38 - 7.25 (m, 4H), 7.16 - 6.68 (m, 10H), 4.27 - 3.94 (m, 4H), 1.78 - 1.64 (m, 4H), 1.46 - 1.20 (m, 20H), 0.93 - 0.82 (m, 6H).

^{13}C-NMR (126 MHz, CD_2Cl_2, 298 K):
δ [ppm]: 163.8, 163.7, 139.4, 139.3, 138.8, 138.7, 136.7, 136.1, 136.0, 135.7, 135.6, 135.5, 135.4, 135.3, 135.1, 135.1, 135.0, 134.7, 134.6, 132.3, 132.2, 132.1, 130.9, 130.8, 130.6, 129.4, 129.2, 128.8, 128.7, 128.6, 128.5, 128.3, 128.1, 127.8, 126.9, 126.8, 126.7, 126.6, 126.0, 125.8, 125.7, 125.6, 125.1, 125.0, 123.3, 123.2, 123.1, 123.0, 41.0, 40.1, 32.5, 32.4, 30.6, 30.3, 30.2, 30.0, 29.9, 29.8, 28.6, 27.7, 27.6, 24.5, 23.3, 23.2, 14.5, 14.4, 13.9.

IR spectrum (ATR):
ν_{max} [cm^{-1}] = 2923, 2853, 1695, 1654, 1588, 1500, 1432, 1403, 1326, 1241, 1169, 1103, 1045, 931, 835, 812, 750, 690.

UV-Vis spectrum (CH_2Cl_2):
λ_{max} [nm] (ϵ [$M^{-1}cm^{-1}$])= 512 (27,869).

FD-MS-Spektrum (8 kV):
m/z = 1106.6, calculated: 1106.24

Elemental analysis ($C_{64}H_{54}N_2O_4S_6$):
calculated: 69.41% C, 4.91% H, 2.53% N, 17.37% S
found: 69.14% C, 5.03% H, 2.41% N, 16.38% S

N,N'-Bisoctyl-1,7-bis(2,2':5'2"-terthien-5-yl)-perylene-3,4:9,10-tetracarboxy diimide

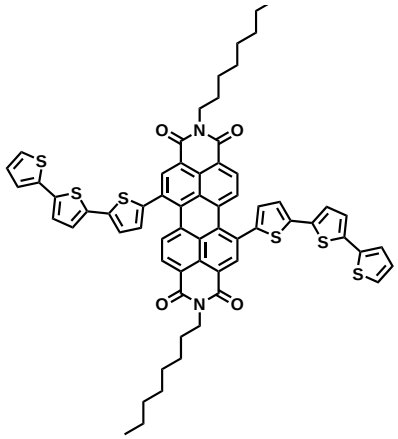

180 mg of *N,N'*-bisoctyl-1,7-dibromo-perylene-3,4:9,10-tetracarboxy diimide (0.233 mmol), 190 mg of 5-(4,4,5,5-tetramethyl-[1,3,2]dioxaborolan-2-yl)-2,2':5',2"-terthiophene (0.508 mmol), and 850 mg of potassium carbonate (6.159 mmol) were dissolved in 18 mL of toluene, 1.8 mL of water, and 0.18 mL of ethanol in a Schlenk tube. The solution was deoxygenated with argon, 100 mg of tetrakis(triphenylphosphine)palladium (0.090 mmol) were added and the solution was stirred under argon at 80°C for three days. The reaction mixture was extracted with dichloromethane and dried over magnesium sulfate. The solvent was evaporated under reduced pressure and the resulting solid was purified by column chromatography on silica gel with dichloromethane.

Yield 120 mg dark green solid (44%)

^{1}H-NMR (250 MHz, CD_2Cl_2, 298 K):
δ [ppm]: 8.58 (d, J = 2.7, 2H), 8.31 - 8.16 (m, J = 8.1, 4H), 7.26 - 6.94 (m, 16H), 4.17 -

3.96 (m, 4H), 1.77 - 1.53 (m, J = 6.5, 11.9, 4H), 1.36 - 1.09 (m, 20H), 0.85 - 0.74 (m, 6H).

^{13}C-NMR (126 MHz, $C_2Cl_4D_2$, 393 K):
δ [ppm]: 163.0, 142.6, 140.3, 137.6, 136.9, 135.4, 135.3, 134.6, 133.2, 132.7, 129.8, 129.6, 129.4, 129.1, 128.5, 128.1, 127.9, 125.3, 125.0, 124.7, 124.3, 122.8, 122.7, 120.4, 40.7, 31.7, 29.2, 29.0, 28.2, 27.1, 22.4, 13.8.

IR spectrum (ATR):
ν_{max} [cm^{-1}] = 2919, 2852, 1695, 1657, 1592, 1465, 1435, 1403, 1324, 1245, 1172, 1128, 1034, 863, 835, 822, 812, 794, 757, 715, 701.

UV-Vis spectrum (CH_2Cl_2):
λ_{max} [nm] (ϵ [$M^{-1}cm^{-1}$])= 376 (61,861); 488 (22,205), 610 (15,426.

FD-MS-Spektrum (8 kV):
m/z = 1107.3, calculated: 1106.24

Elemental analysis ($C_{64}H_{54}N_2O_4S_6$):
calculated: 69.41% C, 4.91% H, 2.53% N, 17.37% S
found: 69.24% C, 4.91% H, 2.49% N, 17.07% S

Bibliography

[1] Feiler, L., Langhals, H., Polborn, K., *Liebigs Annalen* **1995**, *1995*, 1229–1244.

[2] Li, C., Schöneboom, J., Liu, Z., Pschirer, N. G., Erk, P., Herrmann, A., Müllen, K., *Chemistry - A European Journal* **2009**, *15*, 878–884.

[3] Suraru, S.-L., Zschieschang, U., Klauk, H., Würthner, F., *Chemical Communications* **2011**, *47*, 11504–11506.

[4] Newton, J. D. *Uncommon Friends*; Harcourt Brace & Company, 1987; p 31.

[5] Goldemberg, J., Coelho, S. T., *Energy Policy* **2004**, *32*, 711 – 714.

[6] REN21, *Renewables 2011 Global Status Report*; 2011.

[7] Cho, A., *Science* **2010**, *329*, 786–787.

[8] Sun, S.-S., Sariciftci, N. S., Eds. *Organic Photovoltaics - Mechanisma, Materials, and Devices*; Marcel Dekker Inc, 2005.

[9] Jäger-Waldau, A. *PV Status Report 2010*; 2010.

[10] Miles, R. W., Zoppi, G., Forbes, I., *Materials Today* **2007**, *10*, 20 – 27.

[11] Chamberlain, G., *Solar Cells* **1983**, *8*, 47 – 83.

[12] Tang, C. W., *Applied Physics Letters* **1986**, *48*, 183–185.

[13] Green, M. A., Emery, K., Hishikawa, Y., Warta, W., Dunlop, E. D., *Progress in Photovoltaics: Research and Applications* **2011**, *19*, 565–572.

[14] O'Regan, B., Grätzel, M., *Nature* **1991**, *353*, 737–740.

[15] Nazeeruddin, M. K., Baranoff, E., Grätzel, M., *Solar Energy* **2011**, *85*, 1172–1178.

[16] Yella, A., Lee, H.-W., Tsao, H. N., Yi, C., Chandiran, A. K., Nazeeruddin, M., Diau, E. W.-G., Yeh, C.-Y., Zakeeruddin, S. M., Grätzel, M., *Science* **2011**, *334*, 629–634.

[17] Chung, I., Lee, B., He, J., Chang, R. P. H., Kanatzidis, M. G., *Nature* **2012**, *485*, 486–489.

[18] Burschka, J., Dualeh, A., Kessler, F., Baranoff, E., Cevey-Ha, N.-L. C.-H., Yi, C., Nazeeruddin, M. K., Grätzel, M., *Journal of the American Chemical Society* **2011**, *133*, 18042–18045.

[19] Anscombe, N., *Nature Photonics* **2011**, *5*, 266–267.

[20] Hagfeldt, A., Boschloo, G., Sun, L., Kloo, L., Pettersson, H., *Chemical Reviews* **2010**, *110*, 6595–6663.

[21] Yoon, J. et al. , *Nature Materials* **2008**, *7*, 907–915.

[22] Bessho, T., Zakeeruddin, S. M., Yeh, C. Y., Diau, E. W., Grätzel, M., *Angewandte Chemie International Edition* **2010**, *122*, 6796–6799.

[23] Tsao, H. N., Yi, C., Moehl, T., Yum, J.-H., Zakeeruddin, S. M., Nazeeruddin, M. K., Grätzel, M., *ChemSusChem* **2011**, *4*, 591–594.

[24] Bach, U., Lupo, D., Comte, P., Moser, J. E., Weissörtel, F., Salbeck, J., Spreitzer, H., Grätzel, M., *Nature* **1998**, *395*, 583–585.

[25] Kroeze, J. E., Hirata, N., Schmidt-Mende, L., Orizu, C., Ogier, S. D., Carr, K., Grätzel, M., Durrant, J. R., *Advanced Functional Materials* **2006**, *16*, 1832–1838.

[26] Mishra, A., Fischer, M. K., Bäuerle, P., *Angewandte Chemie International Edition* **2009**, *48*, 2474–99.

[27] Li, C., Liu, Z. H., Schöneboom, J., Eickemeyer, F., Pschirer, N. G., Erk, P., Herrmann, A., Müllen, K., *Journal of Materials Chemistry* **2009**, *19*, 5405–5415.

[28] Hara, K., Sato, T., Katoh, R., Furube, A., Ohga, Y., Shinpo, A., Suga, S., Sayama, K., Sugihara, H., Arakawa, H., *Journal of Physical Chemistry B* **2003**, *107*, 597–606.

[29] Hara, K., Wang, Z.-S., Sato, T., Furube, A., Katoh, R., Sugihara, H., Dan-Oh, Y., Kasada, C., Shinpo, A., Suga, S., *Journal of Physical Chemistry B* **2005**, *109*, 15476–15482.

[30] Horiuchi, T., Miura, H., Sumioka, K., Uchida, S., *Journal of the American Chemical Society* **2004**, *126*, 12218–12219.

[31] Sayama, K., Tsukagoshi, S., Mori, T., Hara, K., Ohga, Y., Shinpou, A., Abe, Y., Suga, S., Arakawa, H., *Solar Energy Materials and Solar Cells* **2003**, *80*, 47 – 71.

[32] Tokuhisa, H., Hammond, P., *Advanced Functional Materials* **2003**, *13*, 831–839.

[33] Funabiki, K., Mase, H., Saito, Y., Otsuka, A., Hibino, A., Tanaka, N., Miura, H., Himori, Y., Yoshida, T., Kubota, Y., Matsui, M., *Organic Letters* **2012**, *14*, 1246 –1249.

[34] Grice, K., Lu, H., Atahan, P., Asif, M., Hallmann, C., Greenwood, P., Maslen, E., Tulipani, S., Williford, K., Dodson, J., *Geochimica et Cosmochimica Acta* **2009**, *73*, 6531 – 6543.

[35] Kardos, M. Vat dye. 1913.

[36] Li, C., Wonneberger, H., *Advanced Materials* **2012**, *24*, 613–636.

[37] Zollinger, H. *Color Chemistry*, 3rd ed.; Wiley-VCH GmbH & Co. KGaA, 2003.

[38] Peneva, K., Mihov, G., Nolde, F., Rocha, S., ichi Hotta, J., Braeckmans, K., Hofkens, J., Uji-i, H., Herrmann, A., Müllen, K., *Angewandte Chemie International Edition* **2008**, *47*, 3372–3375.

[39] Herrmann, A., Müllen, K., *Chemistry Letters* **2006**, *35*, 978–985.

[40] Zhang, X., Rehm, S., Safont-Sempere, M. M., Würthner, F., *Nature Chemistry* **2009**, *1*, 623–629.

[41] Cordes, T., Vogelsang, J., Anaya, M., Spagnuolo, C., Gietl, A., Summerer, W., Herrmann, A., Müllen, K., Tinnefeld, P., *Journal of the American Chemical Society* **2010**, *132*, 2404–2409.

[42] Jordens, S., Belder, G. D., Lor, M., Schweitzer, G., der Auweraer, M. V., Weil, T., Reuther, E., Müllen, K., Schryver, F. C. D., *Photochemical & Photobiological Sciences* **2003**, *2*, 177–186.

[43] Jones, B. A., Facchetti, A., Wasielewski, M. R., Marks, T. J., *Journal of the American Chemical Society* **2007**, *129*, 15259–15278.

[44] Schmidt-Mende, L., Fechtenkötter, A., Müllen, K., Moons, E., Friend, R. H., MacKenzie, J. D., *Science* **2001**, *293*, 1119–1122.

[45] Langhals, H., Krotz, O., Polborn, K., Mayer, P., *Angewandte Chemie International Edition* **2005**, *44*, 2427–2428.

[46] Avlasevich, Y., Li, C., Müllen, K., *Journal of Materials Chemistry* **2010**, *20*, 3814–3826.

[47] Rademacher, A., Märkle, S., Langhals, H., *Chemische Berichte* **1982**, *115*, 2927–2934.

[48] Heek, T., Fasting, C., Rest, C., Zhang, X., Würthner, F., Haag, R., *Chemical Communications* **2010**, *46*, 1884–1886.

[49] Erwin, P., Thompson, M. E., *Applied Physics Letters* **2011**, *98*, 223305.

[50] Graser, F., Hädicke, E., *Liebigs Annalen der Chemie* **1980**, *1980*, 1994–2011.

[51] Hädicke, E., Graser, F., *Acta Crystallographica Section C* **1986**, *42*, 189–195.

[52] Seybold, G., Iden, R., Lardon, H. Fluorescent compounds for light concentration. 1984.

[53] Nakazono, S., Imazaki, Y., Yoo, H., Yang, J., Sasamori, T., Tokitoh, N., Cédric, T., Kageyama, H., Kim, D., Shinokubo, H., Osuka, A., *Chemistry - A European Journal* **2009**, *15*, 7530–7533.

[54] Nakazono, S., Easwaramoorthi, S., Kim, D., Shinokubo, H., Osuka, A., *Org Lett* **2009**, *11*, 5426–5429.

[55] Teraoka, T., Hiroto, S., Shinokubo, H., *Organic Letters* **2011**, *13*, 2532–2535.

[56] Battagliarin, G., Li, C., Enkelmann, V., Müllen, K., *Organic Letters* **2011**, *13*, 3012–3015.

[57] Battagliarin, G., Zhao, Y., Li, C., Müllen, K., *Organic Letters* **2011**, *13*, 3399–3401.

[58] Wang, S., Dössel, L., Mavrinskiy, A., Gao, P., Feng, X., Pisula, W., Müllen, K., *Small* **2011**, *7*, 2841–2846.

[59] Zheng, X., Zhang, D., Zhu, D., *Tetrahedron Letters* **2006**, *47*, 9083 – 9087.

[60] Böhm, A., Helfer, W. Preparation and purification of perylene-3,4-dicarbimides. 1996.

[61] Könemann, M., Blaschka, P., Reichelt, H. Verfahren zur Herstellung von Perylen-3,4-dicarbonsäureimiden. 2006.

[62] ya Tomizaki, K., Thamyongkit, P., Loewe, R. S., Lindsey, J. S., *Tetrahedron* **2003**, *59*, 1191 – 1207.

[63] Wonneberger, H., Pschirer, N., Bruder, I., Schöneboom, J., Ma, C.-Q., Erk, P., Li, C., Bäuerle, P., Müllen, K., *Chemistry - An Asian Journal* **2011**, *6*, 1744–1747.

[64] Robertson, N., *Angewandte Chemie International Edition* **2006**, *45*, 2338–2345.

[65] Nazeeruddin, M. K., Angelis, F. D., Fantacci, S., Selloni, A., Viscardi, G., Liska, P., Ito, S., Takeru, B., Grätzel, M., *Journal of the American Chemical Society* **2005**, *127*, 16835–16847.

[66] Edvinsson, T., Li, C., Pschirer, N., Schöneboom, J., Eickemeyer, F., Sens, R., Boschloo, G., Herrmann, A., Müllen, K., Hagfeldt, A., *Journal of Physical Chemistry C* **2007**, *111*, 15137–15140.

[67] Li, C., Liu, M., Pschirer, N. G., Baumgarten, M., Müllen, K., *Chemical Reviews* **2010**, *110*, 6817–6855.

[68] Tasios, N., Grigoriadis, C., Hansen, M. R., Wonneberger, H., Li, C., Spiess, H. W., Müllen, K., Floudas, G., *Journal of the American Chemical Society* **2010**, *132*, 7478–7487.

[69] Ferrere, S., Zaban, A., Gregg, B. A., *Journal of Physical Chemistry B* **1997**, *101*, 4490–4493.

[70] Zafer, C., Kus, M., Turkmen, G., Dincalp, H., Demic, S., Kuban, B., Teoman, Y., Icli, S., *Solar Energy Materials and Solar Cells* **2007**, *91*, 427–431.

[71] Planells, M., Cespedes-Guirao, F. J., Goncalves, L., Sastre-Santos, A., Fernandez-Lazaro, F., Palomares, E., *Journal of Materials Chemistry* **2009**, *19*, 5818–5825.

[72] Liu, B., Zhu, W. H., Wu, W. J., Ri, K. M., Tian, H., *Journal of Photochemistry and Photobiology A* **2008**, *194*, 268–274.

[73] Jin, Y. H., Hua, J. L., Wu, W. J., Ma, X. M., Meng, F. S., *Synthetic Metals* **2008**, *158*, 64–71.

[74] Shibano, Y., Umeyama, T., Matano, Y., Imahori, H., *Organic Letters* **2007**, *9*, 1971–1974.

[75] Ferrere, S., Gregg, B. A., *Journal of Physical Chemistry B* **2001**, *105*, 7602–7605.

[76] Ferrere, B. A., Sue; Gregg, *Proceedings - Electrochemical Society 2001* **2001**, *2001-10*, 161–172.

[77] Matsui, M., Dentani, T., Funabiki, K., Jin, J. Y., Yoshida, T., Minoura, H., *Dyes and Pigments* **2007**, *72*, 303–307.

[78] Otsuki, Y. T. D. K. P. S. S. P. I. A. H. L., Joe; Takaguchi, *Advances in Optoelectronics* **2011**, *2011*, 1–7.

[79] Cappel, U. B., Karlsson, M. H., Pschirer, N. G., Eickemeyer, F., Schöneboom, J., Erk, P., Boschloo, G., Hagfeldt, A., *Journal of Physical Chemistry C* **2009**, *113*, 14595–14597.

[80] Müllen, K., Li, C., Liu, Z. H., Schöneboom, J., Eickemeyer, F., Pschirer, N. G., Erk, P., Herrmann, A., *Journal of Materials Chemistry* **2009**, *19*, 5405–5415.

[81] Li, C., Yum, J.-H., Moon, S.-J., Herrmann, A., Eickemeyer, F., Pschirer, N. G., Erk, P., Schöneboom, J., Müllen, K., Grätzel, M., Nazeeruddin, M. K., *ChemSusChem* **2008**, *1*, 615–618.

[82] Yang, L., Cappel, U. B., Unger, E. L., Karlsson, M., Karlsson, K. M., Gabrielsson, E., Sun, L., Boschloo, G., Hagfeldt, A., Johansson, E. M. J., *Physical Chemistry Chemical Physics* **2012**, *14*, 779–789.

[83] Imahori, H., Mathew, S., *Journal of Materials Chemistry* **2011**, *21*, 7166–7174.

[84] Le Pleux, L., Smeigh, A. L., Gibson, E., Pellegrin, Y., Blart, E., Boschloo, G., Hagfeldt, A., Hammarstrom, L., Odobel, F., *Energy & Environmental Science* **2011**, *4*, 2075–2084.

[85] Hagfeldt, A., Morandeira, A., Fortage, J., Edvinsson, T., Le Pleux, L., Blart, E., Boschloo, G., Hanmiarstrom, L., Dobel, F., *Journal of Physical Chemistry C* **2008**, *112*, 1721–1728.

[86] Nattestad, A., Mozer, A. J., Fischer, M. K., Cheng, Y. B., Mishra, A., Bäuerle, P., Bach, U., *Nature Materials* **2010**, *9*, 31–5.

[87] Li, C. Novel Functional Rylene Dyes for Dye-Sensitized Solar Cells. Ph.D. thesis, Johannes Gutenberg-Universität Mainz, 2008.

[88] Hagberg, D. P., Yum, J.-H., Lee, H., De Angelis, F., Marinado, T., Karlsson, K. M., Humphry-Baker, R., Sun, L., Hagfeldt, A., Grätzel, M., Nazeeruddin, M. K., *Journal of the American Chemical Society* **2008**, *130*, 6259–6266.

[89] Qin, P., Zhu, H., Edvinsson, T., Boschloo, G., Hagfeldt, A., Sun, L., *Journal of the American Chemical Society* **2008**, *130*, 8570–8571.

[90] Segura, J. L., Herrera, H., Bäuerle, P., *Journal of Materials Chemistry* **2012**, *22*, 8717–8733.

[91] Cadogan, J. I. G., Cameronw.M,, Mackie, R. K., Searle, R. J. G., *Journal of the Chemical Society* **1965**, 4831–4837.

[92] Quante, H., Müllen, K., *Angewandte Chemie International Edition in English* **1995**, *34*, 1323–1325.

[93] Oesterling, I., Müllen, K., *Journal of the American Chemical Society* **2007**, *129*, 4595–4605.

[94] Weil, T., Reuther, E., Beer, C., Müllen, K., *Chemistry - A European Journal* **2004**, *10*, 1398–1414.

[95] Nolde, F., Pisula, W., Müller, S., Kohl, C., Müllen, K., *Chemistry of Materials* **2006**, *18*, 3715–3725.

[96] Langhals, H., Saulich, S., *Chemistry* **2002**, *8*, 5630–5643.

[97] Cotlet, M., Vosch, T., Habuchi, S., Weil, T., Müllen, K., Hofkens, J., Schryver, F. D., *Journal of the American Chemical Society* **2005**, *127*, 9760–9768.

[98] Fron, E., Puhl, L., Oesterling, I., Li, C., Müllen, K., De Schryver, F. C., Hofkens, J., Vosch, T., *ChemPhysChem* **2011**, *12*, 595–608.

[99] Mor, G. K., Basham, J., Paulose, M., Kim, S., Varghese, O. K., Vaish, A., Yoriya, S., Grimes, C. A., *Nano Letters* **2010**, *10*, 2387–2394.

[100] Kroeze, J. E., Hirata, N., Schmidt-Mende, L., Orizu, C., Ogier, S. D., Carr, K., Grätzel, M., Durrant, J. R., *Advanced Functional Materials* **2006**, *16*, 1832–1838.

[101] Cohen, A. J., Mori-Sánchez, P., Yang, W., *Science* **2008**, *321*, 792–794.

[102] Ziegler, T., Seth, M., Krykunov, M., Autschbach, J., Wang, F., *Journal of Molecular Structure: THEOCHEM* **2009**, *914*, 106 – 109.

[103] Kwon, Y. S., Lim, J., Song, I., Song, I. Y., Shin, W. S., Moon, S.-J., Park, T., *Journal of Materials Chemistry* **2012**, *22*, 8641–8648.

[104] Becker, S., Böhm, A., Müllen, K., *Chemistry - A European Journal* **2000**, *6*, 3984–3990.

[105] Thomas, K. R. J., Hsu, Y. C., Lin, J. T., Lee, K. M., Ho, K. C., Lai, C. H., Cheng, Y. M., Chou, P. T., *Chemistry of Materials* **2008**, *20*, 1830–1840.

[106] Fischer, M. K. R., Wenger, S., Wang, M. K., Mishra, A., Zakeeruddin, S. M., Grätzel, M., Bäuerle, P., *Chemistry of Materials* **2010**, *22*, 1836–1845.

[107] Ning, Z. J., Tian, H., *Chemical Communications* **2009**, 5483–5495.

[108] Wonneberger, H., Ma, C. Q., Gatys, M. A., Li, C., Bäuerle, P., Müllen, K., *Journal of Physical Chemistry B* **2010**, *114*, 14343–14347.

[109] Choi, H., Baik, C., Kang, S. O., Ko, J., Kang, M. S., Nazeeruddin, M. K., Grätzel, M., *Angewandte Chemie-International Edition* **2008**, *47*, 327–330.

[110] Kroeze, J. E., Hirata, N., Koops, S., Nazeeruddin, M. K., Schmidt-Mende, L., Grätzel, M., Durrant, J. R., *Journal of the American Chemical Society* **2006**, *128*, 16376–83.

[111] Wiberg, J., Guo, L. J., Pettersson, K., Nilsson, D., Ljungdahl, T., Martensson, J., Albinsson, B., *Journal of the American Chemical Society* **2007**, *129*, 155–163.

[112] Erten, S., Eren, E., Icli, S., *The European Physical Journal - Applied Physics* **2007**, *38*, 227–230.

[113] Holtrup, F. O., R. J. Müller, G., Quante, H., De Feyter, S., De Schryver, F. C., Müllen, K., *Chemistry - A European Journal* **1997**, *3*, 219–225.

[114] Kohl, C., Becker, S., Müllen, K., *Chemical Communications* **2002**, 2778–2779.

[115] Pschirer, N. G., Kohl, C., Nolde, F., Qu, J., Müllen, K., *Angewandte Chemie International Edition* **2006**, *45*, 1401–1404.

[116] Müller, S. Farbe und Funktion neuer Molekülarchitekturen auf Rylencarbonsäureimid-Basis. Ph.D. thesis, Johannes Gutenberg-Universität Mainz, 2006.

[117] Shi, F., Larock, R. C. In *C-H Activation*; Jin-Quan,, Shi, Z. Y., Eds.; Topics in Current Chemistry; Springer Berlin / Heidelberg, 2010; Vol. 292; pp 123–164.

[118] Worlikar, S. A., Larock, R. C., *Organic Letters* **2009**, *11*, 2413–2416.

[119] Ishiyama, T., Takagi, J., Hartwig, J. F., Miyaura, N., *Angewandte Chemie International Edition* **2002**, *41*, 3056–3058.

[120] Ishiyama, T., Nobuta, Y., Hartwig, J. F., Miyaura, N., *Chemical Communications* **2003**, 2924–2925.

[121] Lütke Eversloh, C., Avlasevich, Y., Li, C., Müllen, K., *Chemistry - A European Journal* **2011**, *17*, 12756–12762.

[122] Boschloo, G., Cappel, U. B., Smeigh, A. L., Plogmaker, S., Johansson, E. M. J., Rensmo, H., Hammarstrom, L., Hagfeldt, A., *Journal of Physical Chemistry C* **2011**, *115*, 4345–4358.

[123] Tam-Chang, S.-W., Seo, W., Rove, K., Casey, S. M., *Chemistry of Materials* **2004**, *16*, 1832–1834.

[124] Tam-Chang, S.-W., Seo, W., Iverson, I. K., *The Journal of Organic Chemistry* **2004**, *69*, 2719–2726.

[125] Tröster, H., *Dyes and Pigments* **1983**, *4*, 171 – 177.

[126] Wang, S., Li, Y., Du, C., Shi, Z., Xiao, S., Zhu, D., Gao, E., Cai, S., *Synthetic Metals* **2002**, *128*, 299 – 304.

[127] Hunsdiecker, H., Hunsdiecker, C., *Berichte der deutschen chemischen Gesellschaft (A and B Series)* **1942**, *75*, 291–297.

[128] Bronstein, H. E., Choi, N., Scott, L. T., *Journal of the American Chemical Society* **2002**, *124*, 8870–8875.

[129] Meyers, A. I., Fleming, M. P., *The Journal of Organic Chemistry* **1979**, *44*, 3405–3406.

[130] Camps, P., Lukach, A. E., Pujol, X., Vázquez, S., *Tetrahedron* **2000**, *56*, 2703 – 2707.

[131] Naskar, D., Chowdhury, S., Roy, S., *Tetrahedron Letters* **1998**, *39*, 699 – 702.

[132] Qu, J., Pschirer, N. G., Könemann, M., Müllen, K., Avlasevic, Y. Heptarylene and octarylene tetracarboxylic acid diimides, and production thereof. 2008.

[133] Lütke Eversloh, C., Li, C., Müllen, K., *Organic Letters* **2011**, *13*, 4148–4150.

[134] Wakim, S., Leclerc, M., *Synlett* **2005**, *2005*, 1223,1234.

[135] Bouchard, J., Wakim, S., Leclerc, M., *The Journal of Organic Chemistry* **2004**, *69*, 5705–5711.

[136] Du, C., Chen, J., Guo, Y., Lu, K., Ye, S., Zheng, J., Liu, Y., Shuai, Z., Yu, G., *The Journal of Organic Chemistry* **2009**, *74*, 7322–7327.

[137] Balaji, G., Shim, W. L., Parameswaran, M., Valiyaveettil, S., *Organic Letters* **2009**, *11*, 4450–4453.

[138] Jiang, W., Qian, H. L., Li, Y., Wang, Z., *Journal of Organic Chemistry* **2008**, *73*, 7369–7372.

[139] Miyaura, N., Suzuki, A., *Chemical Reviews* **1995**, *95*, 2457–2483.

[140] Hartwig, J. F., *Angewandte Chemie International Edition* **1998**, *37*, 2046–2067.

[141] Cid, J.-J., Yum, J.-H., Jang, S.-R., Nazeeruddin, M. K., Martínez-Ferrero, E., Palomares, E., Ko, J., Grätzel, M., Torres, T., *Angewandte Chemie International Edition* **2007**, *46*, 8358–8362.

[142] Ogura, R. Y., Nakane, S., Morooka, M., Orihashi, M., Suzuki, Y., Noda, K., *Applied Physics Letters* **2009**, *94*, 073308.

[143] Yum, J.-H., Jang, S.-R., Walter, P., Geiger, T., Nuesch, F., Kim, S., Ko, J., Gratzel, M., Nazeeruddin, M. K., *Chemical Communications* **2007**, 4680–4682.

[144] Wang, H.-X., Wu, H.-F., Yang, X.-L., Ma, N., Wan, L., *Polyhedron* **2007**, *26*, 3857 – 3864.

[145] Curiel, D., Más-Montoya, M., Uruvakili, A., Orenes, R. A., Pallamreddy, H., Molina, P., *Organic Letters* **2010**, *12*, 3164–3167.

[146] Jones, B. A., Ahrens, M. J., Yoon, M.-H., Facchetti, A., Marks, T. J., Wasielewski, M. R., *Angewandte Chemie International Edition* **2004**, *43*, 6363–6366.

[147] Wang, B., Yu, C., *Angewandte Chemie International Edition* **2010**, *49*, 1485–1488.

[148] Huang, C., Barlow, S., Marder, S. R., *The Journal of Organic Chemistry* **2011**, *76*, 2386–2407.

[149] Zhan, X., Facchetti, A., Barlow, S., Marks, T. J., Ratner, M. A., Wasielewski, M. R., Marder, S. R., *Advanced Materials* **2011**, *23*, 268–284.

[150] Mishra, A., Ma, C.-Q., Bäuerle, P., *Chemical Reviews* **2009**, *109*, 1141–1276.

[151] Huang, J., Fu, H., Wu, Y., Chen, S., Shen, F., Zhao, X., Liu, Y., Yao, J., *The Journal of Physical Chemistry C* **2008**, *112*, 2689–2696.

[152] Chen, S., Liu, Y., Qiu, W., Sun, X., Ma, Y., Zhu, D., *Chemistry of Materials* **2005**, *17*, 2208–2215.

[153] Ma, C.-Q., Mena-Osteritz, E., Debaerdemaeker, T., Wienk, M. M., Janssen, R. A. J., Bäuerle, P., *Angewandte Chemie International Edition* **2007**, *46*, 1679–1683.

[154] Fischer, M. K. R., Kaiser, T. E., Würthner, F., Bäuerle, P., *Journal of Materials Chemistry* **2009**, *19*, 1129.

[155] Zhan, X., Tan, Z., Zhou, E., Li, Y., Misra, R., Grant, A., Domercq, B., Zhang, X.-H., An, Z., Zhang, X., Barlow, S., Kippelen, B., Marder, S. R., *Journal of Materials Chemistry* **2009**, *19*, 5794–5803.

[156] An, Z., Odom, S. A., Kelley, R. F., Huang, C., Zhang, X., Barlow, S., Padilha, L. A., Fu, J., Webster, S., Hagan, D. J., Van Stryland, E. W., Wasielewski, M. R., Marder, S. R., *The Journal of Physical Chemistry A* **2009**, *113*, 5585–5593.

[157] Vajiravelu, S., Ramunas, L., Juozas Vidas, G., Valentas, G., Vygintas, J., Valiyaveettil, S., *Journal of Materials Chemistry* **2009**, *19*, 4268.

[158] Huang, J., Wu, Y., Fu, H., Zhan, X., Yao, J., Barlow, S., Marder, S. R., *The Journal of Physical Chemistry A* **2009**, *113*, 5039–5046.

[159] Li, J. L., Kastler, M., Pisula, W., Robertson, J. W. F., Wasserfallen, D., Grimsdale, A. C., Wu, J. S., Müllen, K., *Advanced Functional Materials* **2007**, *17*, 2528–2533.

[160] Bouzzine, S. M., Bouzakraoui, S., Bouachrine, M., Hamidi, M., *Journal of Molecular Structure: THEOCHEM* **2005**, *726*, 271 – 276.

[161] Jayasuriya, N., Kagan, J., Owens, J. E., Kornak, E. P., Perrine, D. M., *Journal of Organic Chemistry* **1989**, *54*, 4203–4205.

[162] Taerum, T., Lukoyanova, O., Wylie, R. G., Perepichka, D. F., *Org Lett* **2009**, *11*, 3230–3233.

[163] Balaji, G., Kale, T. S., Keerthi, A., Della Pelle, A. M., Thayumanavan, S., Valiyaveettil, S., *Organic Letters* **2011**, *13*, 18–21.

[164] Snaith, H. J., Grätzel, M., *Advanced Materials* **2007**, *19*, 3643–3647.

[165] Kroon, J. M. et al. , *Progress in Photovoltaics: Research and Applications* **2007**, *15*, 1–18.

[166] Hardin, B. E., Snaith, H. J., McGehee, M. D., *Nature Photonics* **2012**, *6*, 162 –169.

[167] Ahlrichs, R., Bär, M., Häser, M., Horn, H., Kölmel, C., *Chemical Physics Letters* **1989**, *162*, 165 – 169.

[168] Becke, A. D., *Physical Review A* **1988**, *38*, 3098–3100.

[169] Perdew, J. P., *Physical Review B* **1986**, *33*, 8822–8824.

[170] Eichkorn, K., Weigend, F., Treutler, O., Ahlrichs, R., *Theoretical Chemistry Accounts: Theory, Computation, and Modeling (Theoretica Chimica Acta)* **1997**, *97*, 119–124.

[171] Schäfer, A., Horn, H., Ahlrichs, R., *Journal of Chemistry Physics* **1992**, *97*, 2571–2577.

[172] Peng, B., Jungmann, G., Jager, C., Haarer, D., Schmidt, H. W., Thelakkat, M., *Coordination Chemistry Reviews* **2004**, *248*, 1479–1489.

[173] Veldman, D., Chopin, S. M. A., Meskers, S. C. J., Janssen, R. A. J., *The Journal of Physical Chemistry A* **2008**, *112*, 8617–8632.

Summary

Focus of this dissertation is the orbital and absorption tuning of perylene monoimides and diimides with respect to their application in organic photovoltaics (OPV). There, broad absorption plays a major role to harvest as much light as possible which is then converted into electrical energy. In order to ensure that the cells work efficiently, orbital tuning is a second important prerequisite.

Three new concepts of sensitiser design for perylene monoimides and their use in solid-state dye sensitised solar cells (sDSSCs) are explored. The synthesis of the molecules, their optical and electronic properties as well as their performance in sDSSC devices are described and discussed.

The concepts demonstrated in this work range from π-spacer introduction over new functionalisations to core extension of perylene monoimides. The push-pull character of the systems varies from strong coupling to complete decoupling of donor and acceptor, strongly influencing the absorption and HOMO/LUMO energy levels of the compounds.

Some of these concepts can be transferred to perylene diimides. One example of colour tuning in perylene diimides (PDIs) is demonstrated by a set of three terthiophene PDIs.

Zusammenfassung

Die vorliegende Dissertation beschäftigt sich mit der Steuerung der Absorption und Orbitalenergien von Perylenmonoimiden und Perylendiimiden für die Anwendung in organischer Photovoltaik (OPV). Eine breite Absorption spielt hier eine wichtige Rolle, um möglichst viel Licht zu ernten, das dann in elektrische Energie umgewandelt wird. Um sicher zu stellen, dass die Zelle effizient arbeiten kann, ist die Abstimmung von Orbitalenergien eine zweite wichtige Voraussetzung.

Es werden drei neue Design-Konzepte für Perylenmonoimid-Sensibilatoren für Festkörper-Farbstoffsolarzellen (solid-state dye-sensitised solar cells - sDSSCs) untersucht. Die Synthese, die optischen und elektronischen Eigenschaften der neuen Sensibilisator-Verbindungen sowie ihre Leistungsdaten in sDSSCs werden beschrieben und diskutiert.

Die in dieser Arbeit vorgestellten Konzepte reichen von der Einführung von π-Abstandhaltern über neue Funktionalisierungen bis hin zur Erweiterung der Perylenmonimid Grundkörper. Der *Push-Pull*-Charakter der Systeme variiert von starker Kopplung bis zu kompletter Entkopplung des Donors vom Akzeptor. Dies hat einen starken Einfluss sowohl auf die Absorptionseigenschaften, als auch auf die HOMO/LUMO Energie-Niveaus der Verbindungen.

Einige der Konzepte können auf Perylendiimide übertragen werden. Ein Beispiel von Perylendiimid (PDI)-Farbsteuerung wird an einer Reihe von drei Terthiophen-PDIs gezeigt.